

**Proceedings**  
**of the**  
**5<sup>th</sup> Joint Russian-American**  
**Computational Mathematics**  
**Conference**

**September 2-7, 1997**

*Hosted By:*  
**Sandia National Laboratories**  
**Albuquerque, NM, USA**



**SANDIA REPORT**  
**SAND98-1591**  
Unlimited Release  
Printed

The papers in this book comprise the proceedings of the meeting mentioned on the cover and title page. They reflect the authors' opinions and, in the interest of timely dissemination, are published as presented and without change. Their inclusion in this publication does not necessarily constitute endorsements by Sandia Corporation, the United States Government, or the other authors.

© 1997 by Sandia Corporation. All rights reserved

Issued by Sandia National Laboratories, operated for the United States Department of Energy by Sandia Corporation.

**NOTICE:** This report was prepared as an account of work sponsored by an agency of the United States Government. Neither the United States Government nor any agency thereof, nor any of their employees, nor any of their contractors, subcontractors, or their employees, make any warranty, express or implied, or assumes any legal liability or responsibility for the accuracy, completeness, or usefulness of any information, apparatus, product, or process disclosed, or represents that its use would not infringe privately owned rights. Reference herein to any specific commercial product, process, or service by trade name, trademark, manufacturer, or otherwise, does not necessarily constitute or imply its endorsement, recommendation, or favoring by the United States Government, any agency thereof or any of their contractors or subcontractors. The views and opinions expressed herein do not necessarily state or reflect those of the United States Government, any agency thereof or any of their contractors.

Printed in the United States of America. This report has been reproduced directly from the best available copy.

# Proceedings of the 5<sup>th</sup> Joint Russian-American Computational Mathematics Conference

September 2-7, 1997  
Coronado Club, Sandia National Laboratories  
Kirtland Air Force Base  
Albuquerque, New Mexico, USA

Conference Organizer &  
Proceedings Editor

Grant S. Heffelfinger  
Manager  
Materials Simulation Science Department  
Sandia National Laboratories  
Albuquerque, NM 87185-1111

## Abstract

These proceedings contain a record of the talks presented and papers submitted by participants of the 5<sup>th</sup> Joint Russian-American Computational Mathematics Conference. The conference participants represented three institutions from the United States, Sandia National Laboratories (SNL), Los Alamos National Laboratory (LANL), Lawrence Livermore National Laboratory (LLNL), and two from Russia, Russian Federal Nuclear Center – All Russian Research Institute of Experimental Physics (RFNC-VNIIEF/Arzamas-16), and Russian Federal Nuclear Center – All Russian Research Institute of Technical Physics (RFNC-VNIITF/Chelyabinsk-70).

## Table of Contents

List of Attendees .....	iii
Agenda .....	iv
List of Abstracts .....	viii
List of Conference Papers Submitted for Proceedings .....	xii
Conference Abstracts .....	1
Conference Papers .....	67
Index of Authors & Co-Authors .....	296
Distribution .....	298

## List of Attendees

### **Arzamas-16, VNIIEF**

#### **Russia**

Bakhrakh, Samuel  
Delov, Valeri  
Pavlenko, Olga  
Pevnaya, Polina  
Rasskazova, Vera  
Shagaliyev, Rashit  
Sofronov, Ivan  
Tikhomirov,  
Volkov, Stanislav  
Voronin, Boris  
Yanilkin, Yuri

### **Chelyabinsk-70, VNIITF**

#### **Russia**

Baidine, Grigori  
Elsoukov, Vassili  
Kandiev, Iadgar  
Kozmanov, Mikhail  
Talantova, Lada

### **Lawrence Livermore National Laboratory**

#### **USA**

Belak, Jim F.  
Boercker, Dave  
Clouse, Christopher J.  
Cox, Larry J.  
Ferguson, Jim  
Nielsen, Dale  
Procassini, Richard  
Rathkopf, Jim  
Ritchie, Burke  
Schach Von Wittenau, Alex E  
Svatos, Michelle M.

### **Los Alamos National Laboratory**

#### **USA**

Caramana, Ed  
Clover, Michael R.  
Collins, Lee A.  
Dilts, Gary  
Hammerberg, James E.  
Kirkpatrick, Ronald  
Linn, Rodman R.  
Morel, Jim E.  
Pepin, Jason  
Powers, Bill  
Riley, Merle  
Shahskov, Mikhail  
Shaw, Milton S.  
Sheehey, Peter T.  
Smolarkiewicz, Piotr  
Steinkamp, Michael  
Tonks, Davis  
Vold, Erik  
Zocher, Marvin A.

### **Sandia National Laboratories**

#### **USA**

Blanford, Mark  
Fang, H. Eliot  
Greenberg, David  
Heffelfinger, Grant S.  
Heinstein, Martin  
Key, Samuel W  
Leland, Robert W.  
Mitchell, Scott A.  
Ober, Curtis  
Pohl, Phillip  
Summers, Randall M.  
Taylor, Paul  
Trucano, Tim G.

# Agenda

## Fifth Joint Russian-American Conference on Computational Mathematics

Tuesday, September 2, 1997

### Presentations - Abstract Title and Author(s)

#### Early Morning Session

- 8:30 - 8:50 *Paralleling Calculations in 3D Electromagnetic Simulation Code*, G. A. Adamkevich, G. V. Baidin, I. A. Litvinenko, V. A. Rotko
- 8:50 - 9:10 *Parallelization Methods for Numerical Solution of 3D Group Non-Stationary Equation of Neutron Diffusion for Nuclear Power Plant Safety Calculations*, A. V. Alexeyev, O. A. Zvenigorodskaya, R. M. Shagaliyev
- 9:10 - 9:30 *Methods for Improving Accuracy of the First-Order Approximation Scheme for Solving Systems of Equations for Radiation Transfer*, E. S. Andreyev, V. Yu. Gusev, M. Yu. Kozmanov
- 9:30 - 9:50 *A Technique for Radiation Transfer Computation With Account of Anisotropic Emission of Boundary Surface*, S. V. Bazhenov, P. I. Pevnaya
- 9:50 - 10:10 BREAK

#### Late Morning Session

- 10:10 - 10:30 *Numerical Simulation in Diffusive-Vacuum Approximation of Radiant Energy Transfer in Thermonuclear Targets*, A. A. Bazin, V. V. Vatulin, Yu. A. Demytyev, V. F. Mironova, G. I. Skidan, E. N. Tikhomirova, B. P. Tikhomirov
- 10:30 - 10:50 *Computational Simulation of Non-Equilibrium Processes During Thermonuclear Fusion*, I. M. Belyakov, S. A. Belkov, V. V. Vatulin, L. L. Vakhlamova, O. A. Vinokurov, S. G. Garanin, V. F. Yermolovich, N. P. Pleteneva, G. N. Remizov, V. Yu. Rezchikov, N. A. Ryabikina, I. D. Sofronov, L. P. Fedotova, R. M. Shagaliyev
- 10:50 - 11:10 *Elimination of Artificial Grid Distortion and Hourglass-Type Motions by Means of Lagrangian Subzonal Masses and Pressures*, E. J. Caramana, M. J. Shashkov
- 11:10 - 11:30 *Parallel Deterministic Neutronics with AMR in 3D*, C. Clouse, J. Ferguson, C. Hendrickson
- 11:30 - 1:00 LUNCH

#### Early Afternoon Session

- 1:00 - 1:20 *Source Description and Sampling Techniques used in PEREGRINE Monte Carlo Calculations of Dose Distributions for Radiation Oncology*, L. J. Cox, P. M. Bergstrom, Jr., W. P. Chandler, S. M. Hornstein, A. E. Schach von Wittenau, C. L. Hartmann Siantar
- 1:20 - 1:40 *The Moving-Least-Squares-Particle Hydrodynamics Method (MLSPH)*, G. Dilts
- 1:40 - 2:00 *Monte-Carlo Simulation of Biological Protection at Repetitive Pulse Electron Accelerator*, Ia. Z. Kandiev, V. V. Plokhoy
- 2:00 - 2:20 *The Energetic Alpha Particle Transport Method (EATM)*, R. C. Kirkpatrick
- 2:20 - 2:40 BREAK

## Agenda

**Tuesday - (Continued)**

### Late Afternoon Session

- 2:40 - 3:00 *Time Dependent View Factor Methods*, R. C. Kirkpatrick  
3:00 - 3:20 *Implementation of Numerical Simulation Techniques in Analysis of the Accidents in Complex Technological Systems*, G. S. Klishin, V. E. Seleznev, V. V. Aleoshin  
3:20 - 3:40 *3D Unstructured-Mesh Radiation Transport Codes*, J. Morel  
3:40 - 4:00 *Boundary Acquisition for Setup of Numerical Simulation*, C. Diegert  
4:00 - 4:20 *An Analytically Solvable Problem for A Sliding Interface*, J. Pepin and J. E. Hammerberg  
4:20 - 4:30 Wrap-up/Discussion  
6:30 - 9:00 RECEPTION - GRUET WINERY

**Wednesday, September 3, 1997**

### Presentations - Abstract Title and Author(s)

#### Early Morning Session

- 8:30 - 8:50 *Three Dimensional Finite Element Formulation For Thermoviscoelastic Orthotropic Media*, M. A. Zocher  
8:50 - 9:10 *Computational Modeling of Joint U. S. - Russian Experiments Relevant to Magnetic Compression/Magnetized Target Fusion (MAGO/MTF)*, P. T. Sheehey, R. J. Faehl, R. C. Kirkpatrick, I. R. Lindemuth  
9:10 - 9:30 *ALEGRA--A Massively Parallel H-Adaptive Code for Solid Dynamics*, R. M. Summers, M. K. Wong, E. A. Boucheron, J. R. Weatherby  
9:30 - 9:50 *Application of CHAD Hydrodynamics to Shock-Wave Problems*, H. E. Trease, P. J. O'Rourke, M. S. Sahota  
9:50 - 10:10 BREAK

#### Late Morning Session

- 10:10 - 10:30 *Nonregular Free-Lagrangian "Medusa" Technique*, S. G. Volkov, B. M. Zhogov, V. D. Malshakov, I. D. Sofronov  
10:30 - 10:50 *Numerical Simulation of Close and Remote Zones of Accident Outburst and Explosion*, Yu. V. Yanilkin, V. N. Sofronov, V. I. Tarasov, V. P. Statsenko, V. N. Piskunov, N. P. Kovalyov, O. A. Dibirov, A. L. Stadnik, T. A. Toropova, G. G. Ivanova, A. A. Shanin  
10:50 - 11:10 *Variational Difference Flow-Type Scheme for 3D Diffusion Equation on Grids of Arbitrary Hexahedrons*, S. V. Bazhenov, S. P. Belyayev, Yu. A. Bondarenko, V. V. Gorev, T. V. Korol'kova, P. I. Pevnaya  
11:10 - 11:30 *Hexahedral Mesh Generation Via the Dual Arrangement of Surfaces*, S. A. Mitchell, T. J. Tautges  
11:30 - 1:00 LUNCH

#### Early Afternoon Session

- 1:00 - 1:20 *Numerical Preservation of Symmetry Properties of Continuum Problems*, E. J. Caramana, P. Whalen  
1:20 - 1:40 *A New 2-d, Limited, Zone-Centered Artificial Viscosity Tensor*, M. R. Clover, C. W. Cranfill  
1:40 - 2:00 *Solving the Transport Equation with Quadratic Finite Elements: Theory and Applications*, J. M. Ferguson  
2:00 - 2:20 *Modeling By Value Implemented in Prizma Code*, Ia. Z. Kandiev, G. N. Malyshkin  
2:20 - 2:40 BREAK

## Agenda

**Wednesday – (Continued)**

### Late Afternoon Session

- 2:40 - 3:00 *An 8-Node Tetrahedral Finite Element Suitable For Explicit Transient Dynamic Simulations*, S. W. Key, M. W. Heinstein, C. M. Stone
- 3:00 - 3:20 *MPDATA: A Positive Definite Solver for Geophysical Flows*, P. K. Smolarkiewicz, L. G. Margolin
- 3:20 - 3:40 *Load Balancing of Parallel Computations*, Robert W. Leland, Bruce Hendrickson, Karen Devine
- 3:40 - 4:00 *Numerical Simulation of Turbulent Mixing in 2D Flows*, V. V. Nikiforov, Yu. V. Yanilkin, G. V. Zharova, Yu. A. Yudin
- 4:00 - 4:20 *Analytical and Numerical Study of Accelerated Thin Layer Instability*, S. M. Bakhrah, G. P. Simonov
- 4:20 - 4:30 Wrap-up/Discussion

DINNER - OPEN

**Thursday, September 4, 1997**

### Presentations - Abstract Title and Author(s)

#### Early Morning Session

- 8:30 - 8:50 *Calculation Technique for 3-D Gas Dynamics Problems on Nonregular Lagrangian Grids*, V. V. Rasskazova
- 8:50 - 9:10 *3-D Parallel Program for Numerical Calculation of Gas Dynamics Problems with Heat Conductivity on Distributed Memory Computational Systems (CS)*, I. D. Sofronov, B. L. Voronin, O. I. Butnev, A. N. Bykov, A. M. Yerofeyev, A. I. Skripnik, D. Nielsen, Jr., N. Medsen, R. Evans, S. Brandon
- 9:10 - 9:30 *Mathematical Methods for Protein Science*, W. Hart, S. Istrail, J. Atkins
- 9:30 - 9:50 *Development of Difference Schemes for Computing Multidimensional Non-Stationary Elastic-Plastic Flows on the Base of the Mutual Transition Law for Kinetic and Internal Energies*, V. B. Vershinin, V. I. Delov, O. V. Senilova, I. D. Sofronov
- 9:50 - 10:10 BREAK

#### Late Morning Session

- 10:10 - 10:30 *Molecular Dynamics Modeling of Solidification in Metals*, D. B. Boercker, J. Belak, J. Glosli
- 10:30 - 10:50 *Quantum Molecular Dynamics Simulations of Dense Matter*, L. Collins, J. Kress, N. Troullier, T. Lenosky, I. Kwon
- 10:50 - 11:10 *Simulation of Thermomechanical Fatigue in Solder Joints*, H. E. Fang, V. L. Porter, R. M. Fye, E. A. Holm
- 11:10 - 11:30 *Computation Technique for Elastic-Plastic Flows with Account of Material Destruction and Fragmentation*, A. V. Gorodnichev, G. P. Siminov, Yu. V. Yanilkin
- 11:30 - 1:00 LUNCH

## Agenda

Thursday – (Continued)

### Presentations - Abstract Title and Author(s)

#### Early Afternoon Session

- 1:00 - 1:20 *Recent Work on Material Interface Reconstruction*, S. J. Mosso, B. K. Swartz  
1:20 - 1:40 *Molecular Dynamics Computer Simulation of Permeation in Solids*, P. I. Pohl, G. S. Heffelfinger, D. K. Fidler, D. M. Ford  
1:40 - 2:00 *An Implicit Fast Fourier Transform Method for Integration of the Time Dependent Schrodinger Equation*, M. E. Riley, A. B. Ritchie  
2:00 - 2:20 *Efficient Single Scatter Electron Monte Carlo Simulation*, M. Svatos, J. Rathkopf  
2:20 - 2:40 BREAK

#### Late Afternoon Session

- 2:40 - 3:00 *Transverse Isotropic Modeling of the Ballistic Response of Glass Reinforced Plastic Composites*, P. A. Taylor  
3:00 - 3:20 *Spallation Studies on Shock Loaded Uranium*, D. L. Tonks, R. Hixson, R. L. Gustavsen, J. E. Vorthman, A. Kelly, A. K. Zurek, W. R. Thissell  
3:20 - 3:40 *Propagation of an Ultra-short, Intense Laser in a Relativistic Fluid*, A. B. Ritchie, C. D. Decker  
3:40 - 4:00 *A Transport Model for Computer Simulation of Wildfires*, R. Linn, F. Harlow  
4:00 - 4:20 *Experiences with Electromagnetic Particle-in-Cell Simulation on the Teraflop Computer*, Mark L. Kiefer  
4:20 - 4:30 Wrap-up/Discussion  
6:30 – 9:00 SOCIAL EVENING – TOWN PARK CLUB HOUSE

Friday, September 5, 1997

### Presentations - Abstract Title and Author(s)

#### Early Morning Session

- 8:30 - 8:50 *Molecular Dynamics of Shock Loading of Metals with Defects*, J. F. Belak  
8:50 - 9:10 *Solution of Large Nonlinear Quasistatic Structural Mechanics Problems on Distributed-Memory Multiprocessor Computers*, M. Blanford  
9:10 - 9:30 *Providing Scalable System Software for High-End Simulations*, D. Greenberg  
9:30 - 9:50 *Architecture of a Multicomputer's Commutation Network and of Difference Grid for Computational Physics Problems*, I. D. Sofronov  
9:50 - 10:10 BREAK

#### Late Morning Session

- 10:10 - 10:30 *Establishing Confidence in Complex Physics Codes: Art or Science?*, T. Trucano  
10:30 - 10:50 *Explosive Deceleration and Fragmentation of Meteorites in the Atmosphere*, V. P. Elsukov, D. V. Petrov, V. A. Simonenko, O. N. Shubin  
10:50 - 11:10 *Numerical Simulation of Experiments with Fuel Pellets at Pulse Reactor Facility*, Ia. Z. Kandiev, R. M. Kozybayev  
11:10 - 11:30 *Seismic Imaging using Finite-Differences and Parallel Computers*, C. C. Ober  
11:30 – 12:00 Wrap-up/Discussion

## List of Abstracts

Adamkevich, G.A., Baidin, G.V., Litvinenko, I.A., Rotko, V.A., RFNC-VNIITF, Russia, <i>Parallel Calculations in 3D Electromagnetic Simulation Code</i> .....	3
Alexeyev, A.V., Zvenigorodskaya, O.A., Shagaliyev, R.M., RFNC-VNIIEF, Russia, <i>Parallelization Methods for Numerical Solution of 3D Group Non-Stationary Equation of Neutron Diffusion for Nuclear Power Plant Safety Calculations</i> .....	4
Andreyev, E.S., Gusev, V. Yu, Kozmanov, M. Yu, RFNC-VNIITF, Russia, <i>Methods for Improving Accuracy of the First-Order Approximation Scheme for Solving Systems of Equations for Radiation Transfer</i> .....	5
Bakhrakh, S.M. and Simonov, G.P., RFNC-VNIIEF, Russia, <i>Analytical and Numerical Study of Accelerated Thin Layer Instability</i> .....	6
Bazhenov, S.V. and Pevnaya, P.I., RFNC-VNIIEF, Russia, <i>A Technique for Radiation Transfer Computation with Account of Anisotropic Emission of Boundary Surface</i> .....	7
Bazhenov, S.V., Belyayev, S.P., Bondarenko, Yu.A., Gorev, V.V., Korol'kova, T.V., Pevnaya, P.I., RFNC-VNIIEF, Russia, <i>Variational Difference Flow-Type Scheme for 3D Diffusion Equation on Grids of Arbitrary Hexahedrons</i> .....	8
Bazin, A.A., Vatulin, V.V., Dementyev, Yu.A., Mironova, V.F., Skidan, G.I., Tikhomirova, E.N., Tikhomirov, B.P., RFNC-VNIIEF, Russia, <i>Numerical Simulation in Diffusive Vacuum Approximation of Radiant Energy Transfer in Thermonuclear Targets</i> .....	9
Belak, J.F., LLNL, <i>Molecular Dynamics of Shock Loading of Metals with Defects</i> .....	10
Belyakov, I.M., Beklov, S.A., Vatulin, V.V., Vakhlamova, L.L., Vinokurov, O.A., Garanin, S.G., Yermolovich, V.F., Pleteneva, N.P., Remizov, G.N., Rezchikov, V. Yu, Ryabikina, N.A., Sofronov, I.D., Fedotova, L.P., Shagaliyev, R.M., RFNC-VNIIEF, Russia, <i>Computational Simulation of Non-Equilibrium Processes During Thermonuclear Fusion</i> .....	11
Blanford, M., SNL, <i>Solution of Large Nonlinear Quasistatic Structural Mechanics Problems on Distributed-Memory Multiprocessor Computers</i> .....	12
Boercker, D.B., Belak, J., and Glosli, J., LLNL, <i>Molecular Dynamics Modeling of Solidification in Metals</i> .....	13
Caramana, E.J., and Shashkov, M.J., LANL, <i>Elimination of Artificial Grid Distortion and Hourglass-Type Motions by Means of Lagrangian Subzonal Masses and Pressures</i> .....	14
Caramana, E.J., and Whalen, P., LANL, <i>Numerical Preservation of Symmetry Properties of Continuum Problems</i> .....	15

## List of Abstracts (Continued)

Clouse, C., Ferguson, J., Hendrickson, C., LLNL, <i>Parallel Deterministic Neutronics With AMR in 3D</i> .....	16
Clover, M.R., and Cranfill, C.W., LANL, <i>A New 2-D, Limited, Zone-Centered Artificial Viscosity Tensor</i> .....	17
Collins, L., Kress, J., Troullier, N., Lenosky, T., and Kwon, I., LANL, <i>Quantum Molecular Dynamics Simulations of Dense Matter</i> .....	18
Cox, L., Bergstrom Jr., P.M., Chandler, W.P., Hornstein, S.M., Schach von Wittenau, A.E., Hartmann Sinatar, C.L., LLNL, <i>Source Description and Sampling Techniques Used in Peregrine Monte Carlo Calculations of Dose Distributions for Radiation Oncology</i> .....	19
Diegert, C., SNL, <i>Boundary Acquisition for Setup of Numerical Simulation</i> .....	20
Dilts, G., LANL, <i>The Moving-Least-Squares-Particle Hydrodynamics Method (MLSPH)</i> .....	21
Elsukov, V.P., Petrov, D.V., Simonenko, V.A., Shubin, O.N., RFNC-VNIITF, Russia, <i>Explosive Deceleration and Fragmentation of Meteorites in the Atmosphere</i> .....	22
Fang, H.E., Porter, V.L., Fye, R.M., Holm, E.A., SNL, <i>Simulation of Thermomechanical Fatigue in Solder Joints</i> .....	23
Ferguson, J.M., LLNL, <i>Solving the Transport Equation with Quadratic Finite Elements: Theory and Applications</i> .....	25
Gorodnichev, A.V., Siminov, G.P., Yanilkin, V.Yu, RFNC-VNIIEF, Russia, <i>Computation Technique for Elastic-Plastic Flows With Account of Material Destruction and Fragmentation</i> .....	26
Greenberg, D., SNL, <i>Providing Scalable System Software for High-End Simulations</i> .....	27
Hart, W., Istrail, S., Atkins, J., SNL, <i>Mathematical Methods for Protein Science</i> .....	28
Kandiev, Ia.Z., and Malyshkin, G.N., RFNC-VNIITF, Russia, <i>Modeling by Value Implemented in Prizma Code</i> .....	30
Kandiev, Ia.Z., and Plokhoy, V.V., RFNC-VNIITF, Russia, <i>Monte-Carlo Simulation of Biological Protection at Repetitive Pulse Electron Accelerator</i> .....	32
Kandiev, Ia.Z., and Kozybayev, R.M., RFNC-VNIITF, Russia, <i>Numerical Simulation of Experiments With Fuel Pellets at Pulse Reactor Facility</i> .....	33
Key, S.W., Heinstejn, M.W., Stone, C.M., SNL, <i>An 8-Node Tetrahedral Finite Element Suitable for Explicit Transient Dynamic Simulations</i> .....	34

## List of Abstracts (Continued)

Kirkpatrick, R.C., LANL, <i>The Energetic Alpha Particle Transport Method (EATM)</i> .....	35
Kirkpatrick, R.C., LANL, <i>Time Dependent View Factor Methods</i> .....	36
Klishin, G.S., Seleznev, V.E., Aleoshin, V.V., RFNC-VNIIEF, Russia, <i>Implementation of Numerical Simulation Techniques in Analysis of the Accidents in Complex Technological Systems</i> .....	37
Linn, R., LANL, <i>A Transport Model for Computer Simulation of Wildfires</i> .....	38
Margolin, L.G., LANL, <i>On Simulating Flow with Multiple Time Scales Using a Method of Averages</i> .....	39
Mitchell, S.A., and Tautges, T.J., SNL, <i>Hexahedral Mesh Generation Via The Dual Arrangement of Surfaces</i> .....	40
Morel, J., LANL <i>3D Unstructured-Mesh Radiation Transport Codes</i> .....	41
Mosso, S.J., and Swartz, B.K., LANL, <i>Recent Work on Material Interface Reconstruction</i> .....	42
Nikiforov, V.V., Yanilkin, Yu.V., Zharova, G.V., Yudin, Yu.A., RFNC-VNIIEF, Russia, <i>Numerical Simulation of Turbulent Mixing in 2D Flows</i> .....	43
Ober, C.C., SNL, <i>Seismic Imaging Using Finite-Differences and Parallel Computers</i> .....	44
Pohl, P.I., Heffelfinger, G.S., Fisler, D.K., and Ford, D.M., SNL, <i>Molecular Dynamics Computer Simulation of Permeation in Solids</i> .....	45
Procassini, R.J., LLNL, <i>Parallel Monte Carlo Transport Modeling in The Context of a Time-Dependent, Three-Dimensional Multi-Physics Code</i> .....	46
Rasskazova, V.V., RFNC-VNIIEF, Russia, <i>Calculation Technique for 3-D Gas Dynamics Problems on Nonregular Lagrangian Grids</i> .....	47
Riley, M.E., SNL, and Ritchie, A.B., LLNL, <i>An Implicit Fast Fourier Transform Method for Integration of the Time Dependent Schrodinger Equation</i> .....	48
Ritchie, A.B., and Decker, C.D., LLNL, <i>Propagation of an Ultra-Short, Intense Laser in a Relativistic Fluid</i> .....	49
Sheehey, P.T., Faehl, R.J., Kirkpatrick, R.C., and Lindemuth, I.R., LANL, <i>Computational Modeling of Joint U.S.-Russian Experiments Relevant to Magnetic Compression/ Magnetized Target Fusion (MAGO/MTF)</i> .....	50
Smolarkiewicz, P.K., and Margolin, L.G., LANL, <i>MPData: A Positive Definite Solver for Geophysical Flows</i> .....	51

## List of Abstracts (Continued)

Sofronov, I.D., RFNC-VNIIEF, Russia, <i>Architecture of a Multicomputer's Commutation Network and of Difference Grid for Computational Physics Problems</i> .....	52
Sofronov, I.D., Voronin, B.L., Butnev, O.I., Bykov, A.N., Yerofeyev, A.M., and Skripnik, A.I., VNIIEF, Russia, Nielsen Jr., D., Medsen, N., Evans, R., and Brandon, S., LLNL, <i>3-D Parallel Program for Numerical Calculation of Gas Dynamics Problems with Heat Conductivity on Distributed Memory Computational Systems (CS)</i> .....	53
Summers, R.M., Wong, M.K., Boucheron, E.A., Weatherby, J.R., SNL, <i>Alegra—A Massively Parallel H-Adaptive Code for Solid Dynamics</i> .....	54
Svatos, M., and Rathkopf, J., LLNL, <i>Efficient Single Scatter Electron Monte Carlo Simulation</i> .....	55
Taylor, P.A., SNL, <i>Transverse Isotropic Modeling of the Ballistic Response of Glass Reinforced Plastic Composites</i> .....	56
Tonks, D.L., Hixson, R., Gustavsen, R.L., Vorthman, J.E., Kelly, A., Zurek, A.K., and Thissell, W.R., LANL, <i>Spallation Studies on Shock Loaded Uranium</i> .....	57
Trease, H.E., O'Rourke, P.J., and Sahota, M.S., LANL, <i>Application of Chad Hydrodynamics to Shock-Wave Problems</i> .....	58
Trucano, T., SNL, <i>Establishing Confidence in Complex Physics Codes: Art or Science?</i> .....	59
Vershinin, V.B., Delov, V.I., Senilova, O.V., Sofronov, I.D., RFNC-VNIIEF, Russia, <i>Development of Difference Schemes for Computing Multidimensional Non-Stationary Elastic-Plastic Flows on the Base of the Mutual Transition Law for Kinetic and Internal Energies</i> .....	60
Volkov, S.G., Zhogov, B.M., Malshakov, V.D., Sofronov, I.D., RFNC-VNIIEF, Russia, <i>Nonregular Free-Lagrangian "Meducs" Technique</i> .....	62
Yanilkin, Yu.V., Sofronov, V.N., Tarasov, V.I., Statsenko, V.P., Piskunov, V.N., Kovalyov, N.P., Dibirov, O.A., Stadnik, A.L., Toropova, T.A., Ivanova, G.G., Shanin, A.A., RFNC-VNIIEF, Russia, <i>Numerical Simulation of Close and Remote Zones of Accident Outburst and Explosion</i> .....	63
Zocher, M.A., LANL, <i>Three Dimensional Finite Element Formulation for Thermoviscoelastic Orthotropic Media</i> .....	65

## List of Conference Papers Submitted for Proceedings

<i>Analytical and numerical study of accelerated thin layer instability</i> , S. M. Bakhrakh, G. P. Simonov, RFNC-VNIIEF, Arzamas-16, Russia .....	69
<i>Architecture of a Multicomputer's Commutation Network and a Difference Grid for Mathematical Physics Problems</i> , I. D. Sofronov, VNIIEF, Russia .....	75
<i>The Calculations of Radiant Energy Transfer in Thermonuclear Targets in Diffusion-Vacuum Approximation</i> , A. A. Bazin, V. V. Vatulin, Yu. A. Dementyev, V. F. Mironova, G. I. Skidan, B. P. Tikhomirov, E. N. Tikhomirova, Russia .....	79
<i>Computation of Radiation Transport at Boundary Surface Anisotropic Light Emission</i> , S. V. Bazhenov, P. I. Pevnaya, Russia .....	83
<i>Difference Scheme Construction for Computing 2D Time-Dependent Elastic-Plastic Flows Basing on the Law of Kinetic and Internal Energy Interconversion</i> , V. I. Delov, O. V. Senilova, I. D. Sofronov, VNIIEF, Arzamas-16, Russia .....	87
<i>Efficient Single Scatter Electron Monte Carlo</i> , M. M. Svatos and J. A. Rathkopf, LLNL, USA .....	91
<i>The Energetic Alpha Particle Transport Method EATM</i> , Ronald C. Kirkpatrick, LANL, USA .....	97
<i>Explosive Deceleration and Fragmentation of Meteorites in Atmosphere</i> , D. V. Petrov, O. N. Shubin, V. P. Elsukov, V. A. Simonenko, RFNC-VNIITF, Russia .....	105
<i>Explosive Deceleration and Fragmentation of Meteorites in the Atmosphere</i> , D. V. Petrov, O. N. Shubin, V. P. Elsukov, V. A. Simonenko, RFNC-VNIITF, Russia .....	123
<i>Implementation of Numerical Simulation Techniques in Analysis of the Accidents in Complex Technological Systems</i> , G. S. Klishin, V. E. Seleznev, V. V. Aleoshin, VNIIEF, Russia, Presented by P. I. Pohl, SNL, USA .....	135
<i>An Implicit Fast Fourier Transform Method for Integration of the Time Dependent Schrodinger Equation</i> , Merle E. Riley, SNL, and A. Burke Ritchie, LLNL, USA .....	143
<i>Importance Biasing Scheme Implemented in Prizma Code</i> , Ia.Z. Kandiev, G. N. Malyshkin, RFNC-VNIITF, Russia .....	149
<i>Irregular Free-Lagrangian "Medusa" Technique</i> , S. G. Volkov, B. M. Zhogov, V. D. Malshakov, I. D. Sofronov, Arzamas-16, VNIIEF, Russia .....	159

<i>Irregular Free-Lagrangian Technique “Meduza.”</i> S. G. Volkov, B. M. Zhogov, V. D. Malshakov, I. D. Sofronov, VNIIEF, Russia .....	165
<i>Method for Material Failure and Fragmentation Computation in Egak Program System.</i> A. V. Gorodnichev, G. P. Simonov, Yu. V. Yanilkin, RFNC-VNIIEF, Russia .....	195
<i>Molecular Dynamics Simulation of Permeation in Solids,</i> Phillip I. Pohl, Grant S. Heffelfinger, Diana K. Fisler and David M. Ford, SNL, USA .....	199
<i>Monte-Carlo Simulation of Biological Protection for Repetitive Pulse Electron Accelerator,</i> Ya.Z. Kandiev, V. V. Plokhov, RFNC-VNIITF, Russia .....	209
<i>Multi-Parameter Model of Turbulent Mixing in Two-Dimensional Flows,</i> V. V. Nikiforov, Yu. V. Yanilkin, G. V. Zharova, Yu. A. Yudin, RFNC-VNIIEF, Russia .....	219
<i>Numerical modeling of experiments with fuel pellets at pulse reactor,</i> Ya. Z. Kandiev, R. M. Kozybayev, RFNC-VNIITF, Russia .....	225
<i>Numerical Simulation of Near and Far Areas of Accidental Releases and Explosions,</i> Yu. V. Yanilkin, V. N. Sofronov, V. I. Tarasov, V. P. Statsenko, V. N. Piskunov, N. P. Kovalev, O. A. Dibirov, A. L. Stadnik, T. A. Toropova, G. G. Ivanova, A. A. Shanin, RFNC-VNIIEF, Russia .....	235
<i>Numerical Simulation of Thermonuclear Fusion Non-equilibrium Processing Using 2D Software Packages,</i> I. M. Belyakov, S. A. Belkov, V. V. Vatulin, L. L. Vakhlamova, O. A. Vinokurov, S. G. Garanin, V. F. Yermolovich, N. P. Pleteneva, G. N. Remizov, V. Yu. Rezchikov, N. A. Ryabikina, I. D. Sofronov, L. P. Fedotova, R. M. Shagaliev, Russia.....	239
<i>Parallelization Methods for Numerical Solution of 3D Group Non-stationary Equation of Neutron Diffusion for Nuclear Power Plant Safety Calculations,</i> A. V. Alekseyev, O. A. Zvenigorodskaya, R. M. Shagaliev, VNIIEF, Russia .....	245
<i>Propagation of an ultrashort, intense laser pulse in a relativistic plasma,</i> Burke Ritchie and Christopher D. Decker, LLNL, USA .....	249
<i>Source Description and Sampling Techniques in PEREGRINE Monte Carlo Calculations of Dose Distributions for Radiation Oncology,</i> A. E. Schach von Wittenau, L. J. Cox, P. M. Bergstrom, Jr., W. P. Chandler, C. L. Hartmann-Siantar, and S. M. Hornstein , LLNL, USA .....	259
<i>The technique for solving 3D hydrodynamics problems on irregular Lagrangian grids,</i> V. N. Motlokhov, V. V. Rasskazova, P. A. Rasskazov, A. N. Shaporenko, VNIIEF, Russia .....	265

<i>A Three Dimensional Finite Element Formulation for Thermoviscoelastic Orthotropic Media.</i> Marvin A. Zocher, LANL, USA .....	271
<i>3-D Parallel Program for Numerical Solution of Gas Dynamics Problems with Heat Conduction on Distributed-Memory Computers. Results of Computations on MP-3, Meiko CS-2 and SP2 Computers,</i> I. D. Sofronov, B. L. Voronin, O. I. Butnev, A. N. Bykov, A. M. Yerofeev, S. I. Skrypnik, VNIIEF, Russia, D. Nielson, Jr., B. J. Uyemura, R. Evans, S. Brandon, M. Nemanic, C. Okuda, LLNL, USA .....	275
<i>Time Dependent View Factor Methods,</i> Ronald C. Kirkpatrick, LANL, USA .....	285
<i>Variational-Difference Flow-Type Scheme for 3D Diffusion Equation on Grids of Arbitrary Hexahedrons,</i> S. V. Bazhenov, S. P. Belayaev, Yu. A. Bondarenko, V. V. Gorev, T. V. Korolkova, P. I. Pevnaya, Russia .....	291

# **Conference Abstracts**



# PARALLELING CALCULATIONS IN 3D ELECTROMAGNETIC SIMULATION CODE

G. A. Adamkevich, G. V. Baidin, I. A. Litvinenko, V. A. Rotko,  
RFNC-VNIITF, Russia

## Abstract

Presentation touches upon the issues related to a structure of code for 3D simulation of plasma electrodynamics problems which will enable to parallel the code efficiently on available multiprocessors. Peculiarities of 3D calculations and hybrid description of charge carriers are considered as elements specifying data and code structure, determining specifics of selection of paralleling option.

# PARALLELIZATION METHODS FOR NUMERICAL SOLUTION OF 3D GROUP NON-STATIONARY EQUATION OF NEUTRON DIFFUSION FOR NUCLEAR POWER PLANT SAFETY CALCULATIONS

A. V. Alexeyev, O. A. Zvenigorodskaya, R. M. Shagaliyev,  
RFNC-VNIIEF, Russia

## Abstract

The paper presents an iterative parallelization method for 3D diffusion problems implemented in reactor program KORAT 3D. It is based on geometric decomposition concept which provides the possibility of parallelization on a great number of distributed-memory processors.

As it is known, the idea of geometric decomposition method is in the fact that the initial problem solution domain is split into a number of subdomains (to be called mathematical domains below) and the diffusion equation is solved separately by mathematical domains. The interaction of solutions obtained in different mathematical domains is accounted by the internal boundary conditions whose interchange takes place on special iterations (on iterations by internal boundary conditions).

The parallelization method implemented in KORAT 3D program is peculiar for the use of a special kind of internal boundary conditions. These internal boundary conditions are a combination of a full flow function and the desired function with a coefficient selected in this combination basing on a multidimensional analog of a limiting run coefficient.

The paper presents the results of analytical estimations of the iterative process convergence rate by internal boundary conditions along with the results of numerical evaluations of parallelization efficiency exemplified on a 3D test problem for channel-type reactor.

# METHODS FOR IMPROVING ACCURACY OF THE FIRST-ORDER APPROXIMATION SCHEME FOR SOLVING SYSTEMS OF EQUATIONS FOR RADIATION TRANSFER

E. S. Andreyev, V. Yu. Gusev, M. Yu. Kozmanov,  
RFNC-VNIITF, Russia

## Abstract

Methods are considered to improve schemes of the first order of accuracy enabling to achieve required accuracy using even a coarse spatial grid. Results are illustrated by the examples. To build the scheme, principle of maximum [1,2] is used, a system of non-linear difference equations obtained is solved with the method of iterations [3]. The paper sets forth development of results presented at the previous conference of five nuclear labs described in [4].

## Reference

1. E.S. Andreyev, M.Yu. Kozmanov, E.B. Rachilov Principle of Maximum for a System of Equations of Energy and Non-stationary Radiation Transfer.- Zhurnal Vychislitel'noy Matematiki i Matematicheskoy Fiziki. 1983, v.23, #1, pp.152-159.
2. M. Yu. Kozmanov Existence Theorem of Solution for Non-Linear System of Equations of Non-Stationary Radiation Transfer. - Voprosy Atomnoy Nauki i Tekhniki Ser. Matematicheskoe Modelirovanie Physicheskikh Processov. 1989 Issue 2, pp. 47-50.
3. V.Yu. Gusev, M.Yu. Kozmanov Methods for Solving of Difference Equations Approximating Equations of Thermal Radiation Transfer. - Zhurnal Vychislitel'noy Matematiki i Matematicheskoy Fiziki. 1986, v.26, #11, pp.1654-1660.
4. V.Yu. Gusev, M.Yu. Kozmanov Conservative Schemes Using Characteristics and Anti-Diffusion Velocities to Solve Transfer Equations. - Voprosy Atomnoy Nauki i Tekhniki Ser. Matematicheskoe Modelirovanie Physicheskikh Processov. 1996. Issue 1-2, pp. 24-32.
5. M. Yu. Kozmanov Monotone Schemes for the Systems of Radiation Transfer Equations. - Voprosy Atomnoy Nauki i Tekhniki Ser. Matematicheskoe Modelirovanie Physicheskikh Processov. 1989 Issue 2, pp. 51-54.

# ANALYTICAL AND NUMERICAL STUDY OF ACCELERATED THIN LAYER INSTABILITY

S. M. Bakhrah and G. P. Simonov,  
RFNC-VNIIEF, Russia

## Abstract

New analytical solutions for Rayleigh-Taylor thin layer instability on a non-linear in observer space process stage have been obtained presenting the main equations in Lagrangian variables.

Analytical solutions have been obtained for a liquid layer and an elastic one with both 2D and 3D perturbations present. Perturbation evolution dependence is studied in respect of perturbation kinds (perturbation of middle surface, layer thickness and perturbations in layer velocities) and of non-dimensional parameters determining the perturbation nature. Both exponentially growing and bounded solutions exist depending on the parameter values.

The relations of perturbation growth increment and critical acceleration have been obtained for a thin elastic layer, the boundaries of solution limitation have been defined. The relations determining the strength effect on perturbation growth, particularly on their limitation conditions, have been obtained.

The 3D elastic layer perturbations (with a considerably large shift module) are shown to grow no faster than the 2D.

The analytical solutions obtained are tested by means of a complete system of conservation laws for a compressible continuum.

The obtained thin layer perturbation growth regularities are observed to take place in a semispace of compressible both liquid and elastic continuum.

The analytical solutions obtained are good tests for 2D and 3D numerical techniques for continuum flow calculations.

# A TECHNIQUE FOR RADIATION TRANSFER COMPUTATION WITH ACCOUNT OF ANISOTROPIC EMISSION OF BOUNDARY SURFACE

S. V. Bazhenov and P. I. Pevnaya,  
RFNC-VNIIEF, Russia

## Abstract

The technique is intended for the solution of radiation transfer equation in optically-transparent domain in the case when boundary surface radiation intensity distribution is arbitrary enough.

To solve the problem, the method based on angular coefficients is used.

The equation of radiation exchange between boundary surfaces is derived from the expression for one-way radiation flux outgoing through the unit boundary area of surface.

The scheme of calculations proposed by the authors to solve the problem is strictly conservative for a common case when the form of the boundary surface depends on time.

While setting the boundary condition the technique gives an ability to use various boundary condition types in different areas of the boundary surface.

The given technique is implemented by the RADIBS program.

Using this program one may obtain more exact values of geometric ranges which will allow to compute radiation transfers in a domain of a small size (as compared to the range length in the material) by the diffusion approximation technique.

# VARIATIONAL DIFFERENCE FLOW-TYPE SCHEME FOR 3D DIFFUSION EQUATION ON GRIDS OF ARBITRARY HEXAHEDRONS

S. V. Bazhenov, S. P. Belyayev, Yu. A. Bondarenko, V. V. Gorev,  
T. V. Korol'kova, P. I. Pevnaya,  
RFNC-VNIIEF, Russia

## Abstract

The presentation describes the construction of a difference scheme for 3D equation of nonstationary linear isotropic and anisotropic diffusion by variational technique using flow-type form of diffusion equation (generalization for 3D case of the following technique: Tishkin V.F., Favorskii A.P., Shashkov M.Yu. Variational difference schemes for heat conduction equation on nonregular grids// Doklady of the USSR Acad.Nauk .-1979, Vol.246, No.6, pp.1342-1346). An arbitrary grid composed of hexahedrons whose bounds are ruled surfaces and edges are segments of straight lines is used. Temperature values being averaged over hexahedral cell volumes are used. Flows being used are determined at hexahedrons' bounds, they are averaged over bound surface values of flow components normal to bounds. The energy conservation law is being approximated in each hexahedron in a standard manner. The relation between flows at bounds and temperatures in cells is obtained from the minimality condition for the functional

$$\Phi(\vec{W}) = \int_{\Omega} D^{-1} \vec{W}^2 d\Omega - 2 \int_{\Omega} U \cdot \text{div} \vec{W} d\Omega$$

which is approximated in a simplest manner and in which only flow components normal to hexahedron bounds are varied. As a result, the difference between temperatures of two neighboring hexahedral cells is expressed via some linear combination of flows through these two cells' bounds. Then temperatures in the upper layer are excluded using the energy conservation law written in implicit form and this results in linear system of equations for normal flows. After approximate calculation of the equation system temperatures are being found from the energy balance equation. The scheme version for anisotropic diffusion is developed for an arbitrary symmetric positively defined tensor of diffusion coefficients and the minimized functional is modified correspondingly.

To solve numerically the obtained system of difference equations, iterations with one-dimensional runs are used that always converge due to the strict convexity of the minimized functional. The results of test and methodical computations are given. Calculations on orthogonal and strongly oblique grids show that the number of such iterations is approximately proportional to the square root from the Courant number.

# NUMERICAL SIMULATION IN DIFFUSIVE-VACUUM APPROXIMATION OF RADIANT ENERGY TRANSFER IN THERMONUCLEAR TARGETS

A. A. Bazin, V. V. Vatulin, Yu. A. Dementyev, V. F. Mironova,  
G. I. Skidan, E. N. Tikhomirova, B. P. Tikhomirov,  
RFNC-VNIIEF, Russia

## Abstract

An approximated method of numerical solution for 2D and 3D problems of radiant energy transfer in multilayer systems consisting of optically thick and thin areas is considered. Radiation transfer in optically thick layers is simulated in sectoral approximation by the equation of radiant heat conductivity and gas dynamics. The propagation of X-ray radiation through optically thin layers is described by integral equation of radiation heat conductivity with account of photon delay.

The equations of radiant heat conductivity and gas dynamics are integrated by finite difference method. Integral equation is solved either by a generalized zonal method or by method of large photons. Visibility factors (a slope one and of average distances) are calculated for meshes on vacuum area surface with varied geometry. To obtain solution on a temporal layer a method of separate area calculation is used. Stable exchange boundary conditions are set up between optically thick and thin layers.

An application of diffusive-vacuum method to inertial thermonuclear fusion exemplifies its use.

The characteristics of X-ray radiation field in a construction of a cylindric target for heavy ion fusion with converters placed at lateral surface are studied in 2D and 3D cases.

The influence of target parameters and heavy ion beam on the uniformity of X-ray radiation distribution field on capsule surface is studied.

# MOLECULAR DYNAMICS OF SHOCK LOADING OF METALS WITH DEFECTS

J. F. Belak,  
Lawrence Livermore National Laboratory

## Abstract

The finite rise time of shock waves in metals is commonly attributed to dissipative or viscous behavior of the metal. This viscous or plastic behaviour is commonly attributed to the motion of defects such as dislocations. Despite this intuitive understanding, the experimental observation of defect motion or nucleation during shock loading has not been possible due to the short time scales involved. Molecular dynamics modeling with realistic interatomic potentials can provide some insight into defect motion during shock loading. However, until quite recently, the length scale required to accurately represent a metal with defects has been beyond the scope of even the most powerful supercomputers. Here, we present simulations of the shock response of single defects and indicate how simulation might provide some insight into the shock loading of metals.

Work performed under the auspices of the U.S. DOE by LLNL under contract No. W-7405-ENG-48.

# COMPUTATIONAL SIMULATION OF NON-EQUILIBRIUM PROCESSES DURING THERMONUCLEAR FUSION

I. M. Belyakov, S. A. Belkov, V. V. Vatulin, L. L. Vakhlamova,  
O. A. Vinokurov, S. G. Garanin, V. F. Yermolovich, N. P. Pleteneva,  
G. N. Remizov, V. Yu. Rezhnikov, N. A. Ryabikina, I. D. Sofronov,  
L. P. Fedotova, R. M. Shagaliyev,  
RFNC-VNIIEF, Russia

## Abstract

The paper presents the main possibilities of numerical simulation for the processes of radiation and material energy transfer in 2D problems of thermonuclear fusion implemented in the frames of SATURN and MIMOSA technique communication and their application to solve some thermonuclear fusion problems.

SATURN program set computes the processes of spectral X-ray radiation transfer, energy transfer by ions and electrons with account of environment non-equilibrium, laser radiation energy transfer and absorption and the ionization kinetics in an average ion approximation.

Multicomponent non-equilibrium gas dynamics movements are calculated in MIMOSA code.

Initial differential equations are approximated by grid (finite-difference and finite element) methods. Non-orthogonal spatial grids are used allowing to account the peculiarities of computed geometries with a required degree of detail. Special acceleration methods are used to economize the computations.

The computations with a simultaneous account of all the processes named above are carried out by special communication programs of SATURN and MIMOSA techniques (as a continuous data exchange).

The given program package finds a wide application in studying different constructions for thermonuclear fusion.

The possibilities of the given program package are demonstrated by some numerical simulation results of heavy ion fusion target with elliptic chamber proposed by a group of scientists from Frankfurt University under Prof. Marun I. leadership.

Numerical results by SATURN+MIMOSA codes have allowed to optimize the construction of ellipsoid target. If the radiation field asymmetry on the capsule surface reached 16% in the first construction versions, the improved version based on numerical calculations gave the asymmetry value of 1%.

The work is being continued. Basing on modern physics-mathematical models the program set implies the calculation possibility for the parameters of non-equilibrium multicomponent multicharged plasma in an average ion approximation being taken into account in a series of computations for an American LABYRINTH target. The first preliminary results have been obtained.

SOLUTION OF LARGE NONLINEAR QUASISTATIC STRUCTURAL  
MECHANICS PROBLEMS  
ON DISTRIBUTED-MEMORY MULTIPROCESSOR  
COMPUTERS

M. Blanford,  
Sandia National Laboratories

Abstract

Most commercially-available quasistatic finite element programs assemble element stiffnesses into a global stiffness matrix, then use a direct linear equation solver to obtain nodal displacements. However, for large problems (greater than a few hundred thousand degrees of freedom), the memory size and computation time required for this approach becomes prohibitive. Moreover, direct solution does not lend itself to the parallel processing needed for today's multiprocessor systems.

This talk gives an overview of the iterative solution strategy of JAS3D, our nonlinear large-deformation quasistatic finite element program. Because its architecture is derived from an explicit transient-dynamics code, it does not ever assemble a global stiffness matrix. I will describe the approach we used to implement the solver on multiprocessor computers, and show examples of problems run on hundreds of processors and more than a million degrees of freedom. Finally, I will describe some of the work we are presently doing to address the challenges of iterative convergence for ill-conditioned problems.

# MOLECULAR DYNAMICS MODELING OF SOLIDIFICATION IN METALS

D. B. Boercker, J. Belak, and J. Glosli,  
Lawrence Livermore National Laboratory

## Abstract

Molecular dynamics modeling is used to study the solidification of metals at high pressure and temperature. Constant pressure MD is applied to a simulation cell initially filled with both solid and molten metal. The solid/liquid interface is tracked as a function of time, and the data is used to estimate growth rates of crystallites at high pressure and temperature in Ta and Mg.

Work performed under the auspices of the U. S. DoE by LLNL under contract No. W-7405-ENG-48.

ELIMINATION OF ARTIFICIAL GRID DISTORTION AND  
HOURGLASS-TYPE MOTIONS  
BY MEANS OF LAGRANGIAN SUBZONAL MASSES AND PRESSURES

E. J. Caramana and M. J. Shashkov.  
Los Alamos National Laboratory

Abstract

The bane of Lagrangian hydrodynamics calculations is premature breakdown of the grid topology that results in severe degradation of accuracy and run termination often long before the assumption of Lagrangian zonal mass ceased to be valid. At short spatial grid scales this is usually referred to by the terms "hourglass" mode or "keystone" motion associated in particular with underconstrained grids such as quadrilaterals and hexahedrons in two and three dimensions, respectively.

At longer spatial scales relative to the grid spacing there is what is referred to ubiquitously as "spurious vorticity", or the long-thin zone problem. In both cases the result is anomalous grid distortion and tangling that has nothing to do with the actual solution, as would be the case for turbulent flow. In this work we show how such motions can be eliminated by the proper use of subzonal Lagrangian masses, and associated densities and pressures. These subzonal masses arise in a natural way from the fact that we require the mass associated with the nodal grid point to be constant in time. This is addition to the usual assumption of constant, Lagrangian zonal mass in staggered grid hydrodynamics scheme.

We show that with proper discretization of subzonal forces resulting from subzonal pressures, hourglass motion and spurious vorticity can be eliminated for a very large range of problems. Finally we are presenting results of calculations of many test problems.

# NUMERICAL PRESERVATION OF SYMMETRY PROPERTIES OF CONTINUUM PROBLEMS

E. J. Caramana and P. Whalen,  
Los Alamos National Laboratory

## Abstract

We investigate the problem of perfectly preserving a symmetry associated naturally with one coordinate system when calculated in a different coordinate system. This allows a much wider range of problems that may be viewed as perturbations of the given symmetry to be investigated. We study the problem of preserving cylindrical symmetry in two-dimensional cartesian geometry and spherical symmetry in two-dimensional cylindrical geometry. We show that this can be achieved by a simple modification of the gradient operator used to compute the force in a staggered grid Lagrangian hydrodynamics algorithm. In the absence of the supposed symmetry we show that the new operator produces almost no change in the results because it is always close to the original gradient operator. Our technique thus results in a subtle manipulation of the spatial truncation error in favor of the assumed symmetry but only to the extent that it is naturally present in the physical situation. This not only extends the range of previous algorithms and the use of new ones for these studies, but for spherical or cylindrical calculations reduces the sensitivity of the results to grid setup with equal angular zoning that has heretofore been necessary with these problems. Although this work is in two-dimensions, it does point the way to solving this problem in three-dimensions. This is particularly important for the ASCI initiative. The manner in which these results can be extended to three-dimensions will be discussed.

# PARALLEL DETERMINISTIC NEUTRONICS WITH AMR IN 3D

C. Clouse, J. Ferguson, C. Hendrickson,  
Lawrence Livermore National Laboratory

## Abstract

AMTRAN, a three dimensional Sn neutronics code with adaptive mesh refinement (AMR) has been parallelized over spatial domains and energy groups and runs on the Meiko CS-2 with MPI message passing. Block refined AMR is used with linear finite element representations for the fluxes, which allows for a straight forward interpretation of fluxes at block interfaces with zoning differences. The load balancing algorithm assumes 8 spatial domains, which minimizes idle time among processors.

# A NEW 2-D, LIMITED, ZONE-CENTERED ARTIFICIAL VISCOSITY TENSOR

M. R. Clover and C. W. Cranfill,  
Los Alamos National Laboratory

## Abstract

We have developed a fully 2-d(3-d) formulation of a linear, monotonic limiter for use in conjunction with a new zone-centered Lagrangian Q (which we refer to as a "discretization" viscosity) suitable for arbitrary connectivity. Rather than min-mod'ing  $du/dx$  from two adjacent cells onto a node, as in 1-d, we min-mod each eigenvalue of the strain-rate tensor from all zones adjacent to a node. These are then used to calculate the shock (or discretization) jump across the zone in that eigenvector's direction. We will report results on various test problems (e.g. Saltzman's piston problem, Coggeshall's similarity solution, etc).

# QUANTUM MOLECULAR DYNAMICS SIMULATIONS OF DENSE MATTER

L. Collins, J. Kress, N. Troullier, T. Lenosky, and I. Kwon.  
Los Alamos National Laboratory

## Abstract

We have developed a quantum molecular dynamics(QMD) simulation method for investigating the properties of dense matter in a variety of environments. The technique treats a periodically- replicated reference cell containing  $N$  atoms in which the nuclei move according to the classical equations-of-motion. The interatomic forces are generated from the quantum mechanical interactions of the (between?) electrons and nuclei. To generate these forces, we employ several methods of varying sophistication from the tight-binding(TB) to elaborate density functional(DF) schemes. In the latter case, lengthy simulations on the order of 200 atoms are routinely performed, while for the TB, which requires no self-consistency, upwards to 1000 atoms are systematically treated. The QMD method has been applied to a variety cases: 1) fluid/plasma Hydrogen from liquid density to 20 times volume-compressed for temperatures of a thousand to a million degrees Kelvin; 2) isotopic hydrogenic mixtures, 3) liquid metals(Li, Na, K); 4) impurities such as Argon in dense hydrogen plasmas; and 5) metal/insulator transitions in rare gas systems (Ar,Kr) under high compressions. The advent of parallel versions of the methods, especially for fast eigensolvers, presage LDA simulations in the range of 500-1000 atoms and TB runs for tens of thousands of particles. This leap should allow treatment of shock chemistry as well as large-scale mixtures of species in highly transient environments.

# SOURCE DESCRIPTION AND SAMPLING TECHNIQUES USED IN PEREGRINE MONTE CARLO CALCULATIONS OF DOSE DISTRIBUTIONS FOR RADIATION ONCOLOGY

L. Cox, P. M. Bergstrom, Jr., W. P. Chandler, S. M. Hornstein, A. E. Schach von  
Wittenau, C. L. Hartmann Siantar,  
Lawrence Livermore National Laboratory

## Abstract

The goal of Lawrence Livermore National Laboratory's PEREGRINE project is to provide accurate and fast Monte Carlo calculation of dose distributions for routine clinical use in the radiation treatment of cancer. To attain this goal, an accurate and efficient method of describing and sampling external radiation sources is essential. We combine comprehensive simulations of accelerators with clinical measurements to determine accurate, multiple-component descriptions of the patient-independent radiation field. Monte Carlo simulations of the accelerators are performed with MCNP/4B and/or BEAM96 based on detailed engineering information obtained from the linac manufacturers. In this presentation, we describe the different source component models available in PEREGRINE for defining complex patient-independent bremsstrahlung sources emitted from commercially available linacs. The sampling techniques used with the different source models are explained. PEREGRINE's methods of handling beam modifiers -- such as jaws/collimators, blocks, wedges and multi-leaf collimators -- is described. The important aspects of absolute normalization and dose monitor unit calculations are discussed. Comparisons to clinical measurements and to standard clinical treatment plans are shown.

This work was performed under the auspices of the U.S. Department of Energy by the Lawrence Livermore National Laboratory under contract number W-7405-ENG-48.

# BOUNDARY ACQUISITION FOR SETUP OF NUMERICAL SIMULATION

C. Diegert,  
Sandia National Laboratory

## Abstract

We present a work flow diagram that includes a path that begins with taking experimental measurements, and ends with obtaining insight from results produced by numerical simulation. Two examples illustrate this path:

- (1) Three-dimensional imaging measurement at micron scale, using X-ray tomography, provides information on the boundaries of irregularly-shaped alumina oxide particles held in an epoxy matrix. A subsequent numerical simulation predicts the electrical field concentrations that would occur in the observed particle configurations.
- (2) Three-dimensional imaging measurement at meter scale, again using X-ray tomography, provides information on the boundaries fossilized bone fragments in a *Parasaurolophus* crest recently discovered in New Mexico. A subsequent numerical simulation predicts acoustic response of the elaborate internal structure of nasal passageways defined by the fossil record.

We must both add value, and must change the format of the three-dimensional imaging measurements before the define the geometric boundary initial conditions for the automatic mesh generation, and subsequent numerical simulation. We apply a variety of filters and statistical classification algorithms to estimate the extents of the structures relevant to the subsequent numerical simulation, and capture these extents as faceted geometries. We will describe the particular combination of manual and automatic methods we used in the above two examples.

# THE MOVING-LEAST-SQUARES-PARTICLE HYDRODYNAMICS METHOD (MLSPH)

G. Dilts,  
Los Alamos National Laboratory

## Abstract

An enhancement of the smooth-particle hydrodynamics (SPH) method has been developed using the moving-least-squares (MLS) interpolants of Lancaster and Salkauskas which simultaneously relieves the method of several well-known undesirable behaviors, including spurious boundary effects, inaccurate strain and rotation rates, pressure spikes at impact boundaries, and the infamous tension instability. The classical SPH method is derived in a novel manner by means of a Galerkin approximation applied to the Lagrangian equations of motion for continua using as basis functions the SPH kernel function multiplied by the particle volume. This derivation is then modified by simply substituting the MLS interpolants for the SPH Galerkin basis, taking care to redefine the particle volume and mass appropriately. The familiar SPH "kernel approximation" is now equivalent to a collocation-Galerkin method. Both classical conservative and recent non-conservative formulations of SPH can be derived and emulated. The non-conservative forms can be made conservative by adding terms that are zero within the approximation at the expense of boundary-value considerations. The familiar Monaghan viscosity is used. Test calculations of uniformly expanding fluids, the Swegle example, spinning solid disks, impacting bars, and spherically symmetric flow illustrate the superiority of the technique over SPH. In all cases it is seen that the marvelous ability of the MLS interpolants to add up correctly everywhere civilizes the noisy, unpredictable nature of SPH. Being a relatively minor perturbation of the SPH method, it is easily retrofitted into existing SPH codes. On the down side, computational expense at this point is significant, the Monaghan viscosity undoes the contribution of the MLS interpolants, and one-point quadrature (collocation) is not accurate enough. Solutions to these difficulties are being pursued vigorously.

# EXPLOSIVE DECELERATION AND FRAGMENTATION OF METEORITES IN THE ATMOSPHERE

V. P. Elsukov, D. V. Petrov, V. A. Simonenko, O. N. Shubin.  
RFNC-VNIITF, Russia

## Abstract

Currently there is a series of experimental facts of observed interaction of meteorites with the atmosphere that have no consistent and logical explanation. First of all this refers to the burst of Tunguska meteorite at some altitude. No meteorite substance was found after this burst. Besides, flashes similar to a fireball of nuclear explosion with the yield of 1-100 kT of TNT are recorded in the Earth's atmosphere regularly. They evidence that under some conditions there exists a physical mechanism of explosive interaction of meteorites with the Earth's atmosphere having characteristic features of above-surface or high-altitude nuclear explosion. Moreover, there is no contradiction-free theory describing fragmentation of meteorites in the atmosphere.

The paper describes simulation-theoretical model of explosive interaction of meteorites with the atmosphere as well as fragmentation of meteorites. This physical model can lead to two outcomes. In the first case meteorites with rather low density and sizes less than critical one are able to reach only some critical altitude above the Earth's surface. Judging by the consequences of Tunguska burst, final sizes of particles are microscopic. In the second scenario when density of meteorite is high or sizes are rather large, fragmentation process have no time to evolve deeply. In this case, chunks falling on the Earth will be of macroscopic size.

Thus, Sikhote-Alin event was not of explosive nature.

# SIMULATION OF THERMOMECHANICAL FATIGUE IN SOLDER JOINTS\*

H. E. Fang, V. L. Porter, R. M. Fye, E. A. Holm,  
Sandia National Laboratories

## Abstract

Thermomechanical fatigue (TMF) is a very complex phenomenon in electronic component systems and has been identified as one prominent degradation mechanism for surface mount solder joints in the stockpile. TMF is caused by different coefficients of thermal expansion (CTE) of the materials in the package, combined with changes in the ambient temperature. In this case different CTEs result in cyclical strain in the assembly, and this strain is concentrated almost entirely in the solder because it is the most deformable portion of the system. Since solder alloy is at a significant fraction of its melting point even at room temperature, the cyclical strain enhances mass diffusion and cause dramatic changes in the joint microstructure over time. As the microstructure changes, the joint weakens and eventually cracks when it can no longer withstand the strain.

In order to precisely predict the TMF-related effects on the reliability of electronic components in weapons, a multi-level simulation methodology is being developed at Sandia National Laboratories. This methodology links simulation codes of continuum mechanics (JAS3D), microstructural mechanics (GLAD), and microstructural evolution (PARGRAIN) to treat the disparate length scales that exist between the macroscopic response of the component and the microstructural changes occurring in its constituent materials. JAS3D is used to predict strain/temperature distributions in the component due to environmental variable fluctuations.

GLAD identifies damage initiation and accumulation in detail based on the spatial information provided by JAS3D. PARGRAIN simulates the changes of material microstructure, such as the heterogeneous coarsening in Sn-Pb solder, when the component's service environment varies.

In a complex electronic component system, such as the MC4352 MET hybrid unit which contains 348 solder joints, each individual JAS3D, GLAD and PARGRAIN calculation is computationally intensive although only part of the TMF phenomenon is modeled. For example, running JAS3D on a single processor of Cray J90 to model strain distribution in MC4352 under TMF would take about 1000 CPU hours to finish one fatigue cycle, while many cycles must be simulated for a complete analysis. PARGRAIN would need a day or more on Sandia's Intel Paragon supercomputer to model grain growth in a volume representative of a solder joint, using the fast Monte Carlo grain growth algorithm recently developed. The limits of computational power from conventional supercomputers prohibited the full implementation of this methodology in achieving realistic problem size, physical complexity, and numerical accuracy. Moving to multi-

teraflop computing is the only solution which can enable the practical interactions required for a full-physics model of a complex electronic system, where TMF in solder joints must be assessed. The preliminary results from our exercises on the Teraflop machine at Sandia show that after full implementations, JAS3D could gain 140-200 times speedup and the run time of PARGRAIN can be shortened to only two hours. Similar performance increase is also expected for GLAD. With the support of US ASCI (Accelerated Strategic Comp[uting Initiative) program and advanced algorithm development, the computational TMF model will enable scientists and engineers to anticipate reliability and performance problems in aging weapon components. This capability in turn will allow early identification of problems so that corrective actions can be efficiently implemented.

-----  
\* Sandia is a multiprogram laboratory operated by Sandia Corporation, a Lockheed Martin Company, for the United States Department of Energy under Contract DE-ACO4-94AL85000.

# SOLVING THE TRANSPORT EQUATION WITH QUADRATIC FINITE ELEMENTS: THEORY AND APPLICATIONS

J. M. Ferguson,  
Lawrence Livermore National Laboratory

## Abstract

At the 4th Joint Conference on Computational Mathematics, we presented a paper introducing a new quadratic finite element scheme (QFEM) for solving the transport equation. In the ensuing year we have obtained considerable experience in the application of this method, including solution of eigenvalue problems, transmission problems, and solution of the adjoint form of the equation as well as the usual forward solution. We will present detailed results, and will also discuss other refinements of our transport codes, particularly for 3-dimensional problems on rectilinear and non-rectilinear grids.

# COMPUTATION TECHNIQUE FOR ELASTIC-PLASTIC FLOWS WITH ACCOUNT OF MATERIAL DESTRUCTION AND FRAGMENTATION

A. V. Gorodnichev, G. P. Siminov, Yu. V. Yanilkin,  
RFNC-VNIIEF, Russia

## Abstract

The paper gives the description of the Lagrangian-Eulerian technique implemented in the EGAK program set [1] and intended for flow simulation with account of elastic-plastic properties of materials. The technique is intended for simulation of 2D flows in multicomponent media whose essential feature is the presence of large deformations. To calculate contact boundaries, the concentration technique is used.

Both simplest models based on the instant destruction with achieving critical tensile stress and more complex models are used to calculate material destruction. The latter include equations for parameters characterizing the degree of material porosity.

To calculate the process of fragmentation of the destructed material, concepts developed in the works by Grady [2] and Ivanov and others [3] were considered.

Computation results are given for several problems: the problem of punching a two-layer aluminum and textolite barrier by a steel ball; impact of two copper plates; punching a plastic material barrier by a steel ball, etc. Fragmentation computation techniques were tested on the last problem.

Computation results are compared to analytical solutions, experiment data and results of computations using other techniques. The results of all computation runs are in good agreement with analytical solutions and experiment data.

## Reference

1. Yanilkin Yu.V., Shanin A.A., Kovalev N.P., Gavrilova E.S., Gubkov E.V., Darova N.S., Dibirov O.A., Zharova G.V., Kalmanovich A.I., Pavlusha I.N., Samigulin M.S., Simonov G.P., Sin'kova O.G., Sotnikova M.G., Tarasov V.I., Toropova T.A. EGAK Program Set for Computation of 2D Multicomponent Medium Flows.// VANT, ser.MMFP, iss.4, 1993.
2. Grady D.E. Local Inertial Effects in Dynamic Fragmentation // J.Appl.Phys.. 1985, v.53, No.1, pp.322-325.
3. Ivanov A.G., Rayevskii V.A., Vorontsova O.S. Material Fragmentation during Explosion. // Fizika Goreniya i Vzryva, 1995, v.31, No.2.

# PROVIDING SCALABLE SYSTEM SOFTWARE FOR HIGH-END SIMULATIONS

D. Greenberg,  
Sandia National Laboratories

## Abstract

Detailed, full-system, complex physics simulations requiring  $10^{15}$  flops and terabytes of data have been shown to be feasible on systems containing thousands of processors. In order to manage these computer systems it has been necessary to create scalable system services. In this talk Sandia's research on scalable systems will be described. The key concepts of low overhead data movement through portals and of flexible services through multi-partition architectures will be illustrated in detail. The talk will conclude with a discussion of how these techniques can be applied outside of the standard monolithic MPP system.

# MATHEMATICAL METHODS FOR PROTEIN SCIENCE

W. Hart, S. Istrail, J. Atkins.  
Sandia National Laboratories

## Abstract

Understanding the structure and function of proteins is a fundamental endeavor in molecular biology. Currently, over 100,000 protein sequences have been determined by experimental methods. The three dimensional structure of the protein determines its function, but there are currently less than 4,000 structures known to atomic resolution. Accordingly, techniques to predict protein structure from sequence have an important role in aiding our understanding of the Genome and the effects of mutations in genetic disease. We describe current efforts at Sandia to better understand the structure of proteins through rigorous mathematical analyses of simple lattice models. Our efforts have focused on two aspects of protein science: mathematical structure prediction, and inverse protein folding.

A variety of methods have been proposed to predict the three-dimensional structure of proteins from their amino acid sequence. Very few of these methods provide the user with a measure of confidence in the predicted structure. We have developed algorithms that generate protein structures in linear time whose energy is guaranteed to be within a fixed fraction of the energy of the optimal protein structure. Our analysis has focused on variants of the hydrophobic-hydrophilic model (Dill 1985), which abstracts the dominant force of protein folding: the hydrophobic interaction. The protein is modeled as a chain of amino acids of length  $n$  which are of two types: H (hydrophobic, i.e., nonpolar) and P (hydrophilic, i.e., polar).

Although a variety of methods like these have been proposed to perform structure prediction, this problem has been difficult to solve exactly in a robust manner. In fact, it is still not known whether there exists an efficient algorithm for predicting the structure of a protein from its amino acid sequence alone. This observation has prompted us to characterize the computational complexity of protein structure prediction in simple lattice models. We have shown that a two broad classes of structure prediction problems are NP-hard. The first illustrates how structure prediction can be NP-hard for any reasonable lattice. The second illustrates how structure prediction can be NP-hard for a broad class of Lennard-Jones-like energy potentials.

Inverse protein folding is a complementary problem to structure prediction. It concerns the identification of an amino acid sequence that folds to a given structure. Sequence design problems attempt to avoid the apparent difficulty of inverse protein folding by defining an energy that can be minimized to find protein-like sequences. We have evaluated the practical relevance of two sequence design problems by analyzing their computational complexity. Our analysis shows how sequence design problems can fail to

reduce the difficulty of the inverse protein folding problem, and highlights the need to analyze these problems to evaluate their practical relevance.

## MODELING BY VALUE IMPLEMENTED IN PRIZMA CODE

Ia. Z. Kandiev and G. N. Malyshkin,  
RFNC-VNIITF, Russia

### Abstract

PRIZMA code was intended for Monte Carlo simulation of linear radiation transfer problems. The code has broad capabilities to describe geometry, sources, material composition, obtain specified results. There is a capability to calculate path of particles of different types (neutrons, photons, electrons, positrons and heavy charged particles) taking into account their transmutations. Scheme of modeling by value [2] was implemented to solve the problems which require calculation of functionals related to small probabilities (for example, problems of protection against radiation, problems of detection, etc.). The scheme enables to adapt algorithm of trajectory building to the problem peculiarities.

Main components of the developed technique are the following.

Problem of any complexity can be presented in the form of combination of (elementary) problems with simpler relations between the source and detector. Totally four classes of elementary problem were defined:

1. Radiation propagation in optically thick medium.
2. Radiation propagation in optically transparent medium.
3. Problem of detection using detector located in vacuum or absorber.
4. Problem of detection using detector located in emitting or scattering medium.

Schemes of non-analogous modeling and principles of building approximate value function and appropriate non-analogous distributions were selected for each class of problems.

Calculation of a specific problem is performed in the following way: problem conditions are analyzed in order to understand peculiarities of the problem; based on the peculiarities initial problem is split into elementary ones, each falling into one of four classes; for each elementary problem approximate solution is built using appropriate procedures and, if necessary, parameters of appropriate non-analogous distributions are determined; modeling scheme obtained is described by initial data in addition to problem conditions and calculation is performed.

### References

1. Ia.Z. Kandiev, E.S. Kuropatenko, I.V. Lifanova et al. Monte-Carlo Calculations of Particle Interaction with Matter in PRIZMA Code. Theses of presentations at III Scientific Conference on Protection against Ionizing Radiation at Nuclear Facilities.

- Tbilisi, 1981, p. 24.

2. J. Spanier, Z. Gelbard. Monte-Carlo Method and Neutron Transport Problems.  
Moscow, Atomizdat, 1972, p. 207

# MONTE-CARLO SIMULATION OF BIOLOGICAL PROTECTION AT REPETITIVE PULSE ELECTRON ACCELERATOR

Ia. Z. Kandiev and V. V. Plokhoy,  
RFNC-VNIITF, Russia

## Abstract

Bremsstrahlung dose rate was calculated. Bremsstrahlung results from the interaction of electron beam of 1MeV accelerator operating in repetitive pulse mode with the foil of a beam-exit hole and layer of air where beam is decelerated behind biological protection.

It is shown that high repetition frequency (~500 Hz) of pulses of accelerated electrons leads to ~100cm width of concrete wall necessary to ensure personnel protection against radiation.

Technique is described enabling Monte-Carlo simulation of bremsstrahlung dose behind the obstacle with large optical thickness. This technique provides estimates with rather small dispersion in acceptable run time. Calculations were performed using PRIZMA code [1] which allows to consider the complete problem statement taking into account combined electrons and photons transport in the real geometry.

To verify the results obtained, gamma-radiation dose from  $^{60}\text{Co}$  isotope source scattered by atmospheric air was calculated at a great distance from the source for geometry described in [2]. Calculation results are compared with "benchmark" experiment results, thus enabling to test the technique developed to estimate bremsstrahlung dose behind biological protection of the accelerator.

With the same purpose technique was tested for calculation of bremsstrahlung yield and energy-angular distribution of photons by comparing measurement results given in [3] with calculation results obtained using PRIZMA code.

## References:

1. Ya.Z. Kandiev, E.S. Kuropatenko, I.V. Lifanova et al., Theses of presentations at the III Scientific Conference on Protection against Ionizing Radiation at Nuclear Facilities. Tbilisi, Tbilisi State University, 1981, p. 24.
2. R.R. Nason, J.K. Shultis, R.E. Saw and C.E. Clifford, "A Benchmark Gamma-Ray SkyShine Experiment", Nucl. Sci. Eng., 79, 404-416, 1981.
3. D.H. Rester, W.E. Dance and J.H. Derrickson, "Thick Target Bremsstrahlung Produced by Electron Bombardment of Targets Be, Sn and Au in the Range 0.2-2.8 MeV", Journ. Appl. Phys., vol. 41, #6, pp.2682-2692, (1970).

# NUMERICAL SIMULATION OF EXPERIMENTS WITH FUEL PELLETS AT PULSE REACTOR FACILITY

Ia. Z. Kandiev and R. M. Kozybayev,  
RFNC-VNIITF, Russia

## Abstract

To solve the problems related to numerical simulation of experiments performed at pulse reactors, PRIZMA-D code which is a modification of the basic PRIZMA code was developed at VNIITF.

Peculiarity of this code is in a special source - fission points distributed in eigenfunction in the reactor core. To diminish constraints on applying non-analogous simulation, process of determining source is distinguished from the process of modeling trajectories to obtain necessary results. This structure of calculation cycle enables to increase effectiveness of calculations. In addition, special method of modeling trajectories of the particles implemented in PRIZMA code enables to obtain correlated results of several problem versions during one calculation. To illustrate the code capabilities, problems are considered related to numerical simulation of experiments with fuel pellets at the pulse reactor.

# AN 8-NODE TETRAHEDRAL FINITE ELEMENT SUITABLE FOR EXPLICIT TRANSIENT DYNAMIC SIMULATIONS

S. W. Key, M. W. Heinstein, C. M. Stone,  
Sandia National Laboratories

## Abstract

Considerable effort has been expended in perfecting the algorithmic properties of 8-node hexahedral finite elements. Today the element is well understood and performs exceptionally well when used in modeling three-dimensional explicit transient dynamic events. However, the automatic generation of all-hexahedral meshes remains an elusive achievement. The alternative of automatic generation for all-tetrahedral meshes is a reality. Unfortunately, in solid mechanics the 4-node linear tetrahedral finite element is a notoriously poor performer, and the 10-node quadratic tetrahedral finite element while a better performer numerically is computationally expensive. To use the all-tetrahedral mesh generation extant today, we have explored the creation of a quality 8-node tetrahedral finite element (a four-node tetrahedral finite element enriched with four mid-face nodal points).

The derivation of the element's gradient operator, studies in obtaining a suitable mass lumping and the element's performance in applications are presented. In particular, we examine the 8-node tetrahedral finite element's behavior in longitudinal plane wave propagation, in transverse cylindrical wave propagation, and in simulating Taylor bar impacts. The element only samples constant strain states and, therefore, has 12 hourglass modes. In this regard, it bears similarities to the 8-node, mean-quadrature hexahedral finite element. Given automatic all-tetrahedral meshing, the 8-node, constant-strain tetrahedral finite element is a suitable replacement for the 8-node hexahedral finite element and "hand-built" meshes.

# THE ENERGETIC ALPHA PARTICLE TRANSPORT METHOD (EATM)

R. C. Kirkpatrick,  
Los Alamos National Laboratory

## Abstract

There have been several methods applied to the problem of energetic (e.g., 14.1 MeV DT) alpha particle transport in fusion plasmas as well as heavy ion transport in high-Z radiation converters for ion beam fusion targets. In addition, the magnetic confinement fusion community has treated the problem of transport in the presence of magnetic fields. However, the problem of energetic charged particle transport in a dynamic magnetized plasma has been inadequately explored. The research code EATM is a first attempt to find an efficient method of treating the transport of energetic charged particles in a dynamic magnetized (MHD) plasma for which the mean free path of the particles and the Larmor radius may be long compared to the gradient lengths in the plasma. The intent is to span the range of parameter with the efficiency and accuracy thought necessary for experimental analysis and design of magnetized fusion targets.

One of the earliest examples of such targets is the Sandia National Lab Phi-target in 1977. However, about the same time Los Alamos was exploring the Fast Liner concept, a larger cylindrical version.

More recently, Los Alamos and the All-Russia Scientific Institute for Experimental Physics have collaborated on the MAGO experiments that are intended to study target plasma formation for magnetized target fusion (MTF).

EATM uses some piecewise analytic solutions and transformations to build transport matrices for single computational cells, and then uses these matrices in a way similar to equations of state or opacities to effect the transport throughout the computational mesh. This approach should be most applicable to codes with fixed orthogonal meshes such as Eulerian algorithms or AMR codes.

# TIME DEPENDENT VIEW FACTOR METHODS

R. C. Kirkpatrick,  
Los Alamos National Laboratory

## Abstract

View factors have been used for treating radiation transport between opaque surfaces bounding a transparent medium for several decades. However, in recent years they have been applied to problems involving intense bursts of radiation in enclosed volumes such as in the laser fusion hohlraums. In these problems, several aspects require treatment of time dependence. These will be discussed and some examples will be provided. Also, the limitations of view factor methods will be discussed.

# IMPLEMENTATION OF NUMERICAL SIMULATION TECHNIQUES IN ANALYSIS OF THE ACCIDENTS IN COMPLEX TECHNOLOGICAL SYSTEMS

G. S. Klishin , V. E. Seleznev, V. V. Aleoshin,  
RFNC-VNIIEF, Russia

## Abstract

Gas industry enterprises such as main pipelines , compressor gas transfer stations, gas extracting complexes belong to the energy intensive industry. Accidents there can result into the catastrophes and great social, environmental and economic losses. Annually, according to the official data several dozens of large accidents take place at the pipes in the USA and Russia. That is why prevention of the accidents, analysis of the mechanisms of their development and prediction of their possible consequences are acute and important tasks nowadays. The accidents reasons are usually of a complicated character and can be presented as a complex combination of natural, technical and human factors.

Mathematical and computer simulations are safe, rather effective and comparatively inexpensive methods of the accident analysis. It makes it possible to analyze different mechanisms of a failure occurrence and development, to assess its consequences and give recommendations to prevent it. Besides investigation of the failure cases, numerical simulation techniques play an important role in the treatment of the diagnostics results of the objects and in further construction of mathematical prognostic simulations of the object behavior in the period of time between two inspections.

While solving diagnostics tasks and in the analysis of the failure cases, the techniques of theoretical mechanics, of qualitative theory of differential equations, of mechanics of a continuous medium , of chemical macro-kinetics and optimizing techniques are implemented in the Conversion Design Bureau #5 (DB#5). Both universal and special numerical techniques and software (SW) are being developed in DB#5 for solution of such tasks. Almost all of them are calibrated on the calculations of the simulated and full-scale experiments performed at the VNIIEF and MINATOM testing sites. It is worth noting that in the long years of work there has been established a fruitful and effective collaboration of theoreticians, mathematicians and experimentalists of the institute to solve such tasks.

# A TRANSPORT MODEL FOR COMPUTER SIMULATION OF WILDFIRES

R. Linn,  
Los Alamos National Laboratory

## Abstract

Realistic self-determining simulation of wildfires is a difficult task because of a large variety of important length scales (including scales on the size of twigs or grass and the size of large trees), imperfect data, complex fluid mechanics and heat transfer, and very complicated chemical reactions. We use a transport approach produce a model that exhibit a self-determining propagation rate. The transport approach allows us to represent a large number of environments such as those with nonhomogeneous vegetation and terrain. We account for the microscopic details of a fire with macroscopic resolution by dividing quantities into mean and fluctuating parts similar to what is done in traditional turbulence modeling. These divided quantities include fuel, wind, gas concentrations, and temperature. Reaction rates are limited by the mixing process and not the chemical kinetics. We have developed a model that includes the transport of multiple gas species, such as oxygen and volatile hydrocarbons, and tracks the depletion of various fuels and other stationary solids and liquids. From this model we develop a simplified local burning model with which we perform a number of simulations that demonstrate that we are able to capture the important physics with the transport approach. With this simplified model we are able to pick up the essence of wildfire propagation, including such features as acceleration when transitioning to upsloping terrain, deceleration of fire fronts when they reach downslopes, and crowning in the presence of high winds.

# ON SIMULATING FLOW WITH MULTIPLE TIME SCALES USING A METHOD OF AVERAGES

L.G. Margolin,  
Los Alamos National Laboratory

## Abstract

We present a new computational method based on averaging to efficiently simulate certain systems with multiple time scales. We first develop the method in a simple one-dimensional setting and employ linear stability analysis to demonstrate numerical stability. We then extend the method to multidimensional fluid flow. Our method of averages does not depend on explicit splitting of the equations nor on modal decomposition. Rather we combine low order and high order algorithms in a generalized predictor-corrector framework. We illustrate the methodology in the context of a shallow fluid approximation to an ocean basin circulation. We find that our new method reproduces the accuracy of a fully explicit second-order accurate scheme, while costing less than a first-order accurate scheme.

# HEXAHEDRAL MESH GENERATION VIA THE DUAL ARRANGEMENT OF SURFACES

S. A. Mitchell and T. J. Tautges,  
Sandia National Laboratories

## Abstract

Given a general three-dimensional geometry with a prescribed quadrilateral surface mesh, we consider the problem of constructing a hexahedral mesh of the geometry whose boundary is exactly the prescribed surface mesh. Due to the specialized topology of hexahedra, this problem is more difficult than the analogous one for tetrahedra. Folklore has maintained that a surface mesh must have a constrained structure in order for there to exist a compatible hexahedral mesh.

However, we have a proof that a surface mesh need only satisfy mild parity conditions, depending on the topology of the three-dimensional geometry, for there to exist a compatible hexahedral mesh. The proof is based on the realization that a hexahedral mesh is dual to an arrangement of surfaces, and the quadrilateral surface mesh is dual to the arrangement of curves bounding these surfaces. The proof is constructive and we are currently developing an algorithm called Whisker Weaving (WW) that mirrors the proof steps.

Given the bounding curves, WW builds the topological structure of an arrangement of surfaces having those curves as its boundary. WW progresses in an advancing front manner. Certain local rules are applied to avoid structures that lead to poor mesh quality. Also, after the arrangement is constructed, additional surfaces are inserted to separate features, so e.g. no two hexahedra share more than one quadrilateral face.

The algorithm has generated meshes for certain non-trivial problems, but is currently unreliable. We are exploring strategies for consistently selecting which portion of the surface arrangement to advance based on the existence proof. This should lead us to a robust algorithm for arbitrary geometries and surface meshes.

# 3D UNSTRUCTURED-MESH RADIATION TRANSPORT CODES

J. Morel,  
Los Alamos National Laboratory

## Abstract

Three unstructured-mesh radiation transport codes are currently being developed at Los Alamos National Laboratory. The first code is ATTILA, which uses an unstructured tetrahedral mesh in conjunction with standard  $S_n$  (discrete-ordinates) angular discretization, standard multigroup energy discretization, and linear-discontinuous spatial differencing. ATTILA solves the standard first-order form of the transport equation using source iteration in conjunction with diffusion-synthetic acceleration of the within-group source iterations. DANTE is designed to run primarily on workstations. The second code is DANTE, which uses a hybrid finite-element mesh consisting of arbitrary combinations of hexahedra, wedges, pyramids, and tetrahedra. DANTE solves several second-order self-adjoint forms of the transport equation including the even-parity equation, the odd-parity equation, and a new equation called the self-adjoint angular flux equation.

DANTE also offers three angular discretization options:  $S_n$  (discrete-ordinates),  $SP_n$  (spherical harmonics), and  $SP_n$  (simplified spherical harmonics). DANTE is designed to run primarily on massively parallel message-passing machines, such as the ASCI-Blue machines at LANL and LLNL. The third code is PERICLES, which uses the same hybrid finite-element mesh as DANTE, but solves the standard first-order form of the transport equation rather than a second-order self-adjoint form.

DANTE uses a standard  $S_n$  discretization in angle in conjunction with trilinear-discontinuous spatial differencing, and diffusion-synthetic acceleration of the within-group source iterations. PERICLES was initially designed to run on workstations, but a version for massively parallel message-passing machines will be built. The three codes will be described in detail and computational results will be presented.

# RECENT WORK ON MATERIAL INTERFACE RECONSTRUCTION

S. J. Mosso and B. K. Swartz,  
Los Alamos National Laboratory

## Abstract

For the last 15 years, many Eulerian codes have relied on a series of piecewise linear interface reconstruction algorithms developed by David Youngs. In a typical Youngs' method, the material interfaces were reconstructed based upon nearby cell values of volume fractions of each material. The interfaces were locally represented by linear segments in two dimensions and by pieces of planes in three dimensions. The first step in such reconstruction was to locally approximate an interface normal. In Youngs' 3D method, a local gradient of a cell-volume-fraction function was estimated and taken to be the local interface normal. A linear interface was moved perpendicular to the now known normal until the mass behind it matched the material volume fraction for the cell in question. But for distorted or nonorthogonal meshes, the gradient normal estimate didn't accurately match that of linear material interfaces. Moreover, curved material interfaces were also poorly represented.

We will present some recent work in the computation of more accurate interface normals, without necessarily increasing stencil size. Our estimate of the normal is made using an iterative process that, given mass fractions for nearby cells of known but arbitrary variable density, converges in 3 or 4 passes in practice (and quadratically - like Newton's method - in principle). The method reproduce a linear interface in both orthogonal and nonorthogonal meshes. The local linear approximation is generally 2nd-order accurate, with a 1st-order accurate normal for curved interfaces in both two and three dimensional polyhedral meshes. Recent work demonstrating the interface reconstruction for curved surfaces will be discussed.

# NUMERICAL SIMULATION OF TURBULENT MIXING IN 2D FLOWS

V. V. Nikiforov, Yu. V. Yanilkin, G. V. Zharova, Yu. A. Yudin,  
RFNC-VNIIEF, Russia

## Abstract

The paper describes 2D multiparameter model of turbulent mixing developed within the EGAK program package. The model use nine independent variables for which evolution equations are solved. The variables are four components of Reynolds tensor, full turbulent energy, viscous dissipation rate of turbulent energy, two components of a velocity vector of turbulent mass flow and squared density pulsation. The model is the two-dimensional generalization of the one-dimensional model of VIKHR' technique.

The results of 1D computations using multiparameter turbulent mixing model under gravitational instability are given. These results are in full agreement with computation results using VIKHR' technique.

The results of computations of 1D problem of shift instability are given in comparison with already known experiment results and computation results using k- $\epsilon$  model of turbulent mixing. Our results are in good agreement both with experimental results and results obtained with k- $\epsilon$  model.

The paper also includes 2D computation results of modeling instability growth at the interface of two different -density gases and liquids and their subsequent turbulent mixing. Results are being compared to experiment data obtained in laboratories headed by Meshkov and Kucherenko. Additionally, the results are also compared to the results obtained using k- $\epsilon$  model of turbulent mixing and results of direct numerical simulations without any turbulence models earlier conducted using other techniques within EGAK program set. Good agreement of computation results using the proposed technique with experiment data and results using other numerical techniques is achieved.

The calculations carried out showed that the multiparameter model has its advantages over other models, the main of them is that it use the same semi-empirical constants for all flows being simulated.

# SEISMIC IMAGING USING FINITE-DIFFERENCES AND PARALLEL COMPUTERS

C. C. Ober,  
Sandia National Laboratories

## Abstract

A key to reducing the risks and costs of associated with oil and gas exploration is the fast, accurate imaging of complex geologies, such as salt domes in the Gulf of Mexico and overthrust regions in U.S. onshore regions. Prestack depth migration generally yields the most accurate images, and one approach to this is to solve the scalar wave equation using finite differences.

Current industry computational capabilities are insufficient for the application of finite difference, 3-D, prestack, depth migration algorithms. A 3-D data set can be several terabytes in size, and the multiple runs necessary to refine the velocity model may take many years. The oil companies and seismic contractors need to be able to perform complete velocity field refinements in weeks and single iterations overnight. High performance computers and state-of-the-art algorithms and software are required to meet this need.

As part of an ongoing ACTI project funded by the U.S. Department of Energy, we have developed a finite difference, 3-D prestack, depth migration code. The goal of this work is to demonstrate that massively parallel computers can be used efficiently for seismic imaging, and that sufficient computing power exists (or soon will exist) to make finite difference, prestack, depth migration practical for oil and gas exploration.

We have had to address several problems to get an efficient code for the Intel Paragon. These include efficient I/O, efficient parallel tridiagonal solves, and high single-node performance. Furthermore, to provide portable code we have been restricted to the use of high-level programming languages (C and Fortran) and interprocessor communications using MPI. We have been using the SUNMOS operating system, which has affected many of our programming decisions.

We will present images created from two verification datasets (the Marmousi Model and the SEG/EAEG 3D Salt Model). Also, we will show recent images from real datasets, and point out locations of improved imaging. Finally, we will discuss areas of current research which will hopefully improve the image quality and reduce computational costs.

# MOLECULAR DYNAMICS COMPUTER SIMULATION OF PERMEATION IN SOLIDS

P. I. Pohl, G. S. Heffelfinger, D. K. Fidler and D. M. Ford,  
Sandia National Laboratories

## Abstract

In this work, we apply classical mechanics and molecular dynamics to better understand the phenomena of atomic and molecular movement in dense and slightly porous solids. Lennard-Jones interaction potentials are used and supplemented with quantum mechanical adjustments where necessary. Novel simulation techniques such as Grand Canonical Molecular Dynamics, transition state theory and diffusion pathways are utilized to understand permeation, diffusion and diffusive pathways. Applications of this theoretical work include development of membranes for gas separations, predictions of oxygen permeation and subsequent oxidation in support of materials degradation research and understanding cation diffusion in meteorite minerals to assess the probability of organic life on the planet Mars.

# PARALLEL MONTE CARLO TRANSPORT MODELING IN THE CONTEXT OF A TIME-DEPENDENT, THREE-DIMENSIONAL MULTI- PHYSICS CODE

R. J. Procassini,  
Lawrence Livermore National Laboratory

## Abstract

The fine-scale, multi-space resolution that is envisioned for accurate simulations of complex weapons systems in three spatial dimensions implies flop-rate and memory-storage requirements that will only be obtained in the near future through the use of parallel computational techniques. Since the Monte Carlo transport models in these simulations usually stress both of these computational resources, they are prime candidates for parallelization. The MONACO Monte Carlo transport package, which is currently under development at LLNL, will utilize two types of parallelism within the context of a multi-physics design code: decomposition of the spatial domain across processors (spatial parallelism) and distribution of particles in a given spatial subdomain across additional processors (particle parallelism). This implementation of the package will utilize explicit data communication between domains (message passing). Such a parallel implementation of a Monte Carlo transport model will result in non-deterministic communication patterns. The communication of particles between subdomains during a Monte Carlo time step may require a significant level of effort to achieve a high parallel efficiency.

This work is performed under the auspices of the U.S. Department of Energy at the Lawrence Livermore National Laboratory under Contract Number W-7405-Eng-48.

# CALCULATION TECHNIQUE FOR 3-D GAS DYNAMICS PROBLEMS ON NONREGULAR LAGRANGIAN GRIDS

V. V. Rasskazova,  
RFNC-VNIIEF, Russia

## Abstract

The technique offered uses both Lagrangian gas dynamics equations and a difference calculation grid connected with a material and moving with it.

The space is filled with figures as computational grid meshes without folds and gaps by nonregular method using convex Dirichlet-Voronoy polyhedrons at initial moment of integration.

To avoid Lagrangian grid calculational distortions during numerical experiment the means of preserving convex trihedral angles are used together with a local grid reconstruction by cutting separate meshes or by spating two neiboring.

The technique and its software can be used for solving problems in the following practical areas:

- ecology problems which need to know the material particles location and pathway;
- calculation of directed explosions when it is necessary to know and be able to define the direction of material-ground being burst out;
- meteorology problems;
- calculation of body co-impact in space and their penetration within each other.

The problems for demonstration of this method capabilities are offered.

# AN IMPLICIT FAST FOURIER TRANSFORM METHOD FOR INTEGRATION OF THE TIME DEPENDENT SCHRODINGER EQUATION

M. E. Riley,  
Sandia National Laboratories,  
and  
A. B. Ritchie.  
Lawrence Livermore National Laboratory

## Abstract

The potential of the new massively-parallel-processor computers to perform "bare-knuckle" numerical solutions of difficult full-dimensional problems prompted us to investigate some modern finite-difference methods for solution the time-dependent Schrodinger equation. One of these is the exponentiated split operator procedure, based on the use of the fast Fourier transform, which has been successfully used for vibration-rotation spectral analysis and molecular dynamics.

Electronic processes such as charge transfer, excitation, and ionization involve the Coulomb interaction which makes the numerical representation of the wave function more difficult than in the previous molecular dynamics studies. We have found that the exponentiated split operator procedure is subject to difficulties in energy conservation when solving the time-dependent Schrodinger equation for Coulombic systems. Stability with respect to time increment variations is a problem for these interactions. We have rearranged the kinetic and potential energy terms in the temporal propagator of the finite difference equations to find a propagation algorithm for three dimensions that looks much like the Crank-Nicholson and alternating direction implicit methods for one- and two-space-dimensional partial differential equations. Stability is greatly improved. We report comparisons of this novel implicit split operator procedure with the conventional exponentiated split operator procedure on hydrogen atom solutions.

# PROPAGATION OF AN ULTRA-SHORT, INTENSE LASER IN A RELATIVISTIC FLUID

A. B. Ritchie and C. D. Decker,  
Lawrence Livermore National Laboratory

## Abstract

A Maxwell-relativistic fluid model is developed to describe the propagation of an ultrashort, intense laser pulse through an underdense plasma. The model makes use of numerically stabilizing fast Fourier transform (FFT) computational methods for both the Maxwell and fluid equations, and it is benchmarked against particle-in-cell (PIC) simulations.

Strong fields generated in the wake of the laser are calculated, and we observe coherent wake-field radiation generated at harmonics of the plasma frequency due to nonlinearities in the laser-plasma interaction. For a plasma whose density is 10% of critical, the highest members of the plasma harmonic series begin to overlap with the first laser harmonic, suggesting that widely used multiple-scales-theory, by which the laser and plasma frequencies are assumed to be separable, ceases to be a useful approximation.

# COMPUTATIONAL MODELING OF JOINT U.S.-RUSSIAN EXPERIMENTS RELEVANT TO MAGNETIC COMPRESSION/MAGNETIZED TARGET FUSION (MAGO/MTF)

P. T. Sheehey, R. J. Faehl, R. C. Kirkpatrick, and I. R. Lindemuth,  
Los Alamos National Laboratory

## Abstract

Magnetized Target Fusion (MTF) experiments, in which a preheated and magnetized target plasma is hydrodynamically compressed to fusion conditions, present some challenging computational modeling problems. Recently, joint experiments relevant to MTF (Russian acronym MAGO, for Magnitnoye Obzhatiye, or magnetic compression) have been performed by Los Alamos National Laboratory and the All-Russian Scientific Research Institute of Experimental Physics (VNIIEF). Modeling of target plasmas must accurately predict plasma densities, temperatures, fields, and lifetime; dense plasma interactions with wall materials must be characterized. Modeling of magnetically driven imploding solid liners, for compression of target plasmas, must address issues such as Rayleigh-Taylor instability growth in the presence of material strength, and glide plane-liner interactions.

Proposed experiments involving "liner-on-plasma" compressions to fusion conditions will require integrated target plasma and liner calculations. Detailed comparison of the modeling results with experiment will be presented.

LA-UR-97-2291

# MPDATA: A POSITIVE DEFINITE SOLVER FOR GEOPHYSICAL FLOWS

P. K. Smolarkiewicz and L. G. Margolin.  
Los Alamos National Laboratory

## Abstract

This paper is a review of MPDATA, a class of methods for the numerical simulation of advection based on the sign-preserving properties of upstream differencing. MPDATA was designed originally as an inexpensive alternative to flux-limited schemes for evaluating the transport of nonnegative thermodynamic variables (such as liquid water or water vapour) in atmospheric models. During the last decade, MPDATA has evolved from a simple advection scheme to a general approach for integrating the conservation laws of geophysical fluids on micro-to-planetary scales. The purpose of this paper is to summarize the basic concepts leading to a family of MPDATA schemes, review the existing MPDATA options, as well as to demonstrate the efficacy of the approach using diverse examples of complex geophysical flows.

# ARCHITECTURE OF A MULTICOMPUTER'S COMMUTATION NETWORK AND OF DIFFERENCE GRID FOR COMPUTATIONAL PHYSICS PROBLEMS

I. D. Sofronov,  
RFNC-VNIIEF, Russia

## Abstract

One of the main reserves of increase of computer system performance is the wide calculating process paralleling when one large problem is being solved using a great number of PEs simultaneously.

Evidently, the efficiency of paralleling process depends on a capability of an algorithm to be paralleled, as well as on specific features of architecture of a multiprocessor computer system in use.

The presentation considers algorithms for solving evolutionary problems in computational physics discretized over difference grids having the architecture of  $\rho$ -dimensional matrix, and peculiarities of these algorithm implementation on multiprocessor computer systems which have a commutation network either with matrix or hypercubic architecture.

In particular, it is shown that with matrix architecture of a commutation network the loss of a middle load of PEs is inevitable if a number of PEs is large enough. With regard to this parameter a hypercubic commutation network has an advantage as compared to a matrix commutation network. Some theoretical estimations have been verified by solving test problems on multiprocessor supercomputers of several types.

# 3-D PARALLEL PROGRAM FOR NUMERICAL CALCULATION OF GAS DYNAMICS PROBLEMS WITH HEAT CONDUCTIVITY ON DISTRIBUTED MEMORY COMPUTATIONAL SYSTEMS (CS)

(Calculation results obtained on MP-3 CS, Meiko CS-2 and SP2)

I. D. Sofronov, B. L. Voronin, O. I. Butnev, A. N. Bykov,  
A. M. Yerofeyev, and A. I. Skripnik, VNIIEF, Russia  
D. Nielsen, Jr., N. Medsen, R. Evans, and S. Brandon,  
Lawrence Livermore National Laboratory

## Abstract

The aim of the work performed is to develop a 3D parallel program for numerical calculation of gas dynamics problem with heat conductivity on distributed memory computational systems (CS), satisfying the condition of numerical result independence from the number of processors involved.

Two basically different approaches to the structure of massive parallel computations have been developed. The first approach uses the 3D data matrix decomposition reconstructed at temporal cycle and is a development of parallelization algorithms for multiprocessor CS with shareable memory. The second approach is based on using a 3D data matrix decomposition not reconstructed during a temporal cycle.

The program was developed on 8-processor CS MP-3 made in VNIIEF and was adapted to a massive parallel CS Meiko-2 in LLNL by joint efforts of VNIIEF and LLNL staffs.

A large number of numerical experiments has been carried out with different number of processors up to 256 and the efficiency of parallelization has been evaluated in dependence on processor number and their parameters.

# ALEGRA--A MASSIVELY PARALLEL H-ADAPTIVE CODE FOR SOLID DYNAMICS

R. M. Summers, M. K. Wong, E. A. Boucheron, J. R. Weatherby,  
Sandia National Laboratories

## Abstract

ALEGRA is a multi-material, arbitrary-Lagrangian-Eulerian (ALE) code for solid dynamics designed to run on massively parallel (MP) computers. It combines the features of modern Eulerian shock codes, such as CTH, with modern Lagrangian structural analysis codes using an unstructured grid. ALEGRA is being developed for use on the teraflop supercomputers to conduct advanced three-dimensional (3D) simulations of shock phenomena important to a variety of systems.

ALEGRA was designed with the Single Program Multiple Data (SPMD) paradigm, in which the mesh is decomposed into sub-meshes so that each processor gets a single sub-mesh with approximately the same number of elements. Using this approach we have been able to produce a single code that can scale from one processor to thousands of processors.

A current major effort is to develop efficient, high precision simulation capabilities for ALEGRA, without the computational cost of using a global highly resolved mesh, through flexible, robust h-adaptivity of finite elements. H-adaptivity is the dynamic refinement of the mesh by subdividing elements, thus changing the characteristic element size and reducing numerical error. This provides for increased resolution wherever and whenever higher precision is necessary to adequately simulate regions of large deformation and transient features such as shocks, burn fronts, and pressure stagnation areas. The h-adaptive version of ALEGRA is called HAMMER.

We are working on several major technical challenges that must be met to make effective use of HAMMER on MP computers. One is efficient parallelization of the basic refinement and unrefinement algorithms. Another is the development of dynamic load balancing techniques to prevent severe overloading of one or more processors as adaptive refinement progresses. Also, appropriate error estimators or refinement indicators must be developed for various physics, and how they should be applied in a multi-physics calculation must be determined.

# EFFICIENT SINGLE SCATTER ELECTRON MONTE CARLO SIMULATION

M. Svatos and J. Rathkopf,  
Lawrence Livermore National Laboratory

## Abstract

A single scatter electron Monte Carlo code (SSMC), CREEP, has been written which bridges the gap between existing transport methods and modeling real physical processes. CREEP simulates ionization, elastic and bremsstrahlung events individually. Excitation events are treated with an excitation-only stopping power. The detailed nature of these simulations allows for calculation of backscatter and transmission coefficients, backscattered energy spectra, stopping powers, energy deposits, depth dose, and a variety of other associated quantities. Agreement of these quantities with experimental values will be shown and is generally excellent.

One application of this code is the generation of probability distribution functions (PDFs) to describe the phase space of a single electron emerging from a sphere of a given material and radius. A library of data sets for such spheres (or "kugels") is being computed for a variety of incident energies, material types, and sizes. These results are stored for subsequent sampling from another electron transport code, Steppenwolf. The goal of this work is to achieve extremely accurate transport results with a efficiency that is similar to condensed history methods. Comparisons of Steppenwolf with CREEP and condensed history codes will be shown.

CREEP, and Steppenwolf, rely on sampling the Lawrence Livermore Evaluated Electron Data Library (EEDL) which has data for all elements with an atomic number between 1 and 100, over an energy range from approximately several eV (or the binding energy of the material) to 100 GeV. Compounds and mixtures may also be used by combining the appropriate element data via Bragg additivity.

# TRANSVERSE ISOTROPIC MODELING OF THE BALLISTIC RESPONSE OF GLASS REINFORCED PLASTIC COMPOSITES

P. A. Taylor,  
Sandia National Laboratories

## Abstract

The use of glass reinforced plastic (GRP) composites is gaining significant attention in the DoD community for use in armor applications. These materials typically possess a laminate structure consisting of up to 100 plies, each of which is constructed of a glass woven roving fabric that reinforces a plastic matrix material. Current DoD attention is focused on a high strength, S-2 glass cross-weave (0/90) fabric reinforcing a polyester matrix material that forms each ply of a laminate structure consisting anywhere from 20 to 70 plies. The resulting structure displays a material anisotropy that is, to a reasonable approximation, transversely isotropic. When subjected to impact and penetration from a metal fragment projectile, the GRP displays damage and failure in an anisotropic manner due to various mechanisms such as matrix cracking, fiber fracture and pull-out, and fiber-matrix debonding.

In this presentation, I will describe the modeling effort to simulate the ballistic response of the GRP material described above using the transversely isotropic (TI) constitutive model which has been implemented in the shock physics code, CTH. The results of this effort suggest that the model is able to describe the delamination behavior of the material but has some difficulty capturing the in-plane (i.e., transverse) response of the laminate due to its cross-weave fabric reinforcement pattern which causes a departure from transverse isotropy.

Sandia is a multiprogram laboratory operated by Sandia Corporation, a Lockheed Martin Company, for the United States Department of Energy under Contract DE-ACO4-94AL85000.

# SPALLATION STUDIES ON SHOCK LOADED URANIUM

D. L. Tonks, R. Hixson, R. L. Gustavsen, J. E. Vorthman, A. Kelly, A. K. Zurek, and W. R. Thissell,  
Los Alamos National Laboratory

## Abstract

Uranium samples at two different purity levels were used for spall strength measurements at three different stress levels. A 50 mm single-stage gas-gun was used to produce planar impact conditions using Z-cut quartz impactors. Samples of depleted uranium were taken from very high purity material and from material that had 300 ppm of carbon added. A pair of shots was done for each impact strength, one member of the pair with VISAR diagnostics and the second with soft recovery for metallographical examination.

A series of increasing final stress states were chosen to effectively freeze the microstructural damage at three places in the development to full spall separation. This allowed determination of the dependence of spall mechanisms on stress level and sample purity.

This report will discuss both the results of the metallurgical examination of soft recovered samples and the modeling of the free surface VISAR data. The micrographs taken from the recovered samples show brittle cracking as the spallation failure mechanism. Deformation induced twins are plentiful and obviously play a role in the spallation process. The twins are produced in the initial shock loading and, so, are present already before the fracture process begins.

The 1 d characteristics code CHARADE has been used to model the free surface VISAR data. The spallation modeling is micromechanically based and involves brittle crack breakout, growth, and coalescence. Calculated free surface particle velocity profiles are compared with the data and conclusions drawn. The results show that the brittle crack model can explain the spall features of the data, except for the very late time behavior. The late time behavior is more complicated because it involves close interactions and couplings between cracks. A preliminary modeling result for the 81 kbar shot is shown in Fig. 1.

# APPLICATION OF CHAD HYDRODYNAMICS TO SHOCK-WAVE PROBLEMS

H. E. Trease, P. J. O'Rourke, and M. S. Sahota.  
Los Alamos National Laboratories

## Abstract

CHAD is the latest in a sequence of continually evolving computer codes written to effectively utilize massively parallel computer architectures and the latest grid generators for unstructured meshes. Its applications range from automotive design issues such as in-cylinder and manifold flows of internal combustion engines, vehicle aerodynamics, underhood cooling and passenger compartment heating, ventilation, and air conditioning to shock hydrodynamics and materials modeling.

CHAD solves the full unsteady Navier-Stoke equations with the k-epsilon turbulence model in three space dimensions. The code has four major features that distinguish it from the earlier KIVA code, also developed at Los Alamos. First, it is based on a node-centered, finite-volume method in which, like finite element methods, all fluid variables are located at computational nodes. The computational mesh efficiently and accurately handles all element shapes ranging from tetrahedra to hexahedra. Second, it is written in standard Fortran 90 and relies on automatic domain decomposition and a universal communication library written in standard C and MPI for unstructured grids to effectively exploit distributed-memory parallel architectures. Thus the code is fully portable to a variety of computing platforms such as uniprocessor workstations, symmetric multiprocessors, clusters of workstations, and massively parallel platforms. Third, CHAD utilizes a variable explicit/implicit upwind method for convection that improves computational efficiency in flows that have large velocity Courant number variations due to velocity or mesh size variations. Fourth, CHAD is designed to also simulate shock hydrodynamics involving multimaterial anisotropic behavior under high shear.

We will discuss CHAD capabilities and show several sample calculations showing the strengths and weaknesses of CHAD.

# ESTABLISHING CONFIDENCE IN COMPLEX PHYSICS CODES: ART OR SCIENCE?

T. Trucano,  
Sandia National Laboratories

## Abstract

The ALEGRA shock wave physics code, currently under development at Sandia National Laboratories and partially supported by the U. S. Advanced Strategic Computing Initiative (ASCI), is generic to a certain class of physics codes: large, multi-application, intended to support a broad user community on the latest generation of massively parallel supercomputer, and in a continual state of formal development. To say that we have "confidence" in the results of ALEGRA is to say something different than that we believe that ALEGRA is "predictive." It is the purpose of this talk to illustrate the distinction between these two concepts. I elect to perform this task in a somewhat historical manner. I will summarize certain older approaches to code "validation". I view these methods as aiming to establish the predictive behavior of the code. These methods are distinguished by their emphasis on "local" information. I will conclude that these approaches are more art than science. It then will follow that newer approaches

---

\*This work performed at Sandia National Laboratories supported by the U. S. Department of Energy under contract number DE-AC04-94AL85000.

# DEVELOPMENT OF DIFFERENCE SCHEMES FOR COMPUTING MULTIDIMENSIONAL NON-STATIONARY ELASTIC-PLASTIC FLOWS ON THE BASE OF THE MUTUAL TRANSITION LAW FOR KINETIC AND INTERNAL ENERGIES

V. B. Vershinin, V. I. Delov, O. V. Senilova, I. D. Sofronov  
RFNC-VNIIEF, Russia

## Abstract

The paper proposes the approach to develop conservative difference-differential equations describing non-stationary elastic-plastic flows via Lagrangian variables. The given technique is the outgrowth of 2D technique of constructing spatial approximations of gas dynamics motion equations. /1/, /2/ for elastic-plastic media. Its distinctive features are simplicity and quickness of obtaining difference motion equations which are close to equations obtained using variational approaches by their structure and quality.

The proposed technique serves for elimination of one of the main drawbacks of Whilkins scheme in the case of axial symmetry related to nonconservation of full system energy.

In the given paper the kinetic energy matrix determining the way of pressure gradient approximation is used in its canonical form being used traditionally in gas dynamic techniques.

The paper includes difference formulas for strain rate tensor components and obtained difference approximations to compute derivatives of components of stress tensor deviator .

There is an information about computation results using the developed difference scheme in which grid value distribution in time is used in the same manner as in "D" technique /3/, time derivative being approximated with the second order.

Obvious advantages of the developed difference scheme are shown for the problem of elastic membrane oscillations in comparison with the classic Whilkins scheme.

Opposite to the difference scheme for gas-dynamic computations /4/ obtained using the same approach to the development of difference schemes, the scheme from the work /2/ and the difference scheme proposed here do not require iterations on the time step to achieve the second order accuracy in time.

## Reference

1. Isayev V.N., Sofronov I.D. Development of Discrete Models for Gas Dynamics Equations on the Base of the Law of Mutual Transition of Kinetic and Internal Continuous Medium Energies. // VANT, Ser. Metodici i Programmy Chisl. Resh. Zadach Mat.Fiz., 1984, iss.1(15), pp.3-7.

2. Delov V.I., Isayev V.N., Sofronov I.D. Conservative and Invariant Difference-Differential Representations of Gas Dynamics Equations in Axial Symmetry Case.// VANT, Ser. Metodici i Programmy Chisl. Resh. Zadach Mat.Fiz., 1987. iss.1. pp.3-10.
3. Dmitriyev N.A., Dmitriyeva L.V., Malinovskaya E.V., Sofronov I.D. The Calculation Technique for Non-Stationary 2D Gas Dynamics Problems in Lagrangian Variables. In the book: Theoretical Foundations and Development of Numerical Algorithms for Computational Physics Problems./Edited by Babenko K.I.- Moscow, Science Publishers , 1979, pp.175-200.
4. Caramana E.J., Whalen P.P. (LANL). Scalable Compatible Energy and Entropy Conserving Hydrodynamics. Third Joint Conference on Computational Mathematics (JCCM3), 1995, Los Alamos.

# NONREGULAR FREE-LAGRANGIAN "MEDUSA" TECHNIQUE

S. G. Volkov, B. M. Zhogov, V. D. Malshakov, I. D. Sofronov  
RFNC-VNIIEF, Russia

## Abstract

"Medusa" technique refers to 2D Lagrangian gas dynamics techniques on non-regular grids adapting to the nature of occurring processes. Using a universally accepted terminology we may refer it to a free-Lagrangian technique class.

The paper gives a brief historic information, describes "Medusa" gas dynamics technique difference scheme, gives a list of physical processes being calculated, describes parallelization methods of calculating the problems on multiprocessor computational systems and gives calculation examples.

The first part tells about "Medusa" technique development, about its implementation on different computers, tells about some interesting calculations performed by this technique and about modern technique implementation.

The second part describes the problem digitization, the obtained difference equations, stresses the main technique peculiarities such as the use of mixed meshes and grid local interpolation.

The third part gives the method of obtaining difference equations to solve a heat conductivity equation on a non-regular grid. Here an approximated method of solving the obtained system by means of balance iterations is given, the one presenting good results even in case of iteration cut resulting from their great number.

The fourth part marks the technique peculiarities allowing to parallelize gas dynamics calculations. Different means of splitting the point sets in the problem for parallel calculations and the peculiarities of parallelization connected with this splitting are considered.

The final part describes the technique application area and calculation results.

# NUMERICAL SIMULATION OF CLOSE AND REMOTE ZONES OF ACCIDENT OUTBURST AND EXPLOSION

Yu. V. Yanilkin, V. N. Sofronov, V. I. Tarasov, V. P. Statsenko,  
V. N. Piskunov, N. P. Kovalyov, O. A. Dibirov, A. L. Stadnik,  
T. A. Toropova, G. G. Ivanova, A. A. Shanin,  
RFNC-VNIIEF, Russia

## Abstract

The paper describes a 3D program package designed for numerical simulation of accident explosion and outburst dynamics and their consequences in a regional scale. The package is implemented in the frames of TREK program complex.

The simulation of a full-scale problem involving accident outbursts is an intricate problem due both to a large number of physical processes to be taken into account and scale diversity of flows at different process stages. The package includes two stages of the considered process: the explosion cloud lifting to the height of stabilization and aerosole transfer in atmosphere above an orographically and thermally non-uniform underlying surface.

The simulation is based on a joint solution of the following physical processes:  
at the first stage

- gas-dynamical flow of polydisperse environment;
- turbulent agitation;
- variation of aerosole particle disperse composition due to coagulation;

at the second stage

- atmosphere hydrothermodynamics;
- particle transfer and turbulent diffusion.

The equation approximation is made in Decartes coordinate system on arbitrary in general case non-rectangular, Eulerian and Lagrangian-Eulerian grids. Such approach allows to use the grids most adapted to the considered flows: first, those accounting local orography and, second, those moving with aerosole cloud. The approach considerably reduces the number of grids used in calculations and the calculation diffusion intrinsic in Eulerian methods as well.

Implicit difference schemes are used to calculate gas-(hydro-)dynamics and diffusion; concentration and FCT methods are used to calculate convective transfer; original algebraic and (k- $\epsilon$ ) -models are used to account turbulence. Multicomponent versions both of carrying and dispersed phases with their unlimited number are assumed.

The examples of numerical solution for several test problems are given:

- spherical cloud transfer;
- Prandtl problem;
- Eckmann problem;
- aerosole propagation with a constant wind, diffusion coefficient and sedimentation coefficient.

The calculation results of real problems are given:

- cloud lifting with account of wind and without it;
- aerosole transfer over the rugged country;
- radiation contamination propagation in the Ural accident.

# THREE DIMENSIONAL FINITE ELEMENT FORMULATION FOR THERMOVISCOELASTIC ORTHOTROPIC MEDIA

M. A. Zocher,  
Los Alamos National Laboratory

## Abstract

This presentation shall be concerned with the development of a numerical algorithm for the solution of the uncoupled, quasistatic initial/boundary value problem involving orthotropic linear viscoelastic media undergoing thermal and/or mechanical deformation. The constitutive equations, expressed in integral form involving the relaxation moduli, are transformed into an incremental algebraic form prior to development of the finite element formulation. This incrementalization is accomplished in closed form and results in a recursive relationship which leads to the need of solving a simple set of linear algebraic equations only for the extraction of the finite element solution. Use is made of a Dirichlet-Prony series representation of the relaxation moduli in order to derive the recursive relationship and thereby eliminate the storage problem that arises when dealing with materials possessing memory. Several illustrative example problems will be presented for the purpose of demonstrating the ability of the formulation, which has been implemented into a three dimensional finite element code, to accurately predict the solution to the class of thermoviscoelastic problems addressed.



# Conference Papers



## Analytical and numerical study of accelerated thin layer instability

*S.M.Bakhrakh, G.P.Simonov*

(RFNC-VNIIEF, Sarov (Arzamas-16), Russia)

Using the representation of the governing equations in Lagrangian variables new analytical solutions are found for problems of Rayleigh-Taylor instability of a thin accelerated layer at the process stage non-linear in the observer's space. The analytical solutions are obtained for a liquid layer and an elastic layer, given both 2D and 3D perturbations.

The analytical solutions found have been verified with solving the complete system of conservation laws for compressible continuum.

Through numerical experiments the found mechanisms of thin layer perturbation growth are shown to take place for a finite thickness layer and compressible continuum half-space.

The analytical solutions provide a deeper insight into the instability nature and mechanisms and constitute good tests for numerical techniques of computing continuum flows.

Studying the Rayleigh-Taylor instability (RTI) is of interest in connection to a number of important and urgent problems which include but are not limited to the following: high-velocity throwing, inertial thermonuclear fusion, structure stability, etc.

For theoretic study of the initial RTI phase representation of the initial equations in the Lagrangian variables proved fruitful. This is related to the fact that in some special cases the equations of motion of an accelerated thin layer in the Lagrangian variables appear linear at large displacements as well [1]. This allows to analyze them in order to describe the perturbation evolution stage non-linear in the observer's space. Thus, refs.[1-4] studied evolution of 2D and 3D perturbations of thin liquid layer shape and thickness; ref.[5] did 2D perturbations of elastic layer thickness.

This paper uses such an approach to study thin elastic layer surface RTI, given both 2D and 3D perturbations.

*Analytical study.* The linearized equations of motion of accelerated thin elastic layer are

$$\begin{aligned}
\frac{\partial^2 x_1}{\partial t^2} &= c_{ob}^2 \frac{\partial^2 x_1}{\partial \xi^2} + c_{sd}^2 \left( \frac{\partial^2 x_1}{\partial \eta^2} + \frac{\partial^2 y_1}{\partial \xi \partial \eta} \right) - a \frac{\partial z}{\partial \xi}; \\
\frac{\partial^2 y_1}{\partial t^2} &= c_{ob}^2 \frac{\partial^2 y_1}{\partial \eta^2} + c_{sd}^2 \left( \frac{\partial^2 y_1}{\partial \xi^2} + \frac{\partial^2 x_1}{\partial \xi \partial \eta} \right) - a \frac{\partial z}{\partial \eta}; \\
\frac{\partial^2 z}{\partial t^2} &= -\alpha \left( \frac{\partial^4 z}{\partial \xi^4} + 2 \frac{\partial^4 z}{\partial \xi^2 \partial \eta^2} + \frac{\partial^4 z}{\partial \eta^4} \right) + a \left( \frac{\partial x_1}{\partial \xi} + \frac{\partial y_1}{\partial \eta} \right).
\end{aligned} \tag{1}$$

Here the median surface of the layer in the unperturbed state is assumed to coincide with the surface  $z=0$ . Next, it is taken that  $x_1=x-\xi$ ,  $y_1=y-\eta$ , where  $\xi, \eta$  are Lagrangian coordinates of the layer particles. The acceleration is  $a=p/\rho h_0$  where  $p$  is retaining pressure;  $h_0, \rho$  are initial thickness and density of the layer, respectively. The values  $c_{ob}, c_{sd}, \lambda$  characterize the elastic properties of the plate material:

$$c_{sd}^2 = G / \rho, \quad c_{ob}^2 = 2G / (\rho(1-\nu)) = 2c_{sd}^2 / (1-\nu), \quad \alpha = c_{ob}^2 h^2 / 12. \tag{2}$$

where  $G$  - shear modulus,  $\nu$  - Poisson ratio.  
Consider the solution to system (1) of the form

$$x_1 = A_1 e^{\omega t} \cos(k\xi) \cos(n\eta); \quad y_1 = A_2 e^{\omega t} \sin(k\xi) \sin(n\eta); \quad z = A_3 e^{\omega t} \sin(k\xi) \cos(n\eta). \tag{3}$$

It is possible to show that the increment  $\omega$  is determined by the equation ( $\lambda = \omega^2$ ):

$$\begin{vmatrix}
\lambda + c_{ob}^2 k^2 + c_{sd}^2 n^2 & -c_{sd}^2 kn & ak \\
-c_{sd}^2 kn & c_{ob}^2 n^2 + c_{sd}^2 k^2 & -an \\
ak & -an & \lambda + \alpha(k^2 + n^2)^2
\end{vmatrix} = 0. \tag{4}$$

At sufficiently large accelerations a governing dispersion equation (4) has real positive roots  $\lambda$  correspondent with exponentially growing solutions.

In this problem, like in the problem of elastic half-space RTI [6], the notion of critical acceleration arises.

We define the critical value of acceleration  $a_*$  as acceleration correspondent with zero value  $\lambda = \omega = 0$ . Assume  $\lambda = 0$  in characteristic equation (4) to arrive at the relation for determination of the critical acceleration  $a_*$ :

$$a_c^2 = \frac{\alpha(k^2 + n^2)^2 \left( (C_{ob}^2 k^2 + C_{sd}^2 n^2)(C_{ob}^2 n^2 + C_{sd}^2 k^2) + C_{sd}^4 k^2 n^2 \right)}{C_{sd}^2 (k^2 - n^2)^2 + 2C_{ob}^2 k^2 n^2} \quad (5)$$

At  $n=0$  we obtain the layer stability criterion given 2D perturbations. In this case the critical acceleration is determined by relation

$$a_c^2 = \alpha c_{ob}^2 k^4 = \frac{G^2 h^2 k^4}{3(1-\nu)^2 \rho^2} \quad (6)$$

At small layer thickness  $h$  the critical acceleration determined from (6) is noticeably less than the critical acceleration for elastic medium half-space [7]  $a_c = 2Gk/\rho$ .

From comparison of (5) and (6) it follows that under certain conditions perturbation introduction along the second direction can lead to total perturbation stabilization, with the material working for strength more intensively. For example, at  $n=k$  the ratio  $q$  of critical acceleration determined by relation (5) to appropriate value from relation (4)  $g$  leads to relation  $q^2 = 1 + (2-\nu)^2$ , that is  $q > 1$ .

The stabilizing effect of perturbation along the second direction is specific for media with strength; in the case of a liquid layer the inverse effect of growth increment increase takes place [4].

**Numerical studies.** To verify the above-described analytical solutions, numerical computations in the continuous compressible elastic medium approximation were conducted. The computations were done in the 2D formulation with technique [8] designed for computation of elastic-plastic continuum flows and in the 3D formulation with the technique extending method [9] to three dimensions. The computations varied the principal parameters of the problem.

It was assumed that  $k=1$ ,  $\nu=0.28$ ,  $n=0$  at setting 2D perturbations and  $n=1$  for 3D perturbations. The equation of state was taken in the Mie-Grueneisen form:  $\rho=7.8$ ,  $c_0=4.6$ . Acceleration, shear modulus  $G$  and layer thickness were varied. At the initial time for the equithick shape-unperturbed layer velocity perturbations with  $r_2=-1$  were given. At the layer boundaries pressure  $p_1=p$  and  $p_2=0$  was given at the "lower" and "upper" boundaries, respectively.

At varying thickness  $h$  the computations proportionally varied the applied boundary pressure, so that acceleration  $a=p/\rho h$  remain invariable. In the first series of 2D computations  $a=1$ ,  $G=5$  were assumed.

In the layers with  $h=0.01$ ;  $0.025$ ;  $0.1$  the perturbations grow. However, the perturbation growth is noticeably less than that in the gas-dynamical (strength-free) computation. The computed data for  $h=1$  and  $h=2$  differ considerably from others. At  $h=2$  the perturbations appear stable; the case of  $h=1$  is at the stability boundary.

It is interesting to compare  $h=2$  layer perturbation growth rates at various accelerations,  $a=0.33$ ;  $1$ ;  $2$ . The critical acceleration for such a layer is  $a^*=1.028$ . The results of the computations under discussion confirmed the theory conclusions.

Computations of a thin layer with 3D perturbations in the continuum approximation also agree with the above analytical solutions.

The work was supported by Russian Fundamental Research Foundation, Project 96-01-00043a.

## REFERENCES

1. Ott E. Phys.Rev.Lett.,1972,Vol.29,p.1429.
2. Manheimer W., Colombant D., Ott E. Phys.Fluids,27(8),Aug,1984, p. 2164-2175.
3. Bakhrakh S.M., Simonov G.P.. VANT. Ser.Mat. Modelir. Fiz. Protsessov, 1995, No.3, p.39-46.
4. Bakhrakh S.M., Simonov G.P.. VANT. Ser.Mat. Modelir. Fiz. Protsessov, 1995, No.3, p.33-38.
5. Nizovtsev P.N., Rayevsky V.A. VANT. Ser. Teor. i Prikl. Fizika, 1991, No.3, p.11-17.
6. Bakhrakh S.M., Kovalev N.P. Chisl. Metody Mekh. Splosh. Sredy, Novosibirsk, 1980, p.5-21.
7. Bakhrakh S.M., Kovalev N.P., Pavlusha I.N. Proc. 3d All-Union Conference on Numerical Methods for Solution of Elasticity and Plasticity Theory Problems. Novosibirsk, 1974, p.22-26.
8. Maichen J., Sak S. Computational methods in hydrodynamics. Moscow, Mir Publishers, 1967, p.185-211.

Point of contact: **Bakhrakh Samuil Mikhailovich**

17 Academician Sakharov street, Nizhni Novgorod region, Sarov,  
607190.

Phone: (83130) 11190

Fax: (83130) 45711

E-mail: [smb@md08.vniief.ru](mailto:smb@md08.vniief.ru)



# Architecture of a Multicomputer's Commutation Network and a Difference Grid for Mathematical Physics Problems

Sofronov I.D.

Russian Federal Nuclear Center - All-Russian Scientific Research  
Institute of Experimental Physics (VNIIEF), Sarov

Problems you meet in various areas of science and technology require computers with very high performance to solve them. To achieve maximum performance, computer designers use different techniques. First of all, we can mention high speed elemental base, vector -pipe approach, concurrent execution of several different instructions- the so-called "wide instruction" and, finally, multiprocessor systems. During the last years the attention to multiprocessor systems greatly increased mainly due to gained successes in microelectronics. In present days a great number of multiprocessor systems of various architectures is being developed. We are interested in two simplest, in some sense, types of multiprocessor systems, namely: multiprocessor systems with common internal memory and multicomputers. The typical feature of computers with common memory is a relatively small number of central processors. To gain maximum performance in this case, very powerful processors are used. Multicomputers achieve high performances at the expense of using a large number of very compact central processors. Therewith we have to use shared memory in lieu of common internal memory. A multicomputer under consideration will be considered to have each central processor equipped with its own local internal memory. Suppose further that all processor elements (PEs) are connected to each other by some commutation network involving  $L$  communication lines (CL). Let  $g$  be the throughput of each line, i.e. each line is capable of sending  $g$  full words per a time unit;  $f$  is an arithmetic performance of one processor element. Thus, maximum achievable throughput of the whole commutation system equals  $Lg$ , and maximum arithmetic performance is

$$V = M * f,$$

where  $M$  is a number of PEs which may be interconnected using commutation systems of different architecture.

The most simple is the matrix architecture when processor elements are connected to each other in such a manner that a set of them has a matrix structure of some dimensionality.

The problem of computation parallelization to a large number of branches becomes more and more actual. Now there are computer systems including thousands of processor elements. In spite of the growing arithmetic performance of each processor element the problem of their number increase in some computer systems doesn't lose its actuality. For this reason we somehow exaggerate the problem, namely: we suppose that we have a computer at our disposal consisting of  $N$  processor elements, where  $N$  may increase with no limit. We also suppose that the problem being solved includes  $N \gg M$  computational points, where  $N$  may also increase with no limit. Assume that a set  $\Omega_N$  of all  $N$  computational points is divided into  $M$  subsets with  $N/M$  points in each of them. Let each subset be processed by an appropriate processor element. Total multicomputer's arithmetic performance is proportional to a number of processor elements  $M$  and increases indefinitely with  $M \rightarrow \infty$ . However, with  $M \rightarrow \infty$  an amount of data transfers between processor elements may increase

indefinitely. Evidently, a question arises: may it be so that the time needed for these transfers becomes essentially larger than the time needed for arithmetic work completion?

Suppose that processor elements under consideration have fixed performance and communication lines have fixed throughput. Further suppose that the difference grid  $\Omega_n$  and the hypergrid constructed on it and containing  $M$  hypernodes both have bounded degrees  $r \leq c$ .

**Statement 1.** With above made assumptions for a multicomputer having a commutation network with an architecture of a full graph of connections the following inequalities are valid under any topology:

$$C_1 \leq T_n/T_A \leq C_2 \quad (1)$$

Here  $T_n$  and  $T_A$  are the times spent by a multicomputer to execute data transfers and arithmetic work,  $C_1$  and  $C_2$  are constants.

To prove this statement, remember that each hypernode has a finite number of grid nodes, therefore, to calculate the step one needs to transfer a finite amount of data from neighboring hypernodes that will implement a finite number of communication lines without any transits because the commutation network has an architecture of a full graph of connections. The above formulated conditions are valid for any  $M$  and  $N$ , i.e. with any  $M$  and  $N$  the average load of a processor element will be positive.

**Statement 2.** Let a multicomputer's commutation network has matrix architecture with a degree  $R \geq r$ . Assume that in the original difference grid topology regularity violates in isolated points<sup>1)</sup>.

Under the above assumptions with  $M \rightarrow \infty$  we may chose the hypergrid with its topology being regular by placing irregular points into hypernodes. Thus, we obtain the task where  $M$  hypernodes have regular hypergrid's topology which is to be solved using a multicomputer which commutation network has an architecture coinciding with the hypergrid topology. Obviously, in the case being considered the time spent for transit data transfers will not decrease and inequalities (1) will be valid.

**Statement 3.** If a difference grid has an unbounded degree, then an average load of processors will approach to zero under the unlimited increase of their number.

To prove the above statements, it is sufficient to consider a case when only in one point the grid's degree appears unbounded. Let the degree of the point  $O$  increases indefinitely. Two cases are possible during the hypergrid construction.

1. A point with an unbounded degree is an internal point of some hypernode.
2. A point with an unbounded degree is a boundary point of a hypernode.

In the first case a situation arises with an increasing  $N$ , when a number of nearest grid neighbors surpasses a maximum admissible number of points in a hypernode. In the last case one will need to remove a part of nearest grid neighbors from the considered hypernode and transfer them to another hypernode, i.e. a point with unbounded degree becomes a boundary point of a hypernode and we obtain the case 2. In this case a part of nearest neighbors of a considered point will be located inside and on the boundary of the same hypernode which the point itself belongs to. With an unbounded increase of  $N$  a number of nearest neighbors of the considered point being located in neighboring hypernodes will increase with no limit. Information about all these neighbors is to be transferred by communication lines to the memory of the processor element formed this hypernode. A number of communication lines

---

<sup>1)</sup> By an isolated point regularity violation we mean a point which is surrounded by a sufficient number of regular points.

converging to the considered node may increase with no limit. But all obtained data must pass through one or several ports having the finite performance, therefore, data transfers may require unlimited time, i.e.

$$\begin{aligned} T_n &\rightarrow \infty \\ N &\rightarrow \infty \end{aligned} \quad (2)$$

$T_A$  being a finite value, inequalities (1) will not take place in the case under consideration and an average load of processors will decrease to zero.

Let us have a multicomputer with matrix structure of commutation network of a degree  $r_1 > 0$ . Assume that in this task the hypergrid topology coincides with the commutation network architecture. Under these assumptions it's not difficult to determine bijection between the commutation grid nodes and the difference hypergrid nodes. Evidently, in this case, if an algorithmic neighborhood coincides with the difference grid neighborhood, then the task solution is possible without transit data transfers. In other words, we have proved the Statement 4. If the difference grid topology coincides with the commutation network architecture and an algorithmic neighborhood follows from grid neighborhood, then computation without transits is possible. Obviously, we may suggest a more strict statement, namely: if in the above described case the commutation network is supplemented by new communication lines, then a possibility of transit-free computation remains. In particular, if the matrix architecture is supplemented up to the torus architecture or up to the matrix of degree  $r_2 \geq r_1$ , then a possibility of transit-free computation remains.

**Statement 5.** If the difference grid topology is contained inside the commutation network architecture, i.e. if by switching off some communication lines it is possible to make the commutation network architecture coinciding with the difference grid topology, then the considered task computation without transits is possible using such multicomputer, if the algorithmic neighborhood follows from the grid neighborhood.

**Statement 6.** If a multicomputer's commutation network architecture is inside the difference grid topology, i.e. by switching off some grid lines it is possible to make the difference hypergrid topology coinciding with the commutation network architecture for the computer in use, then in this case computation without transit transfers is not possible, if algorithmic closeness follows from grid closeness. The same fact may be formulated in the following way: if a hypergrid has a degree  $\rho_1 > 0$ , it is impossible to solve the task without transit transfers using a multicomputer the commutation network architecture of which has a degree  $\rho_2 > 0$  less than  $\rho_1 > 0$  at least in few points.



*THE CALCULATIONS OF RADIANT ENERGY TRANSFER IN THERMONUCLEAR TARGETS IN DIFFUSION-VACUUM APPROXIMATION*

Bazin A. A., Vatulin V.V., Dementyev Yu. A., Mironova V. F., Skidan G. I.,  
Tikhomirov B. P., Tikhomirova E.N.

Numerical evaluation of X-radiation symmetry on the surface of capsule containing thermonuclear fuel is one of the key issues in the problem of adequate numerical description of physical processes in inertial confinement fusion targets. Solution of the problem in its complete statement comprising kinetic equation of radiation transfer and the set of hydrodynamics equations meets certain difficulties.

For this reason simpler mathematical models are used in practice for preliminary choice of initial ICF target design and shape [1]. The paper describes radiant energy transfer in ICF targets in diffusion-vacuum approximation. In the frames of this approximation radiation transfer in optically thick and close to those regions is described by radiant heat conduction while in optically thin and transparent regions by integral equation of radiant heat exchange between radiation absorbing surfaces. The regions in which integral equation is solved are called 'vacuum', other regions are called diffusive. Radiation transfer between diffusion regions through transparent environment is described by integral equation, with account of photon time-delay [2]. For numerical solution integral equation is substituted by a set of algebraic equations which is solved by relaxation method [3]. View factors and average photon time-delay are calculated using the technique presented in [4].

It should be noted that there are two approaches to developing numerical techniques for radiant transfer simulation. Both of them are based on the concept of separate calculation of diffusion and vacuum regions. The initial problem is represented as two simple problems, soluble consistently. The first approach - iterative. The decision is built by a method consecutive approximations. The boundary conditions on a surface non transparency are corrected on each iterative cycle. The method is simple in realization, but requires appreciable expenses of processor time of the computer. The second approach is based, that the exchange of boundary conditions between diffusions and vacuums by areas occurs automatically on each temporary layer. Thus absence necessity of iterative process, that results in economy of processor time. However there is the danger of occurrence of computing instability, as the stability of algorithm as a whole much depends on a way of the task of exchange boundary conditions.

The technique considered stipulates several types of exchange boundary conditions which provide the calculation process stability. Particularly, one-way fluxes might be transferred or self-similar flux and temperature obtained from the solution of the equation of transfer in vacuum region and the equations of radiant heat conduction in diffusion regions are jointly calculated.

For the problems considered the process of reradiation from the cavity wall is described either in black body approximation (model 1) or by boundary conditions of diffusion type (model 2). In the latter case the flux from diffusion region can exceed the value of radiation flux into vacuum. To remove this error an easy method of limiting the diffusion flux is proposed. The flux is determined by the formula:

$$W = \sigma T^4 - \frac{3}{2} J^- + \left| \sigma T^4 - \frac{1}{2} J^- \right|,$$

where  $\sigma$  is Stephen-Boltzmann constant,  $T$  is temperature.

The material motion in diffusion regions is described by gas dynamics equations which are solved by finite-difference method in 1-D sector" approximation [5].

To exemplify application of the given approximation method for radiant energy transfer problems we consider the problems of X-radiation propagation in laser and heavy-ion targets.

### 1. Laser targets.

The calculations have been done for the laser targets of small diameter with laser energy radiation of 8 kJ. Such targets were tested at VNIIEF on "ISKRA-5" facility [6]. The geometry of two targets being studied is presented in Fig.1.

Targets 1, 2.

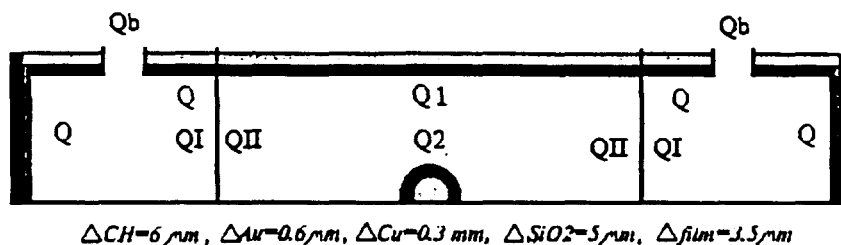


Fig.1.

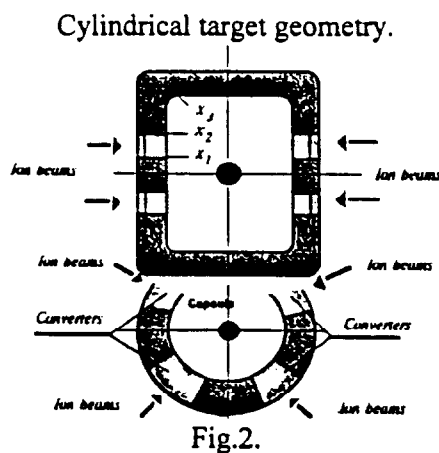
A spherical capsule of 0.095 mm radius is located in the center of a hollow cylinder with inner diameter 0.9 mm and length 3.2 mm. The capsule has a glass casing 5  $\mu m$  thick. The casing is filled with gas with the density 0.004 G/cm<sup>3</sup>. The cylinder casing has two layers. The outer layer 6  $\mu m$  thick is made of polyethylene; the inner layer is sprayed gold 0.6  $\mu m$  thick. The cylinder is sealed by round plates at the ends. The outer plate is copper. It is 0.3 mm thick. The inner plate is made of gold (0.2 mm thick). X-radiation flux as a function of time was set on Q surfaces as a source, the dependence corresponded to the experimental parameters of "Iskra-5" facility laser pulse. The source energy made 2 kJ in all calculations. The condition of energy outlet into vacuum on the Qb surfaces ( $-1.2 \leq X \leq -1.1, 1.1 \leq X \leq 1.2$ ) was set. Exchange boundary conditions were set on Q1, Q2, QI, QII surfaces. The second target differs from the first one by the presence of polyethylene film 3.5  $\mu m$  thick placed at a distance of 7 mm from the target center (see Fig.1) to shield the capsule from laser radiation.

The calculations were mainly aimed at assessing the radiation field symmetry on the spherical capsule surface. The targets were calculated in two versions: with and without account of gas dynamics processes. It was demonstrated that in static case the value of temperature field asymmetry at the moment when the temperature on the equator reached its maximum made 10.5% and 10.6% for the first and for the second targets respectively. In dynamic case these values appeared to be equal to 20% and 16,3% correspondingly.

### 2. Heavy-ion target.

A cylindrical target of 1.3 cm diameter and about 1.6 cm height is considered (see Fig.2). The target is radiated by 10 ion beams with total energy of 10 mJ.

The given target was optimized by means of two-dimensional calculations. In two-dimensional calculations (five cases) the converter width was varied and its position on the side surface along with the cylinder height. The curves are given from these calculations to characterize temperature on the capsule surface as a function of angle  $\theta$ .



To evaluate temperature field asymmetry over the rotation angle  $\varphi$  3-D calculations were made. In three-dimensional problem the converters in the left and right halves of the target were turned relative to each other by the angle of  $\Delta\varphi = 36^\circ$ .

The analysis of results of three-dimensional calculations demonstrated that the temperature field asymmetry on the capsule surface over angle  $\theta$  lies in the range of 1% and over angle  $\varphi$  it does not exceed 0.15%.

The numerical method based on diffusion-vacuum approach to energy transfer description is applicable to other problems of radiation heat exchange found in engineering.

#### REFERENCES

1. Babayev Yu. N., Bazhenov S.V., Bazin A. A. et al. VNIIEF techniques and programs for solving 2D and 3D time-dependent problems of radiant energy transfer in complex-shaped regions using visibility factors. Problems of conversion applications. VANT. Ser. Mat. Modelir. Fiz. Protsessov. 1995. №4. P.3-8.
2. Babayev Yu. N., Bazhenov S. V., Demytyev Yu. A. On solution features of one integral equation of radiation transport. VANT. Ser. Mat. Mod. Fiz. Prots. 1978. №.1(1). P.7-9.
3. Skidan G. I. IVA code for numerical solution of integral equation of radiation transport in a cavity of revolution. VANT. Ser. Met. i Progr. Chisl. Resh. Zad. Mat. Fiziki. 1988. №.2. P.78-79.
4. Demytyev Yu. A., Mashinin R. F., Mironova V. F., Chentsov N.N. Approximate computation of angular distribution factors for time-dependent thermal radiation from a surface of revolution. VANT. Ser. Met. i Progr. Chisl. Resh. Zad. Mat. Fiziki. 1983. №.1(12). P.32-34.
5. Dmitriyev N. A., Sofronov I. D., Tikhomirov B. P. A technique for computation of 1D multi-region high-temperature gas dynamics problems. VANT. Ser. Met. i Progr. Chisl. Resh. Zad. Mat. Fiziki. 1983. №3(14). P.3-8.
6. V. P. Lazarchuk, M. V. Murusov, S. I. Petrov, A. V. Senik. Photochronological methods for recording space and time X ray characteristics on "ISKRA-5" facility. Fizika Plasmy. 1994. V.20. №1. P.101-106.



# COMPUTATION OF RADIATION TRANSPORT AT BOUNDARY SURFACE ANISOTROPIC LIGHT EMISSION

*S.V.Bazhenov, P.I.Pevnaya*

The technique is designed for solving the equation of radiation transport in a radiation-transparent region for the case where the distribution of radiation intensity from the boundary surface is of quite an arbitrary form. The problem solution uses a method based on employment of angular factors.

The equation of radiation exchange among boundary surfaces can be found from the expression for one-way radiation flux  $J^-$  leaving the region through its unit boundary surface

$$(1) \quad J^-(A, t) = \int_{2\pi} I(A, \bar{\Omega}, t) \mu_A d\Omega = \int_{B \in S} I(B, \bar{\Omega}, t - \frac{R_{AB}}{c}) \mu_A \frac{\mu_B dS}{R_{AB}^2}$$

where  $I$  is radiation intensity in direction  $\Omega$ ,  
 $\mu$  - cosine of the angle between the direction in which the intensity is taken and the normal to the surface.

Assuming that the boundary surfaces emit by the Lambert law, i.e. in all directions with identical intensity, the equation transfers to

$$(2) \quad J^-(A, t) = \int_{B \in S} J^-(B, t - \frac{R_{AB}}{c}) \frac{\mu_A \mu_B dS}{R_{AB}^2}$$

The system is closed with setting at the boundary of flow

$$(3) \quad J^- = \frac{\sigma c}{4} T^4 - \frac{1}{2} q$$

and balance relation  $J^- - J^+ = q$ .

To solve the problem, splitting  $S_i$  ( $i=1, \dots, M$ ) is introduced on the surface and the transition is made from integral equation (2) to equation system

$$(4) \quad S_i J_i^-(t) = \sum_{j=1}^M [A_{ij} J_j^+]|_{t-L_{ij}(t)}$$

$i = 1, \dots, M$

where matrices  $A_{ij}$  and  $L_{ij}$  are geometrical integrals

$$A_{ij} = \frac{1}{\pi} \int_{A \in S_i} \int_{B \in S_j} \frac{\mu_A \mu_B}{R_{AB}^2} dS_A dS_B, \quad L_{ij} = \frac{1}{\pi c A_{ij}} \int_{A \in S_i} \int_{B \in S_j} \frac{\mu_A \mu_B}{R_{AB}} dS_A dS_B.$$

When deriving the computational scheme we will base on the assumption that in equations (1) and (2) integration can be done over the surface  $S(t)$ .

In most cases this assumption secures a high accuracy as the boundary surface motion velocity is much higher than light velocity  $C$ .

Let the solution is sought for at time  $t^{n+1}$ .

The left-hand side of equation (3), given multiplied by the timestep  $\tau$ , provides the radiation energy flux flowing out of the region through the surface  $S_i$  per computational timestep

$$(5) \quad S_i^{n+1} J_i^{n+1} \tau = \int_{t^n}^{t^{n+1}} S_i J_i^- dt$$

According to the assumption of integration over the surface  $S(t)$  at time  $t^{n+1}$  at the surface  $S_i$  the radiation arrives which left the surface  $S_j$  at time  $t^{n+1} - L_{ij}^{n+1}$  and at time  $t^n$  at the surface  $S_i$  the radiation arrives which left the surface  $S_j$  at time  $t^n - L_{ij}^n$ .

Hence, during the time interval  $(t^n, t^{n+1})$  at the surface  $S_i$  the radiation arrives which left the surface  $S_j$  within the time interval  $(t^n - L_{ij}^n, t^{n+1} - L_{ij}^{n+1})$ .

And the natural formula for each addend in the right-hand side of system (4) is of the form

$$(6) \quad \left[ A_{ij} J_j^- \right] \Big|_{t-L_{ij}^n} = \frac{1}{\tau} \int_{t^n - L_{ij}^n}^{t^{n+1} - L_{ij}^{n+1}} A_{ij}(t) J_j^+(t) dt.$$

If at computing the integral in (6) one accurately uses the principle like in formula (5), i.e. if one assumes the integrand constant and equal to its value at time  $t^{k+1}$  at each timestep  $(t^k, t^{k+1})$ , then from equation system (4) strict conservativeness of the scheme

$$-\sum_{i=1}^M S_i^{n+1} q_i^{n+1} \tau = E^{n+1} - E^n$$

follows, where  $E^{n+1}, E^n$  is radiation energy in the region at times  $t^{n+1}, t^n$ .

$$E(t^{n+1}) = \frac{1}{c} \int_{A \in S} \int_{2\pi} \left( \int_{t^n - L_{ij}^{n+1}}^{t^{n+1}} I(A, \Omega, t) dt \right) \mu_A d\Omega dS = \sum_{i=1}^M \sum_{j=1}^M \int_{t^{n+1} - L_{ij}^{n+1}}^{t^{n+1}} A_{ij} J_j^- dt$$

Many computations used the Lambert distribution when solving the kinetic equation of radiation transport on the region boundary.

The basis for this is the fact that heat flows to the region walls composed, as a rule, of low-transparency materials are noticeably less than emission of the absolutely black body, i.e.

$$|q| \ll \frac{\sigma c}{4} T^4.$$

At the same time, in many problems there were boundary surface areas where the radiation passage to the region considerably differed from the Lambert distribution.

Indeed, in the computations the vacuum regions can border low-density and fairly radiation-transparent regions energy release from which is computed in the diffusion approximation.

Using the Lambert distribution at the interface between the vacuum and such fairly transparent regions inevitably leads to loss of local approximation in the computation on separate boundary surface areas, and the question of necessity to estimate the region of effect of the errors made inevitably arises.

In practice this was expressed in the fact that, instead of the Lambert distribution,  $I(A, \bar{\Omega}, t) \equiv \frac{1}{\pi} J^+(A, t)$ , relationships of the form

$$I(A, \mu, t) = \frac{1}{\pi} \sum_{k=0}^N F_k \mu^k, \quad N \leq 2$$

or  $I(A, \mu, t) = \frac{1}{\pi} F_0 f(\mu, t),$

are admissible on the boundary surface,  $f(\mu)$  is an arbitrary given function  $\mu$  satisfying the normalization condition

$$\frac{1}{\pi} \int_{2\pi} f(\mu) \mu \, d\Omega = 1$$

To close setting up the problem, functions  $F_k$  are assumed known functions of  $T'$  and heat part of flow  $q_1$ :

$$F_k = AF_{k1} T' - AF_{k2} q_1 + AF_{k3}$$

where  $AF_{kj}$  are known functions of coordinates, time.

The so-called "heat" flow  $q$  is assumed composed of two components: actually heat part of flow  $q_1$  and other losses of energy  $q_2$ , e.g., kinetic energy, etc.

$$q = q_1 + q_2$$

The relation between one-way radiation fluxes takes the form

$$J^- = J^+ + q_1 + q_2$$

Division of the energy flow  $q$  through the boundary region into two components seems justified for the reason that the principal formula for  $J^+$  which is always used in the computations is obtained under the assumption that the following expansion takes place for the region wall temperature:

$$T'(x) = T_G' + \frac{\partial T'}{\partial x} x$$



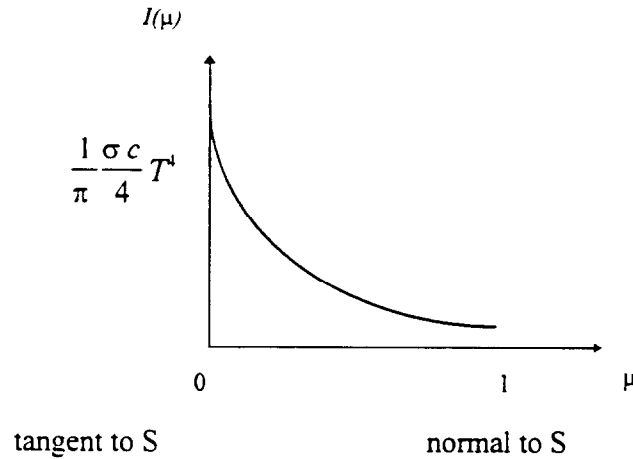
Estimation of emission of the material behind the wall into the region, i.e. of flux  $J^+$ , reduces to integration of the function  $T'(x)$  over the wall material.

The integral of the first addend yields  $\frac{\sigma c}{4} T^4$  and that of the second addend does  $1/2q$ .

From the form of the expansion for  $T'(x)$  it is clear that the second addend is only related to presence of the temperature gradient in the wall material, i.e. only to the thermal flow part.

In particular, note that using the expansion for  $T'(x)$  leads not to the Lambert distribution, but to the formula  $I(A, \mu, t) = \frac{1}{\pi} \left( \frac{\sigma c}{4} T^4 - \frac{3}{4} q_1 \mu \right).$

In our opinion, the need of the quadratic addend in the intensity formula is due to the fact that, as the computations showed, the emission intensity dependence of the wall material on  $\mu$  at the initial phase of its heating is not described with a linear function and is of the form



Using the intensity formulas leads to the equation system

$$S_i (J_i^* + q_{1i} + q_{2i}) = \sum_j^M \sum_{k=0}^N [A_{kij} F_{kj}] \Big|_{t=L_{ij}}$$

where  $A_{kij}$ ,  $L_{kij}$  are geometrical integrals. In the integrand numerator additional multipliers  $\mu_B^k$  or  $f(\mu_B)$  appear, depending on the formula used for the emission intensity.

$$E(t^{n+1}) = \frac{1}{c} \int_{A \in S_{2n}} \int_{t^n - L_{ij}^{n+1}}^{t^{n+1}} I(A, \Omega, t) \mu_{ij} d\Omega dS = \sum_{i=1}^M \sum_{j=1}^M \sum_{k=1}^N \int_{t^n - L_{ij}^{n+1}}^{t^{n+1}} A_{kij} F_{kj} dt$$

The above-discussed approach for provision of scheme conservatism and accounting boundary surface radiation anisotropy is implemented in the RADIBS code.

## Reference

Yu.Babaev, S.V.Bazhenov, A.A.Bazin, E.G.Vasina, V.V.Gorev, Yu.A.Dement'ev, V.G.Zagrafov, E.A.Karpovcev, A.I.Kirillov, V.F.Mironova, P.I.Pevnaja, P.A.Perepelkin, G.I.Skidan, I.D.Sofronov, B.P.Tihomirov, E.N.Tihomirova, N.I.Yurina.

VNIIEF techniques and codes for solution of non-stationary 2D and 3D problems of radiation energy transport in domains of complex shape using view factors. Conversion applications problems.

VANT. Ser. Mathematical Modelling of Physical Processes. I.4, 1995, p.38.

# DIFFERENCE SCHEME CONSTRUCTION FOR COMPUTING 2D TIME-DEPENDENT ELASTIC-PLASTIC FLOWS BASING ON THE LAW OF KINETIC AND INTERNAL ENERGY INTERCONVERSION

VNIIEF, Arzamas-16

Delov V.I., Senilova O.V., Sofronov I.D.

## SUMMARY

The Wilkins scheme /1/ is widely used presently for computations of 2D and 3D continuum gas-dynamical flows in Lagrangian variables. This scheme possesses a number of positive features, however, also has its disadvantages. A number of papers are devoted to its development, as well as description of its application results. The proposed technique for difference scheme construction can be used to eliminate one of the principal drawbacks of the Wilkins scheme in the case of axial symmetry relating to its non-conservation of total energy.

In the presentation the difference schemes for computing 2D time-dependent elastic-plastic flows are constructed in two stages:

At the first stage the conservative differential-difference representations of the equations of motion are derived which describe isotropic axisymmetric time-dependent elastic-plastic flows in Lagrangian variables. The technique under discussion is an extension of the 2D technique for construction of spatial approximations of gas dynamics equations of motion /2/, /3/ for elastic-plastic media. Its distinctive feature is simplicity and fast derivation of the differential-difference equations of motion which are close in their structure and quality to the equations derived using variational approaches.

At the second stage the time discretization of obtained differential-difference equations at the second approximation order is made.

## DERIVATION OF DIFFERENTIAL-DIFFERENCE EQUATIONS OF MOTION

To obtain the differential-difference equations of motion primarily in the region of variation of variables  $(x,y)$  at the initial time it is necessary to choose the approximating grid. Here we restrict our consideration to regular grids. The volume of an elementary tetrahedral grid cell whose sides are straight line segments is evaluated as volume of a body produced by revolution about the axis  $Ox$ .

The grid space distribution of the values is taken as it is a practice in the technique "D" /4/: the velocity and coordinate values are related to the grid nodes and all remaining values to the computational cell centers.

Then the kinetic energy matrix and difference representations of the deformation rate tensor components are determined.

In the presented work the kinetic energy matrix determining the pressure gradient approximation technique is taken in the canonical form which is conventionally used in gas-dynamical techniques. Then the kinetic energy of elementary cell  $i$  is of the following form:

$$K_i = 0.125 \cdot M_i \sum_{j=1}^n (u_j^2 + v_j^2)_i,$$

where  $j$  - the number of the cell vertex,  $M_i = \rho_i V_i$  - mass of the  $i$ -th cell,  $\rho_i$  - material density in the elementary volume,  $V_i$  - the cell volume,  $u, v$  - velocity vector projections on the coordinate axes  $Ox, Oy$ , respectively.

The next step is recording the law of conservation of total energy for the whole computational cell set. Then, taking into account the law of internal energy variation, the law of variation in kinetic energy of the whole elementary volume system under consideration is traced out. Upon transition in the obtained relation to summation over the grid nodes, the differential-difference equations of motion are determined.

## TIME DISCRETIZATION

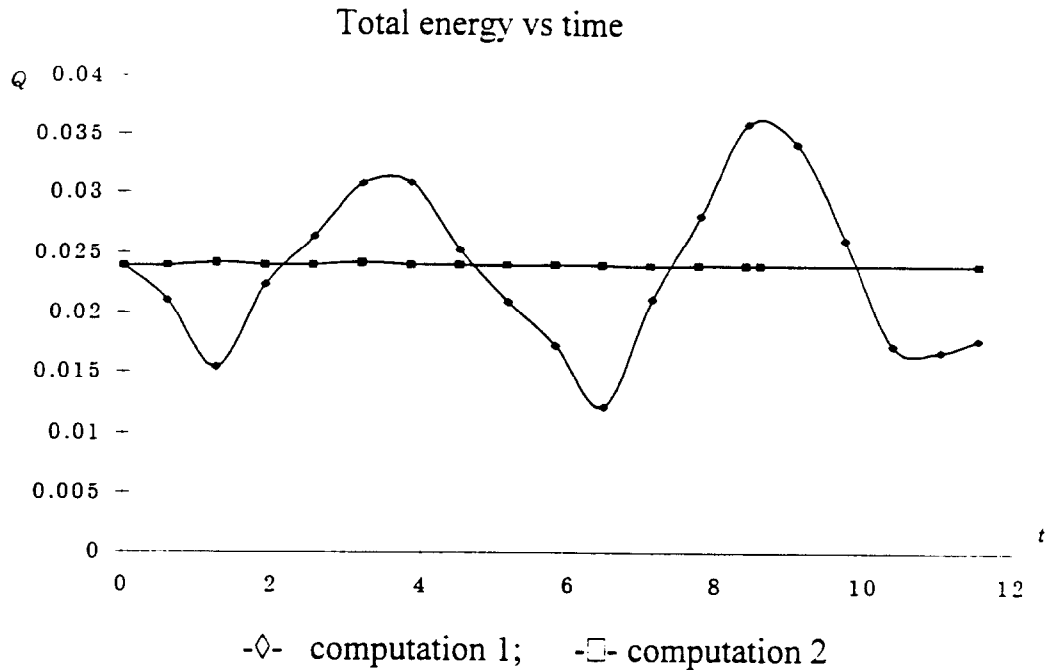
At construction of the proposed difference scheme the grid time distribution of the values is taken as it is a practice in the technique "D": the velocity values are related to half-integer points in time  $t^{n+1/2}$  and all remaining values to integer points in time  $t^n$ , i.e. the time derivatives are approximated within the second order of accuracy.

The increments of the components of the strain tensor per timestep, stress tensor deviator at time  $t^{n+1}$  and the shear strain energy increment are determined according to the Wilkins scheme.

## TEST COMPUTATIONS

The results of two test computations are reported. The problem of planar stress wave in 2D axisymmetric formulation is taken for the first problem. The second problem of elastic membrane vibrations is used as a basis to show the unquestionable advantage of the obtained difference scheme over the classic Wilkins scheme. The figure below illustrates the time history of the plate

total energy which should remain constant in the computation by the Wilkins scheme (computation 1) and by the proposed difference scheme (computation 2)



## REFERENCES

1. Wilkins M.L. Computation of elastic-plastic flows. In: Computational methods in hydrodynamics. Moscow, Mir Publishers, 1967. P.212-263.
2. Isayev V.N., Sofronov I.D. Construction of gas dynamics equation discrete models basing on the laws of continuum kinetic and internal energy interconversion. VANT. Ser.Met. i Progr. Chisl. Resh. Zad. Mat. Fiziki, 1984, No.1(15), p.3-7.
3. Delov V.I., Isayev V.N., Sofronov I.D. Conservative and invariant differential-difference representations of gas dynamics equations in the axisymmetric case. VANT. Ser.Met. i Progr. Chisl. Resh. Zad. Mat. Fiziki, 1987, No.1, p.3-10.
4. Dmitriyev N.A., Dmitriyeva L.V., Malinovskaya E.V., Sofronov I.D. A technique for computing time-dependent 2D gas dynamics problems in Lagrangian variables. In: Theoretic fundamentals and construction of numerical algorithms for computational physics problems/ Ed.by Babenko K.I. Moscow, Nauka Publishers, 1979, p.175-200.



# EFFICIENT SINGLE SCATTER ELECTRON MONTE CARLO

M.M. Svatos and J.A. Rathkopf

Lawrence Livermore National Laboratory  
Livermore, CA 94550

## ABSTRACT

A single scatter electron Monte Carlo code (SSMC), CREEP, has been written which bridges the gap between existing transport methods and modeling real physical processes. CREEP simulates ionization, elastic and bremsstrahlung events individually. Excitation events are usually treated with an excitation-only stopping power, although simulation of individual excitation events is possible. Agreement of these quantities with experimental values is generally quite good.

One application of this code is the generation of probability distribution functions (PDFs) to describe the phase space of a single electron emerging from a sphere of a given material and radius. A library of data sets for such spheres (or "kugels") is being computed for a variety of incident energies, material types, and sizes. The final goal of this work is to achieve extremely accurate transport results with an efficiency that is similar to that of condensed history methods.

## 1 Introduction

Single scatter Monte Carlo (SSMC) physics is gaining attention for electron transport, despite the fact that it is inherently very time consuming. One reason is that since single scatter calculations conform more closely to the physical processes the electron undergoes, they can serve as a means to explore the validity of assumptions used in other transport techniques. The results of SSMC can also be tallied and fed into a more efficient code.

SSMC allows large angle scatter and backscatter measurements to be calculated with greater accuracy in a reliable manner. Large angle scatter and backscatter, being relatively rare, result in much of the seemingly eccentric energy deposition behavior of electron beams (and photon beams for that matter, since photons deposit their energy to the medium through secondary electrons), including lateral blooming with distance and nonuniformities ("hot" or "cold" spots) found near changes in the medium type or density.

CREEP relies on sampling the Lawrence Livermore Evaluated Electron Data Library (EEDL), which was established at LLNL by 1990 to complement the ENDL (Evaluated Nuclear Data Library) and EPDL (Evaluated Photon Data Library). Complete documents detailing its contents, with derivations, are available [1-3]. Cross sections for ionization (by subshell), elastic scatter, bremsstrahlung, and excitation are tabulated on an energy grid with a variable placement of points between 10 eV and 100 GeV, for atomic numbers 1 to 100. Compounds and mixtures may also be used by combining the appropriate element data via Bragg additivity.

One important application of SSMC is to use it as a foundation for other more efficient methods. This has been called a Local-to-Global approach. It works by breaking the calculation into two stages: a local calculation (SSMC) done over small geometries having the size and shape of the "steps" to be taken through the mesh; and a global calculation which relies on a stepping code that samples the stored results of the local calculation. An example of an SSMC-based Local-to-Global code will be introduced in Section 4.

## 2 Single Scatter Monte Carlo Code

The CREEP code is written in FORTRAN and C, in a very simple style with the intent of being extremely portable. Since this code is intended primarily as a means to explore basic physical properties of the

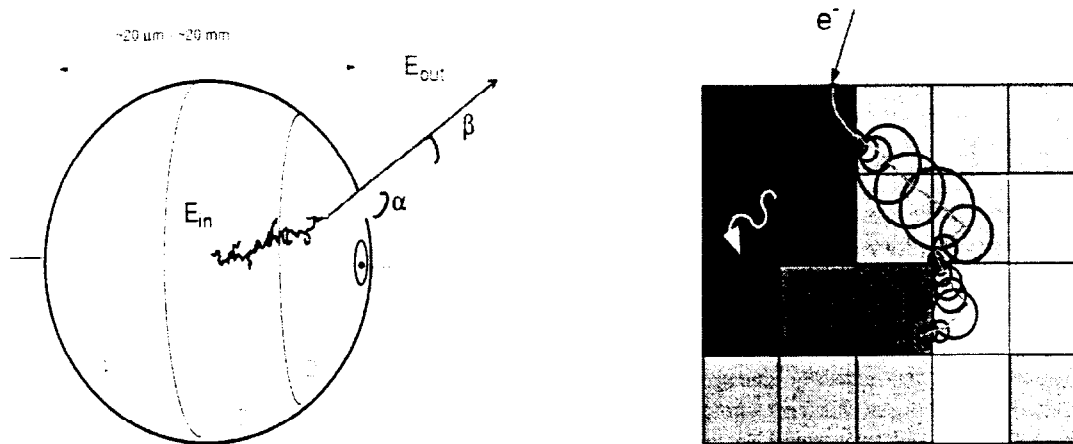


Figure 1: LEFT: The geometry of the local calculation. RIGHT: An example global calculation.

medium. only simple geometries are assumed: either spherical or slab or a slab layered with different materials.

The overall algorithm for a truly single scatter charged particle code is a direct analog of the algorithm that has historically been used in photon and neutron Monte Carlo codes. Briefly, one finds the distance to interaction by finding the total cross section at the present energy and uses the relation  $s = -\lambda \ln(\eta)$ , where  $\eta$  is a random number on the interval  $(0, 1]$ . One then determines which interaction took place, by forming and sampling from a cumulative probability based on the cross sections for each of the four possible interactions (ionization, excitation, elastic scatter, bremsstrahlung). The energy, position and trajectory of the particle are updated to reflect the chosen interaction. Then the same process is begun again, provided the electron has not escaped the medium or fallen below the energy cutoff.

### 3 Results from Single Scatter Monte Carlo

Benchmarking this code with experiment for a variety of elements and select compounds and mixtures, over the energy range of the EEDL database, is a large effort that is still in its infancy.

Historically, backscatter has been difficult for condensed history codes to simulate correctly. Figure 2 shows two examples of backscatter information generated by CREEP compared to experimental values. The agreement is generally quite good.

Comparisons of the CREEP single scatter Monte Carlo (SSMC) code with energy deposition measurements are shown in figure 2. Agreement to experiment is generally quite good for a variety of materials, incident energies, and incident angles. The curves did not require normalization.

In addition to the preceding quantities, CREEP also calculates analog stopping powers (the amount of energy lost per unit distance for both radiative and collisional events), energy deposits due to individual interaction types, and "real" pathlength (cumulative distance between events) which can be used to calculate detour factors (the ratio to the real range compared to the CSDA range).

Obtaining these results is time consuming. Some timings are shown in Table 1. In general, the simulation time increases with the number of histories, the geometry size, and as the energy threshold is lowered.

Table 1: Timings for several CREEP runs on a SunSparc 20 running Solaris OS 2.51. Each medium was a slab of 1 mm thick. Results for the number of interactions, the number of calls to the random number generator (RNG), and the user time are normalized per incident history.

Medium	Density (g/cc)	Interactions	RNG calls	User Time (s)	Ratio
H	$1 \times 10^{-4}$	0.667	8	$2.52 \times 10^{-4}$	1
O	$1.4 \times 10^{-3}$	5.098	39	$1.77 \times 10^{-3}$	7.02
Na	1.0	6714	48001	1.35	5357
$H_2O$	1.0	8057	71714	3.30	13095
Au	19.3	19810	145541	6.98	27698

All of these require more interactions to be simulated. The version of the code which includes compounds and mixtures is also notably slower than the single-element versions. Table 1 gives some feel for how the run time scales with different media.

Clearly if this method is to become practical, there must be a means for a radical speed-up in the execution time. Such a means has been suggested in the Local-to-Global algorithm. [7]

## 4 Using Single Scatter Results in Local-to-Global Transport

In this application, the local calculation is an SSMC (CREEP) run performed in small spheres of various materials. The electron is started in the center and tracked until it crosses the surface of the sphere, at which time the following state variables are tallied: exit energy, exit "position cosine" ( $z/R$ ), elevation angle ( $\beta$ ) and swing angle ( $\alpha$ ) of the trajectory in the exit plane, and the number of secondary particles it set in motion that also escaped the sphere. The sphere, or kugel, is also divided into four surface bands; each band has its tallies kept separately. This geometry is illustrated in figure 1. After many histories, these tallies result in probability distribution functions (PDFs), each having 100 equally-spaced bins, that may be sampled by the global calculation. Knock-on electrons that escape, as well as all photons, are kept in separate distributions.

The global geometry for cases of interest is divided into voxels of varying density and material type. An example is shown in figure 1. For each history, a kugel of appropriate size and incident energy is chosen from the library and centered on the electron's location. The exit conditions are then sampled from that kugel's PDFs, starting with the exit band  $b$ , on which the other variables depend. The exit energy is then sampled, which sets the (target) energy loss,  $E_{loss} = E_{in} - E_{out}$ . The exit trajectory is determined by sampling two correlated angles,  $\alpha$  and  $\beta$ , from which three correlated direction cosines can be obtained. The target exit position on the sphere is found by sampling the  $z$  coordinate, and then randomizing  $x$  and  $y$  on the  $z$ -ring. This exit point is used to define the endpoint of a vector which starts at the center of the kugel. It is along this projected pathlength vector that  $E_{loss}$  is deposited. Since a kugel can be larger than a transport zone, the energy deposited in each zone is scaled by two factors: the fraction of the projected pathlength vector through the zone, and the density of the zone. If the density of a zone is greater than the nominal density that was used in the global calculation, the energy will be deposited before the edge of the kugel was reached; thus a new exit position is found along the same trajectory, but closer to the center (or vice versa for a less dense region). If a new material is encountered during the energy deposition scheme, the step is stopped at the boundary, and only the energy deposited up to that point is subtracted from  $E_{in}$ . The next step is taken in the new material.

After each kugel step, the average number of secondary electrons escaping from (anywhere on) the kugel is sampled,  $n_e$ , given that the primary escaped from band  $b$  with exit energy  $E_{out}$ . The state variables for  $n_e$  secondary electrons are then sampled in a manner exactly like that above, but the results are taken from

the secondary electron distributions. The same is done for photons, which are not tracked, but passed off to another code for transport.

## 5 Summary

Single scatter Monte Carlo provides the most accurate way to simulate electrons, however it is too slow to be practical for general use. It is possible to have a code with both speed and accuracy by using the Local-to-Global method of precalculating distributions. A current implementation of this algorithm uses approximately  $5 \times 10^4$  bytes per kugel PDF set. If the application can be defined by a limited number of materials and step sizes, the total amount of storage is quite feasible.

The speed-up in the global calculation comes from needing a fewer number of steps per history and also a fewer number of operations per step. The accuracy converges to that of the local SSMC calculation as many histories are run, provided the PDF sampling routine is faithful. Further investigation as to the degrees of speed-up and accuracy in various geometries is an ongoing effort.

This work was performed under the auspices of the U.S. Department of Energy by the Lawrence Livermore National Laboratory under contract number W-7405-ENG-48.

## References

- [1] D.E. Cullen and S.T. Perkins. *The Livermore Bremsstrahlung Database*. UCID-21627, 1989. Lawrence Livermore National Laboratory.
- [2] S.T. Perkins and D.E. Cullen. *The Livermore Electron Impact Ionization Database*. UCID-21628, 1989. Lawrence Livermore National Laboratory.
- [3] S.T. Perkins and D.E. Cullen. *The Livermore Electron Elastic Scattering Database*. UCRL-ID-103170, 1990. Lawrence Livermore National Laboratory.
- [4] G.J. Lockwood, L.E. Ruggles, G.H. Miller, and J.A. Halbleib. *Calorimetric Measurement of Electron Energy Deposition in Extended Media - Theory vs Experiment*. Sandia Report SAND79-0414, 1980.
- [5] E.H. Darlington. *Backscattering of 10-100 keV electrons from thick targets*. *J. Phys. D Appl. Phys.*, 8:85-93, 1975.
- [6] G. Neubert and S. Rogaschewski. *Backscattering Coefficient Measurements of 15 to 60 keV electrons for Solids at various angles of incidence*. *Phys. Stat. Sol.*, 59:35-41, 1980.
- [7] M.M. Svatos, C.T. Ballinger, H. Neuenschwander, T.R. Mackie, W.P. Chandler, C.L. Hartmann Siantar, J.A. Rathkopf, and P.J. Reckwerdt. *Electron Transport in Radiotherapy using Local-to-Global Monte Carlo*. In *Proceedings of the International Conference on Mathematics and Computations, Reactor Physics, and Environmental Analyses*, pages 866-875. La Grange Park, IL, 1995. American Nuclear Society, Inc.

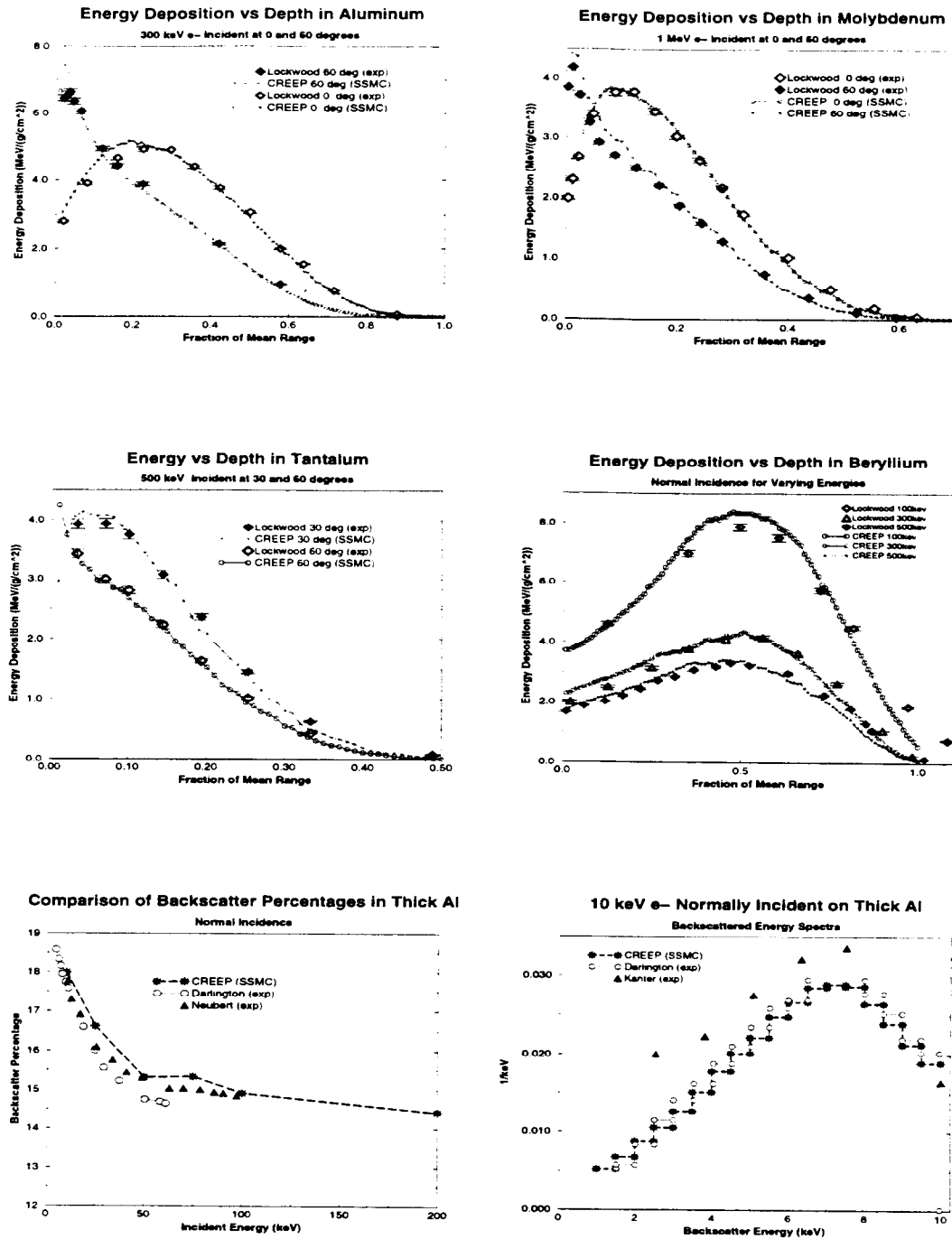


Figure 2: TOP and MIDDLE: Energy deposition is shown as a function of depth into the medium, where the depth has been normalized to the CSDA range of the electron in each case. The points attributed to Lockwood *et al* are from calorimetric measurements [4]; the comparisons are absolute. BOTTOM LEFT: CREEP backscatter percentage (including backscattered secondary electrons) compared to the experiments of Darlington *et al* [5] and Neubert *et al* [6]. BOTTOM RIGHT: The backscattered energy spectrum resulting from a 10 keV electron impinging on an aluminum slab that is large in x, y, and z compared to the mean free path of the incident electron.



# THE ENERGETIC ALPHA PARTICLE TRANSPORT METHOD EATM

Ronald C. Kirkpatrick

Los Alamos National Laboratory

**Abstract:** The EATM method is an evolving attempt to find an efficient method of treating the transport of energetic charged particles in a dynamic magnetized (MHD) plasma for which the mean free path of the particles and the Larmor radius may be long compared to the gradient lengths in the plasma. The intent is to span the range of parameter space with the efficiency and accuracy thought necessary for experimental analysis and design of magnetized fusion targets.

## Introduction

There have been several methods applied to the problem of energetic charged particles (e.g., 3.5 MeV DT alpha particle) transport in unmagnetized fusion plasmas [1-4] as well as heavy ion transport in high-Z radiation converters for ion beam fusion targets [5]. In addition, the magnetic confinement fusion community has treated the problem of transport through very tenuous plasmas in the presence of magnetic fields [6-8]. However, the problem of energetic charged particle transport in a relatively dense, dynamic magnetized plasma has not been adequately explored. The research code EATM is an evolving attempt to find an efficient method of treating the transport of energetic charged particles in a dynamic magnetized (MHD) plasma for which the mean free path of the particles and the Larmor radius are initially long compared to the gradient lengths in the plasma.

The intent of this work is to span the range of parameter space with the efficiency and accuracy thought necessary for experimental analysis and design of magnetized fusion targets. Magnetized target fusion (MTF) [9] attempts to take advantage two benefits of the magnetic field in order to lower the driver requirements for fusion ignition: reduction of thermal conduction across the field and turning of the charged fusion reaction products. It is the second of these benefits that the EATM transport method is intended to elucidate.

One of the earliest examples of MTF targets is the Sandia National Lab Phi-target, devised in 1977 [10-11]. About the same time Los Alamos National Laboratory (LANL) was exploring the Fast Liner concept [12], a larger cylindrical embodiment of MTF, and more recently Los Alamos and the All-Russia Scientific Institute for Experimental Physics (VNIIEF) have collaborated on the MAGO experiments that are intended to study target plasma formation for MTF [13].

The EATM approach is as follows: Use piecewise analytic solutions and transformations to build transport matrices for a range of single computational cell parameters. Then use these matrices to effect the transport throughout the computational mesh. This approach should be most applicable to codes with fixed orthogonal meshes such as Eulerian algorithms or AMR codes. An important property is correct asymptotic behavior for two extreme cases: a) no field and b) zero density. Between these extremes it is necessary to obtain some benchmark for the method. One benchmark is the results of a particle tracking code that has been we have been using to acquire some preliminary results for various static magnetized plasma configurations. The particle tracking code could be extended to dynamic plasmas, but it becomes expensive for complicated configurations.

## Uniform Zone Results

For the case of slowing due to both electrons and ions

$$dE/ds = -b_i E^{-1} - b_e E^{-1} G(x) \quad ,$$

where  $E$  is the particle energy,  $s$  is the distance traversed,  $b_e$  and  $b_i$  are coefficients that depend on the plasma temperature and density,  $x^2 = m_e E / (m kT_e)$ ,

$$G(x) = 2\pi^{-1/2} \operatorname{erf}(x) - (1 + m_e/m) x \exp(-x^2) \\ \approx F^3 / (F^3 + a^3) ,$$

Here we define  $F = E^{1/2}$  and  $a^2 = m kT_e / m_e$ . A factor similar to  $G(x)$  also occurs for the ions, but only near background ion thermal energies does it differ from unity.

By resorting to the above simple approximation for  $G(x)$ , it is possible to get an analytic result for the energy of the particle as a function of time:

$$\Phi e^\Phi = \Phi_0 e^{\Phi_0} e^{-\nu\tau} ,$$

where  $\Phi = (F^3 + H^3) / (\alpha - 1)H^3$ ,  $H^3 = a^3 b_i / (b_i + b_e)$ ,  $\alpha = b_i / (b_i + b_e)$ , and  $\tau = 2 (m/2)^{1/2} a^3 b_e / 3 (b_i + b_e)^2$ . In the fast electron limit  $G(x) \approx F^3 / a^3$ , so that the above result reduces to the form

$$\Phi = \Phi_0 e^{-\nu\tau} .$$

However, for plasma electron temperatures near 1 KeV and below, the fast electron approximation can lead to very large errors, so it is important to avoid this approximation if results that are valid over a wide range of plasma temperatures are desired.

The time interval for slowing from  $F_0$  to  $F$  is

$$t = \tau \{ \ln [(F_0^3 + H^3) / (F^3 + H^3)] + (F_0^3 - F^3) / (\alpha - 1)H^3 \} .$$

The above analytic results apply to the slowing of the DT alpha in a homogeneous medium for any constant value of magnetic field  $B$ . There is an energy dependence in the coulomb logarithm for the ions which was not included in derivation of the analytic results above, so for evaluation of the constant  $b_i$  some mean energy such as  $FF_0$  must be used.

These analytic results connecting  $t$ , and  $E$  (hence  $s$  and  $v$ ) are very useful for facilitating numerical integration and for characterizing the DT alpha trajectory in a uniform computational zone. A table of  $t(F)$  is easily calculated to provide  $\vec{F}(t)$ . It should be noted that direct numerical integration of  $dE/dt = v dE/ds$  can both avoid use of the  $G(x)$  approximation as well as include the dependence of the ion Coulomb logarithm on the energy  $E$ .

In an  $(x,y)$  plane with  $B = B_z$  and  $v_z = v \cos \phi$ , where  $\tan \phi = v_{xy} / v_z$ ,

$$x = \int v_{xy} \sin \omega t dt, \quad y = \int v_{xy} \cos \omega t dt, \quad \text{and } z = \int v_z dt ,$$

where  $v_z = (2/m)^{1/2} F \cos \phi$  and  $v_{xy} = (2/m)^{1/2} F \sin \phi$ .

For slowing by electrons only ( $b_i = 0$ ), these integrals have analytic forms, but for  $b_i > 0$  we have not found an analytic. However, the problem reduces to numerically integrating two functions:

$$\text{sinf}(\theta) = \int f(\theta) \sin \theta \, d\theta \quad \text{and} \quad \text{cosf}(\theta) = \int f(\theta) \cos \theta \, d\theta .$$

where  $\theta = \omega t$  and  $f(\theta)$  is the inversion of

$$\theta(f) = \ln [(f_0^3 + h^3) / (f(\theta)^3 + h^3)] + (f_0^3 - f(\theta)^3) / (\alpha - 1)h^3 .$$

Using a piece-wise linear fit to  $f(\theta)$  allows a piece-wise analytic integration to be carried out to an accuracy that depends only on the step size  $\Delta\theta$  used:

$$\int (c + b \theta) \sin \theta \, d\theta \approx \Sigma \Delta \{ -c \cos \theta + b \sin \theta - b \theta \cos \theta \}$$

and 
$$\int (c + b \theta) \cos \theta \, d\theta \approx \Sigma \Delta \{ c \sin \theta + b \cos \theta + b \theta \sin \theta \} .$$

Only two numerical calculations are needed for a given homogeneous zone, because the transformation properties for the functions  $\text{sinf}(\theta)$  and  $\text{cosf}(\theta)$  allow the results of the two numerical integrations to be reused over and over for many trajectories through that zone.

### Transformation

The integrals  $\text{sinf}(\theta)$  and  $\text{cosf}(\theta)$  to get  $\text{sinf}'(\theta)$  and  $\text{cosf}'(\theta)$  for which the starting value  $f_0'$  differs from  $f_0$  can be transformed thus (see Figure 1):

$$\begin{aligned} \text{sinf}' &= (\text{cosf} - \text{cosf}_i) \cos \theta_i + (\text{sinf} - \text{sinf}_i) \sin \theta_i & \text{and} \\ \text{cosf}' &= (\text{sinf} - \text{sinf}_i) \cos \theta_i - (\text{cosf} - \text{cosf}_i) \sin \theta_i , \end{aligned}$$

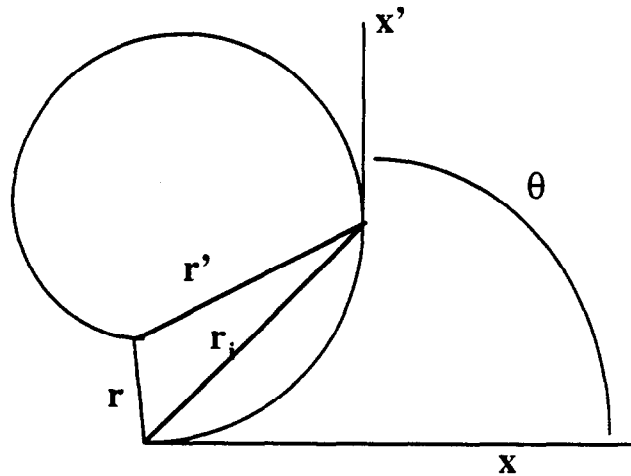


Figure 1. The trajectory in the primed coordinate system is obtained by transforming the trajectory calculated for the original coordinate system.

$$\begin{aligned} \text{where } \text{sinf} &= \text{sinf}(f_0, h, a, \theta), & \text{cosf} &= \text{cosd}(f_0, h, a, \theta), \\ \text{sinf}_i &= \text{sinf}(f_0, h, a, \theta_i), & \text{cosf}_i &= \text{cosd}(f_0, h, a, \theta_i), \\ \text{sinf}' &= \text{sinf}(f_0', h, a, \theta), & \text{cosf}' &= \text{cosd}(f_0', h, a, \theta), \end{aligned}$$

## Crossing Time

It is possible to calculate the time when the DT alpha particle crosses a specified plane. For simplicity the case of slowing by electrons only ( $b_i = 0$ ) is used to illustrate the procedure. For the magnetic field in the z direction and the x direction in the direction of  $\mathbf{v} \times \mathbf{B}$ , the path of a DT alpha particle entering a homogeneous region at the origin will be:

$$x(t) = v_{y0} \tau ( \omega \tau - e^{-\omega \tau} ( \sin \omega t + \omega \tau \cos \omega t ) ) / (1 + \omega^2 \tau^2)$$

$$y(t) = v_{y0} \tau ( 1 - e^{-\omega \tau} ( \cos \omega t - \omega \tau \sin \omega t ) ) / (1 + \omega^2 \tau^2)$$

$$z(t) = v_{z0} \tau ( 1 - e^{-\omega \tau} ) .$$

The equation for a plane in that coordinate system is  $A x + B y + C z = D$ , where  $A = d_x/d$ ,  $B = d_y/d$ ,  $C = d_z/d$ , and  $D = d$ . Here,  $d$  is the distance between the point of entry into a computational cell at (0,0,0) and the plane defining one side of the cell.

Defining the coefficients:  $C_1 = ( v_{y0} \tau (A \omega \tau + B) + C v_{z0} \tau - D )$ ,  $C_2 = v_{y0} \tau A / C_1 (1 + \omega^2 \tau^2)$ ,  $C_3 = v_{y0} \tau B / C_1 (1 + \omega^2 \tau^2)$ ,  $C_4 = C v_{z0} \tau / C_1$ , solving

$$e^{-\omega \tau} [ (C_2 - C_3 \omega \tau) \sin \omega t + (C_3 + C_2 \omega \tau) \cos \omega t + C_4 ] = 1$$

for the minimum crossing time  $t$  (there are potentially several crossings), and substituting  $t$  into the above equations provides the exit point  $(x,y,z)$ . Since there are more than one plane that define the cell, the minimum time among all of them must be found.

Tables can be made for the solutions to  $e^{+a \sin \theta} = a \sin \theta + b \cos \theta + c$ , and an interpolation used to efficiently find solutions. The most convenient approach is to write the equation as

$$e^{q \theta} = a \sin \theta + b \cos \theta + c = R \sin (\theta + \gamma) + c ,$$

and then solve for  $q(\theta) = 1/\omega \tau$ , interpolating to get the  $x$  that satisfies the equation for a given  $q$ . It should be noted that since  $\omega \tau > 0$ ,  $q > 0$  for physically meaningful solutions. For a given value of  $q$  there are multiple values of  $\theta = \omega t$ . Since we want the first crossing time, we choose the smallest value. For a zone defined by multiple planes ( $A_n x + B_n y + C_n z = D_n$ ), the smallest from among all  $\omega t_n$  is selected.

This procedure can be extended to the case of slowing by ions and electrons, but becomes more complicated simply because the path for a DT alpha can't be expressed analytically for that case:

$$(2/m)^{1/2} [ \sin \phi \{ A \int F \sin \omega t dt + B \int F \cos \omega t dt \} + C \cos \phi \int F dt ] = D ,$$

which reduces to solution for  $\theta$  in an analogous equation:

$$a \operatorname{sinf}(\theta) + b \operatorname{cosf}(\theta) + c \int f(\theta) d\theta = 1 .$$

For a given zone  $f(\theta)$  is calculated first and  $\int f(\theta) d\theta$  is easily evaluated, so the functions  $\operatorname{sinf}(\theta)$  and  $\operatorname{cosf}(\theta)$  can be calculated. The transformation procedure can then be used to provide

intermediate values for these functions. Then the crossing time is obtained by solving for the smallest value of  $\theta$  that satisfies an equation analogous to the one for crossing time with slowing due to electrons only.

### Applications of the Analytic Results

The above results have two potential applications. One is in the implementation of a Monte Carlo approach to Charged particle transport. For the case of high plasma temperature such as may occur in a burning DT fusion plasma, or for very energetic particles such as the  $D^3He$  proton, the nuclear scattering cross section becomes important, because the Rutherford scattering cross section diminishes. Monte Carlo has been used in the past to obtain particle range-energy results for these cases [Evans & Talley].

The other potential application is in the construction of a database of transport matrices.

Upon specifying a zone geometry and content ( $\rho$ ,  $T_e$ , and  $B$ ), the analytic results and a single numerical trajectory calculation can be transformed repeatedly to build up a collection of weighted outgoing particle directions, energies, and times. The fractional contribution of each incoming particle to the outgoing particle in a particular distribution is used to build a transport matrix. This approach is similar to that of reference [14]. The transport matrix describes the coupling between a pair of surfaces that are part of the bounding surfaces that define the zone. Each pair of surfaces coupled will have its own matrix, so there will be several matrices per zone, as illustrated in Figure 2.

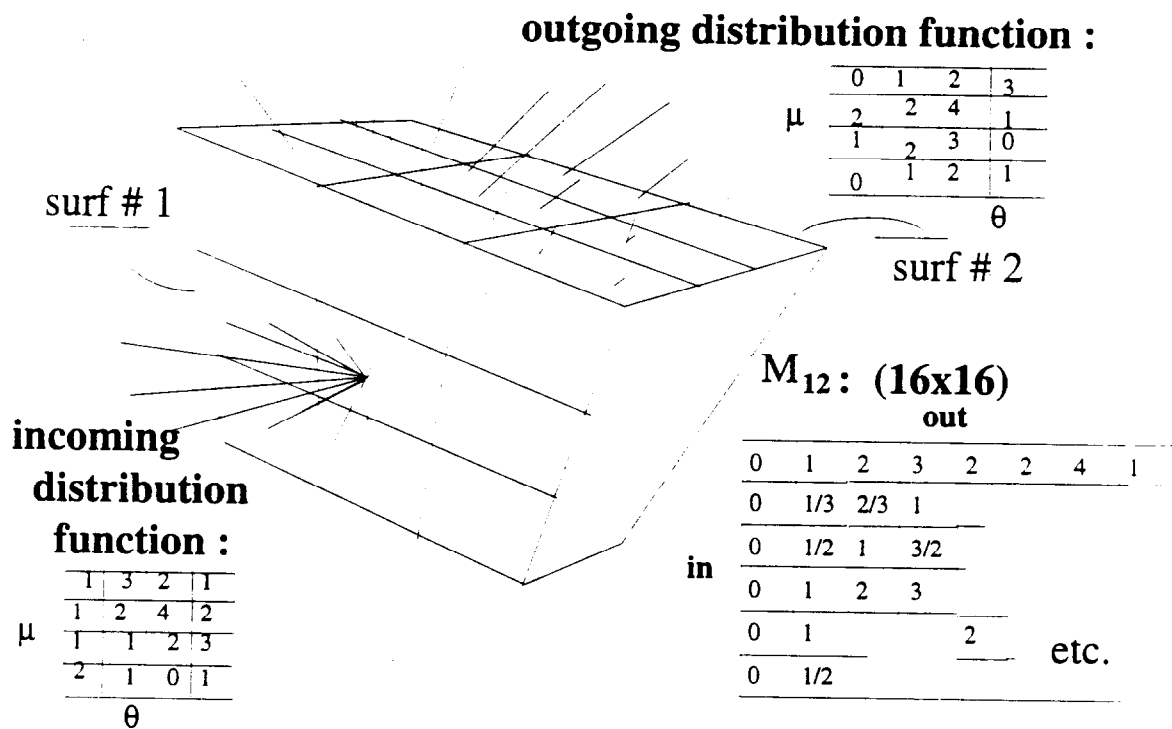


Figure 2. Building a transport matrix. The faces of the zone defined by intersecting planes is divided into several sub areas and a chosen number of trajectories are used to get the exit directions, energies, etc.

## Potential Improvement

Some improvement may be necessary to increase the flexibility of the above results. The analysis of the DT alpha trajectory is based on the assumption of uniform zones. It would be desirable to handle gradients in the various intensive zone quantities ( $\rho$ ,  $T_e$ , and  $B$ ). The prospect for a general analytic approach to gradients is poor, but an efficient numerical approach may be possible. The idea is to break up a zone with a gradient into several volume elements and do the transport through these zones, each of which has uniform density, temperature and field values that reflect the gradient within the parent zone. The results of two successive breakups ( $N$ ) can be extrapolated in  $1/N$  to get the result that would have been obtained for very large  $N$ . This assumes that the gradient can be approximated by many small steps. This assumption can be tested against special cases that have analytic solutions and against a particle tracking code.

## References

- [1] Foster Evans, "Note on the Calculation of Energy Deposition of Alpha Particles in a DT Plasma by Rutherford Scattering," LA-5448-MS, Los Alamos National Laboratory (1973).
- [2] R. Cooper and F. Evans, *Phys. Fluids*, 18, 332 (1975).
- [3] M. J. Antal and C. E. Lee, "Charged particle energy deposition in an inertially confined thermonuclear plasma," *Nucl. Science & Engineering*, 64, 379-383 (1977).
- [4] A. M. Oparin, S. I. Anisimov, J. Meyer-Ter-Vehn, "Kinetic simulation of DT Ignition and burn in ICF targets," *Nucl. Fusion*, 36, p. 443 (1996).
- [5] G. Maynard and C. Deutch, "Born Random Phase Approximation for Ion Stopping in an Arbitrary Degenerate Electron Fluid", *J. Physique* 46 (1985) 71.
- [6] S. Wang and L. Qiu, "Alpha Particle Classical Transport in Tokomaks," *Nuclear Fusion* 36 (1996) 557.
- [7] S.J. Zweben, et al., "Alpha Particle Loss in the TFTR DT Experiments," *Nuclear Fusion* 35 (1995) 893.
- [8] M.H. Redi, et al., "Collisional Stochastic Ripple Diffusion of Alpha Particles and Beam Ions on TFTR," *Nuclear Fusion* 36 (1996) 1193.
- [9] R. C. Kirkpatrick, I. R. Lindermuth and M. S. Ward, "An Overview of Magnetized Target Fusion," *Fusion Technology*, 27, p. 201 (1995).
- [10] M.M. Widner, "Neutron Production from Relativistic Electron Beam Targets", *Bull. Am. Phys. Soc.* 22 (1977) 1139.
- [11] I.R. Lindemuth and M.M. Widner, "Magnetohydrodynamic Behavior of Thermonuclear Fuel in a Preconditioned Electron Beam Imploded Target", *Phys. Fluids* 24 (1981) 753.
- [12] R.A. Gerwin and R.C. Malone, "Adiabatic Plasma Heating and Fusion Energy Production by a Compressible Fast Liner", *Nuclear Fusion* 19 (1979) 155.
- [13] I.R. Lindemuth et al., *Phys. Rev. Lett.* 75 (1995) 1953.

- [14] G.J. Parker, W.N.G. Hitchon, E.R. Keiter, "Transport of Ions During Implantation". Phys. Rev. E 54 (1996) 938.



## EXPLOSIVE DECELERATION AND FRAGMENTATION OF METEORITES IN ATMOSPHERE

*D.V.Petrov, O.N.Shubin, V.P.Elsukov, V.A.Simonenko,  
RFNC—VNIITF*

### ABSTRACT

At this juncture there is a series of interactions between meteorites and the atmosphere experimentally observed but remained without any coherent reasoning. First of all, it is the explosion of the Tunguska meteorite at certain height. After this explosion no meteorite matter was found. Moreover, in the Earth atmosphere one can regularly register the bursts like fire ball of a nuclear explosion yielded of 1 to 100 kilotons of trotyl [1]. This evidences that under certain conditions a physical mechanism exists which governs the explosive interaction between a meteorite and the Earth atmosphere possessing specific features of the nuclear explosion in the air or above ground. There is also no a consistent theory describing meteorite fragmentation in the atmosphere.

The work offers the theoretico-computational model describing the explosive interaction between meteorites and the atmosphere, as well as the meteorite fragmentation. Fundamental assumption of the theory are as follows. When a meteorite enters the atmosphere, it interacts with approach stream of air that results in large-scale loss of hydrodynamic stability. This causes meteorite disintegration into several approximately equal fragments. Later for each of the fragments resulted the process is repeated - one can observe a chain reaction of meteorite fragmentation, the fragments being decelerated in the atmosphere.

This physical model can lead to two consequences. In the first one, the meteorites which have rather small density and size less than critical can reach only certain critical height above the Earth surface. In this case the spatial region, where the meteorite "pieces" transfer their energy to the atmosphere during relatively short time (as compared with flight time), has the sizes comparable (with one order accuracy) with the initial dimension of the meteorite. The final size of fragments felt down onto the ground according to this scenario will apparently be defined by existence of certain minimal size of a particle and/or critical velocity of these particles in the atmosphere. Judging on result of the Tunguska explosion the final particles are of microscopic dimensions. In the second scenario, when density and dimensions are large enough, fragmentation process has no time to develop comprehensively. In this case dimensions of fragments which have achieved the ground, will be macroscopic. For example, the Sikhote-Alin event was not the explosive one.

## TABLE OF CONTENTS

1. Overview
  2. Physical Model
    - 2.1. Null Approximation
    - 2.2. Results of Mathematical Simulation
  3. Analytical Estimates
    - 3.1. Exponential Atmosphere
    - 3.2. Atmosphere of Constant Density
  4. Comparison of Analytical Estimates with Results of Mathematical Simulation
  5. Comparison of Different Models
- The Bottom Line  
Acknowledgments  
References

## 1. OVERVIEW

Currently most of researchers use as the initial hypotheses the theory of gas dynamic deceleration and ablation of meteorites in the Earth atmosphere which is described, for example, in [2]. The equations it uses are in the following form:

$$\begin{cases} M \frac{dv}{dt} = -G \rho_a S v^2 n & (1.1) \\ \frac{dM}{dt} = -\frac{\Lambda}{Q} \rho_a S v^3 & (1.2) \end{cases}$$

where  $G$ ,  $\Lambda$  are unitless coefficients,

$S$  - effective maximum midsection,

$Q$  - ablation energy of unit mass,

$M$  - meteorite mass (initial mass  $M_0$ ),

$n$  - unit vector along trajectory,

$\rho_a$  - air density,

$v$  - meteorite velocity.

In principle, the equations should contain Earth gravity, however, for considering the fundamental issues it is not principal character..

In [3] for the case of exponential atmosphere the analytical solution (1.1) in quadratures was derived for "spherical meteorite".

Let us consider the major advantages and disadvantages of the theory.

### *Advantages*

1. The theory (given appropriate choice of constants) qualitatively well describes deceleration of a single meteorite in the middle part of trajectory.

### *Disadvantages*

1. As only velocity vs. altitude is known from direct experimental observations, then there are rather great uncertainties in selection of constants in the system (1.1-1.2). This is especially actual for determining the initial dimensions, mass, and, respectively, energy.

2. As it was noted by the author of [6], the ablation equation at certain velocities contradicts to the energy conservation law.

3. The theory does not offer neither qualitative nor quantitative evidences of potential fragmentation of meteorites, meanwhile investigations of meteorites felt down show that meteorite fragmentation is most probably a rule - single meteorites are rare.

4. The theory does not offer the qualitative evidence of meteorite explosion in the atmosphere: the Tunguska and Sikhote-Alin events. It follows from solutions of the system (1.1-1.2) that a meteorite loses energy relatively smoothly with height. Moreover,  $dE/dH$  is smeared practically over the entire atmosphere [3].

In some studies the attempts were undertaken to avoid these disadvantages and complete the theory [3-6].

In [3] it was noted that pressure to a meteorite due achieved maximum, if meteorite mass did not exceed certain value. In this case pressure of air even to relatively slow meteorites can reach great values essentially exceeding strength of meteorite matter. That is why the

authors of [3] describe the process of fragmentation (explosion), phenomenologically introducing the notion of "fractional pressure"  $P_{fr}$ . On their estimates, for iron meteorites  $P_{fr} \approx 650$  atm. for stone ones  $P_{fr} \approx 50$  atm.

To describe the Tunguska event the authors of [4] completed the system (1.1-1.2) with the equations describing changes in meteorite cross section while it travels through the atmosphere (model cylinder of height  $h$  and diameter  $2r$ ) under pressure on the front surface (pressure on the back surface is neglected). It should be noted that in the model, deformation and, respectively, fragmentation begin after pressure has exceeded compression strength of meteorite matter.

Asteroid fragmentation is studied in [5]. As in [3], it is considered that fragmentation of asteroid (or further fragmentation of its fragments) occurs if pressure exceeds asteroid matter strength. In this case cross section of "asteroid" increases with respect to velocity with which fragments fly apart in space, which in turn is derived from the relationship for the pressure difference work and kinetic energy of fragments scattered. Fragmentation proceeds repeatedly: the next phase begins when radius of the cloud increases twice; it is supposed that in this case fractures become wide enough to allow penetration of approach air and each fragment has its own pressure difference. Fragmentation stops if pressure does not exceed strength. From this moment each fragment gets its own pressure difference and their deceleration in the atmosphere is calculated independently.

The model described in [6] was designed as a simple analytical model intended for illustrating calculated with the STN code results of the Shoemaker-Levy comet disruption in the Jupiter atmosphere. The authors of [6] noted that ablation equation (1.2) at certain velocities contradicts to the energy conservation law. This is associated with the fact that actually ablation mass does not disappear from the system, more correct relation for  $Q$  is:

$$Q = Q_0 + \frac{1}{2}v^2.$$

The second term is dominant at  $v > 5$  km/s for all matters of concern for the problem under consideration. If one neglects the first term, the modified ablation equation is:

$$\frac{dM}{dt} = -2\Lambda\rho_a S. \quad (1.3)$$

In addition, the authors of the model took into account formation of a layer of evaporated matter and hydrodynamic expansion of asteroid - a result of Kelvin-Helmholtz instability.

It is evident from the above that in order to describe fragmentation and/or explosion, the initial model (system (1.1-1.2)) is modified in two ways:

1. Introducing phenomenological pressure of disruption (references [3,5]).
2. Deforming a meteorite to increase its resistance and "lead" it to the explosion (references [4,6]).

In the last case it is a need to complete the model with some constants and assumptions which are unknown a priori. It should be noted here that different authors use different constants in the initial system (1.1-1.2). Thus, we have to say that provision of the problem with constants is beneath criticism (consequences of a very poor experimental data). Hence, there are certain doubts whether the physical model and actual picture are adequate.

In our view, all the above shows that this modification of the initial model is not challenging. Mathematical simulation is the most direct way to solve this problem (experiments are expensive and often impossible). Unfortunately, it is not easy to describe the problem completely because there is a lack of knowledge in the processes and there are no adequate

models of matter. Therefore, the theoretico-computational approach is the most promising because every step of the theoretical model is verified by mathematical simulation.

In the work this theoretico-computational approach was implemented for the problem of clarifying the explosion and fragmentation of meteorites and asteroids.

## 2. PHYSICAL MODEL

### 2.1 NULL APPROXIMATION

The phenomenon of fragmentation and explosion (since it is observed) should not be the "thin" physical effect. It should have a simple qualitative reasoning. Therefore, for qualitative understanding, most likely, ablation can be neglected in the first approximation because it should only strengthen the basic effect. Since fragmentation and explosion do not follow from the first equation (1.1), it is a need in the physical hypothesis which could result in the above effects.

The fundamental hypothesis of the model is the following. When a meteorite enters the atmosphere, it interacts with the approach stream of air that results in large-scale loss of hydrodynamic stability. It disintegrates into several parts approximately equal to one another. Then the process reproduces itself - one can observe the chain reaction of meteorite fragmentation, the fragments being decelerated in the atmosphere.

We will consider the meteorites in the form of a ball.

At first, let us assume fragmentation proceeds discretely and the time from one disintegration to another does not depend on both velocity (i.e. we assume that in the "null approximation" a meteorite and its fragments are not decelerated) and air density.

Let us introduce the following designations:

$R_0$  - meteorite initial radius;

$m$  - fragmentation step,  $m=1,2,\dots$ ,  $m=0$  means initial state;

$R_m$  - radius of a fragment at the  $m$ -th step;

$\tau_m$  - time from one disintegration to another at the  $m$ -th step;

$n$  - number of fragments;

$\tau$  - time during which a fragment of unit size disintegrates;

$N$  - total number of fragments.

Then one can write the following relationships:

$$\begin{aligned} R_m &= n^{-m/3} R_0, \\ \tau_m &= \tau n^{-m/3} R_0, \\ N(m) &= n^m. \end{aligned} \quad (2.1.1)$$

Respectively, current time  $t_m$  can be expressed as:

$$t_m = \sum_{k=0}^m \tau_k = \sum_{k=0}^m \tau \cdot R_0 \left(\frac{1}{n}\right)^{k/3} = \tau \cdot R_0 \frac{1-x^{m+1}}{1-x}, \quad \text{where } x=n^{-1/3}, \quad m \geq 1. \quad (2.1.2)$$

It is seen from the formula that there exists the ultimate time of meteorite fragmentation which is equal to:

$$t_f = \tau \cdot R_0 \frac{1}{1-x} = \tau \cdot R_0 \frac{\sqrt[3]{n}}{\sqrt[3]{n}-1} \quad (2.1.3)$$

If during this time meteorite has not reached the Earth, it will naturally disintegrate in air.

Then it is more convenient to transfer from the discrete variable  $m$  to the continuous one  $t$ . Then we derive the following expressions for number and size of fragments:

$$\begin{cases} N(t) = \frac{1}{\left(1 - \frac{t}{t_f}\right)^3} \\ R(t) = R_0 \left(1 - \frac{t}{t_f}\right) \end{cases} \quad (2.1.4)$$

Since  $t_f$  is proportional to meteorite initial size  $R_0$ , then number of fragments into which it will disintegrate during this time, will mostly depend on just this parameter and be far less sensitive to the rest of ( $n, \tau$ ).

Following the above, in the "null" approximation the meteorite explosion - disintegration into infinite number of fragments - takes place at moment  $t_f$ . Then, if it does not reach the Earth surface, the explosion will occur in the air. In this case the reaching condition (meteorite critical size) can be estimated from the following relation:  $t_{nv} = h/v < t_f$ , where  $h$  is the atmosphere height,  $v$  is meteorite velocity. From this one can derive the expression for meteorite critical size:

$$R_0 \geq \frac{h}{v} \cdot \frac{1}{\tau} \left(1 - \frac{1}{\sqrt[3]{n}}\right) \quad (2.1.5)$$

To transfer to numerical estimates, we need to know  $\tau$ . Generally saying,  $\tau$  depends on velocity. Looking ahead, we can say that  $\tau$  obtained by numerical estimation for the ice meteorite is about  $40 \mu\text{s/cm}$  when velocity is equal to  $20 \text{ km/s}$ . Given atmosphere height of  $10 \text{ km}$ , we obtain that  $R_c > 60 \text{ m}$  for  $n=8$ .

## 2.2. RESULTS OF MATHEMATICAL SIMULATION

Naturally, any physical hypothesis needs experimental confirmation. In our case it is rather difficult. Therefore, to verify its plausibility, let us use mathematical simulation. The following calculation was performed with 2D hydrodynamic code MECH [7,8] (without accounting for ablation). A ball of  $1 \text{ cm}$  in radius and  $1 \text{ g/cm}^3$  in density was winded by air flow of velocity in  $20 \text{ km/s}$  and density  $\rho_a = 0.00129 \text{ g/cm}^3$  (air density at sea level). Equation of state of the ball matter was taken in the simplest form:

$$P = \rho_0 c_0^2 (\delta - 1), \quad (2.2)$$

where  $P$  is pressure,

$\rho_0$  - initial density,

$c_0$  - effective speed of sound ( $c_0 = 2.5 \text{ km/s}$ ),

$\delta$  - compression.

In fact, it is equation of state for ice at small compression and pressure. Really, pressure realized in these processes is not high,  $P \approx \rho_0 v^2 \approx 5 \text{ kbar}$ .

Air was considered as ideal gas with  $\gamma = 1.2$ .

Figures 2.2.1 - 2.2.4 depict gas dynamic flow implemented.

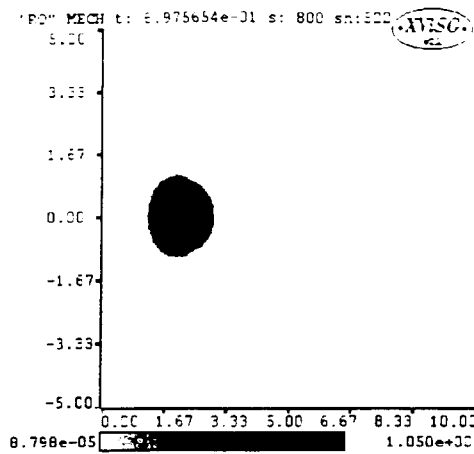


Fig.2.2.1

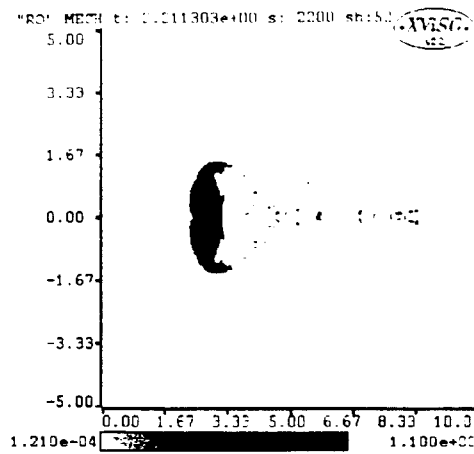


Fig.2.2.2

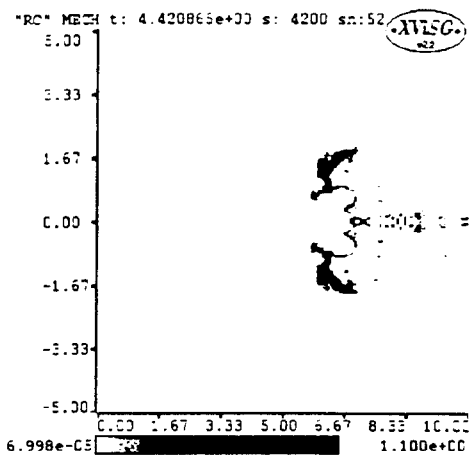


Fig.2.2.3

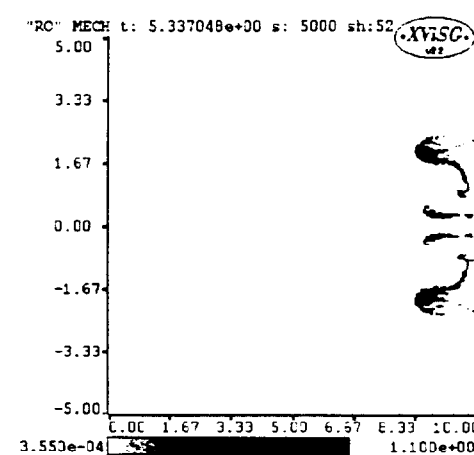


Fig. 2.2.4

Fig. 2.2.1 presents the moment when flow achieved equilibrium. On Fig. 2.2.2 one can see how a hole is being formed at the axis of symmetry. On Fig 2.2.3 we see that the initial ball has become torus and Fig 2.2.4 shows two tori formed from the first one. So, we see the process reproduces itself. Of course, the problem should be calculated for three spatial variables, however, main features of the phenomenon may be seen from 2D calculations. The ball has become torus during  $\approx 40 \mu\text{s}$ . Apparently, this time is close to the disruption time desired and it was used for the estimation of paragraph 2.1.

A series of runs were proceeded which varied in velocities of approach flow at normal air density. Specifically, the values were obtained for resistance coefficient  $G$  in the motion equation (1.1), which was fitted on calculated results.

Main calculated results are presented in table 2.2.1.

Table 2.2.1.

$v_0$ , km/s	$G$	$t_d$ , $\mu\text{s}$
5	1.313	193
10	1.381	84
20	1.408	40
30	1.404	29.5
50	1.219	17.7
70	1.15	14

As it is seen from table 2.2.1, resistance coefficient is almost constant within a wide range of initial velocities. Certain deviation takes place at high velocities which can be easily explained: at these velocities both pressure and compression are not already small and application of the equation of state in form (2.2) is hardly correct.

As to time of disruption, it is seen from Fig. 2.2.5 that it is simply inversely proportional to initial velocity.

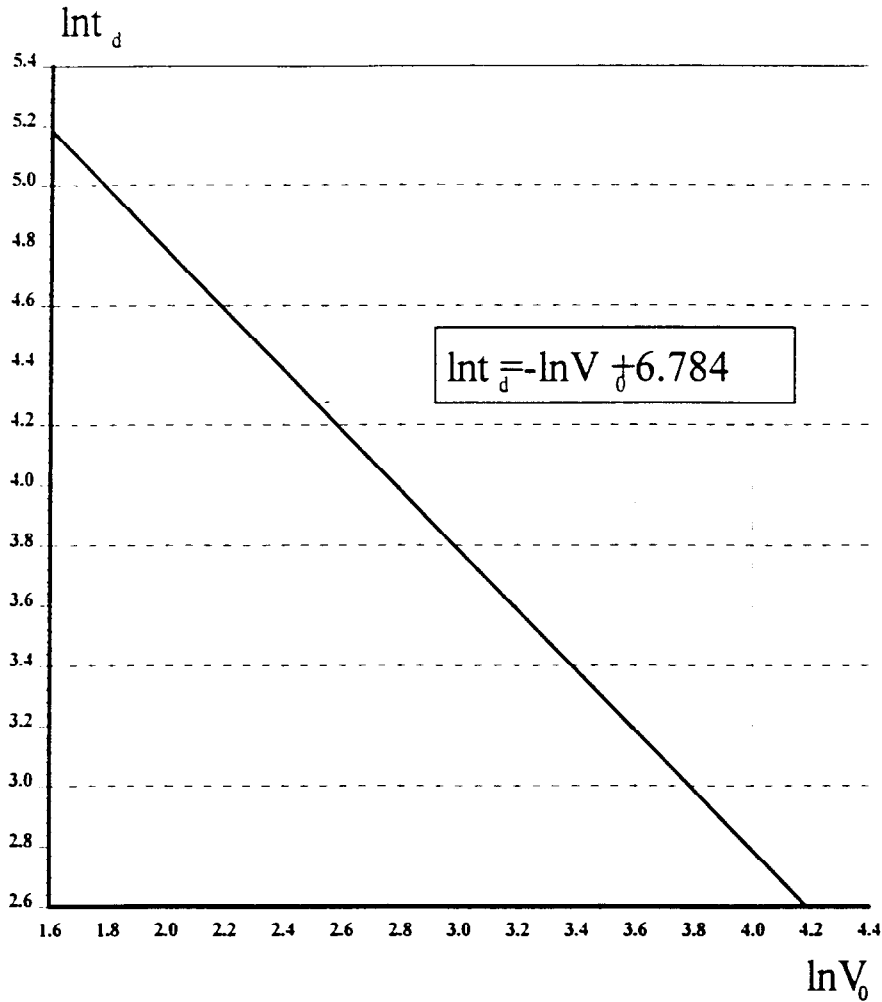


Fig.2.2.5

Thus, mathematical simulation verifies on the whole the mechanism used and obtained relations and patterns, as well as their numerical values we will use in further development of the analytical model and numerical simulation which will be considered in the next section.

### 3. ANALYTICAL ESTIMATES

#### 3.1. EXPONENTIAL ATMOSPHERE

With relation to practice, real interaction with exponential atmosphere of the Earth is of most interest. In this case the system of equations will be written as follows.

Equation of motion in ballistic form

$$\frac{dv^2}{dz} = \frac{2GA}{\rho_M^{2/3} M_m^{1/3} \cos \varphi} \rho_a v^2, \quad (3.1.1)$$

where  $z$  is coordinate above the Earth surface:

$\varphi$  - angle of meteorite enter into the atmosphere;

$M_m$  - mass of a fragment at the  $m$ -th step;

$\rho_M$  - meteorite density;

$A$  - unitless coefficient defined from the relation  $\frac{S_m}{M_m} = \frac{A}{\rho_M^{2/3} M_m^{1/3}}$ ;

$S_m$  - maximum midsection square;

$\rho_a$  - current air density,  $\rho_a = \rho_0 \exp(-z/h)$ ;

$h$  - Earth atmosphere height.

Integration limits in this equation can be defined by the following relation:

$$t_{m-1} - t_m = \tau_m. \quad (3.1.2)$$

To complete the system of equations, it is a need to write the equation for  $\tau_m$ . For this purpose let us introduce the notion of destruction velocity so as

$$\int_{t_{m-1}}^{t_m} v_d dt = \int_{t_{m-1}}^{t_m} \frac{dt}{\tau(v, \rho_a)} = R_{m-1}. \quad (3.1.3)$$

To continue, on the basis of numerical calculations it is necessary to make some assumptions concerning the form of function  $v_d = 1/\tau(v, \rho_a)$ . Considering dimensionality,

$\tau = \frac{1}{v} f\left(\frac{\rho_a}{\rho_M}, \frac{c_0}{v}, \frac{c_a}{v}, \gamma, \text{etc.}\right)$  ( $c_a$  - speed of sound in air). As it was shown in paragraph 2.2,

$\tau_m \sim 1/v_0$  and, since prior the disruption meteorite velocity varies relatively weakly (paragraph 2.2), one can neglect the dependence on parameters of type  $c/v \ll 1$ . Then

$$\tau = \frac{1}{v} f\left(\frac{\rho_a}{\rho_M}\right). \quad (3.1.4)$$

Really, when air density is constant, substituting (3.1.4) into (3.1.3) we obtain:

$$R_{m-1} = \int_{t_{m-1}}^{t_m} \frac{v dt}{f\left(\frac{\rho_a}{\rho_M}\right)} \approx \frac{v_{m-1} \tau_m}{f\left(\frac{\rho_a}{\rho_M}\right)},$$

that agrees with calculated results.

To facilitate computing, we will consider then that

$$\tau = \frac{1}{v} f\left(\frac{\rho_a}{\rho_M}\right) = \frac{1}{v} B \frac{\rho_a}{\rho_M}. \quad (3.1.5)$$

Substituting (3.1.5) into (3.1.3) and integrating with respect to  $z$  we will obtain the following relationship:

$$B\rho_M R_{m-1} \cos \varphi = h(\rho_m - \rho_{m-1}) = h\Delta\rho_m. \quad (3.1.6)$$

where  $\rho_m = \rho_a(z_m)$ .

If we integrate equation (3.1) over  $z$  from  $z_{m-1}$  to  $z_m$ , we will obtain:

$$v_m = v_{m-1} \exp\left(-\frac{h\gamma}{2} \Delta\rho_m \frac{1}{\cos \varphi}\right), \quad (3.1.7)$$

where  $\gamma = \frac{2GA}{\rho_M^{2/3} M_{m-1}^{1/3} \cos \varphi}$ .

Combining (3.1.6) and (3.1.7):

$$v_m = v_{m-1} \exp\left(-\frac{GA}{\left[\frac{4\pi}{3}\right]^{1/3} B}\right) = v_{m-1} f \quad (3.1.8)$$

and

$$v_m = v_0 f^m$$

Respectively, energy loss is:

$$\Delta E_m = E_0 f^{2m} \left(1 - \frac{1}{f^2}\right).$$

After  $m$  acts of fragmentation the meteorite will lose the following amount of energy

$$\Delta E(m) = -E_0 \left(1 - \frac{1}{f^2}\right) \sum_{n=1}^m f^{2n} = E_0 (1 - f^{2m}). \quad (3.1.9)$$

To clarify the issue on distribution of energy losses over height, let us return to formula (3.1.6) and rewrite it for variables  $R_0$  and  $x$ :

$$\Delta\rho_m = B\rho_M \frac{R_0}{h} x^{m-1}.$$

Hence we have the equation:

$$e^{-z_m/h} - e^{-z_{m-1}/h} = B \frac{\rho_M}{\rho_0} \frac{R_0}{h} x^{m-1} = \xi x^{m-1}.$$

So,

$$e^{-z_m/h} = e^{-z_0/h} + \xi \sum_{n=1}^m x^{n-1}, \quad m \geq 1.$$

Assuming  $z_0 \rightarrow +\infty$  and summing the series, we obtain:

$$e^{-z_m/h} = \xi \sum_{n=1}^m x^{n-1} = \xi \frac{1-x^m}{1-x}, \quad m \geq 1. \quad (3.1.10)$$

When  $m \rightarrow \infty$ , meteorite will reach only finite height

$$z_f = h \cdot \ln \frac{1-x}{\xi} = h \cdot \ln \frac{1 - \frac{1}{\sqrt[3]{n}}}{B \frac{\rho_M}{\rho_0} \frac{R_0}{h}}. \quad (3.1.11)$$

If  $z_r < 0$ , meteorite fragments will fall down onto the Earth, if  $z_r > 0$ , meteorite will explore in air. On results of calculations of paragraph 2.2. B-0.1. Then critical radius of the ice meteorite makes up about 50 m.

Using the above formulas, the calculations were proceeded for the ice meteorite of 30m in radius and velocity of 20 km/s normal to the Earth surface. Kinetic energy of such meteorite makes up 5.4 Mt. Figures 3.1.1-3.1.2 depict how meteorite kinetic energy depends on height and time at the moment of fragmentation.

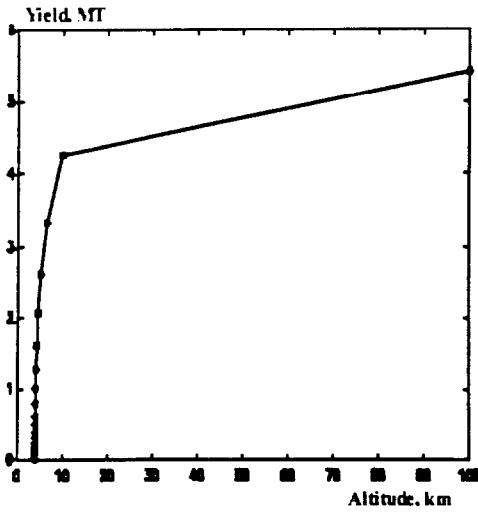


Fig. 3.1.1

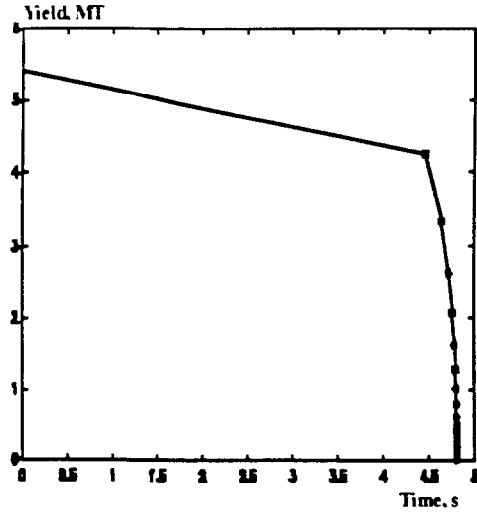


Fig.3.1.2

As it is seen, the first fragmentation occurs at height of ~10 km, after 5 acts of fragmentation it is already at the ultimate height of 4 km where it disintegrates completely. Near this height during the time of ~0.01s energy of 1.5 Mt is being lost along the distance of about 100 m.

The issue remains on the character of energy release in this process. We have failed to derive the explicit analytical expression for exponential atmosphere and this model. However, due to the fact that almost all energy loss is concentrated within narrow range of heights: 50% of energy is lost at 1 km, then one can accept the atmosphere has constant density in this region. Solution of such problem is offered below.

### 3.2. ATMOSPHERE OF CONSTANT DENSITY

Likewise paragraph 3.1, integrating the equation (3.1.1) over time, we obtain:

$$\left( \frac{1}{v_m} - \frac{1}{v_{m-1}} \right) = \frac{GA\rho_a}{\rho_M M_{m-1}^{2/3}} (t_m - t_{m-1}).$$

To derive the explicit analytical formula for function  $E(t)$ , we will use formula (2.1.1):

$\tau_m = \tau \cdot n^{-m/3} R_0$ ,  $R_m = n^{-m/3} R_0$ . Then

$$\left( \frac{1}{v_m} - \frac{1}{v_{m-1}} \right) = \alpha = GA\tau \frac{\rho_a}{\rho_M} \left( \frac{3}{4\pi} \right)^{1/3}. \quad (3.2.1)$$

Generally saying, as it was shown above, this is not correct. Really the right part of the last equation should be inversely proportional to  $v_{m-1}$  (in this case formula (3.2.1) becomes

(3.1.8) at small  $\alpha$ ). In fact, this results in slower energy losses from one fragmentation to another. However, since in the model described the time from one disintegration to another is understated as compared with exponential atmosphere, one could anticipate compensation and hope the approach will give not bad estimate.

It follows from formula (3.2.1) that:

$$v_m = \frac{v_0}{1 + m\alpha v_0}.$$

Hence,

$$\Delta E_m = E_0 \left( \frac{1}{[1 + m\alpha v_0]^2} - 1 \right),$$

and meteorite kinetic energy is:

$$E_0 - E(m) = E_0 - \sum_{k=1}^m \Delta E_m = \frac{E_0}{[1 + m\alpha v_0]^2}. \quad (3.2.2)$$

Transferring from variable  $m$  to time with the use of relation (2.1.2)

$$m = \frac{\ln(1 - t/t_f)}{\ln x} \quad \text{we obtain:}$$

$$E(t) = \frac{E_0}{\left[ 1 + \alpha v_0 \frac{\ln(1 - t/t_f)}{\ln x} \right]^2}. \quad (3.2.3)$$

When  $t \rightarrow t_f$ ,  $dE/dt \rightarrow -\infty$ . It is the explosive process.

Generally saying, in formulas (3.2.1-3.2.3) some effective parameters ( $E_0$ ,  $v_0$ ,  $t_f$ ) should be "sewed" with the solution for exponential atmosphere.

Really rate of energy loss is surely limited. Most likely, its maximum value is determined by finite size of macro particles and/or by finiteness of velocity.

#### 4. COMPARISON OF ANALYTICAL ESTIMATES WITH RESULTS OF MATHEMATICAL SIMULATION FOR EXPONENTIAL ATMOSPHERE

To verify validity of estimates offered in paragraph 3.1. the interaction of meteorite with the Earth atmosphere was computed. Initial conditions were as follows: at height of 25.5 km a meteorite of radius in 30 m had initial velocity of 20 km/s.

The run showed that the destruction has occurred after 0.511s. i.e. after the asteroid has covered ~10 km. Deceleration coefficient made up  $G=1.3$  indicating that it depended on atmosphere density.

It should be noted that the estimation with the formulas of paragraph 3.1. gives the results which somewhat differ from those obtained through mathematical simulation: The first fragmentation occurs at the height of 8.64 km in 0.81 s. This evidences that everything goes faster in mathematical simulation. This might be reasoned by the fact that in analytical estimates of the disruption model we considered that disruption time vs. density is  $\sim \rho_a$ . actually it may be not so strong.

Since the analytical estimates of explosion strength have appeared even less optimistic than results of mathematical simulation. it has meaning to consider the problem of the Tunguska explosion from analytical standpoint.

Let us consider it was a ball of 46 m in radius, 20 km/s speed, entry angle of  $45^\circ$ . Total energy was 20 MT.

Trajectory is shown in Fig.4.1.

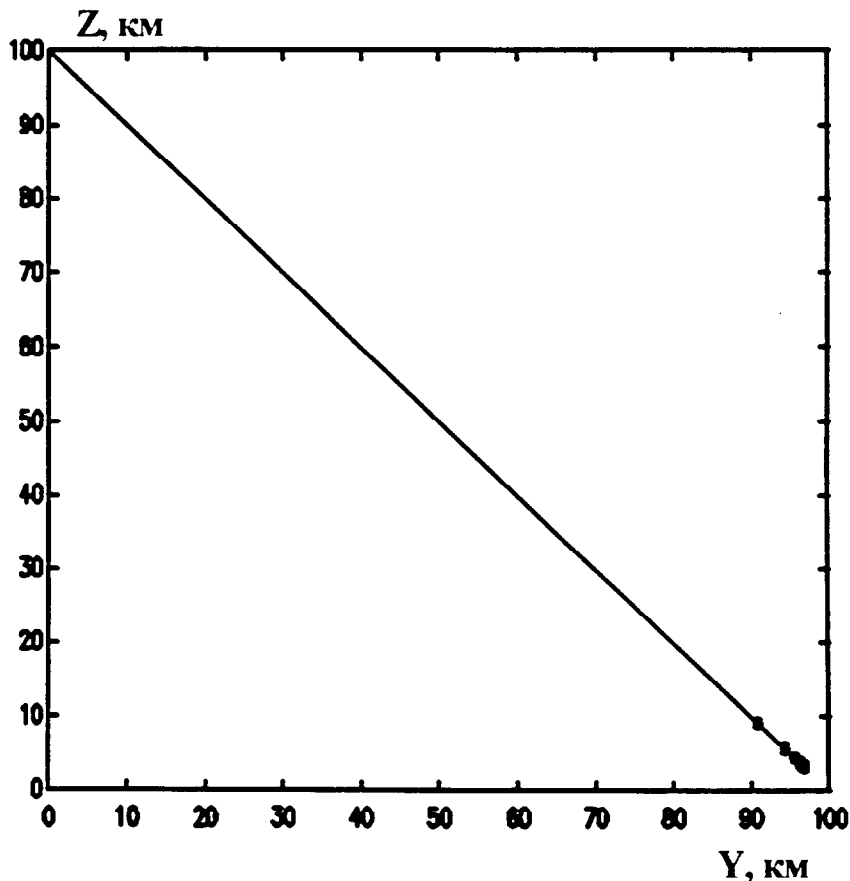


Fig.4.1.

Fig. 4.2 and 4.3. depict energy vs. height (here the first point corresponds to the first fragmentation).

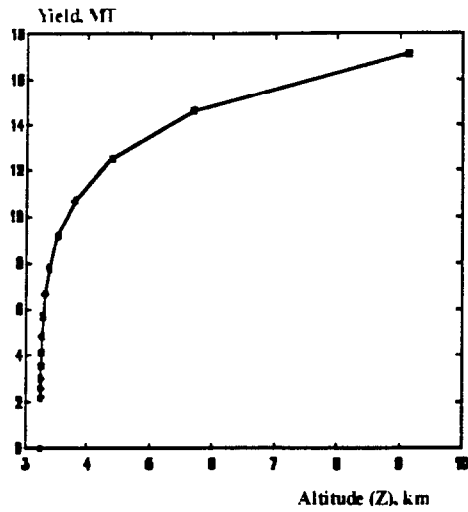


Fig.4.2.

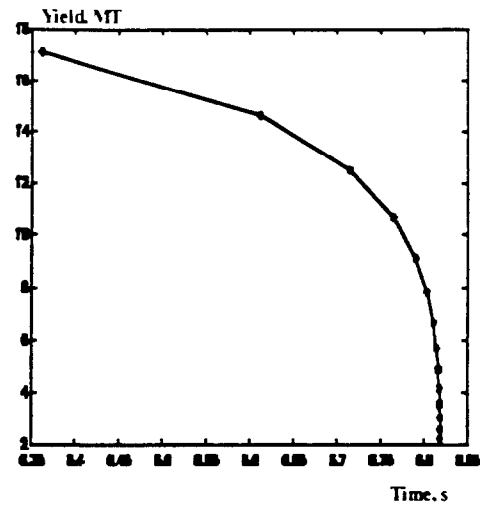


Fig.4.3.

Ultimate height achievable by the meteorite fragments is 3.24 km. As it is seen from the plots, about 8 Mt of energy are released by the explosion.

To illustrate the capabilities of the model proposed, let us compare it with both hydrodynamic model and hydrodynamic model with ablation. Ablation coefficient was taken from [2]. The calculations were done for the ice meteorite which was 20 km/s speed and had energy of 5.4 Mt.

Dependencies of typical quantities are presented in Fig. 4.4 - 4.7.

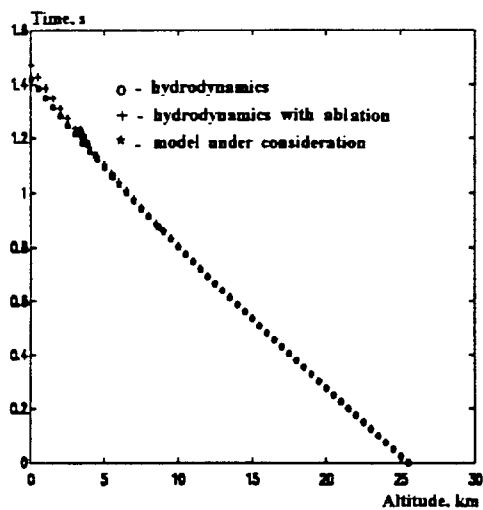


Fig. 4.4.

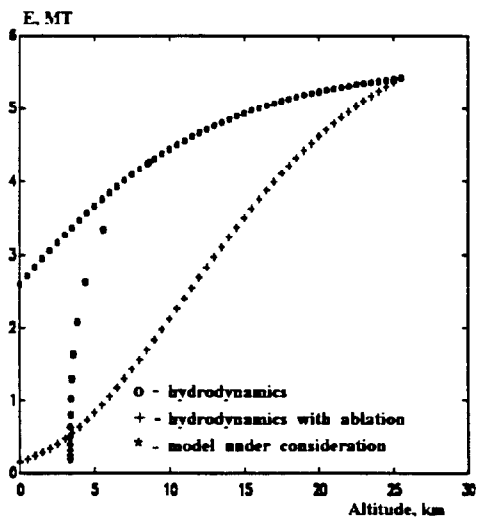


Fig. 4.5.

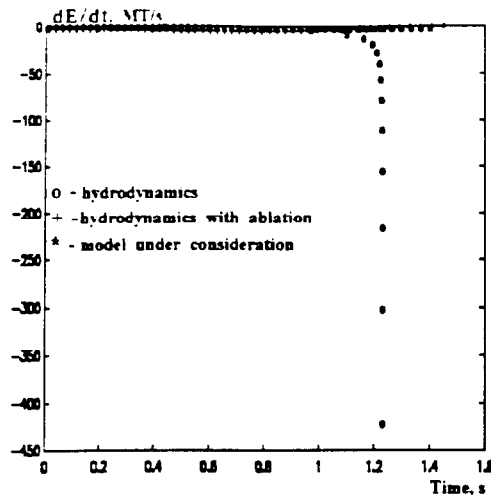


Fig. 4.6.

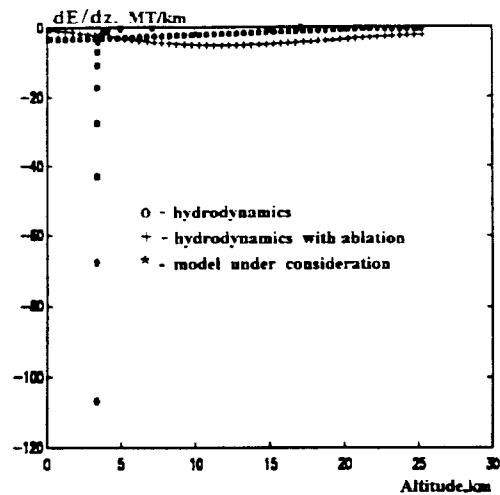


Fig. 4.7.

It is seen from the plots that the model proposed offers qualitatively new results. In hydrodynamic model and model with ablation meteorite reaches the Earth surface with “smooth” release of energy, while in the mechanism proposed it “explores” at finite height. It is also seen ablation affects trajectory not essentially. At the same time, if the model is completed with ablation, energy release due to less radii will proceed faster.

## THE BOTTOM LINE

Theoretico-computational model of the asteroid explosion and fragmentation in the Earth atmosphere has been designed. Fundamental assumptions of the model are as follows. When a meteorite enters the atmosphere, it interacts with approach stream of air that results in large-scale loss of hydrodynamic stability. It disintegrates into several approximately equal fragments. Then each of the fragments reproduces the process - one can observe a chain of fragmentation and deceleration of the meteorite in the atmosphere. Based on the mechanism proposed, radius of the ice asteroid which can achieve the Earth surface was estimate, it is ~50 m. Really, as it follows from mathematical simulation, this radius is smaller. If the meteorite does not reach the Earth surface, its energy loss is of explosive character - the most portion of energy is lost at the distance of several meteorite typical sizes.

Based on the results obtained the areas for further research can be defined:

1. Effects of matter (ice, stone, iron), as well as its porosity on fragmentation.
2. Effects of meteorite (asteroid) form on fragmentation.
3. 3D mathematical simulation of fragmentation processes.
4. Comparison of experimental observations in explosions in the atmosphere with results of mathematical simulations and the estimations with the analytical model.
5. Calibration of physical models and mathematical codes with experimental results.
6. Detailed study on how the resistance coefficient and disruption time depend on air density.

## ACKNOWLEDGMENTS

The authors express their acknowledgments to R.Dudnik and V.Zolotova for their help in proceeding the runs.

## REFERENCES

1. Y. Shoemaker.  
Oral presentation.
2. I.S. Astapovich  
Meteorite Phenomena in the Earth Atmosphere  
И.С. Астапович. Москва. 1958
3. E.I. Zababakhin. M.N. Nechaev  
On Meteorite Movement in the Exponential Atmosphere along the Middle Part of the Trajectory  
In the proceeding of the Zababakhin's Scientific Readings, Chelyabinsk-70, 14-17 January, 1987
4. C.F. Chuba, P.J. Thomas, K.J. Zahnle  
The 1908 Tunguska Explosion: Atmospheric Disruption of a Stony Asteroid
5. J.G. Hills. M.P. Goba  
The Fragmentation of Small Asteroid in the Atmosphere. 1993
6. D.A. Crawford  
Models of Fragment Penetration and Meteorite Evolution In the Collision of Comet Shoemaker-Levy 9 with Jupiter. Cambridge University Press, 1997
7. N.N. Anuchina  
On Computational Methods for Compressible Flows with Strong Deformations.  
Collection *Computational Methods for Solid Media Mechanics*, v. 1, 4, 1970
8. E.N. Avrorin, N.N. Anuchina, V.V. Gadzhieva, V.P. Elsukov, B.P. Mordvinov  
Numerical Simulation of the Interaction between the Galley Comet Particles and a Spacecraft.  
Keldysh Institute for Applied Mathematics. Preprint 177, 1985



# EXPLOSIVE DECELERATION AND FRAGMENTATION OF METEORITES IN THE ATMOSPHERE

*D.V. Petrov, O.N. Shubin, V.P. Elsukov, V.A. Simonenko*

*RFNC-VNIITF*

## Contents

1. Overview
  2. Physical Model
    - 2.1. Zero Approximation
    - 2.2. Results of Mathematical Modeling
  3. Analytical Estimates
    - 3.1. Exponential Atmosphere
    - 3.2. Atmosphere of Constant Density
  4. Comparison of Analytical Estimates with the Results of  
Mathematical Modeling
  5. Comparison of Models
- Conclusion  
Acknowledgments

### Experimental Facts:

- burst of Tunguska meteorite;
- flashes are recorded similar to fireball of nuclear explosion with the yield of 1-100 kT of TNT.

## 1. OVERVIEW

Initial system

$$\begin{cases} M \frac{dv}{dt} = -G\rho_a S v^2 n \\ \frac{dM}{dt} = -\frac{L}{Q} \rho_a S v^3 \end{cases}$$

*Advantages:*

1. This theory describes quite well deceleration of a single meteorite at the intermediate part of trajectory (under appropriate selection of the constants).

*Disadvantages:*

1. Rather large uncertainties in selection of system constants.
2. At some specific velocities equation of ablation contradicts the law of energy conservation.
3. Opportunity of meteorite fragmentation does not succeed.
4. Opportunity of meteorite «burst» in the atmosphere does not succeed:  $dE/dH$  spreads over the whole atmosphere.

Two ways of modification:

1. Phenomenological pressure of destruction is introduced.
2. Meteorite is strained in order to increase its strength and «lead to» burst.

These modifications of the initial model are not promising. Mathematical modeling is the most direct way of solving the problem (because experiments are too expensive, and often impossible).

The most promising way is simulation-theoretical when each step of physical model is verified with mathematical calculations.

## 2. PHYSICAL MODEL

### 2.1. ZERO APPROXIMATION

#### Principal Assumption of the Model:

When meteorite enters the atmosphere, it interacts with a windstream and this results in a large-scale loss of hydrodynamic stability of the meteorite. It disintegrates into several nearly equal fragments. Later this process reproduces itself - chain reaction of meteorite fragmentation, and deceleration in the atmosphere are observed.

Meteorite is a sphere.

Fragmentation is discrete and interval between two fragmentations does not depend on velocity and air density.

Assume  $n$  to be a number of chunks resulting from fragmentation.

Final time of meteorite destruction is:

$$t_r = \tau \cdot R_0 \frac{\sqrt[3]{n}}{\sqrt[3]{n} - 1}$$

Number and sizes of the chunks are calculated in the following way:

$$\begin{cases} N(t) = \frac{1}{\left(1 - \frac{t}{t_r}\right)^3} \\ R(t) = R_0 \left(1 - \frac{t}{t_r}\right) \end{cases}$$

«Burst» of meteorite, i.e. disintegration into an infinite number of fragments, occurs at the moment  $t_r$ . If meteorite does not reach the Earth's surface by this moment, the burst will occur in the air.

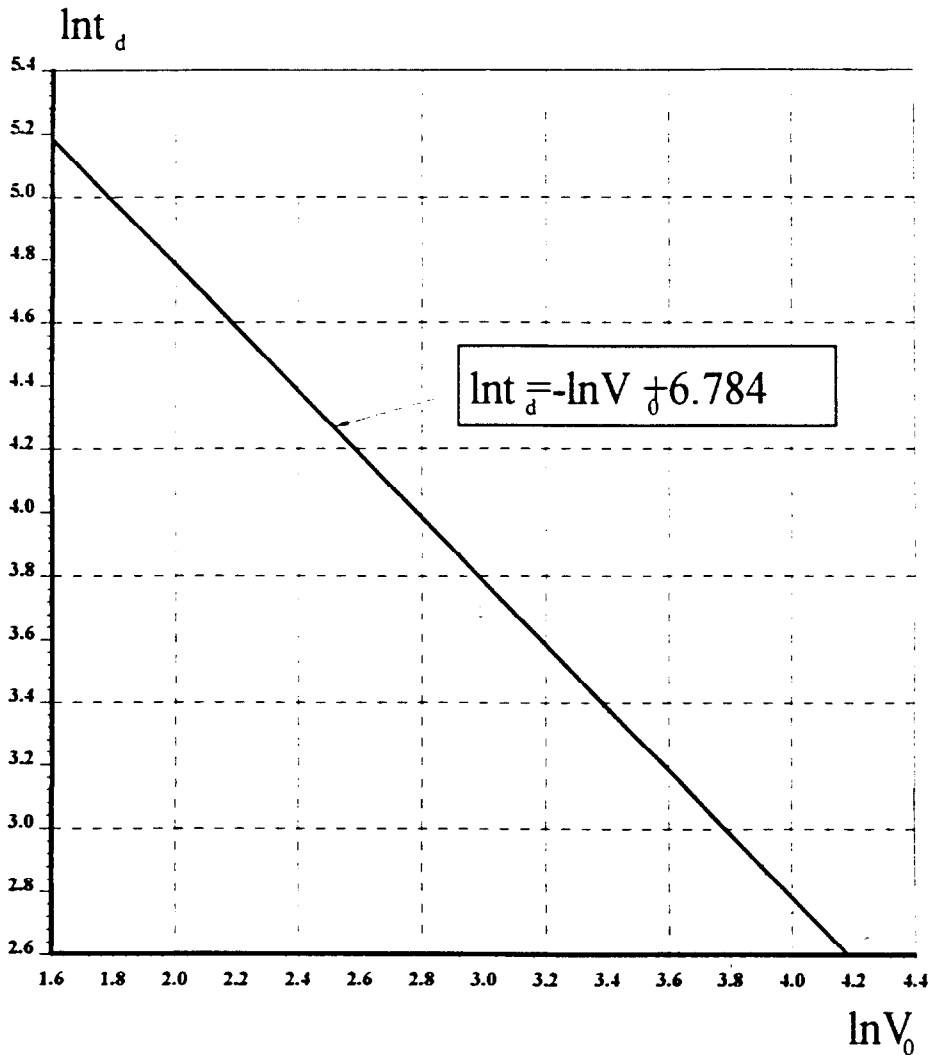
## 2.2.RESULTS OF MATHEMATICAL MODELING

Assume, that meteorite is of unit size and unit density.

Equation of state is  $P = \rho_0 c_0^2 (\delta - 1)$ .

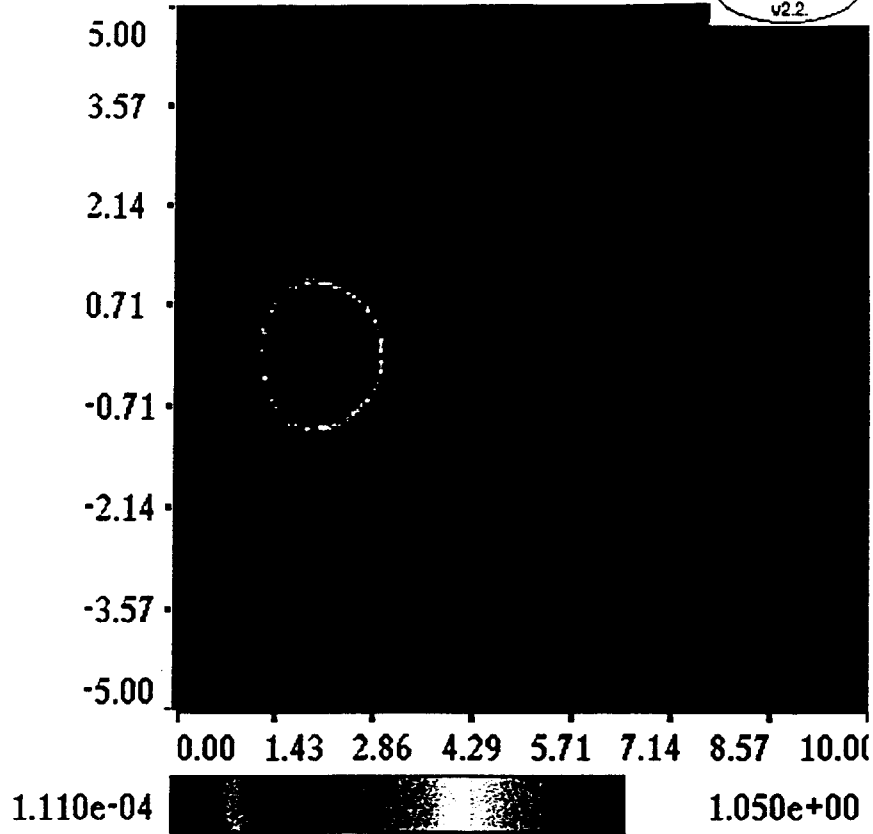
$V_0$ , km/s	G	$t_d$ , $\mu$ s
5	1.313	193
10	1.381	84
20	1.408	40
30	1.404	29.5
50	1.219	17.7
70	1.15	14

$t_d$  is destruction time.



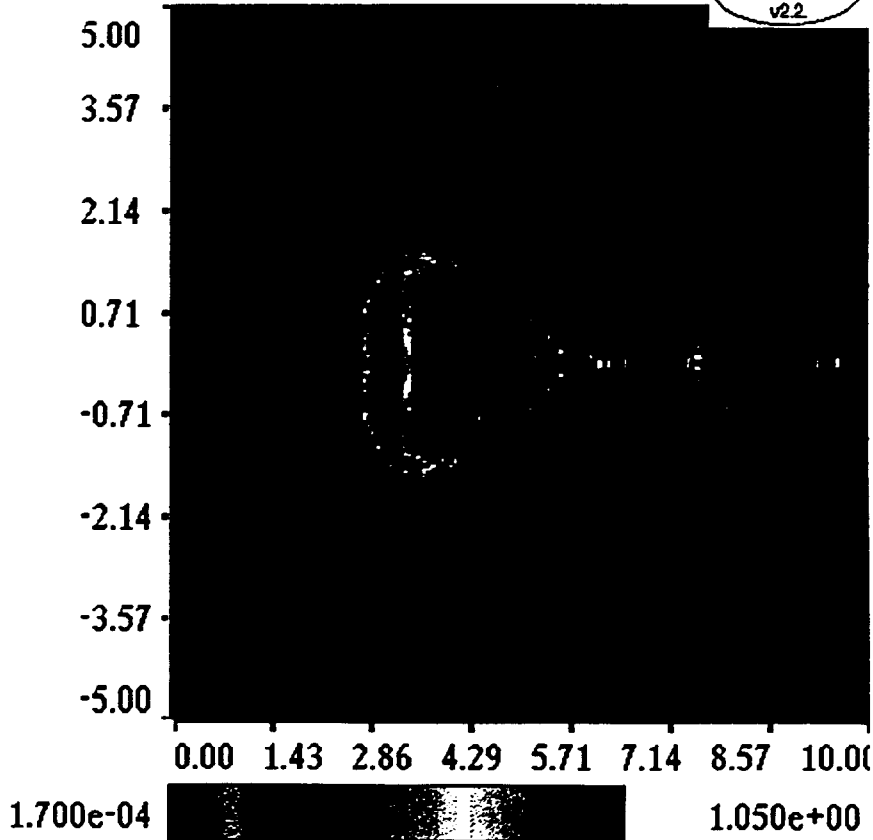
"RO" MECH t: 6.724602e-01 s: 800 sh:522000

XVISG.  
v2.2

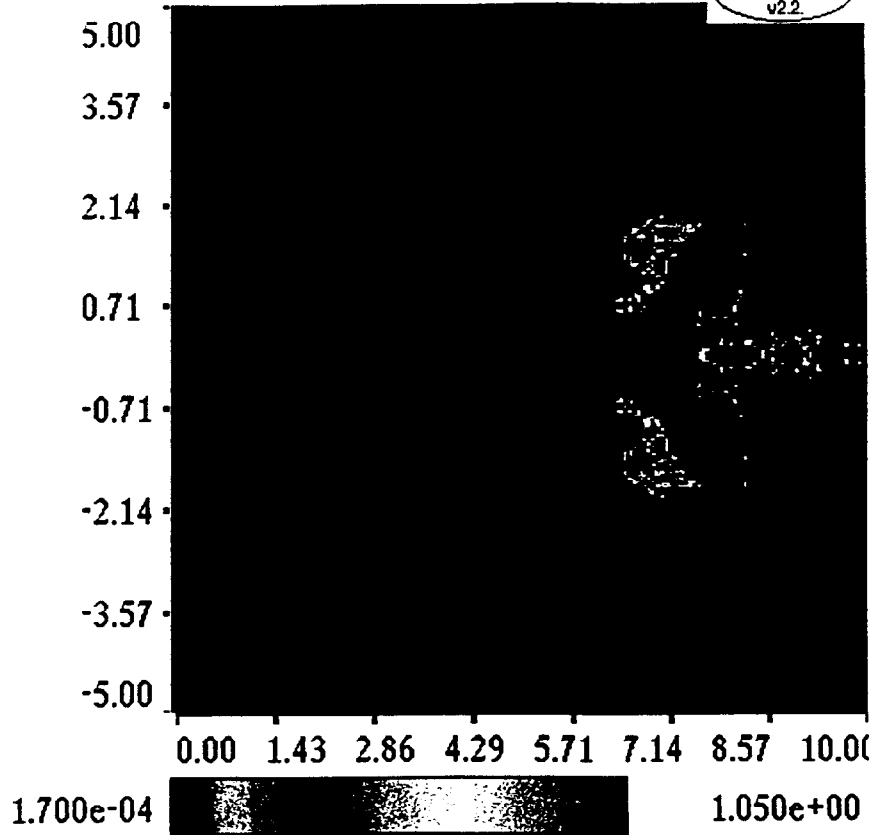


"RO" MECH t: 2.627710e+00 s: 2600 sh:522000

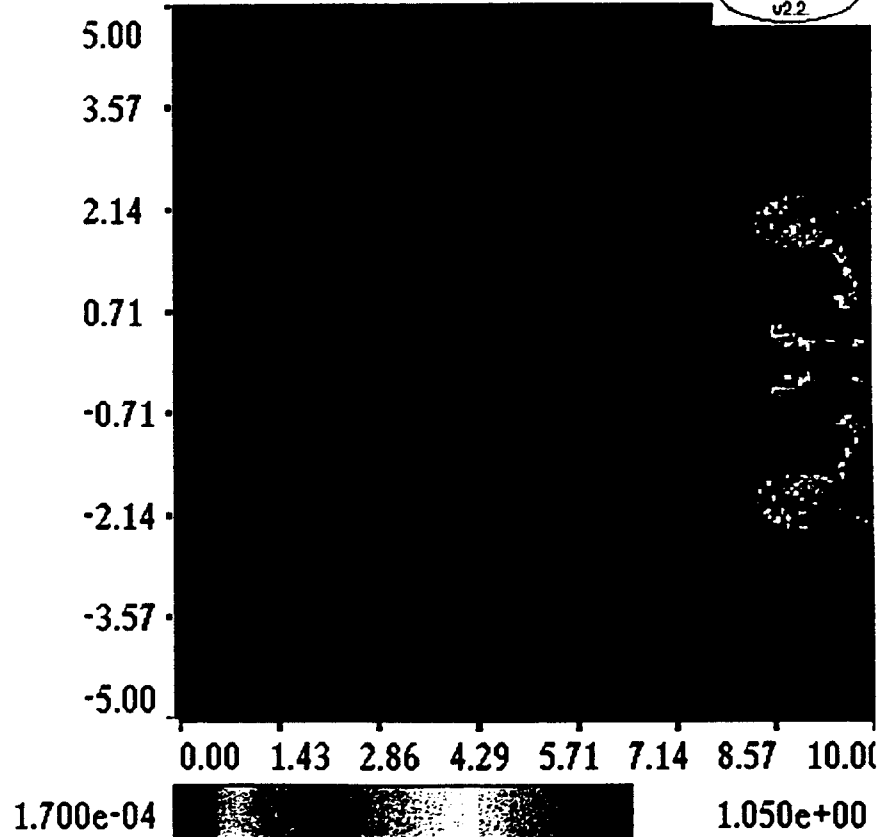
XVISG.  
v2.2



"RO" MECH t: 4.647995e+00 s: 4400 sh:522000 (.XVISG.v22)



"RO" MECH t: 5.337048e+00 s: 5000 sh:522000 (.XVISG.v22)



### 3. ANALYTICAL ESTIMATES

#### 3.1. EXPONENTIAL ATMOSPHERE

$$\frac{dv^2}{dz} = \frac{2GA}{\rho_M^2 M_{\bullet}^{1/3} \cos \varphi} \rho_a v^2$$

Integration limits:  $t_{\bullet} - t_{\bullet-1} = \tau_{\bullet}$

$$\int_{t_{\bullet-1}}^{t_{\bullet}} v_a dt = \int_{t_{\bullet-1}}^{t_{\bullet}} \frac{dt}{\tau(v, \rho_a)} = R_{\bullet-1}$$

Proceeding from dimensionality  $\tau = \frac{1}{v} f\left(\frac{\rho_a}{\rho_M}, \frac{c_0}{v}, \frac{c_a}{v}, \gamma, \text{etc.}\right)$

$$\tau = \frac{1}{v} f\left(\frac{\rho_a}{\rho_M}\right)$$

Assume, that  $\tau = \frac{1}{v} B \frac{\rho_a}{\rho_M}$

Integrating :  $B \rho_M R_{\bullet-1} \cos \varphi = h(\rho_{\bullet} - \rho_{\bullet-1}) = h \Delta \rho_{\bullet}$  and

$$v_{\bullet} = v_{\bullet-1} \exp\left(-\frac{GA}{\left[\frac{4\pi}{3}\right]^{1/3} B}\right) = v_{\bullet-1} f$$

$$\Delta E_{\bullet} = E_0 f^{2m} \left(1 - \frac{1}{f^2}\right)$$

After  $m$  fragmentations meteorite will lose the following amount of energy:

$$\Delta E(m) = -E_0 \left(1 - \frac{1}{f^2}\right) \sum_{n=1}^m f^{2n} = E_0 (1 - f^{2m})$$

Using variables  $R_0$  and  $x=n^{-1/3}$  for  $\cos \varphi=1$  we obtain the following relations:

$$e^{-z_{\bullet}/h} = e^{-z_0/h} + \xi \sum_{n=1}^m x^{n-1}, \quad m \geq 1, \quad \xi = B \frac{\rho_M R_0}{\rho_0 h}$$

If  $m \rightarrow \infty$ , meteorite will be able to reach only a final altitude

$$z_r = h \cdot \ln \frac{1-x}{\xi} = h \cdot \ln \frac{1 - \frac{1}{\sqrt[3]{n}}}{B \frac{\rho_M R_0}{\rho_0 h}}$$

Calculations show that  $B \sim 0.1$ . In this case critical radius of the icy meteorite will make up about 50 m.

### 3.2. ATMOSPHERE OF CONSTANT DENSITY

Similarly to the previous case:

$$\left( \frac{1}{v_n} - \frac{1}{v_{n-1}} \right) = \frac{GA\rho_a}{\rho_M^{2/3} M_{n-1}^{1/3}} (t_n - t_{n-1})$$

For explicit analytical dependence  $E(t)$  the following formulas are used:

$$\tau_n = \tau \cdot n^{-n/3} R_0, \quad R_n = n^{-n/3} R_0$$

Then

$$\left( \frac{1}{v_n} - \frac{1}{v_{n-1}} \right) = \alpha = GA\tau \frac{\rho_a}{\rho_n} \left( \frac{3}{4\pi} \right)^{1/3}$$

This leads to

- less energy loss at fragmentation;
- longer time interval between fragmentations.

Balancing can be expected and this approach will, probably, give a good estimate.

$$E(t) = \frac{E_0}{\left[ 1 + \alpha v_0 \frac{\ln(1 - t/t_f)}{\ln x} \right]}$$

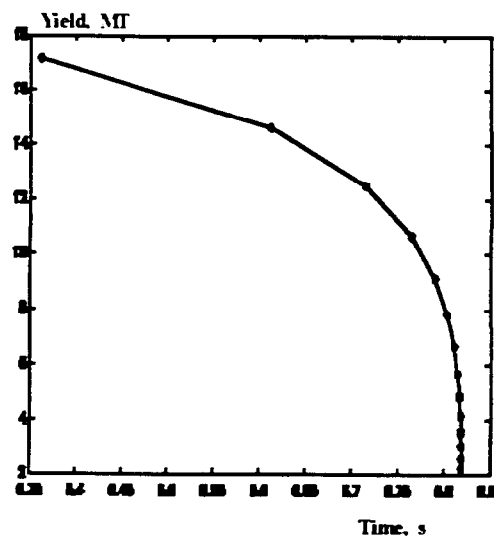
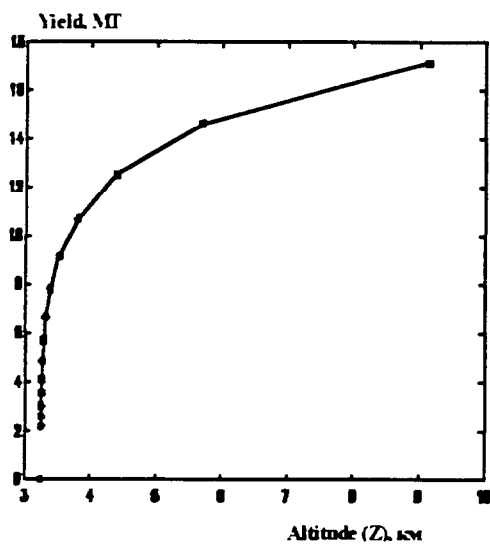
For  $t \rightarrow t_f$ ,  $dE/dt \rightarrow -\infty$ . This is an explosive process.

#### 4. COMPARISON OF ANALYTICAL ESTIMATES WITH THE RESULTS OF MATHEMATICAL MODELING

Initial conditions are the following: at the altitude of 25.5 km meteorite of 60 m in diameter had the initial velocity of 20 km/s.

	Mathematical modeling	Calculation
Time of destruction, s	0.511	0.81
Altitude of destruction, km	15.5	8.64

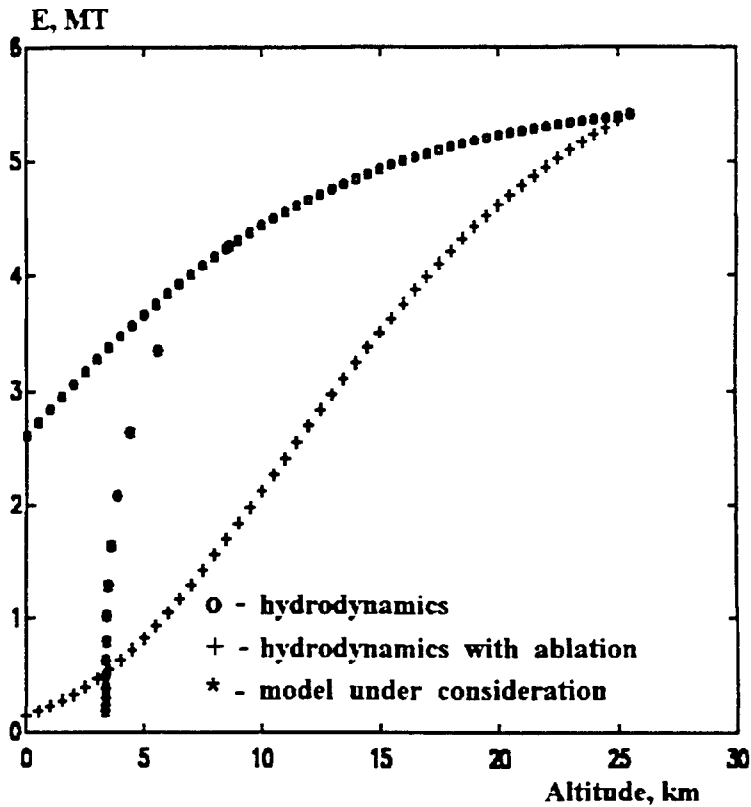
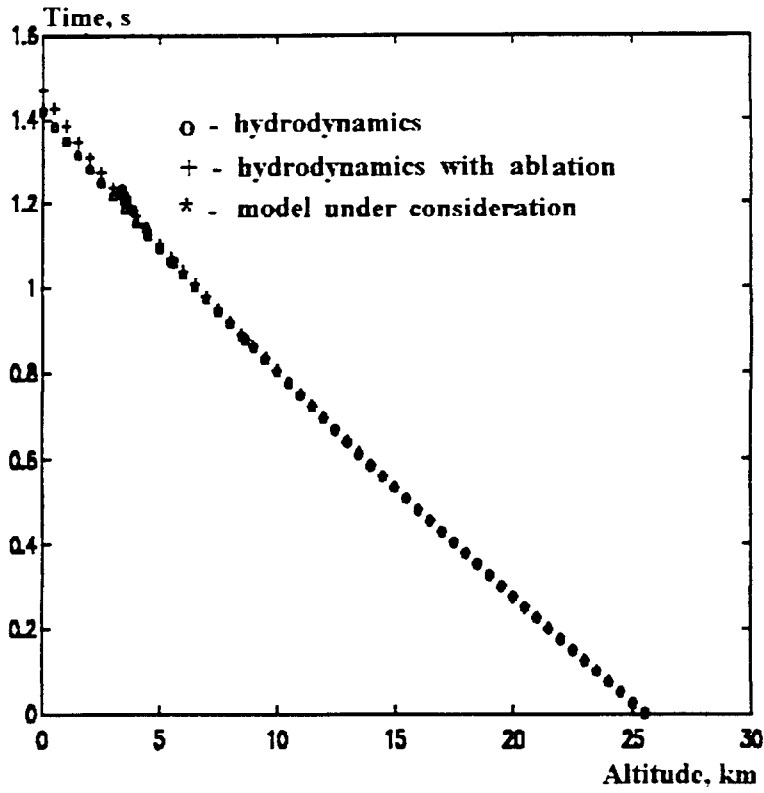
Burst of Tunguska meteorite from the analytical viewpoint: sphere had radius of 46 m, velocity of 20 km/h, angle of incidence of  $45^{\circ}$ , total yield of 20 MT.

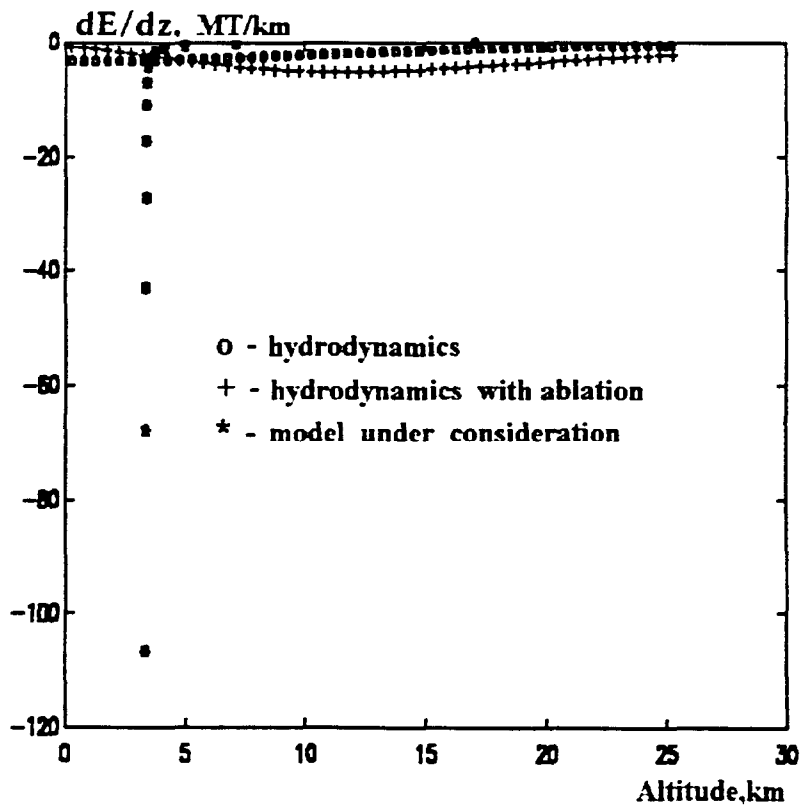
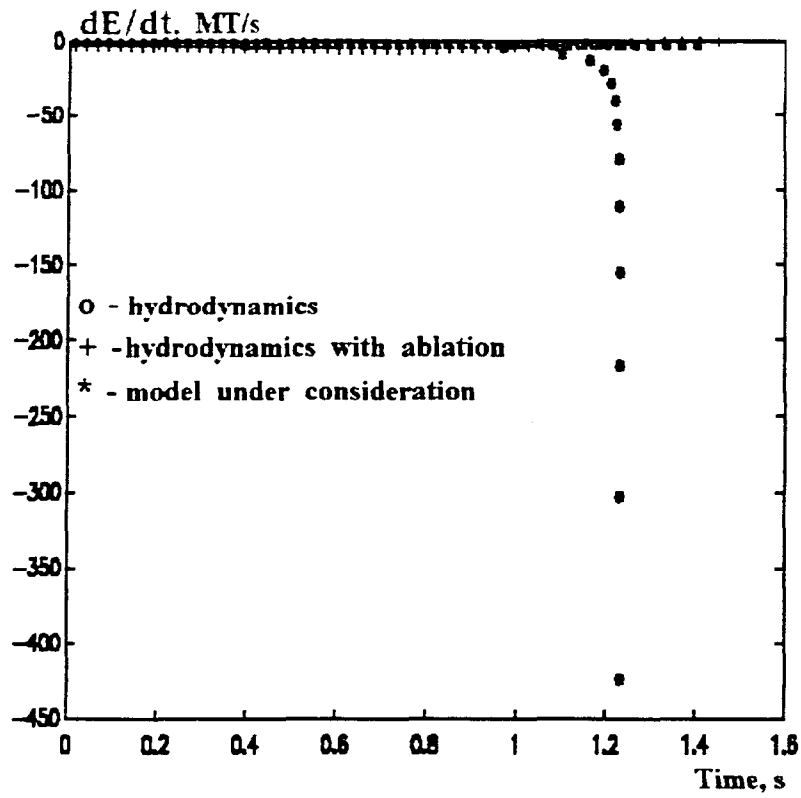


Fragments of meteorite can maximally reach the altitude of 3.24 km.

Explosive process results in the loss of about 8 MT of energy.

# COMPARISON OF DIFFERENT MODELS





## **CONCLUSION**

**Based on the results obtained, directions for further research can be determined:**

- 1. Effect of material type (ice, stone, iron) and porosity on the process of fragmentation.**
- 2. Effect of meteorite (asteroid) form on fragmentation.**
- 3. 3D mathematical modeling of fragmentation processes.**
- 4. Comparison of experimental observations of bursts in the atmosphere with the results of mathematical modeling and calculations according to the analytical model.**
- 5. Calibration of physical models and mathematical codes on the basis of experimental results.**
- 6. Detailed study of how resistance coefficient and destruction time depend on air density.**

## **ACKNOWLEDGMENTS**

**Authors express their gratitude to R. Dudnik and V. Zolotova for assistance with calculations.**

## **Implementation of Numerical Simulation Techniques in Analysis of the Accidents in Complex Technological Systems**

**G. S. Klishin, V. E. Seleznev, V. V. Aleoshin, Russian Federal Nuclear Center-VNIIEF, Russia  
Presented by P. I. Pohl, Sandia National Laboratories, Albuquerque, NM**

Gas industry enterprises such as main pipelines, compressor gas transfer stations, gas extracting complexes belong to the energy intensive industry. Accidents there can result into catastrophes and great social, environmental and economic losses. Annually, according to official data several dozens of large accidents take place at the pipes in the USA and Russia. That is why prevention of the accidents, analysis of the mechanisms of their development and prediction of their possible consequences are acute and important tasks.

The accidents reasons are usually of a complicated character and can be presented as a complex combination of natural, technical and human factors. In the RAO "GAZPROM" there is a subdivision of the reasons of accidents into the following groups:

- environmental interference;
- defects and drawbacks of the pipes and auxiliary equipment manufacture;
- mistakes in the pipelines operation;
- damages during the pipelines construction;
- unauthorized interference in the gas pipes operation.

Mathematical and computer simulations are safe, rather effective and comparatively inexpensive methods of the accident analysis. It makes it possible to analyze different mechanisms of a failure occurrence and development, to assess its consequences and give recommendations to prevent it. The difficulties in mathematical and computer simulations of accidents at the pipelines objects can be explained by :

- a wide spectrum of the failures reasons and consequences;
- the variety of the accidents mechanisms and ways of their development;
- an integrated influence of the damaging factors.

Besides investigation of the failure cases, numerical methods play an important role in the treatment of the object's diagnostics results and in further construction of mathematical prognostic models of the object behavior during the period of time between two inspections.

While solving the diagnostics tasks and in the analysis of the failure cases, the techniques of theoretical mechanics, of qualitative theory of differential equations, of mechanics of a continuous medium, of chemical macro-kinetics and optimizing techniques are implemented in the Conversion Design Bureau #5 (DB#5). Both universal and special numerical techniques and software are being developed in DB#5 to solve such tasks. Almost all of them are calibrated on the calculations of the simulated and full-scale experiments performed at the VNIIEF and MINATOM testing sites. It is

worth noting that in the long years of work there has been established a fruitful and effective collaboration of theoreticians, mathematicians and experimentalists of the institute for solution of such tasks.

Let's consider in more details the approaches and mathematical simulation techniques implemented in DB#5, VNIIEF for the pipelines failures analysis. Big movements, shifts and spread of the construction elements of the pipeline equipment during an accident can be well described with the help of the theoretical mechanics equations. Theoretical mechanics techniques are often used during a simplified numerical analysis of the equipment behavior in the emergency mode of operation.

For example, with their help the oscillations of the air column between blades of the compressor, located at the compressor gas transfer station, during the surge can be described in the first approximation. The task of the surge simulation in this case can be presented as the analysis of a usual system of differential equations with the given boundary conditions. This analysis is done in accordance with the qualitative theory of differential equations. It makes it possible to evaluate surge stability and character, to predict the accident development. Figures 1.2 show an example of the surge phenomenon analysis with the help of computer simulation performed for GTU-16Ö, that is located in one of the shops of the compressor station «Morkinskaya», «Volgotransgaz» subsidiary.

In investigation of fires, a combination of three-dimensional finite element and one-dimensional finite difference models is often implemented. They are investigated with the help of the finite element techniques (FET) and finite difference techniques. Let's consider this approach using the following example. The gas pipe in the building is ruined, a combustible mixture of methane and air is formed. It has filled the building inside. There was a heating source in one of the rooms of the building. To analyze the possible inflaming of the combustible mixture, there were performed non-stationary three-dimensional thermal calculations with the help of a finite element technique. In three-dimensional thermal calculations a gas mixture was assumed as an inert one. This approach in the analysis of the air-methane mixture heating is quite authorized, as the processes of the mixture enflaming take place in a very narrow layer adjacent to the heater. (As a rule, the thickness of the heated layer is considerably less than the distance between the adjacent joints of the finite element grid (graticule) implemented in thermal calculations).

So, at every time step of the finite element technique, after three dimensional thermal areas were calculated, the most heated micro-volumes of the combustible mixture were selected. In these volumes the combustible mixture was considered as a mixture where exothermic chemical reactions take place. We performed one-dimensional non-stationary thermal calculations with consideration of kinetics of a chemical exothermic mixture decomposition to assess the possibility of enflaming of the selected micro-volumes. Here finite difference techniques with the adaptive grid were used.

As a rule, in an emergency at the gas pipeline, the magnitudes of one or several parameters characterizing the design of the equipment or its operation, reach their extremes. That is why, in simulation of emergency cases at the gas pipelines optimizing techniques are widely used in VNIIEF. In this case, a target function of the optimizing task describes critical parameters of the gas transfer system as a function of control efforts induced on the pipeline equipment. Task limitation functions reflect constructive and technological limitations of the pipeline equipment or the gas transfer process.

Taking into account the complexity of the gas pipeline systems, the target function and the limitation functions are non-linear multi-parameter functions. The problem of gas transportation operating costs reduction can also be presented as an optimizing task (Fig. 3,4). So, we are facing the need to solve a non-linear multi-parameter task of a conditional optimization, that looks like:

$$F(X) \Rightarrow \min, \quad G(X)=0, \quad P(X)>0, \quad A > X > B,$$

where  $F(X)$  is a target function,  $G(X)$ ,  $P(X)$ , are given limitation functions,  $X$  is a vector of controlling influences,  $A$ ,  $B$  are the given vectors that belong to the  $n$ -dimensional Euclidean space. For solution of optimizing tasks a library of optimization programs is developed in DB#5, VNIIEF. Original algorithms of solution the tasks of linear, non-linear and mini-maximum optimization are realized. Special algorithms to analyze the obtained solution for its extremity are developed. Many years of work with the optimization library confirmed its operability and sufficient effectiveness of the algorithms in it.

Besides the analysis of different accidents at the gas pipelines, mathematical simulation techniques, that were originally developed in RFNC-VNIIEF for to solution of the tasks of gas industry and pipeline transportation, could be implemented in :

- the analysis of the main pipelines state;
- localization of the places of the pipeline destruction;
- in creation of new generation information and control systems for pipeline transportation.

Figure 1. Stable Equilibrium System State

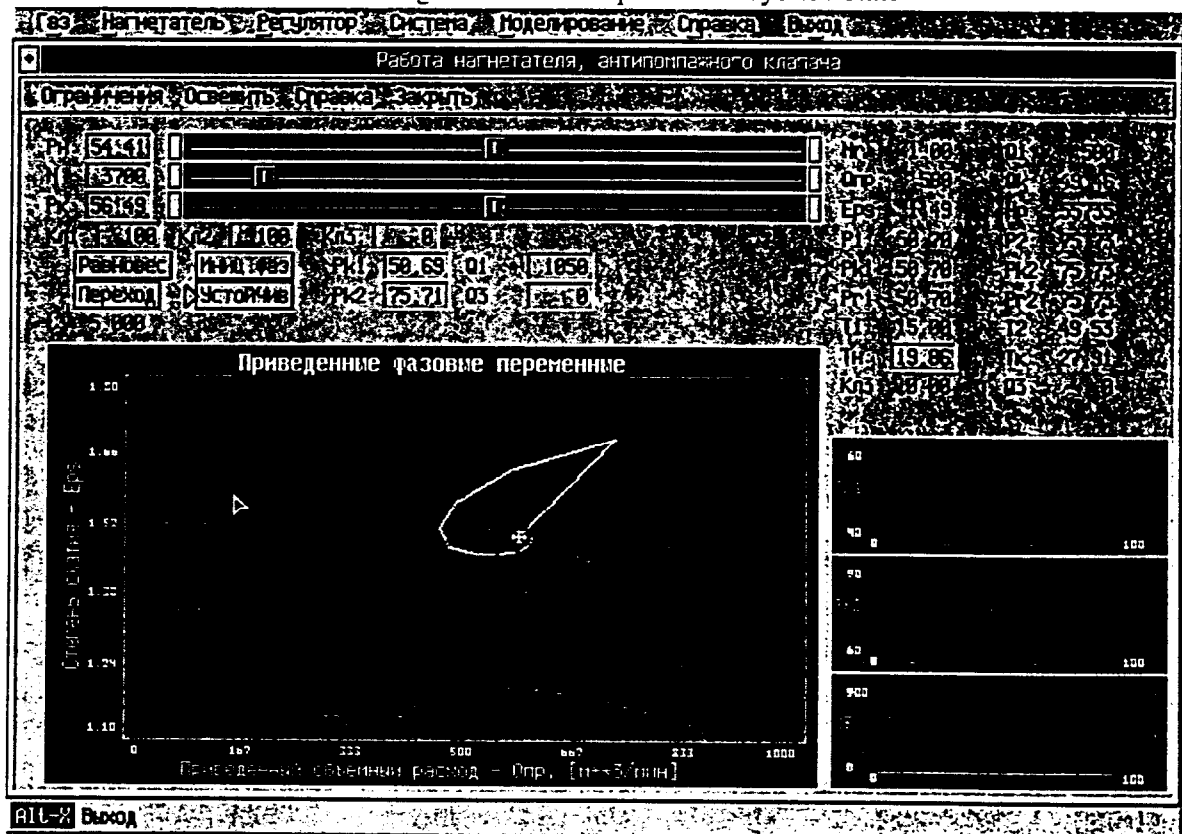


Figure 2. Hard Mode of the Excitation of the Surge

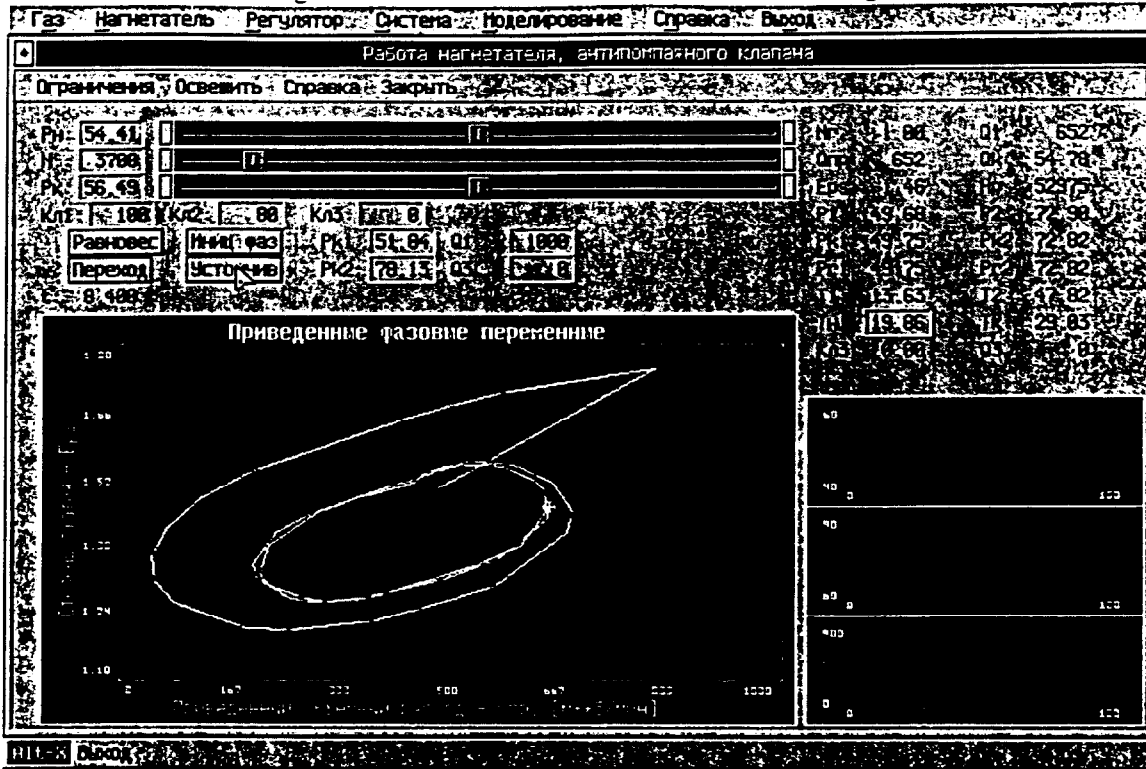


Figure 3. Initial Position in an Example

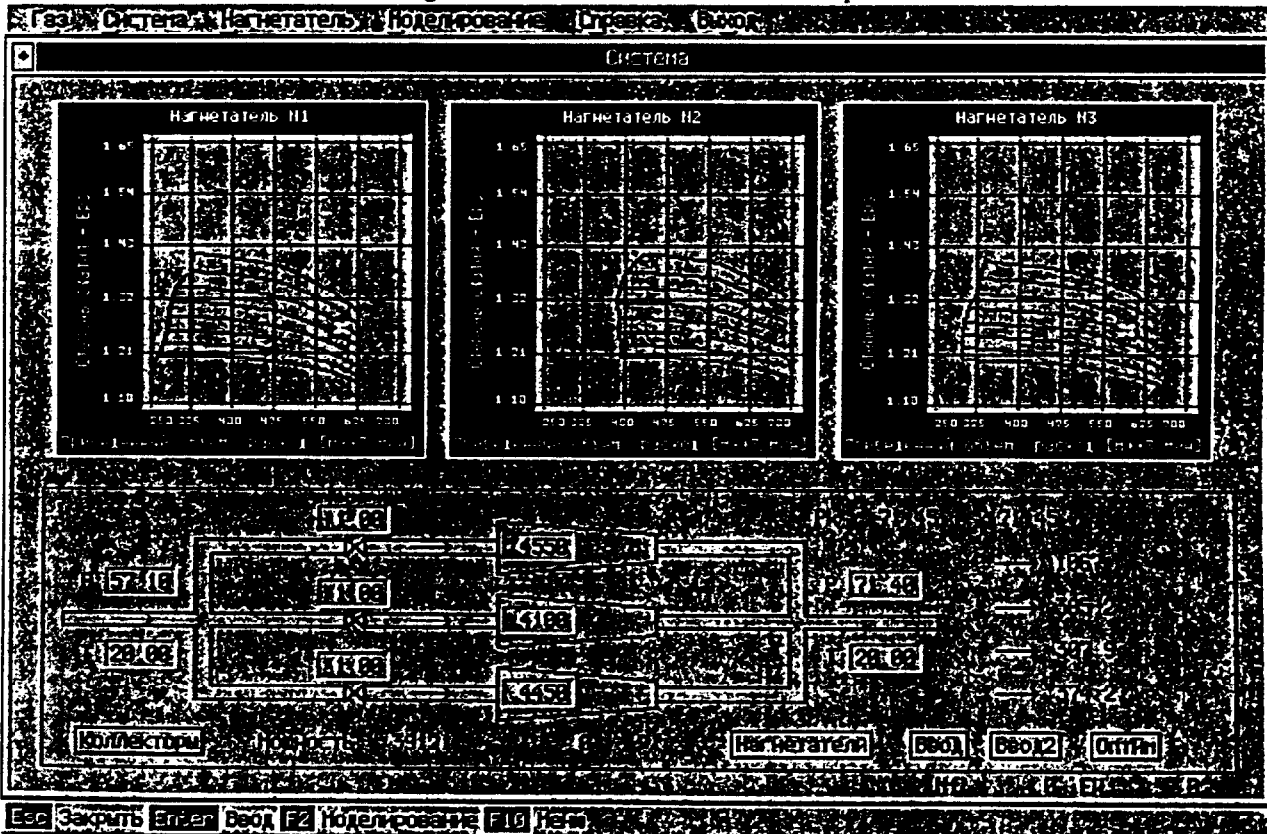
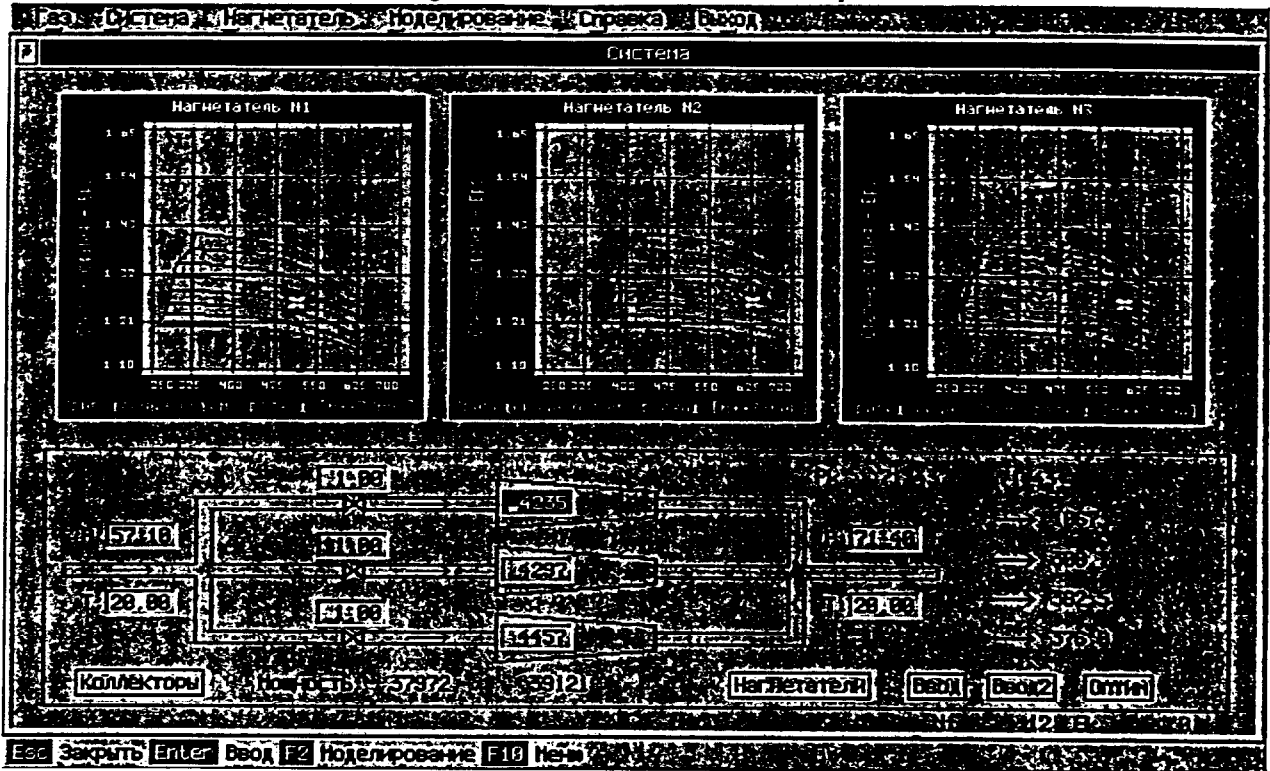


Figure 4. Final Position in an Example



Let's consider implementation of numerical simulation for assessment of the pipeline state that is based on the results of the external and internal pipe diagnostics. To evaluate the state of the main pipelines from the point of view of their strength an external pipe and internal diagnostics is performed from time to time. In the DB#5, RFNC-VNIEEF pipeline state assessment from the point of view of their strength is usually performed with the help of the techniques of the continuous medium mechanics, in particular FEM that is widely used nowadays. Here the approach is based on a consequent implementation of the beam models, shell models and voluminous finite element models. Calculations on the beam models (Fig.5,6) and shell models (Fig.7,8) are of evaluating character are mainly used for specifications of boundary conditions for FEM calculations

Figure 5. Actual Displacement of the Pipeline as Compared to the Designed One

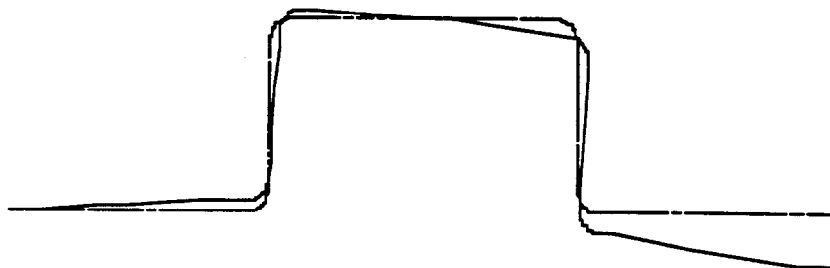
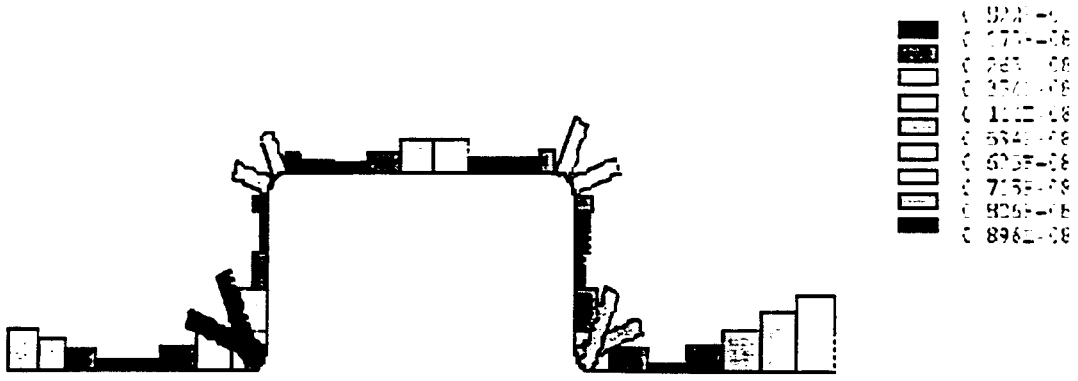
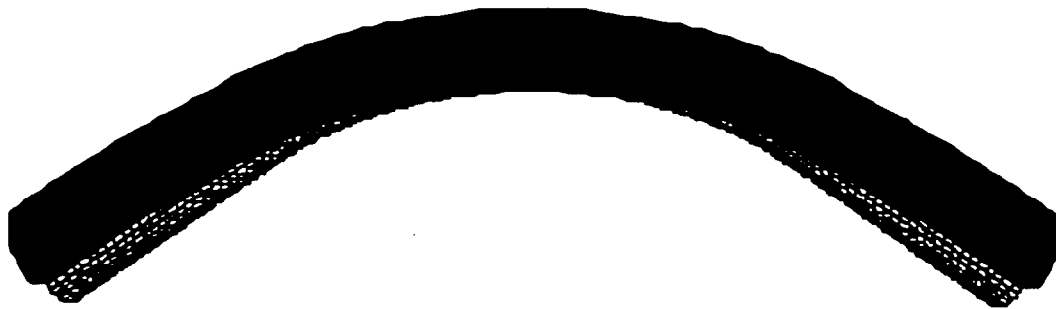


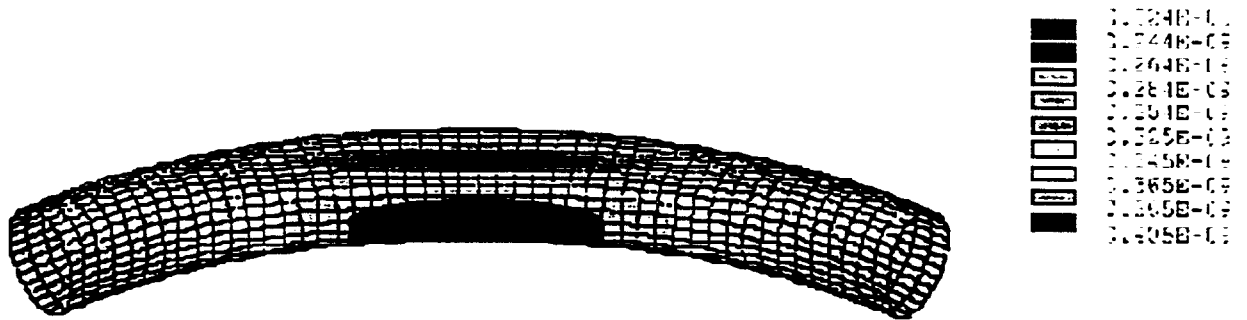
Figure 6. Stress Intensity at the Pipeline Section



**Figure 7. Deformation of the Pipeline Curve Where A Corrosion Defect is Located**

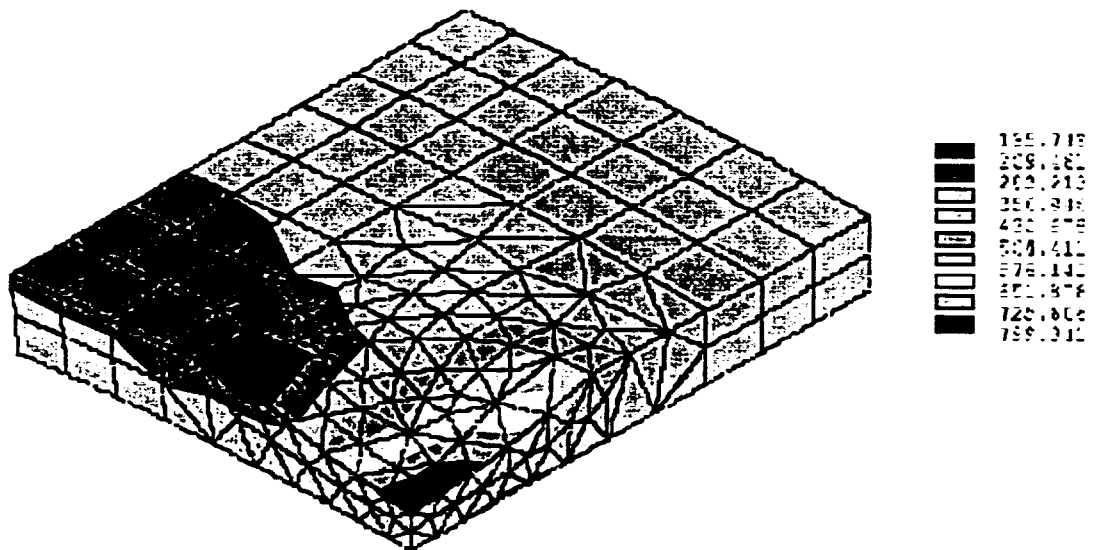


**Figure 8. Stress Intensity at the External Side of the Pipeline Curve Where A Corrosion Defect is Located**



basing on the finite element model (Fig.9). This approach allows to consider the deformation influence of the whole pipeline section on the stress and strain state in the defective zone.

**Figure 9. Stress Intensity in the Defective Zone**



Analysis of the calculation results allows one to make a conclusion, based on the criteria of strength and destruction, about the carrying capability of the defective pipeline section. This conclusion serves as a basis for decision about this section replacement, repair or prolongation of its service lifetime.



# **An Implicit Fast Fourier Transform Method for Integration of the Time Dependent Schrodinger Equation**

Merle E. Riley

Laser, Optics, and Remote Sensing Department

Sandia National Laboratories

Albuquerque, NM USA 87185-1423

and

A. Burke Ritchie

Lawrence Livermore National Laboratory

Livermore, CA USA 94550

## **Abstract**

One finds that the conventional exponentiated split operator procedure is subject to difficulties when solving the time-dependent Schrodinger equation for Coulombic systems. By rearranging the kinetic and potential energy terms in the temporal propagator of the finite difference equations, one can find a propagation algorithm for three dimensions that looks much like the Crank-Nicholson and alternating direction implicit methods for one- and two-space-dimensional partial differential equations. We report investigations of this novel implicit split operator procedure. The results look promising for a purely numerical approach to certain electron quantum mechanical problems. A charge exchange calculation is presented as an example of the power of the method.

## **I. Introduction**

The potential of fast computers to solve difficult full-dimensional problems prompted us to investigate some modern finite-difference methods for solution of partial differential equations of interest, among these the time-dependent Schrodinger equation (TDSE). One of the more interesting choice methods for integration of the TDSE<sup>1</sup> is the exponentiated split operator procedure (ESOP),<sup>1,2</sup> based on the use of the fast Fourier transform (FFT), which has been successfully used for vibration-rotation spectral analysis and simple scattering situations.<sup>1,3,4</sup>

Electronic processes such as charge transfer, excitation, and ionization involve the Coulomb interaction which makes the numerical representation of the wave function more difficult than in the molecular dynamics studies.<sup>2,3,4</sup> We find that the ESOP tends to be very sensitive to the integration step size in Coulombic problems: the solutions become inaccurate very abruptly as the time increment is increased. Overall, one would prefer a method with the inherent stability of implicit numerical procedures which, although inaccurate for large step sizes, remain stable and acceptable in overall character. We review the ESOP and introduce a novel numerical method, the implicit split

operator procedure (ISOP), which is reminiscent of the Crank-Nicolson (CN) and alternating-direction implicit (ADI) methods<sup>5</sup> for integrating the TDSE.

The TDSE is written as  $\dot{\Psi} = -i H \Psi$  in Hartree atomic units (denoted au). The Hamiltonian operator is:

$$H = T + V, \quad T = -\frac{1}{2} \nabla^2. \quad (1)$$

where the potential  $V$  is a function of position and time. The ESOP formulates the numerical integration as the repeated application of the factored (split) incremental propagator:

$$\Psi_{t+dt} = \exp(-\frac{1}{2}i T dt) \exp(-i V dt) \exp(-\frac{1}{2}i T dt) \Psi_t. \quad (2)$$

By using the speed of the FFT to convert from the space to momentum representation and back, one can always apply *diagonal* operators to the wave function. The ESOP conserves norm but not energy due to the lack of commutation of the incremental propagator with the Hamiltonian. The procedure is correct through order  $(dt)^2$ .

In certain atomic physics applications we found that the truncation error in the ESOP grew faster than we could tolerate with time steps that would have appeared to be adequate for a second-order-accurate method. These were applications with a Coulomb potential and a hydrogen 1s orbital as a part of the wave function. We begin by writing down the second-order-accurate, time-symmetric form of the finite difference advance in the TDSE, analogous to the CN procedure:

$$\Psi_{t+dt} + \frac{1}{2}i H dt \Psi_{t+dt} = \Psi_t - \frac{1}{2}i H dt \Psi_t. \quad (3)$$

A direct numerical solution of Eq.(3) is impractical due to the difficulties in resolving the implicit part of the operator, even with the use of ADI techniques. The truncation error in Eq.(3) is  $O(dt)^3$ , which is precisely the same as in the ESOP in Eq.(2). What is desired is a use of the fast Fourier transform (FFT) methods for resolving Eq.(3) by splitting the space and momentum parts of the Hamiltonian. One way to do this is to rewrite Eq.(3):

$$\Psi_{t+dt} = \frac{1 - \frac{1}{2}i H dt}{1 + \frac{1}{2}i H dt} \Psi_t \quad (4)$$

and to factor the propagator quotient *approximately*, all the while *maintaining* accuracy through  $O(dt)^2$  precisely as in Eq.(2):

$$\Psi_{t+dt} = \left( \frac{1 - \frac{1}{4}i T dt}{1 + \frac{1}{4}i T dt} \right) \left( \frac{1 - \frac{1}{2}i V dt}{1 + \frac{1}{2}i V dt} \right) \left( \frac{1 - \frac{1}{4}i T dt}{1 + \frac{1}{4}i T dt} \right) \Psi_t. \quad (5)$$

The advantage of this factorization or splitting is that the operator is now a product of momentum and coordinate dependencies which allows the FFT procedure to be applied as in the ESOP. The form in Eq.(5) is our implicit split operator procedure (ISOP)<sup>6,7</sup>.

## II. Numerical Study of Stationary State

Our first numerical study compared calculations on the stationary 1s hydrogen atom ground state with the ESOP and ISOP methods. We used computational cubes of 10, 20, and 40 au on a side, all with an FFT grid of  $(64)^3$ , symmetrically centered about the Coulomb singularity. The time solution went from zero to 200 au. The space points were element centered and quadratures were performed by the trapezoidal rule. We varied the time increments  $dt$  from 0.02 to 0.5 au.

What we found was that the ESOP calculations were unstable with diverging energy for  $dt = 0.05$  in the  $10^3$  box, for  $dt=0.1$  in the  $20^3$  box, and for  $dt = 0.5$  in the  $40^3$  box. The ISOP was stable for all boxes and space grid sizes for *all* these time increments. Note the resemblance to a “Courant-like” condition in the fact that a larger space increment allows stable integration with a larger time step for the ESOP. Of course the accuracy is not as good for the coarser grids even in the ISOP. A detailed examination of the numerical ESOP wavefunction shows that the unstable propagation error is rapidly varying in space and thus appears in the kinetic energy.

## III. Numerical Study of Charge Exchange

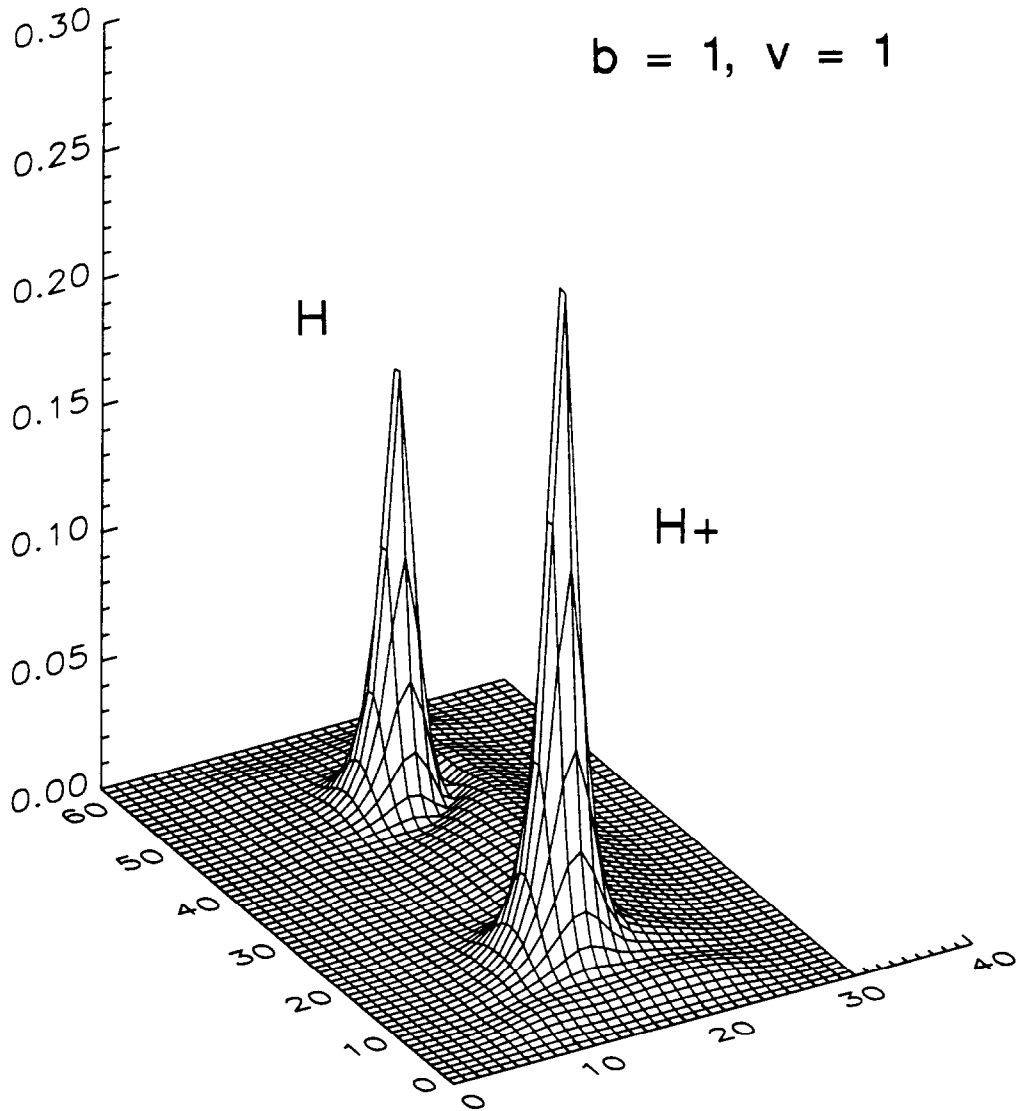
Quantum charge exchange is a notorious multi-arrangement-channel scattering problem of great mathematical and numerical complexity. Even the simple idea of expanding in atomic orbital and/or molecular orbital bases is complicated. We have done a small set of charge exchange calculations of protons on H in the mixed classical-quantum picture. Our results agree quantitatively with experiment and the best prior theory. The potential energy for two moving nuclei is written as:  $V = -Z_a / r_a(t) - Z_b / r_b(t)$ . The presence of ionization in fast collisions requires us to put absorbing boundaries<sup>8</sup> on the computational box. In so doing the periodic boundary conditions of the FFT do not cause interference within the free unbounded ionized channel. One of the most impressive aspects of the present numerical treatment of the quantum charge exchange problem is the simple and straightforward formulation of the theory. The Figure illustrates a slice through the nuclei of the modulus of the wavefunction after the collision with a relative velocity ( $v$ ) of 1 au and a collision impact parameter ( $b$ ) of 1 au. Part of the ionized electron is still leaving the vicinity of the scattering center.

## IV. Discussion and Conclusion

To conclude, we feel that the improved stability and energy conservation of the ISOP affords direct numerical approaches to the solution of certain quantum mechanical problems. Some of these problems are: strong-field excitation and ionization, charge exchange, multichannel reactive scattering, and wave packet dynamics. The new massively parallel computers can make such approaches practical.

## Appendix

A uniformly spaced cartesian grid with points centered about the Coulomb singularity defines its own cutoff of the potential. However one can see that an arbitrarily positioned gridwork



can create a large error in the numerical representation of the potential operator if a grid point lies too near the singular point. We make the following argument for the modification of the Coulomb field when used with the FFT grids. Consider the integral over a spherical volume of radius  $R$  centered about the singular point of the potential: If we equate the spherical volume element to the volume of a rectilinear cartesian volume element,  $dV = dx \times dy \times dz$ , we find for the sphere's radius:  $R = (3dV / 4\pi)^{1/3}$ . If we now equate the integral over the Coulomb singularity to the trapezoidal value of that integral with a cutoff of  $r_x$  imposed in the Coulomb potential, we have  $2\pi R^2 = (1 / r_x) (dx)^3$ , from which we can now solve for  $r_x$  using the above value of  $R$ :  $r_x = (2dV / 9\pi)^{1/3}$ . The Coulomb potential is simply evaluated with  $r = \max[r, r_x]$ .

### Acknowledgments

We wish to thank Charles Cerjan and Mike Feit for useful information and discussions regarding this work. This work was performed under the auspices of the U. S. Department of Energy by Lawrence Livermore National Laboratory under Contract No. W-7405-ENG-48 and was also supported by the United States Department of Energy under Contract DE-AC04-94AL85000 at Sandia National Laboratories. Sandia is a multiprogram laboratory operated by Sandia Corporation, a Lockheed Martin Company, for the United States Department of Energy.

### References:

1. C. Leforestier, R. H. Bisseling, C. Cerjan, M. D. Feit, R. Friesner, A. Guldberg, A. Hammerich, G. Jolicard, W. Karrlein, H.-D. Meyer, N. Lipkin, O. Roncero, and R. Kosloff, "A Comparison of Different Propagation Schemes for the Time Dependent Schrodinger Equation," *J. Comput. Phys.*, 94, 59-80 (1991).
2. M. D. Feit, J. A. Fleck, Jr., and A. Steiger, *J. Comput. Phys.*, "Solution of the Schrodinger Equation by a Spectral Method," 47, 412-433 (1982).
3. M. D. Feit and J. A. Fleck, Jr., "Wave packet dynamics and chaos in the Henon-Heiles system," *J. Chem. Phys.*, 80, 2578-2584 (1984).
4. M. D. Feit and J. A. Fleck, Jr., "Solution of the Schrodinger equation by a spectral method II: vibrational energy levels of triatomic molecules," *J. Chem. Phys.*, 301-308 (1983).
5. W. H. Press, B. P. Flannery, S. A. Teukolsky, and W. T. Vetterling, "Numerical Recipes- The Art of Scientific Computing," Camb. Univ. Press, Camb. and NY (1989).
6. A. Burke Ritchie and Merle E. Riley, Sandia National Laboratories Technical Report SAND97-1205, June 1997
7. B. Ritchie, P. Dykema, and D. Braddy, "Use of Fast Fourier Transform Computational Methods in Radiation Transport," *Phys. Rev. E*, 57, 2217, 1997.
8. K. C. Kulander, "Multiphoton ionization of hydrogen: A time-dependent theory," *Phys. Rev. A*, 35, 445-447 (1987).



# IMPORTANCE BIASING SCHEME IMPLEMENTED IN PRIZMA CODE

*Ia.Z. Kandiev, G.N. Malyshkin*

**Russian Federal Nuclear Center - All-Russia Scientific-Technical Institute of Technical Physics (RFNC-VNIITF), Snezhinsk, Russia, 456770**

## Introduction

PRIZMA code [1] is intended for Monte Carlo calculations of linear radiation transport problems. The code has wide capabilities to describe geometry, sources, material composition, obtain parameters specified by user. There is a capability to calculate path of particle cascade (including neutrons, photons, electrons, positrons and heavy charged particles) taking into account possible transmutations.

Importance biasing scheme [2] was implemented to solve the problems which require calculation of functionals related to small probabilities (for example, problems of protection against radiation, problems of detection, etc.). The scheme enables to adapt trajectory building algorithm to problem peculiarities.

The scheme was developed employing idea of step-by-step calculation of complicated problems according to which initial problem is split into several subproblems which are solvable and are solved successively (results of the first subproblem become input data for the second and so on). Main drawbacks of this way of solving are, first, error emerging due to data conversion at the moment of transit from one subproblem to another and, second, uncertainty in estimating statistical error of the final result.

Scheme implemented in PRIZMA code enables to obtain final result in one through calculation and use splitting into subproblems in order to use methods of non-analog modeling at different steps.

For this purpose we defined four classes of problems with simple relations between source and detector (elementary problems) so that majority of conventional problems of linear transport theory can be reduced to some combinations of them. Schemes of non-analog modeling and principles of building approximate importance function and appropriate non-analog distributions were selected for each class of problems. Special tool for "calculation control" was created allowing to transit from one elementary problem to another during the process of building trajectory.

## Non-analog modeling

When solving integral-differential Boltzmann transport equation we deal with two forms of its integral representation written for density of particles (density of collisions) prior to collision  $\psi(\mathbf{P})$  and after it  $\chi(\mathbf{P})$ :

$$\Psi(P) = \int K(P, P') * \Psi(P') dP' - \psi_1(P) \quad (1)$$

$$\chi(P) = \int L(P, P') * \chi(P') dP' - \chi_0(P) \quad (2)$$

Here

$P = P\{r, \bar{\Omega}, E, t\}$  - is phase space point characterized by the position  $r$ , direction  $\bar{\Omega}$ , energy  $E$  and time  $t$ ;

$\Psi_1(P)$  - is density of first collisions;

$K(P, P')$  - is transition kernel from point  $P$  prior to collision to point  $P'$ ;

$\chi_0(P)$  - is distribution density of the source;

$L(P, P')$  - is transition kernel from point  $P$  after collision to point  $P'$ ;

In the course of building trajectories transitions take place from one form of integral equation to another and vice versa.

In practice importance biasing scheme should be implemented as follows:

1. Calculate approximate importance function meeting functional of the problem under consideration. Approximate importance function should be rather simple in order to provide appropriate nonanalog distributions.
2. In compliance with the importance function obtained build nonanalog distributions with parameters selected to minimize fluctuations of particle statistical weight  $w$ .
3. Introduce special procedure into random walk scheme allowing to eliminate fluctuations of particle weight: reducing statistical weight  $w$  to the value of weight function  $W(P)$  which is inversely proportional to importance function.

## Importance biasing scheme in PRIZMA code

### Elementary problems

PRIZMA code employs estimate “on visits”, i.e. result is recorded only if particle passes through the region of detection. In this case statistical error of estimate of any functional will be large if probability of particle hitting detector is very small. Consequently, to estimate any functionals it is necessary to model trajectories in such way that to increase the number of particles hitting the detector. This means that it is necessary to increase artificially both density of collisions in the vicinity of detector and inside detector and density of particles moving to detector and its vicinity. Thus, problem of estimating any functional is reduced to the problem of estimating solutions  $\psi(P)$  and  $\chi(P)$ , ignoring dependence of importance function on the form of particular functional.

Each of these two groups of problems has its own peculiarities but they are related since turn into one another in the course of modeling. Problems of each group are also divided into two groups. Totally there are four classes of problems to solve which it is necessary to apply nonanalog modeling:

1. Radiation transport in optically thick medium. Calculation of density  $\Psi(P)$ .
2. Radiation transport in optically transparent medium. Calculation of density  $\Psi(P)$ .
3. Radiation transport into detector located in vacuum or absolute absorber. Calculation of density  $\chi(P)$ .

4. Radiation transport into detector located in emitting and scattering medium. Calculation of density  $\chi(P)$

Problem falling into one of these classes with simple relation between source and detector is referred to as elementary. Most problems of linear radiation transport theory can be reduced to a combination of elementary problems.

### Importance function

For the simplest case (one-group (with constant energy) radiation transport problem in homogeneous infinite medium with point isotropic source) the following relation can be obtained based on reciprocity law:

$$\Psi_{r_d}^*(r) = \Psi_r(r_d) \quad (3)$$

where  $\psi$  and  $\psi^*$  are solutions of direct and adjoint equations;

$r$  is source point;

$r_d$  is detector point.

To calculate weight function  $W(r)$ , importance function  $\psi$  is normalized to its value at the source point  $r_0$ :

$$\Psi'(r) = \frac{1}{W(r)} = \frac{\Psi_r(r_d)}{\Psi_{r_0}(r_d)} \quad (4)$$

For the problems with arbitrary geometry, medium properties are symmetrized in accordance with 1D geometry (plane, cylindrical or spherical) specified by detector geometry. But it is required to meet the following condition :

$$\Psi_r(r_d) \geq \max \Psi_{\bar{R}}(\bar{R}_d), \quad \bar{R}, \bar{R}_d \in S \quad (5)$$

where  $S$  is a set of pairs of points matching pair  $r, r_d$  in 1D geometry.

For spectral problems approximate solutions of one-group problems are used

$$\Psi'(r, E) = \frac{\Psi_r(r_d, E)}{\Psi_{r_0}(r_d, E_0)}, \quad (6)$$

where  $\Psi_r(r_d, E)$  is non-increasing function of  $E$ ,  $E_0$  is maximal source energy,

and the following condition should be satisfied

$$\Psi_r(r_d, E_1) \leq \Psi_r(r_d, E_2) \quad (7)$$

where  $E_1$  is incidence energy,  $E_2$  is secondary or scattered energy

Similarly, expression for importance function  $\chi$  from equation (2) is as follows

$$\chi'(r, \bar{\Omega}) = \frac{\chi_r(r_d, \bar{\Omega})}{\chi_{r_0}(r_d, \bar{\Omega})} \quad (8)$$

## Schemes for elementary problems

For specified classes of elementary problems importance functions and brief description of applied methods are given below

**Class 1.** Problems of radiation transport in optically thick media

Importance function reads as

$$\psi'(r, E) = e^{C_0 * r_0^{eff}} * e^{-C(E) * r^{eff}} = N e^{-C(E) * r^{eff}} \quad (9)$$

where  $r$  is distance from a current point to detector;

$r_0$  is distance between source and detector;

$C_0 = C(E_0)$ , where  $E_0$  is maximal energy of the source.

And  $C(E) < \Sigma'(E) \leq \Sigma(E)$ , where  $\Sigma(E)$  is total macroscopic cross-section of interaction,  $C(E)$  and  $\Sigma'(E)$  are non-increasing functions and  $C(E)$  and  $r^{eff}$  are selected to satisfy conditions (5), (7).

Main methods of calculations are geometrical splitting and exponential transformation.

**Class 2.** Problems of radiation transport in optically transparent media.

Importance function is

$$\Psi'(r, E) = \frac{1}{\Delta\tau} \quad (10)$$

where  $\Delta\tau$  is optical thickness of the system ( $\Delta\tau \ll 1$ ).

Main method of calculation is method of forced collisions when density of collisions in the medium is artificially increased.

**Class 3.** Problems of detecting with detector located in absolute absorber (or vacuum) at a rather large distance from emitting and scattering medium.

Importance function is specified in the form

$$\chi'(r, \bar{\Omega}) = \begin{cases} 1/\Delta\mu_0 & \bar{\Omega} \in \varpi \\ 1 & \bar{\Omega} \notin \varpi \end{cases} \quad (11)$$

Here:

$\Delta\mu_0 = 1 - \mu_0$ ,  $\mu_0 = \sqrt{(r_0^2 - R_d^2)/r_0^2}$ ,  $r_0$ ,  $r_0$  is minimal distance from scattering medium to the center of spherical detector with radius  $R_d$ ;

$\varpi$  is a set of directions from point  $r$  to spherical detector.

Main method applied is method of "test" particles in which two particles instead of one are emitted from escape point. One of them moves in a cone of directions  $\varpi$ : its escape angle with respect to direction to detector is selected from uniform distribution

$$\frac{1}{1 - \mu_d}$$

where  $\mu_d$  is cosine angle between tangent to sphere of  $R_d$  radius from point  $r$  and direction to the center of detector.

Escape angle of the second particle results from physical distribution sampling within the range (-1,1) with failure: if selected direction is within  $\varpi$  then particle is considered to be absorbed at the escape point, otherwise it continues motion with the previous weight. Extension for  $m$  detectors is allowed.

**Class 4.** Problems of detecting with detector located in emitting and scattering medium. Importance function is the following:

$$\chi'(r, \bar{\Omega}) = \frac{\Delta\mu_r}{\Delta\mu_c} = \frac{1-\mu_r}{1-\mu_c} \quad (12)$$

where  $r$  is distance between current point and detector center.

$r_0$  is distance between source and detector center,

$\mu_r$  is cosine angle between particle direction and direction to the center of detector.

$$\begin{aligned} \mu_r &= \sqrt{((r_\mu^2 - R_d^2) / r_\mu^2)} \\ r_\mu &= \begin{cases} R_d, & r_\Omega \leq R_d \\ r_\Omega, & R_d < r_\Omega < r_0 \\ r_0, & r_\Omega > r_0 \end{cases} \\ r_\Omega &= \begin{cases} r\sqrt{(1-\mu^2)}, & \mu > 0 \\ r, & \mu \leq 0 \end{cases} \end{aligned} \quad (13)$$

Main method of calculations is method of concentric detectors which implies the following. All space is covered with the net of  $m$  concentric spheres (detector is the first of them)  $R_d = R_1 < R_2 < \dots < R_m$ .

Assume that it is necessary to game escape angle of the particle which is at the distance  $r > R_1$  from the center of detector. Let  $A_i$  be a set of directions from point  $r$  to detector  $R_i$ ,  $i = 1, k$ , where  $k = m$ , if  $r > R_m$  or  $k = l$ , if  $R_{l-1} < r \leq R_l$ ,  $l = 2, m$ , assuming that  $R_1 = r$ . Whole set  $\omega$  of possible particle directions is divided into sub-sets  $\omega_i$  where  $\omega_1 = A_1$ ,  $\omega_i = A_i - A_{i-1}$ ,  $i = 2, k$ ,  $\omega_{k-1} = \omega - \Sigma A_k$ .

Escape angle for detector  $R_1$  is selected from uniform distribution,

$$\frac{1}{1-\mu_1}$$

and for detectors  $R_i$ ,  $i = 2, k$  is proportional to the function

$$f(\mu) = \frac{1}{1-\mu}, \quad \mu_i < \mu \leq \mu_{i-1} \quad (14)$$

where  $\mu_i = \sqrt{((r^2 - R_i^2) / r^2)}$ .

Bias obtained is compensated with weights.

For  $\omega_{k-1}$  particle direction is sampled from physical distribution with failure. If selected direction is within  $\omega_{k-1}$  then particle is considered to be absorbed at the escape point. Otherwise it continues motion with the previous weight. Thus, at once  $(k+1)$  particles instead of one can start from the escape point.

### Change of statistical weight

The following procedure is implemented to reduce statistical particle weight  $w$  to a specified value of weight function  $W(P)$  at point  $P$ . Depending on relation between value  $n = w/W(P)$  and specified interval of values  $(n_1, n_2)$ ,  $n_1 < 1$ ,  $n_2 \geq 2$ , three outcomes are possible

- a)  $n > n_2$ . Splitting  $N$  particles instead of one continue random walk, each with weight  $w = w/N$ , where  $N = [n/n_2] - 1$ . Here square brackets mean integral part of number,
- b)  $n < n_1$ . Russian roulette: particle is "knocked on" with probability  $p = 1 - n$  and with probability  $p = n$  continues random walk with weight  $W(P)$ ,
- c)  $n_1 < n < n_2$ . Particle continues random walk with the previous weight  $w$ .

Interval  $(n_1, n_2)$  specifies range of admissible oscillations of statistical particle weight in the vicinity of prescribed value  $W(P)$ . Interval  $(0.5, 2)$  is usually used in calculations.

The above procedure of reducing statistical weight can be applied at the following phases of modeling particle: after obtaining initial parameters of source particle, prior to particle collision, after selection of type of particle interaction with matter, after sampling of scattering. Weight function can be defined in the form multiply of some functions.

### Scheme of initial problem calculation

The following phases can be defined in solving initial problem from statement to solution.

1. Analysis of problem conditions. Understanding of peculiarities. Problem reduction to elementary ones in compliance with the peculiarities.
2. For each elementary problem importance function is derived and importance biasing scheme is selected. According to importance function obtained, parameters of nonanalog distributions are calculated.
3. Problem is calculated by building trajectories in the real system but at every moment particle trajectory is built in compliance with importance biasing scheme of elementary problem within which the particle is.

### Calculation efficiency

Assume that in addition to some functionals nonanalog calculation gives average number  $I_n$  of particles caught by detector for the first time. Let  $\sigma_n$  be relative statistical error of this result and  $t_n$  be total calculation time. Then efficiency of this calculation is estimated using the known formula:

$$k_n = \frac{1}{\sigma_n^2 t_n} \quad (15)$$

For the case of analog modeling,  $I_A$  and  $\sigma_A$  are calculated using the following formulas:

$$\sigma_A = \frac{1}{\sqrt{m}} \quad (16)$$

$$I_A = \frac{m}{N}, \quad (17)$$

if  $I_A \ll 1$ .

Assuming  $I_A = I_n$  and  $\sigma_A = \sigma_n$ , we obtain

$$K_A = \frac{I_n}{t_1}, \quad (18)$$

where  $t_1$  is mean time required to calculate one history during analog modeling. Using formulas (15) and (18) we obtain expression to estimate prize of nonanalog calculation in comparison with that of analog.

$$K_F = \frac{K_p}{K_A} = \frac{t_1}{\sigma_n^2 I_n t_n} \quad (19)$$

### Examples of calculations

Examples are given below of several model problems calculated using the above approach.

**Problem 1.** Consider infinite homogeneous medium with two types of interaction: scattering at probability  $q=0.9$  and absorption; full macroscopic interaction cross-section being  $\Sigma=1$ . It is required to estimate flux of particles  $\Phi(R)$  at the different distances  $R$  (up to 100 optical thicknesses) from a point isotropic source. This problem falls into the class of elementary problems of radiation transport in optically thick media. Calculation method is exponential transformation.

Table 1 contains precise (up to 5 digits) values of flux  $\Phi(R)$  [3], calculated values of flux,  $\bar{\Phi}(R)$  calculated values of first collisions  $J_1(R)$  and values of prize  $K_B$  (19) at distances  $R=10, 20, \dots, 100$ . Hereinafter relative statistical percentage error is given in brackets.

Table 1.

R, cm	10	20	30	40	50
$\Phi(R) * 4\pi R^2$	1.3182e-1	1.3773e-3	1.0794e-5	7.5201e-8	4.9116e-10
$\bar{\Phi}(R) * 4\pi R^2$	1.312e-1 (0.47)	1.3774e-3 (0.56)	1.086e-5 (0.67)	7.59e-8 (0.80)	4.91e-10 (0.90)
$J_1(R)$	3.93e-2 (0.40)	3.97e-4 (0.50)	3.09e-6 (0.60)	2.135e-8 (0.72)	1.385e-10 (0.83)
$K_p$	0.95	4.0e1	2.7e3	2.3e5	2.2e7

R, cm	60	70	80	90	100
$\Phi(R) * 4\pi R^2$	3.0796e-12	1.8773e-14	1.1210e-16	6.5894e-19	3.8256e-21
$\bar{\Phi}(R) * 4\pi R^2$	3.06e-12 (1.1)	1.88e-14 (1.3)	1.12e-16 (1.5)	6.57e-19 (1.9)	3.88e-21 (2.3)
$J_1(R)$	8.63e-13 (1.0)	5.26e-15 (1.2)	3.13e-17 (1.4)	1.85e-19 (1.7)	1.09e-21 (2.0)
$K_p$	2.1e9	2.2e11	2.4e13	2.5e15	2.5e17

**Problem 2.** This problem differs from problem 1 because it takes into account spectral content of radiation. Point isotropic source of  $E_\gamma=300$  KeV gamma-quanta is located in the center of infinite homogeneous zinc medium (zinc density is derived from  $\Sigma(E_0)\approx 1$  and is equal to  $8.77193\text{g}\cdot\text{cm}^{-3}$ ). Source energy is determined from condition  $q(E_0)\approx 0.9$ . This problem falls into the class of elementary problems of radiation transport in optically thick media. Calculation method is exponential transformation.

Calculation results for  $R=50$  are given in table 2.

Table 2

$R, \text{cm}$	50
$\overline{\Phi(R)} \cdot 4\pi R^2$	2.00e-19 (1.1)
$J_1(R)$	1.25e-19 (1.05)
$K_p$	2.6e16

**Problem 3.** Consider infinite medium with the same optical properties as problem 1. It is required to estimate number of particles  $J$  hitting spherical detector with radius  $r=0.1\text{cm}$ , located at the distance of  $R=50\text{cm}$  from the source. This problem includes two elementary problems which turn one into another: particles transport in optically thick medium (calculation method is exponential transformation) and detection problem in scattering medium (calculation method is method of concentric detectors).

Calculations gave the following value:  $J=5.09\text{e-}16$  at statistical error  $\sigma=4.5\%$ . Transforming to flux  $\Phi(R)$ , we obtain  $\Phi(50)=1.62\text{e-}14$ , that practically coincides with result obtained for the previous problem where  $\Phi(50)=1.6\text{e-}14$ . According of formula (19) we have  $K_p = 1.5\text{e}^{11}$ .

**Problem 4.** This problem illustrates application of the method of forced collisions to estimate electron yield obtained from plane aluminium layer 0.5cm depth exposed to plane-parallel flux of 1MeV gamma-quanta. Two calculations were done: analog and nonanalog. Run times were the same. Tables 3 and 4 show calculated fluxes of electrons at the left and right boundaries of the layer.

Table 3. Flux of electrons  $J_1$  at the left boundary of the layer

	Analog modeling	Method of forced collision
$J_1$	2.58e-4	2.56e-4
$\sigma, \%$	16.8	5.23

Table 4. Flux of electrons  $J_2$  at the right boundary of the layer

	Analog modeling	Method of forced collision
$J_2$	4.88e-3	5.03e-3
$\sigma, \%$	3.77	1.17

Tables show that nonanalog calculation gives a prize of  $K_B \approx 10$  if compared with analog one.

## References

1. Ia.Z. Kandiev, E.S. Kuropatenko, I.V. Lifanova et al. *Monte-Carlo Calculations of Particle Interaction with Matter in PRIZMA Code*. Theses of presentations at III Scientific Conference on Protection against Ionizing Radiation at Nuclear Facilities. - Tbilisi, 1981, p. 24 (in Russian)
2. J. Spanier, E.M. Gelbard. *Monte-Carlo Principles and Neutron Transport Problems*. Moscow, Atomizdat, 1972, p. 207 (in Russian).
3. K. Case, P. Zweifel. *Linear Transport Theory*. Moscow, Mir, 1972 (in Russian).

## IRREGULAR FREE-LAGRANGIAN "MEDUSA" TECHNIQUE.

S.G.Volkov, B.M.Zhogov, V.D.Malshakov, I.D.Sofronov

Arsamas-16, VNIIEF, Russia

### Annotation.

"Medusa" technique refers to two-dimensional free-Lagrangian numerical methods solving gas-dynamics equations. The technique uses an irregular spatial grid reflecting the current neighborhood of computational points while solving difference equations.

The paper presents the scheme of difference gas-dynamics equations and the sequence of their solution. It describes main technique peculiarities such as the use of local interpolations and mixed cells. The paper gives a brief solution of heat conductivity equation on the grids the technique uses.

Finally, the paper discusses the issues on calculation parallelization and gives a computation illustration by means of the given technique.

### Introduction.

"Medusa" technique has been developed and improved by a large team of investigators for a number of years. The early publications on "Medusa" technique date back to 1972. Refs./1,2/ describe the technique and its first program implementation. Ref./3/ includes an English version of the technique description. There are several papers devoted to the computations using this technique /4,5/.

"Medusa" technique is applied to compute gas-dynamic flows assuming shock waves and tangential gaps that are complex both in their geometry and in the nature of motion. One is sure to confront certain difficulties when computing the flows of the kind by regular techniques.

"Medusa" technique automatically makes the grid adaptable to the solution in the sense that when computing the unknowns at each point it uses the information on solution value at the neighboring for the given moment points. As a result, a set of neighboring points might vary during the solution with computations run on metrically close neighbors.

#### 1. Problem discretization.

"Medusa" technique is used to solve 2D (plane or axially symmetric) gas dynamics equations in Lagrangian variables:

$$\frac{dU}{dt} = -V \text{grad}(P + Q) + VF,$$

$$\frac{J}{V} = \text{const},$$

$$\frac{dE}{dt} + (P + Q) \frac{dV}{dt} = 0,$$

$$E = E(P, V).$$

Here  $U$  - velocity vector,  $V$  - specific volume,  $P$  - pressure,  $F$  - external force vector,  $E$  - specific internal energy,  $Q$  value - computational viscosity. The second equation of the system is the equation of conservation for Lagrangian particle mass.  $J$  value in this equation is the transformation Jacobian from the initial Eulerian particle coordinates to the current ones with regard to problem symmetry. The given equation system is solved in some connected 2D domain whose boundary is assigned boundary conditions of geometric (rigid wall) or dynamic (assigned pressure or velocity) type. Within the domain the initial values are given.

To discretize the problem within the domain and on its boundary some points are selected. The point location is arbitrary. The boundary points should not be precisely on the boundary, it is sufficient that they should be closer to the corresponding boundary section than non-boundary points. To select the integration pattern a set of neighboring points is defined for each point. A set of points closest to the considered one than to any other within a selected set of points is considered to be point neighbors. Additional fictitious neighbors are defined for boundary points, namely: left and right boundary conditions are added as neighboring. A set of neighbors for each point are put in order in a counter-clockwise direction.

A cell - as an area of influence - is constructed for each point by means of neighbors. It is a polygon whose vertexes are comprised by triangle centers of gravity defined by the point and two consecutive neighbors. In case with one fictitious neighbor the vertex is the middle of the sector connecting the point with non-fictitious neighbor projected to the corresponding boundary. In case with two fictitious neighbors the point itself is projected. The problem is discretized by applying the equation of motion to cells.

The gradient of  $(P=Q)$  value is found by means of contour integral as to the cell perimeter. Contour integrals are calculated by linear interpolation of  $P$  and  $Q$  functions on triangles. The values on domain boundaries are taken from boundary conditions. As a result we obtain:

$$F_x = \frac{\partial(P+Q)}{\partial x} = \sum P_n (y_{i+1} - y_i) / S,$$

$$F_y = \frac{\partial(P+Q)}{\partial y} = \sum P_n (x_i - x_{i+1}) / S.$$

Where  $P_n$  is  $(P+Q)$  on the side connecting the  $i$  and  $i+1$  vertexes. This function for boundary sides is taken from corresponding boundary condition.

We would obtain the following formulas for velocity components at the next computational step:

$$U^{n+1} = U^n + V^n \cdot (F_x + G_x) \cdot dt,$$

$$W^{n+1} = W^n + V^n \cdot F_y \cdot dt.$$

The equation for conservation of mass is discretized directly. An average specific cell volume results from the cell volume divided into mass. Thus we obtain:

$$V^{n+1} = v^{n+1} / M^{n+1}, M^{n+1} = M^n.$$

In plane case the cell volume equals to domain, in axisymmetric case it equals to the volume of cell rotation around the X axis to one radian.

The equation for energy is discretized as follows:

$$E^{n+1} = E^n + (0.5 \cdot P^{n+1} + 0.5 \cdot P^n + Q^{n+1}) \cdot (V^n - V^{n+1}).$$

Computational viscosity for compressible cells is defined by the formula:

$$Q = (k \cdot l \frac{V^{n+1} - V^n}{dt^n} / V^n)^2 / V^n.$$

With  $V^{n+1} > V^n$  viscosity sets to zero.

$l$  - the cell size directed to pressure gradient,  $k$  - an empirical coefficient, presently equal to 1.6. It represents a quadratic viscosity proportional to the squared number of velocity divergence with the first order of accuracy.

The next step is calculated as follows. The specific cell volume is computed at the beginning of the next step. Computational viscosity is found by variation value of specific volume. Then the adiabatic equation computes the energy, pressure, and sound velocity in the cell. The allowable time step for the given point is calculated by dividing the characteristic cell size by sound velocity. A characteristic size results from the cell domain divided by its perimeter.

The second step computes the pressure (+viscosity) gradients, the sizes of cells in gradient direction and new velocities. With rigid walls restricting the domain, the velocities of corresponding boundary points are adjusted so that the points would keep within the walls during the computation step.

Local grid variations when some points either shift or change their neighbors are carried out after the second step. Along with this, the grid functions are varied as well.

At the final computation step the points acquire new coordinates according to the formulas:

$$x^{n+1} = x^n + U^{n+1} dt,$$

$$y^{n+1} = y^n + W^{n+1} dt.$$

These actions completed, everything is ready for the next step.

"Medusa" with irregular grid is specifically featured by the opportunity of local grid variations. The main variations of the kind are extensions and reconstructions.

The extension deals with the scheme aligning and the cell construction technique. Some of the points may fall out of the cell. To remedy the situation, the points that got close to the boundary of their cell different from the problem boundary or those having left the cell are shifted to the center of cell gravity to a certain part of the segment connecting the point with this center.

Reconstructions remedy the pattern of point neighborhood. The technique supports the point property to have only closest ones as its neighbors. The neighborhood is varied at local level.

Some parts of the cells enter others both during extension and reconstruction processes. When values are recalculated these parts carry mass, total energy and pulses along the axis. A part of the value to be carried is proportional to the volume part being carried in comparison to the total cell volume. Interpolations result in kinetic energy transfer to internal.

"Medusa" technique uses a mixed cell model when computing interfaces. A point is supposed to contain one material or several having their own equations of state. Points with one material are referred to as pure, those with several - mixed. A mixed cell model is supposed to have several separated materials. The material volumes of one cell summed up equals to a total cell volume. The equations of energy for each material are integrated into a system and additional conditions are assigned. One of them requires the equality of the cell volume and the summed volume of component materials. The given model fits well the cases with perturbation propagation perpendicular to material interfaces. Cases when movement along interfaces prevails require the selection of computational grid.

## 2. Heat conduction implementation.

Implementation of heat conduction as of other additional physical processes is based on splitting the problem as to physical processes. The point parameters imply additional grid functions, e.g. temperature, and the corresponding equation is computed on a stationary grid for the same cells as used in gas dynamics. Dcretization in time uses the same computational step as in gas dynamic computations.

When solving the equation for heat conduction

$$\frac{\partial \mathcal{E}}{\partial t} = -div(K grad T),$$

where K is thermal conductivity dependent on the solution, the implicit difference scheme was used

$$\frac{E^{n+1} - E^n}{dt} = \sum_{i=1}^R A_i (T_i^{n+1} - T_i^n),$$

where  $T$  - temperature at the main point,  $T_i$  - temperatures at the points neighboring to that being calculated,  $R$  - number of neighbors,  $A_i$  factors are computed by some averaging the heat conduction factors  $K$  both in the point under computation and its neighbors.

The implicit equation obtained is solved by local balance iterations. The method applies heat flows resulted from local iterations of the points having been computed.

### 3. Parallelization features.

"Medusa" technique provides great opportunities for gas dynamic equations to be computed parallel on a large number of processors. Some computation step stage is defined by the neighboring points data resulted from the previous stage or from the last stage of the previous computation step. Thus, both shared-memory and distributed memory schemes suit "Medusa" equally well.

Parallelization scheme is as follows. Each stage of computation step is computed by processors separately, splitting a set of all points into subsets. These subsets are computed by their processors. To balance the load a number of points is assigned to a processor or the splitting into subsets takes place followed by automatic balancing. When the memory is sufficient to store the previous stage results one processor is capable of computing several stages synchronically. This brings up the question of duplicating several computations. In case of distributed memory the issue of data transfer becomes critical. Each processor needs the data on its points as well as on the neighboring ones. In a shared-memory case the subset configuration is of no importance whereas in distributed memory the subset form determines the transferred data volume.

### 4. Computation illustration.

Computation results represented graphically illustrate the most specific features of the technique. The problem solution for the case with automatic channel pinch is demonstrated.

The problem geometry is as follows. A sealed chamber contains gas under a high pressure. The gas may leak out through a narrow channel in the wall constraining the gas. We need to define whether the channel can be shut or not depending on properties of the material the channel walls are made of. Mathematically the problem is formulated as follows: one halfspace in initial state is filled with ideal gas whose pressure is  $P_1$ , density is  $\rho_1$  and adiabatic exponent is  $\gamma_1$ ; the second halfspace is filled with ideal gas having  $P_2=0$  pressure,  $\rho_2$  density and adiabatic exponent  $\gamma_2$ . There is a cylinder channel in the second halfspace with  $r_0$  radius, free of material, and having an axis perpendicular to the plane dividing the halfspaces. What we need to require is the system behavior in time.

Fig.1 shows the initial problem geometry and the difference grid to be used for computations.

Fig.2 illustrates the material disposition near the channel at the moment of its pinching.

### References

1. Glagoleva Yu.P., Zhogov B.M., Malshakov V.D., Nesterenko L.V., Podlivayev I.F., Sofronov I.D. Fundamentals of "Medusa" technique and of 2D numerical calculations for non-stationary gas dynamics problems. Numerical methods for continuum mechanics. Novosibirsk, volume 3, # 2, 1972.
2. Glagoleva Yu.P., Ilyasova Ye.B., Malshakov V.D., Nesterenko L.V., Podlivayev I.F., Sofronov I.D. "Medusa" program arrangement. Collection of scientific papers "Computational Physics Program Systems" Novosibirsk, 1972
3. Nesterenko L.V., Rasskasova V.V., Sofronov I.D. The use of non-regular grids for solving 2D non-stationary problems in gas dynamics. Collection "Numerical methods in fluid dynamics"

4. Zhmaylo V.A., Giagoleva Yu.P., Malshakov V.D., Nesterenko L.V., Sofronov I.D., Statsenko V. P., Ring vortex formation at light gas floating up in a heavy one. Numerical methods for continuum mechanics. Novosibirsk, volume 5, # 1, 1974
5. Giagoleva Yu.P., Malshakov V.D., Rodigin V.N., Sofronov I.D., Shustova E.F. Numerical solution of the problem on shutting the channel in the wall by gas pressing it. Numerical methods for continuum mechanics Novosibirsk, volume 6, # 4, 1976.

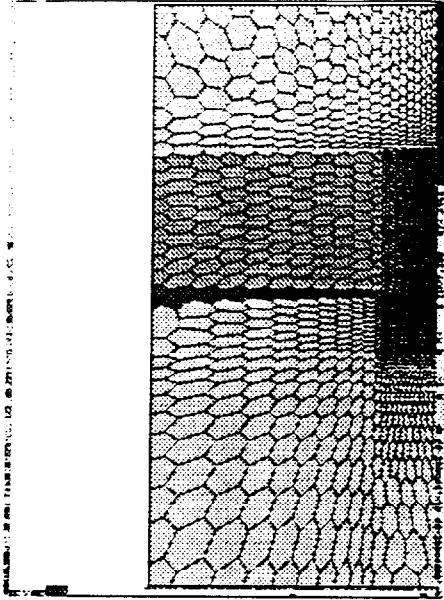


Fig. 1

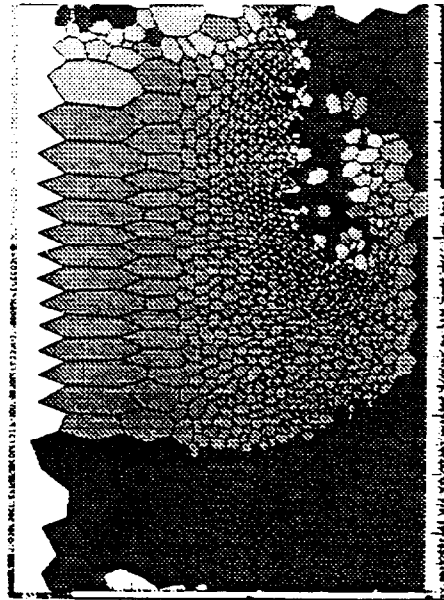


Fig. 2



**Russian Federal Nuclear Center (VNIEF)**  
**PRESENTATION**  
**IRREGULAR FREE-LAGRANGIAN TECHNIQUE**  
**"MEDUZA"**

**S.G.Volkov, B.M.Zhogov, V.D.Malshakov, I.D.Sofronov**

**1997**

## **INTRODUCTION 3**

1. PROBLEM DISCRETIZATION 3
2. TECHNIQUE PROGRAM IMPLEMENTATIONS 9
3. IMPLEMENTATION OF HEAT CONDUCTION AND DETONATION PROCESSES 10
4. PARALLELIZATION FEATURES. 11

## **CONCLUSION 13**

## **REFERENCES 30**

## INTRODUCTION

The technique "Meduza" was developed and improved by a large team of investigators during many years. An incomplete list of the technique investigators can be drawn up basing on the lists of authors of papers devoted to description of the technique and computations conducted with this technique. The early publications devoted to the technique "Meduza" go back to 1972. Refs. /1,2/ describe the technique and its first program implementation. Ref. /3/ includes the English version of the technique description. There are several papers devoted to the computations conducted using this technique /4, 5/. The list of the presentation authors includes its original developers. They pursue the current technique development and maintenance.

It is impossible to realize reliable gas-dynamical computations of complex products by some one numerical technique due to gas-dynamical flow features, computational algorithms, limited capabilities of computers and many other reasons. It is a common practice to conduct computations with different techniques in order to see the effect of methodic errors by result comparison. Of course, in each computation it would be desirable to refine the mesh so that the results in no way depend on that taken at the initial time. However, as a rule, this is impossible, and one has to take it for granted that the quality of the obtained results depends on the mesh cell size. Therefore, in the division there are several techniques for solving gas-dynamical problems. "Meduza" is one of the Lagrangian techniques. In the technique "Meduza" the grid is automatically adapted to the solution in the sense that the computation of unknowns at each point uses the data of the solution value at the points which are neighboring at that time. The latter circumstance leads to the fact that during the solution the set of neighboring points can change, with the computations being conducted each time by metrically close neighbors. The technique refers to free-Lagrangian.

The experience of many years of the technique employment showed that the technique can be used to solve very complex 2D gas-dynamical problems. At a reasonable construction of the initial grid the qualitative pattern of flows has always been proper. To enhance the accuracy achieved, one usually increases the number of the points either over the whole problem or at its regions where the flow gradient has proved especially high and a noticeable loss of accuracy has taken place.

### 1. Problem discretization

The technique "Meduza" is used to solve 2D (plane or axisymmetric) gas dynamics equations in Lagrangian variables:

$$\frac{dU}{dt} = -V \text{grad} (P + Q) + VF,$$

$$\frac{J}{V} = \text{const},$$

$$\frac{dE}{dt} + (P + Q) \frac{dV}{dt} = 0,$$

$$E = E(P, V).$$

Here  $U$  - velocity vector,  $V$  - specific volume,  $P$  - pressure,  $F$  - external force vector,  $E$  - specific internal energy. The value  $Q$ , computational viscosity, is some fictitious value relating to the problem discretization and depending on the grid sizes. The second equation of the system, the equation of conservation of Lagrangian particle mass, the value  $J$  in this equation, is the Jacobian of the transformation from the initial Eulerian particle coordinates to the current taking into account the problem symmetry. The above equation system is solved in some connected 2D region on whose boundary geometric type (rigid wall) or dynamic (given pressure or velocity) type boundary conditions are given. Inside the region the initial values are given.

To discretize the problem inside the region and on its boundary some points are taken. The point position is arbitrary. It is only necessary that they map a given problem in some way, for example, where the density is higher, the points should be more condensed. The boundary points should not necessarily be precisely on the boundary, it is sufficient that they were closer to the corresponding segment of the boundary than the non-boundary points.

The region triangulation is made using a set of points taken. Any triangulation type is possible in principle. The technique essentially employs the triangulation related to the Dirichlet (or Voronoi) cells. The Dirichlet cell for a point is the set of all region points which are closer to the point of concern than to any other one from the point set taken. In the general case the Dirichlet cell will be a convex polygon produced from intersection of semiplanes determined by perpendiculars to the straight line segments connecting various points of the set taken and passing through the middles of these segments. The points are declared neighboring if their Dirichlet cells have a common side. Connection of all the neighbors with straight line segments results in region fragmentation into polygons. Having passed diagonals in the obtained polygons we obtain the region triangulation. When no four points lie on a single circumference, the Dirichlet cells determine the triangulation without passing diagonals.

The triangulation is used to determine a set of neighboring points for each point. Two points are neighbors if they comprise one triangle. For boundary points further fictitious neighbors are determined, namely: on the left and on the right boundary conditions are added as neighbors. The set of neighbors for each point is ordered in the counter-clockwise bypassing direction.

For each point the neighbors are used to construct a cell, the influence region. This is a polygon whose vertices are the centers of gravity of the

triangles determined by the point and two successive neighbors. When one neighbor is fictitious, the vertex is the projection of the middle of the straight line segment connecting the point to the non-fictitious neighbor onto the corresponding boundary. In the event of two fictitious neighbors the point itself is projected. The problem discretization is found by applying the equations of motion toward the cells.

The gradient of the value (P+Q) is found by applying the theorem of mean and Green formula to the contour integrals:

$$\oint f dy = \iint \frac{\partial f}{\partial x} dx dy,$$

$$-\oint f dx = \iint \frac{\partial f}{\partial y} dx dy.$$

The function (P+Q) is taken for the function f. The partial derivative values are substituted with the cell-mean value equal to the quotient of division of the integral over area by the cell area. The integrals over area of the derivatives are substituted with the contour integrals of the functions themselves. The contour integrals are computed by linear interpolation of the functions P and Q on triangles. On the region boundaries the values are taken from the boundary conditions. Finally we obtain

$$F_x = \frac{\partial(P+Q)}{\partial x} = \sum P_{ii} (y_{i+1} - y_i) / S,$$

$$F_y = \frac{\partial(P+Q)}{\partial y} = \sum P_{ii} (x_i - x_{i+1}) / S.$$

where  $P_{ii}$  is (P+Q) on the side connecting the vertices i and i+1. For the boundary sides this function is taken from the relevant boundary condition. At every next computational step for the velocity components we find the formulas

$$U^{n+1} = U^n + V^n \cdot (F_x + G_x) \cdot dt,$$

$$W^{n+1} = W^n + V^n \cdot F_y \cdot dt.$$

The equation of conservation of mass is discretized directly. The mean specific cell volume is found by the cell volume division by mass which is computed by the initial density and varies only at the interpolations. Thus, we obtain

$$V^{n+1} = v^{n+1} / M^{n+1}, M^{n+1} = M^n.$$

In the planar case the cell volume equals the area, in the axisymmetric case it equals the volume of the cell revolution about the axis X by one radian.

The equation of energy is discretized as follows:

$$E^{n+1} = E^n + (0.5 \cdot P^{n+1} + 0.5 \cdot P^n + Q^{n+1}) \cdot (V^n - V^{n+1}).$$

This equation and the equation of state are used to determine pressure and energy with the method of iterations.

The computational viscosity for compressing cells is found by the formula

$$Q = (k \cdot l \frac{V^{n+1} - V^n}{dt^n \cdot \dot{V}^n})^2 / V^n.$$

At  $V^{n+1} > V^n$  viscosity vanishes. In this formula  $l$  is the cell size in the pressure gradient direction,  $k$  is an empirical factor currently equal to 1.6. This is quadratic viscosity proportional to squared velocity divergence of the first order of accuracy.

For every next step the computations are arranged as follows. When at the previous step the new point coordinates have been computed, at the beginning of the next step the specific cell volume is computed. The computational viscosity is computed by the value of variation in the specific volume. Then the adiabat equation is used to compute energy, pressure, and sound speed in the cell. The permissible time step for a given point is computed through division of the characteristic cell size by sound speed. For the characteristic size the quotient from division of the cell area by the cell perimeter is taken. The above computations are conducted for all the points and constitute the computation contents of the first stage of the computational step.

At the second stage the pressure (+viscosity) gradients, cell sizes in the gradient direction and new velocities are computed. Given rigid walls bounding the region, the velocities of relevant boundary points are modified so that the points do not go beyond the walls during the computational step.

Following the second stage, local modifications to the grid are made at which some points change their neighbors or are shifted. In so doing the grid functions change as well.

At the final step computation stage the points acquire new coordinates by the formulas

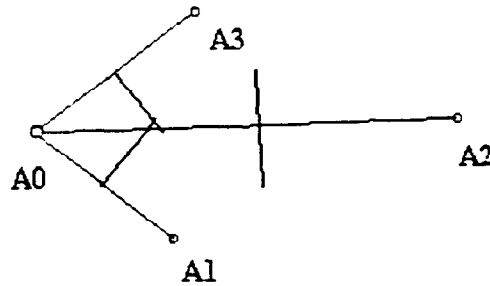
$$\begin{aligned} x^{n+1} &= x^n + U^{n+1} dt, \\ y^{n+1} &= y^n + W^{n+1} dt. \end{aligned}$$

Then everything is ready for conduct of the next step.

The main "Meduza" feature relating to the irregular grid is the capability to make local grid changes. The basic types of such changes are extensions and reconstructions.

The extension relates to the scheme centering and cell construction method. In the scheme discussed the points do not "notice" the approach of their neighbors. It is best to show the position using a one-dimensional model example. Consider a set of points on a straight line segment uniformly distributed at the initial time. The points of odd numbers do not move, while the points of even numbers have one and the same velocity. Pressure is identical at all the points. Upon execution of a computational step like in "Meduza" the points away from the boundary will displace from the cell centers, but cell volumes (lengths) will not change and, hence, the gas-dynamical parameters will not change as well. In the general case the cell drops behind the point or the point tries to go outside the cell. To remedy the situation, the points which came close to the boundary of their cell other than the problem boundaries are shifted toward the center of gravity of the cell at some fraction of the length of the straight line segment connecting the point to that center.

The reconstructions remedy the point neighborhood pattern. The technique maintains the property of the points to have only the points as their neighbors which are neighbors in terms of the Dirichlet cells. The check for the Dirichlet cell criterion is made at the local level, i.e. for one neighborhood generation. Consider some point and its three successive neighbors.



Point A2 will not be a neighbor of point A0 if the point of intersection of the perpendiculars to the middles of the segments A0-A1 and A0-A3 and point A0 lie in one of the semiplanes determined by the perpendicular to the middle of the segment A0-A2. The critical case is when all the three perpendiculars intersect at one point, i.e. the above four points lie on one circumference. Point A2 is brought out of the neighborhood if it has traveled quite far beyond the circumference passing through points A0, A1, A3 (>10% of radius). When point A2 goes out of the number of the neighbors of point A0, its two other neighbors, A1 and A3, become neighbors of each other.

Both at extensions and reconstructions some parts of cells transfer to other cells. At updating mass, total energy (internal + kinetic), and momenta along the axes are transferred together with these parts. The transferred fraction is proportional to the transferred volume fraction as compared to the total cell volume. On transference of all the parts involved in the current re-interpolation the velocities are obtained by division of momenta by masses. Internal energy is obtained by subtraction of the newly obtained kinetic energy from total energy. In any case the re-interpolations result in conversion of the kinetic energy to the internal, similar to a number of absolutely inelastic impacts of the transferred parts to the remaining.

When computing interfaces, the technique "Meduza" uses the model of mixed cells. It is assumed that a point can contain one or more materials which have their equations of state. One-material points are referred to as pure and several-material points as mixed. At the initial time the mixed points are obtained at material interfaces. Later on due to the re-interpolations the mixed points can become pure, while the pure mixed. At material transfer from one point to another the percent composition of the recipient point is maintained. A pure point becomes mixed when transfer of material not contained in it is forced.

The mixed cell model provides for several segregated materials. The sum of material volumes of one cell equals the total cell volume. The equations of energy for each material are integrated into a system and additional conditions are imposed. One of these conditions expresses equality of the cell volume to

the sum of composing material volumes. Other conditions relate pressures and energies of various materials. For example, in pure gas dynamics the condition of equal pressures is used. A computation with heat conduction may use the condition of equal temperatures if density differences between cell materials are not very large. The above model works well at perturbation distribution perpendicularly to the material interfaces. At a predominant motion along interfaces the computational grid should be fit.

## *2. Technique program implementations*

The technique program implementations introduce some peculiarities relating to computer capabilities. For example, memory economy can result in asymmetry caused by the fact that at some points either values from different time templates or interpolated and non-interpolated values are used. Small main memory sizes require using the external memory and appropriate computation tactics.

Three main technique implementations can be distinguished: on BESM-6 computer, on ES series machines, and on personal computers.

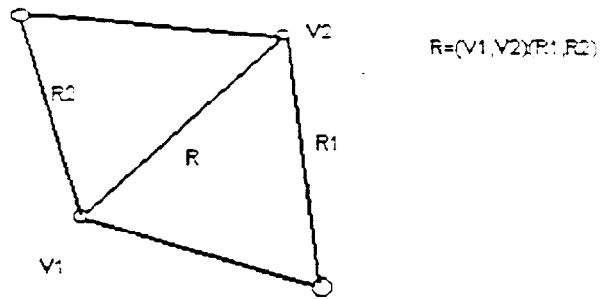
The principal feature of the BESM implementation is a small main memory at quite a high performance. The problem computation employed splitting a set of computational points into so-called computational compacts. The number of points of one compact corresponded to the standard unit communication with the external memory. The point computation till the end of the computational step was conducted compact-by-compact. For points of other compacts only the computations were conducted which are required for computation of the main compact.

The step computation for the compact was split into stages approximately as it was stated in the previous section. Upon the computation of the compact it turned out that its points were not needed for the step computation of other compacts and it could be transferred, if necessary, to the external memory. The compact computation required presence only of the compact itself and several neighboring compacts in the main memory. In this manner it was possible to increase the volume of the points considerably in the problems computed. The limitations were even in the digit quantity of the points used for numbers. The digits were as follows: the main memory allowed to allocate about 1600 points, the splitting into compacts could be used to be able to compute problems with 16000 points.

In addition, one may mention a dense packing of point data and using various programs for initial template computation, gas dynamics computation, and computed data output. Neighbor lists were used for the point neighborhood description, and each element of the list was composed of a group of neighbors which could be fit into one machine word. The program was implemented in the machine codes.

The ES implementation did not use the splitting into compacts. Short integers were used for numbering points and edges. As a result, the maximum permissible number of points equaled 10000. The characteristic features of the ES implementation were as follows: location of all points in main memory, using the dynamic memory for arrays and tables, point neighborhood description using the edge scheme.

The edge scheme provides for the point neighborhood storage as a graph. Each graph edge is described with two points in an arbitrary order and with two neighboring edges following the described one in the order of counter-clockwise bypassing for each of the points composing the edge. The order of appearance of the neighboring edges is consistent with the order of point appearance.



This scheme requires approximately two times more memory than the neighbor lists, but is of a regular character which is more suitable for language implementations.

The ES program was implemented in the PL1 language. The initial data computation, gas dynamics computation, and data output were located in one load module. The computation was controlled with the task text interpretation program.

The technique "Meduza" was implemented on personal computers with i486 and higher processors. The whole computational part was implemented on the FORTRAN pre-processor SVIFT. This pre-processor generated the text for the Fortran-77 compiler translated by many available compilers. Basing on test problem computation a compiler was taken which generates a fastest code, Watcom 9.5. This program version uses the computation control language allowing the on-line interaction with the user. At any instant of the computation it is possible to stop the computation, look through the results, make file outputs, make some modifications and continue the computation or abort the task.

### 3. Implementation of heat conduction and detonation processes

The implementation of further physical processes, such as heat conduction or kinetics, is based on splitting the problem by physical processes. Additional grid functions, for example, temperature or HE concentration, are introduced to the point description, and the relevant equation is solved on an immovable grid for the same cells which are used for gas dynamics. The time discretization employs the same computational step as at the gas dynamics computation.

When solving the equation of heat conduction

$$\frac{\partial \mathcal{E}}{\partial t} = -\text{div}(K \text{grad} T),$$

where  $K$  is the heat conduction factor, generally speaking, depending on the solution, the implicit difference scheme

$$\frac{E_i^{n+1} - E_i^n}{dt} = \sum_{j=1}^R A_{ij} (T_j^{n+1} - T_i^{n+1}),$$

was used where  $T_i$  is temperature at the main point,  $T_j$  are temperatures at the points neighboring with that being computed,  $R$  is the number of neighbors. The factors  $A_{ij}$  are computed using some averaging of the heat conductivity factors  $K$  at the point being computed and its neighbors.

The obtained implicit equation is solved with the method of local balance iterations. This method is well parallelizable.

When solving gas-dynamical problems with detonation simulation, various models were used. The prompt detonation was simulated using replacement of the equation of state and addition of energy release. The assumptions of constant detonation rate and specific energy release were used. Another method of the detonation simulation is taking into account chemical reactions, various dependencies of the reaction rate on thermodynamic parameters of cell materials were used here.

#### *4. Parallelization features.*

The gas dynamics equation solution with the technique "Meduza" provides wide capabilities for computation parallelization on a large number of processors. It should be noted that the computation of a separate computational step stage stated in the first section for each point does not depend on computation of the same stage for other points. The computation of any computational step stage depends on the data for neighboring points computed at the previous stage or at the last stage of the previous computational step. Thus, both shared-memory schemes and distributed-memory schemes are suitable for "Meduza".

On the shared memory the parallelization scheme is as follows. The computation of each computational step stage is distributed among the processors with splitting the set of all the points into subsets. These subsets are computed by their processors. For the load balancing the number of the points on the processors is determined or splitting to small subsets is made and self-balancing is used. When the memory is sufficient to store the results of the previous stages, several stages may be computed on one processor till synchronization. In this case the question about duplication of some computations arises.

For the distributed memory principal becomes the problem of data transfer. The parallelization scheme remains approximately the same as for the shared memory. The set of the computational points is split into subsets which are computed on separate processors. Besides its own points, each processor has to have the neighboring point data as well for the computations. The number of the neighborhood generations depends on the number of the computational step stages computed on one processor till synchronization. As a result, it turns out that if the data transfers occur rarely, the amount of the transferred data is larger. While the subset configuration does not play a large role for the shared memory, the subset type is responsible for the amount of the transferred data for the distributed memory. The problem of the best method of point distribution over subsets has not yet been solved thus far. It is evident intuitively that the subsets should be related to a shortest boundary, something like a circle on the point neighborhood graph.

## CONCLUSION

The technique "Meduza" may be used for computation of flows very complex both regarding geometry and pattern, in particular, allowing for flows with shock waves, tangential discontinuities. For illustration graphic results are given for some computations which show most characteristic features of the solutions computed.

The first computation demonstrates the solution of the channel self-pinch problem. Setting up the problem is as follows. In a closed chamber there is gas under high pressure. This gas can flow out through a narrow channel in the wall bounding the gas. It is necessary to assess the possibility or impossibility of shutting off the channel depending on the properties of the material the channel walls are made of. The mathematical problem is formulated as follows: at the initial state one semispace is filled with ideal gas of pressure  $P_1$ , density  $\rho_1$ , adiabatic exponent  $\gamma_1$ ; the second semispace is filled with ideal gas of pressure  $P_2=0$ , density  $\rho_2$ , adiabatic exponent  $\gamma_2$ . In the second semispace there is a cylindrical channel of radius  $r_0$  not occupied with material whose axis is perpendicular to the plane separating the semispaces. It is necessary to determine the time behavior of the system.

Fig.1 shows the initial geometry of the problem and difference grid used for the computation. The wall is depicted red. Its initial density is 2.56. Gas 34 in pressure and 0.06 in density at the initial time in shown green. The adiabatic exponent of both the materials equals 3. The channel and receiver behind the wall are composed of light gas shown in blue 0.001 in density. Colors other than those of the main materials depict the mixed cells. The horizontal size of the system equals 200, the vertical 100. The channel radius is 4.5.

Fig.2 shows position of the materials near the channel by the time of beginning of its shutting-off. Fig.3 presents the velocity field at the same place. The arrow length is proportional to the velocity modulus. The mixed cells are drawn completely. The channel is not shut off as there is a positive component along the axis  $X$  over the whole channel length. Fig.4 shows the density distribution. The red and brown points have the highest density (5-7), the white and gray the lowest.

Figs.5, 6, 7 show similar patterns by the time of completely shutting-off of the channel. In Fig.5 one can see cells of the wall material on the axis. Fig.6 shows some points before the channel which have reversed. In this figure the maximum velocity is twice as low as in Fig.3. In Fig.7 the region of the highest density points reaches the axis. In Fig.8 there is the complete flow pattern at the same time.

In this computation one can note a characteristic specific positioning of the points near most interesting places and considerable displacements of one point relative another. Depending on the value  $\gamma_2$  characterizing the wall material compressibility the channel can be shut off as is seen from the presented figures or remain open.

The next problem is opposite to the first in a sense. Penetration of a narrow cylinder through a plate of another material is computed in the gas-dynamical approximation, i.e. without taking into account material strength.

The initial geometry is shown in Fig 9. Fragments of two computations are given here. In the first the plate density was 7.85 and the penetrator density was 2.71. In the second computation the materials exchanged their places. The velocity of the penetrator approach equals 5 in both the computations.

Fig.10 shows the plate and penetrator shapes some time after beginning of the impact for the first computation. The next figure shows the velocity field at the same time.

Figs.12 and 13 show the collision problem where the penetrator density is higher than the plate density. Here the instant is shown when the penetrator has almost flown through the plate. Fig.14 shows the density distribution by the same time.

The next example shows the heat conduction computation with the technique "Meduza". The task consists in computation of the temperature field forming at cooling of an infinite square cross section bar inside which at the initial time  $t=0$  temperature  $T(0,x,y)=1$  is given, while on the outer boundary during all following times zero temperature  $Trp(t)=0$  at  $t \geq 0$ . is maintained. The bar cross section is a unity square:  $0 \leq x \leq 1; 0 \leq y \leq 1$ .

2 computations are presented. In the first computation the grid was taken uniform 40 by 40. Fig.15 presents the graph of the grid and temperature field at time  $t=0.1$ .

In Fig.16 the arrows indicate the heat gradient direction to a scale, the arrow length being proportional to temperature at the point where the maximum arrow length corresponds to the maximum temperature whose value is given in the upper row in the graph.

Fig.17 presents the graphs of the temperature distribution by sections. The right bottom rectangle gives the section along the line: the left point is  $x=0, y=0.5$ ; the right point is  $x=1, y=0.5$ . The left bottom rectangle gives the section along the line: the left point is  $x=0, y=1$ ; the right point is  $x=1, y=0$ . The right top rectangle gives the section along the line: the left point is  $x=0, y=0.1$ ; the right point is  $x=1, y=0.1$ . The left top rectangle gives the section along the line: the left point is  $x=0.1, y=1$ ; the right point is  $x=0.1, y=0$ . The crosses show the analytical solution.

In the next computation the grid was taken uniform by rows and columns with point increasing in a line from the square center from 3 to 40 points on each side. Fig.18 presents the graph of the grid and temperature field at the time  $t=0.1$ .

In Fig.19 the arrows indicate the heat gradient direction to a scale, the arrow length being proportional to temperature at the point where the maximum arrow length corresponds to the maximum temperature whose value is given in the upper row in the graph.

Fig.20 presents the graphs of the temperature distribution by sections. The right bottom rectangle gives the section along the line: the left point is  $x=0, y=0.5$ ; the right point is  $x=1, y=0.5$ . The left bottom rectangle gives the section along the line: the left point is  $x=0, y=1$ ; the right point is  $x=1, y=0$ . The right top rectangle gives the section along the line: the left point is  $x=0, y=0.1$ ; the right point is  $x=1, y=0.1$ . The left top rectangle gives the section along the line: the left point is  $x=0.1, y=1$ ; the right point is  $x=0.1, y=0$ . The crosses show the analytical solution.



Fig. 1

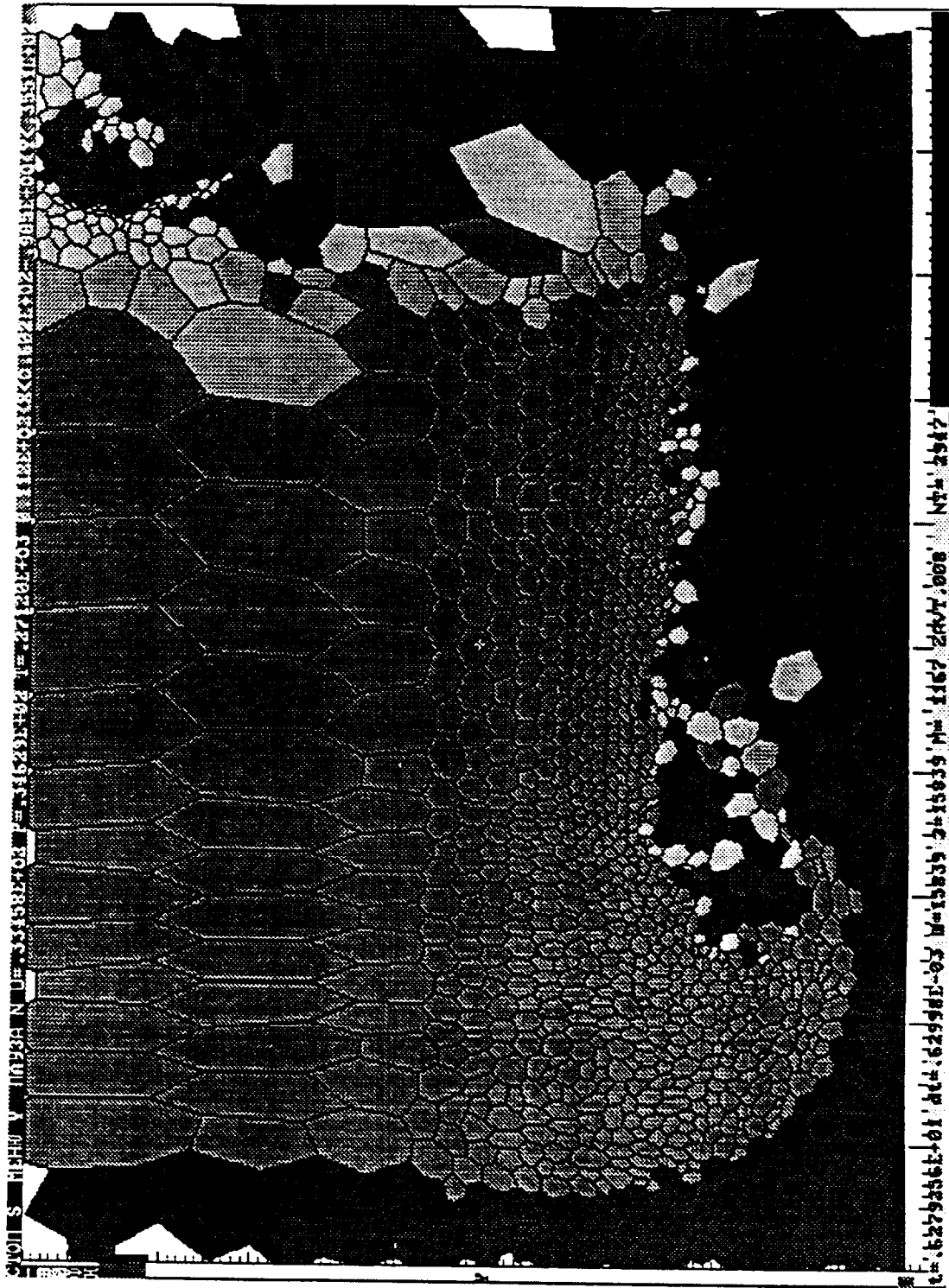


Fig. 2



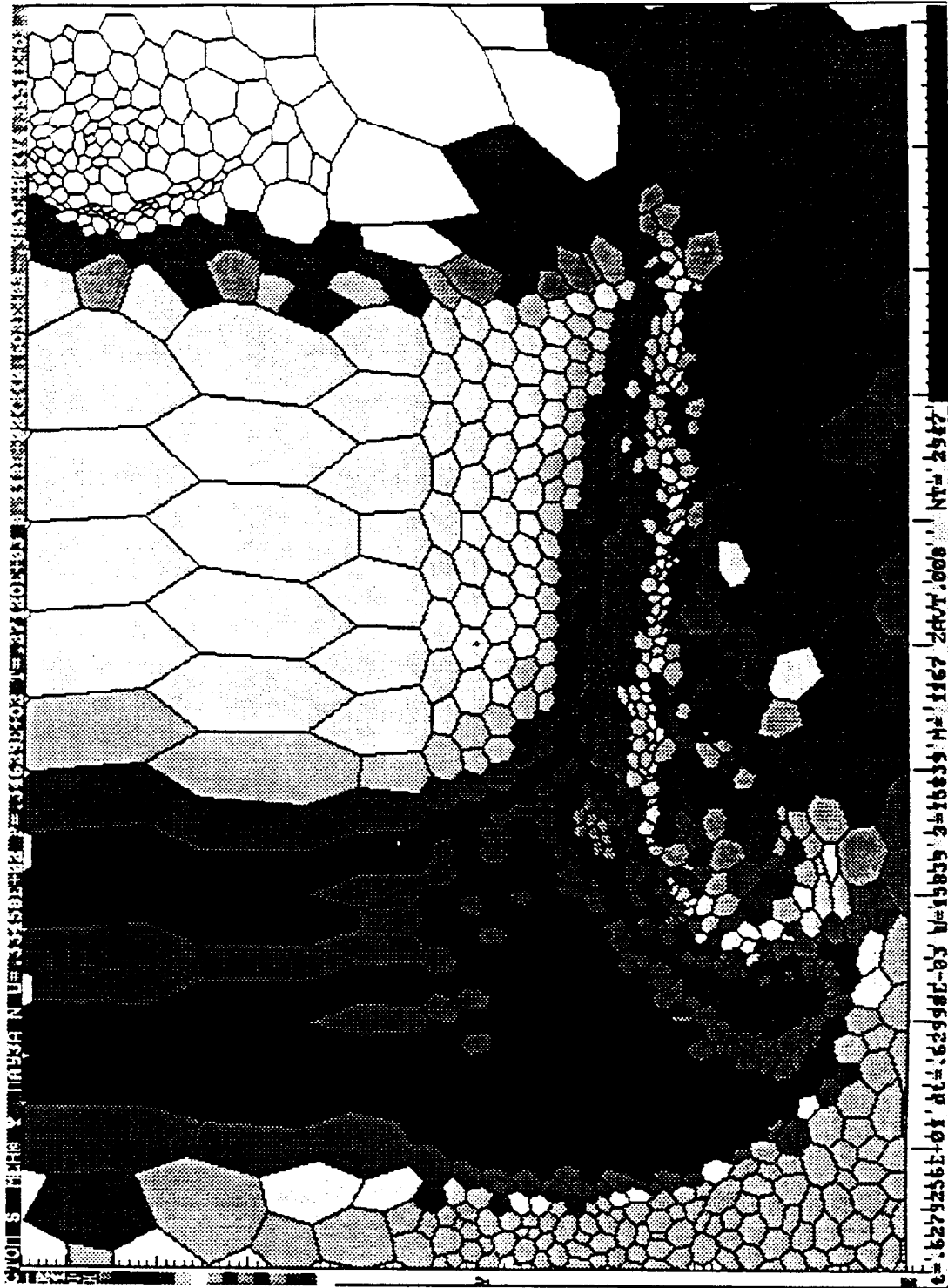


Fig. 4

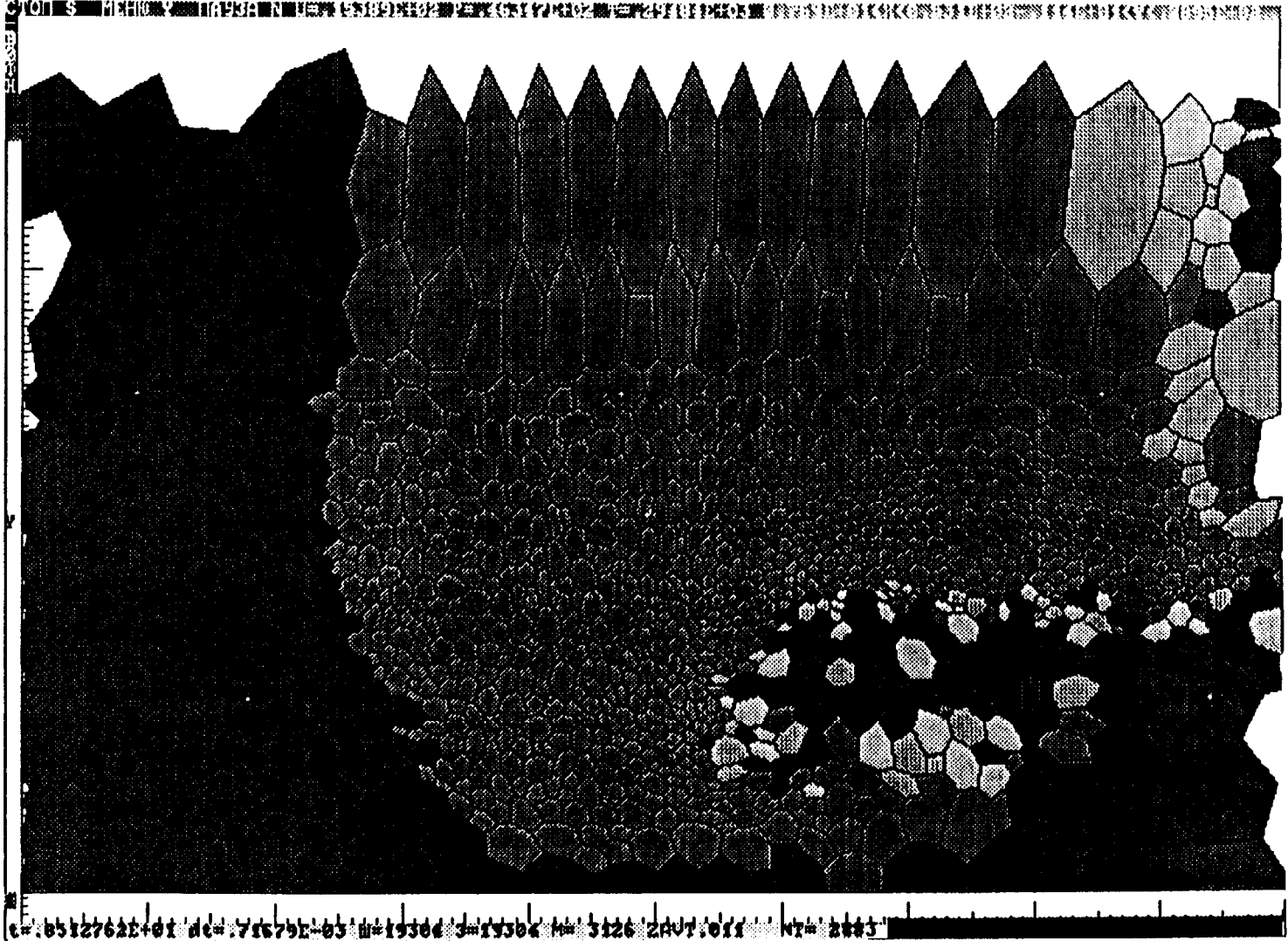


Fig. 5

05127625-01 de=75575E-03 W=19306 3=19306 W= 3126 2A07.011 KR= 2183

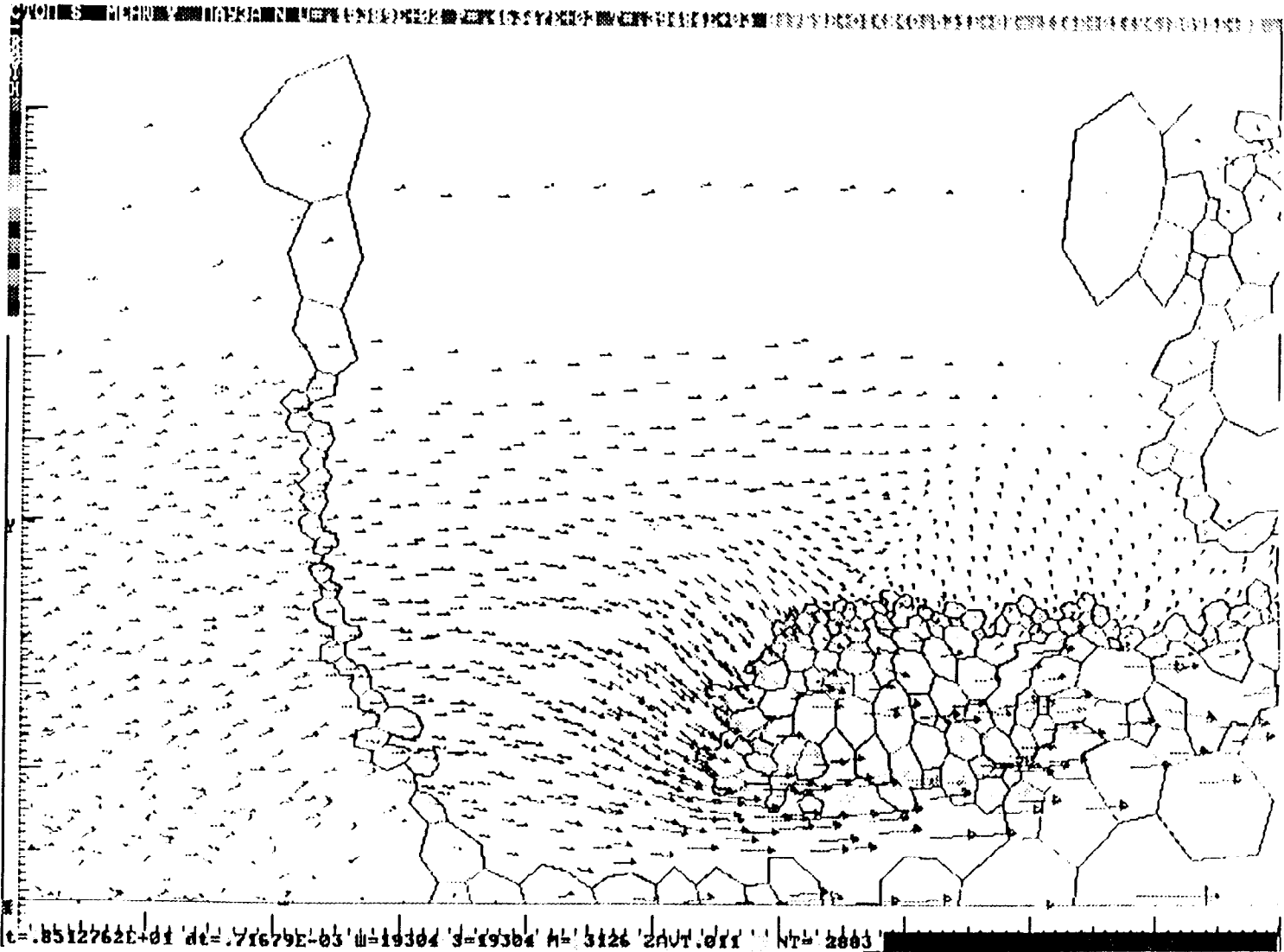


Fig. 6

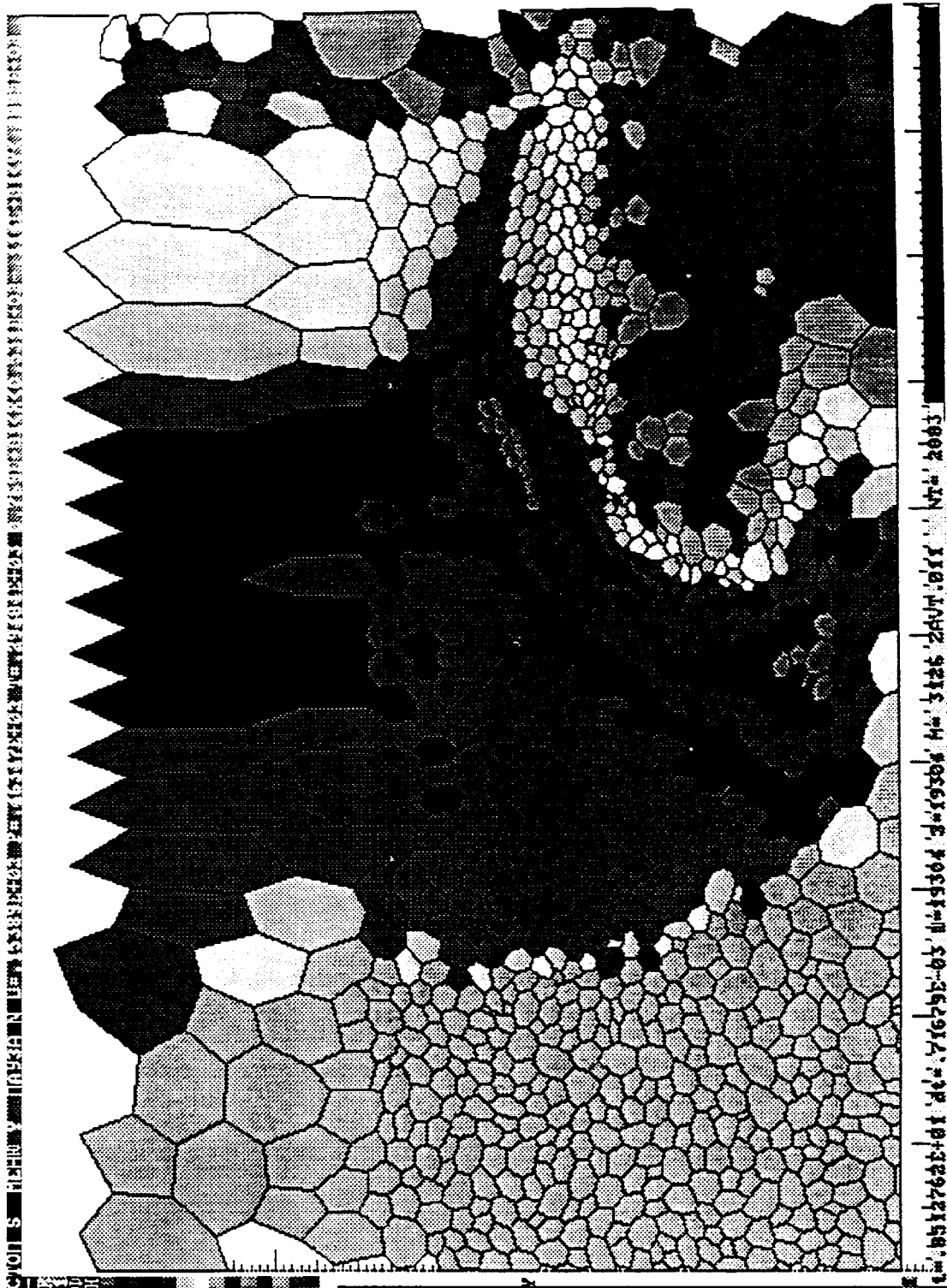


Fig.7

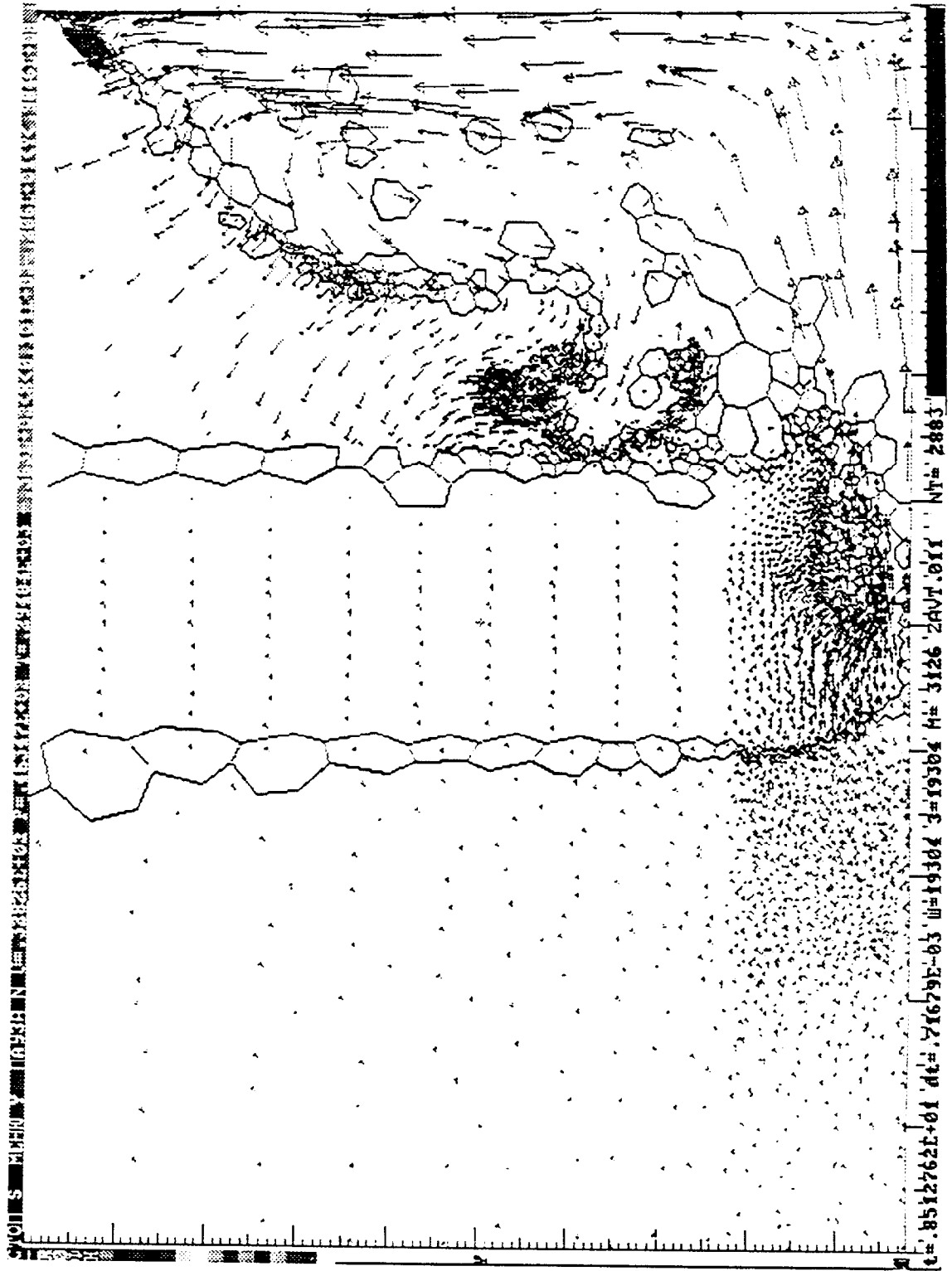


Fig. 8

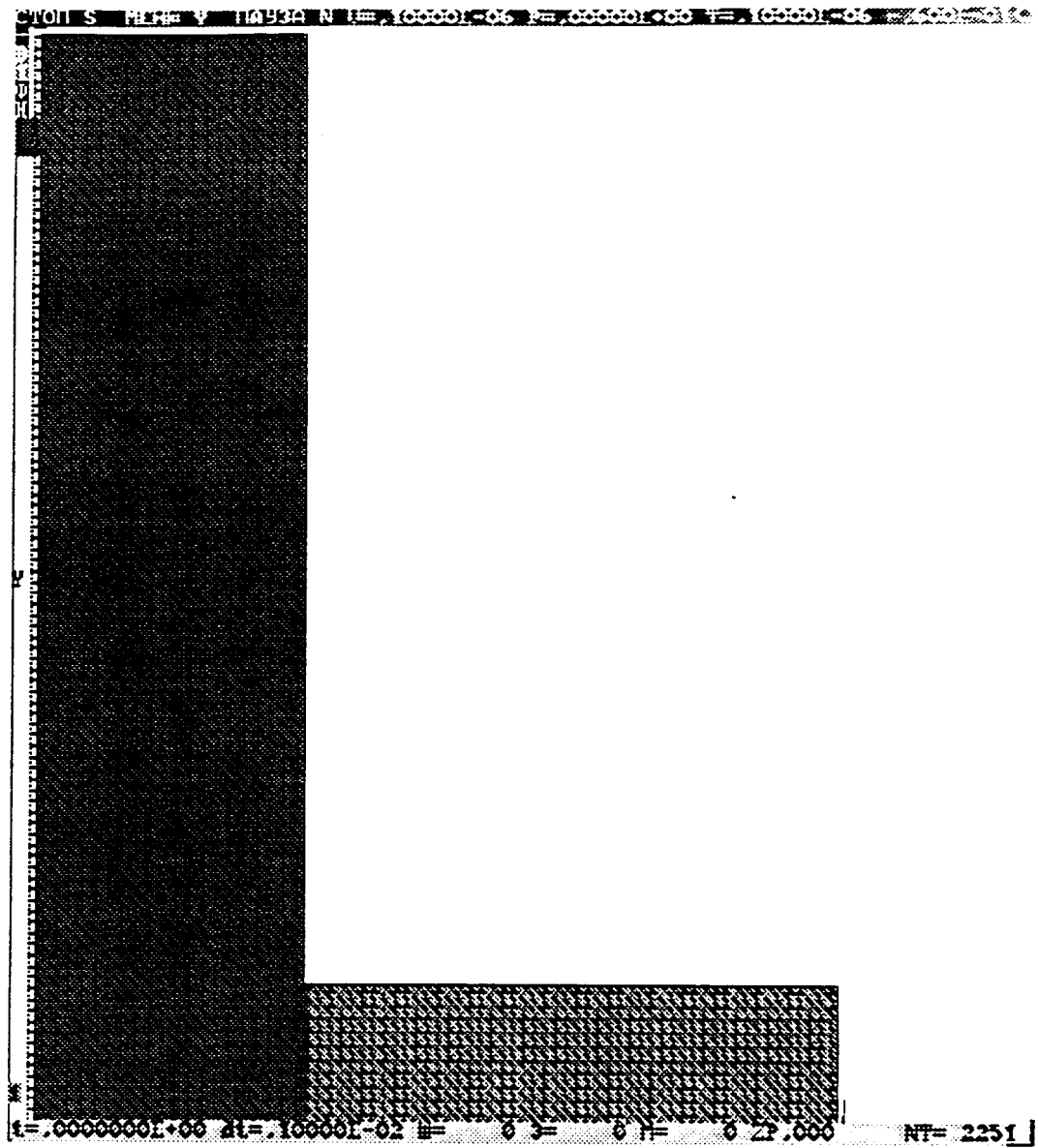


Fig. 9

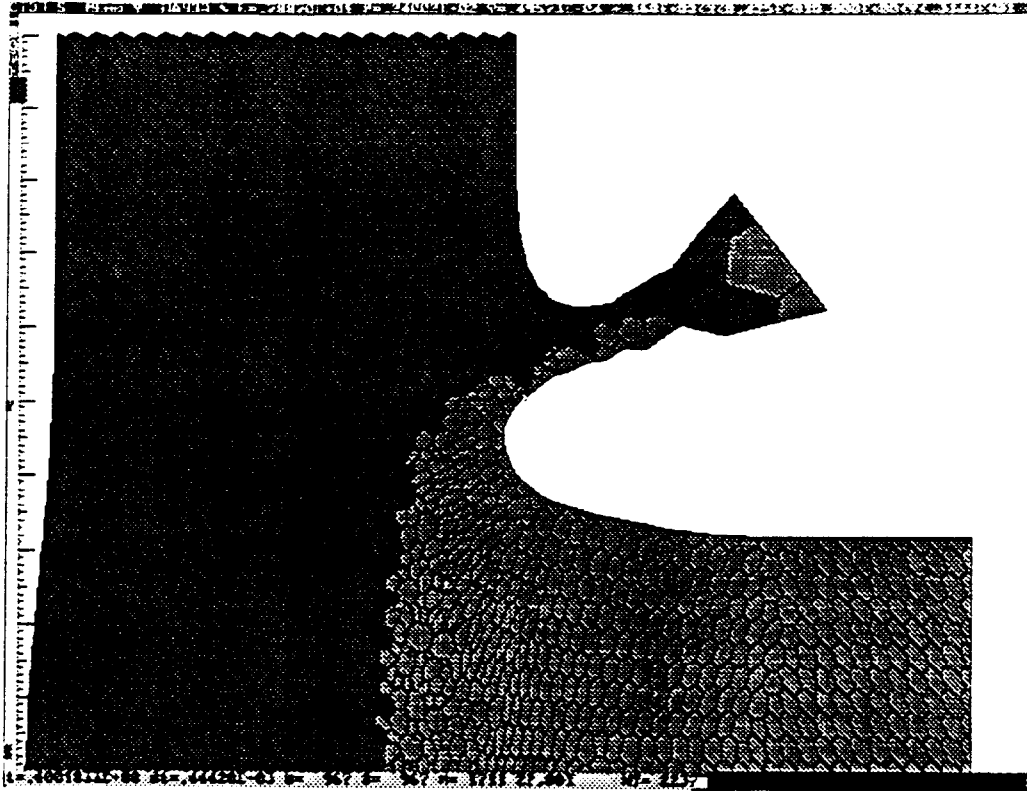


Рис.10

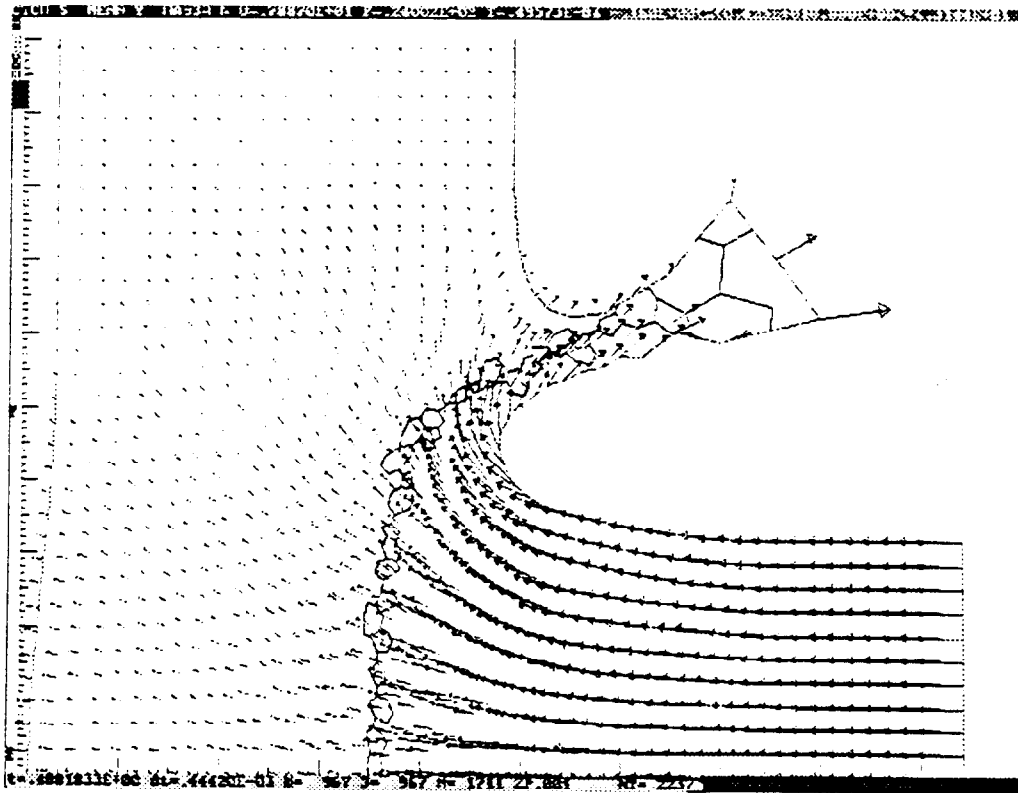


Fig. 11

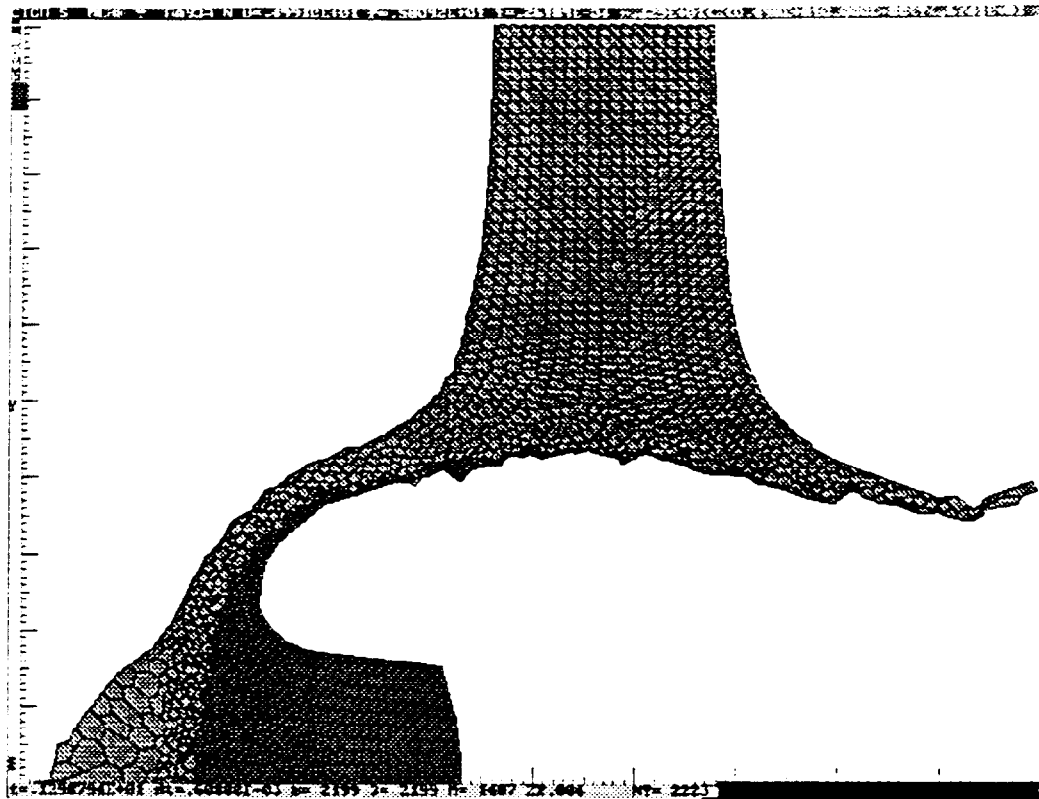


Fig. 12

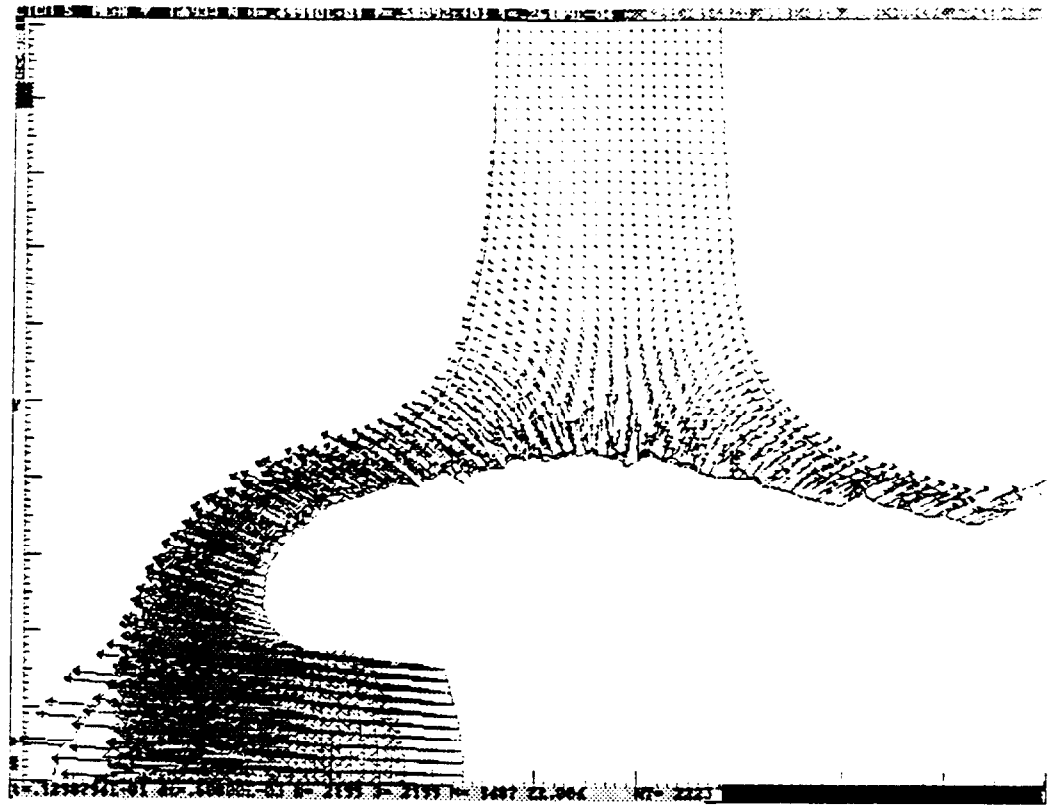


Fig. 13

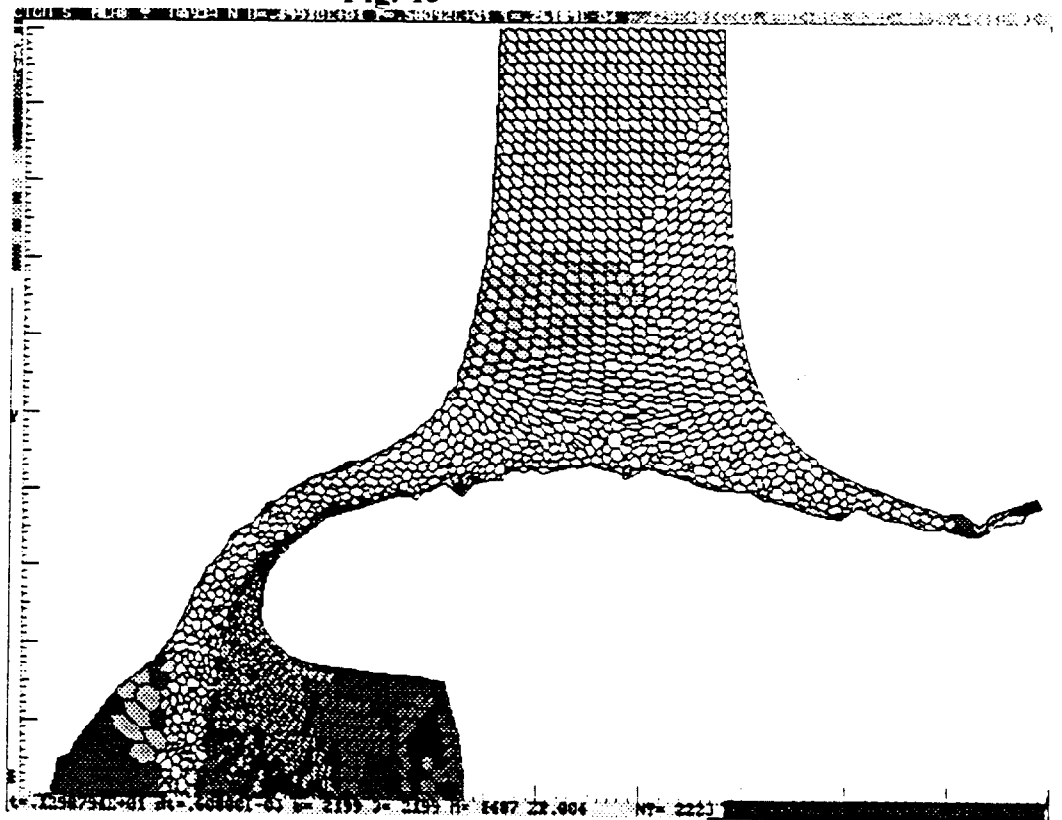


Fig. 14

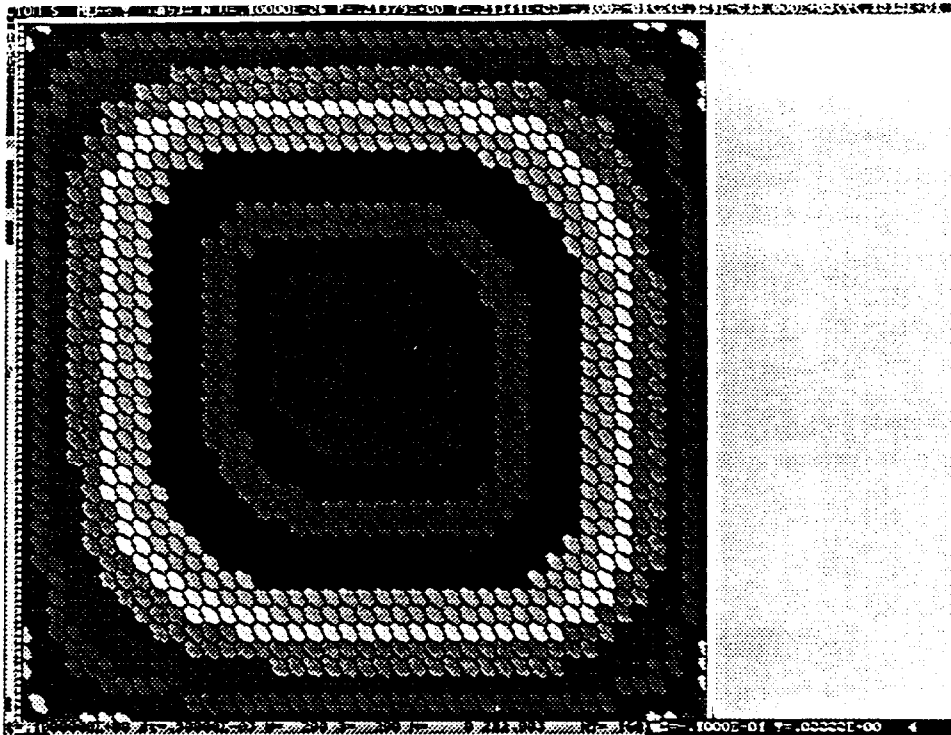


Fig. 15

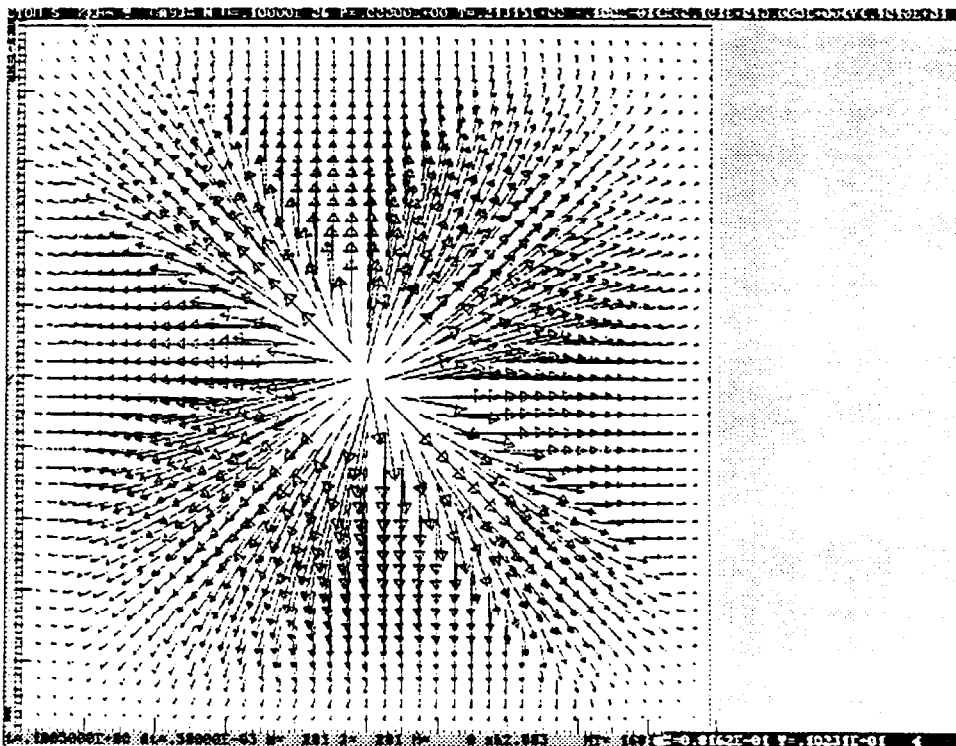


Fig. 16

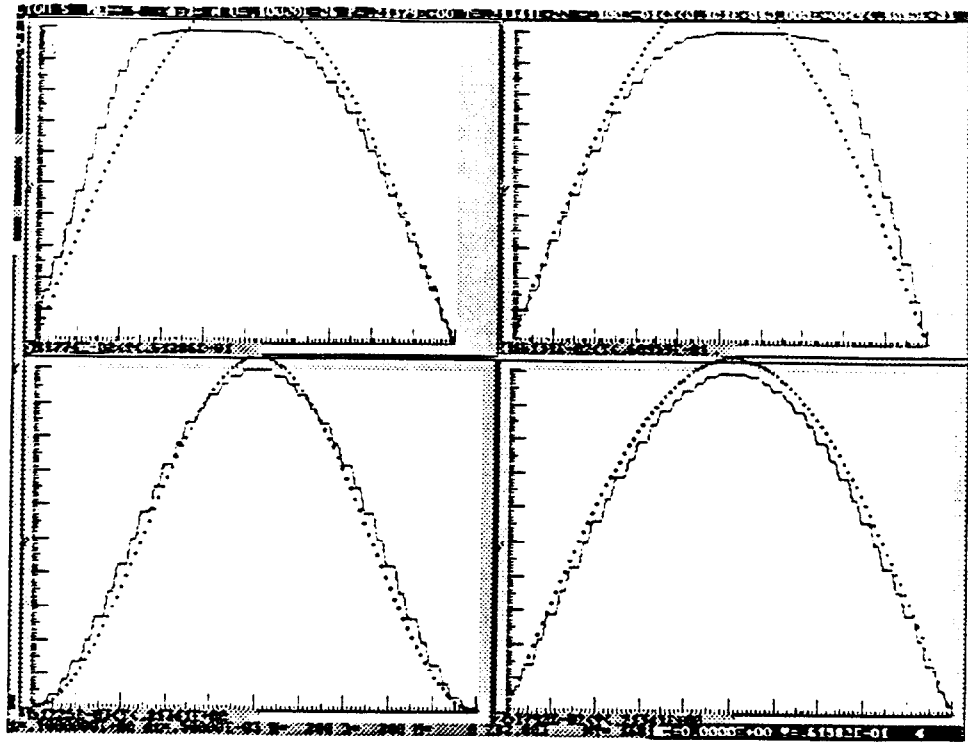


Fig. 17

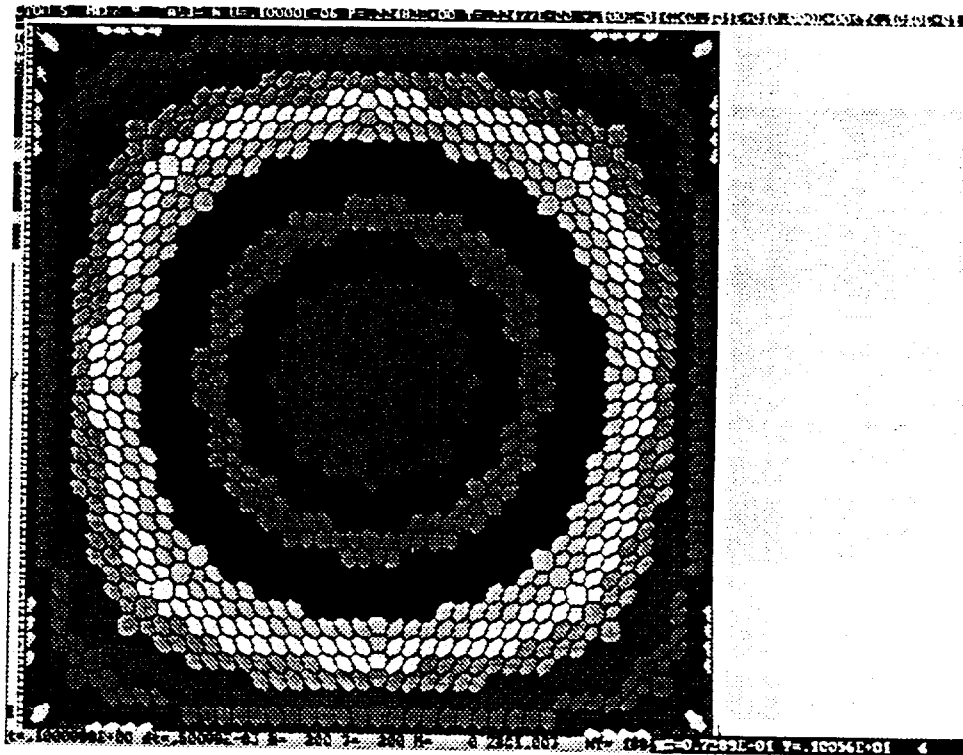


Fig. 18

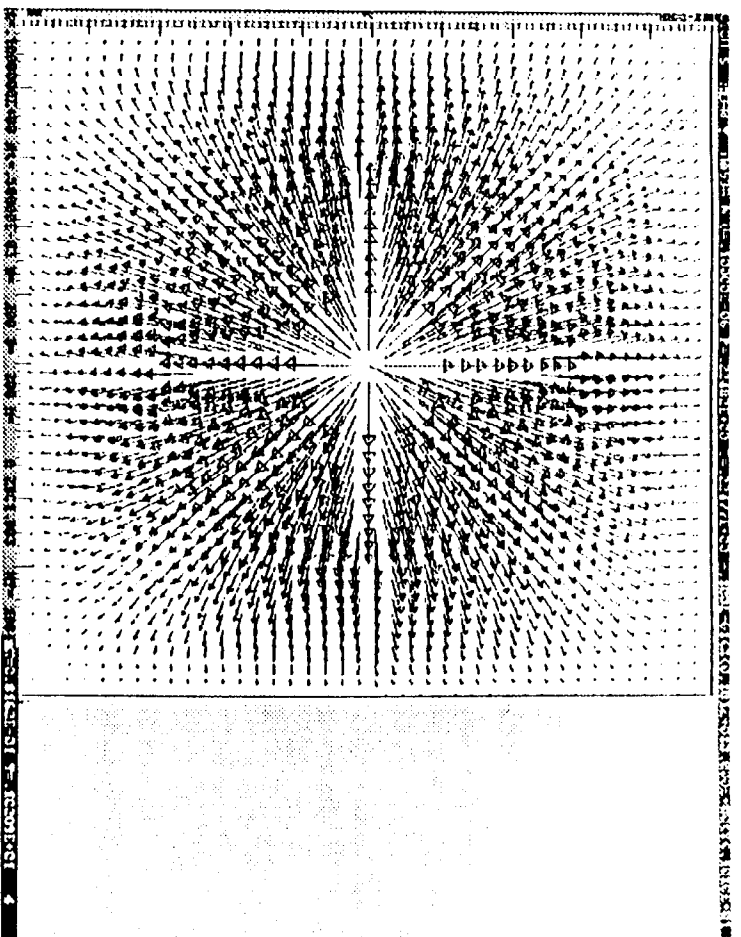


Fig. 19

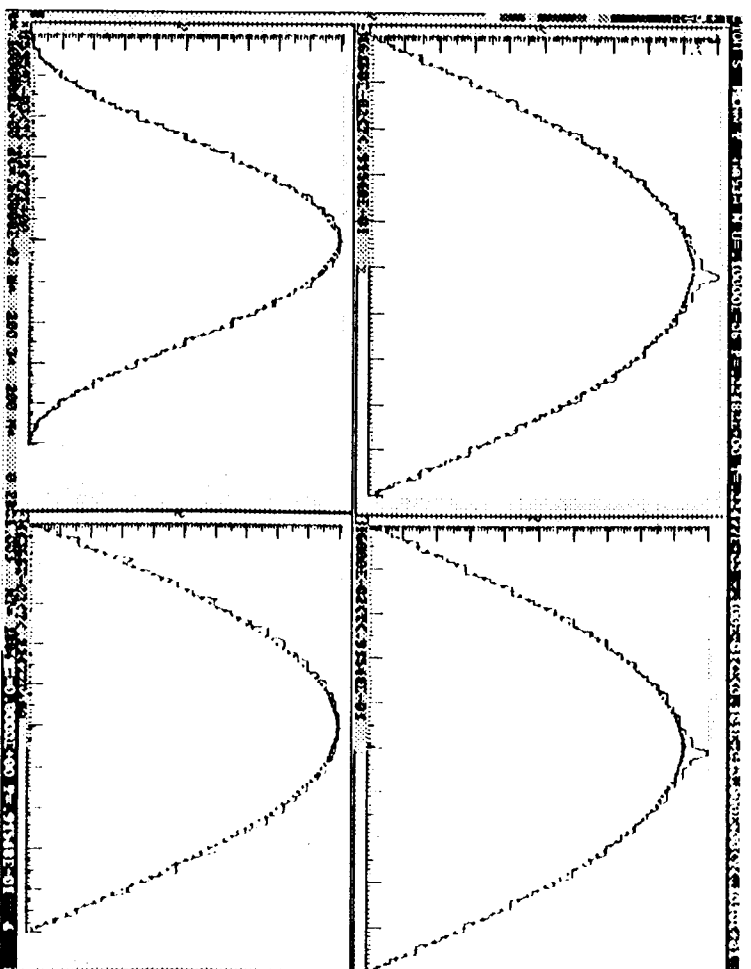


Fig. 20

## REFERENCES

1. Fundamentals of the technique "Meduza". numerical calculation of 2D system non-stationary gas dynamics problems. Glagoleva Yu.P., Zhogov B.M., Malshakov V.D., Nesterenko L.V., Podlivayev I.F., Sofronov I.D. Chisl. Met. Mekh. Splosh. Sredy, Novosibirsk, v.3, No.2, 1972.
2. "Meduza" program arrangement. Glagoleva Yu.P., Ilyasova E.B., Malshakov V.D., Nesterenko L.V., Sofronov I.D., Podlivayev I.F. Collected scientific papers "Computational Physics Program Systems", Novosibirsk, 1972.
3. The use of nonregular nets for solving two-dimensional nonstationary problems in gas dynamics. Nesterenko L.V., Rasskazova V.V., Sofronov I.D. In: "Numerical methods in fluid dynamics", Moscow, Mir Publishers, 1984.
4. Ring vortex generation at floating up of light gas in heavy gas. Zhmailo V.A., Glagoleva Yu.P., Malshakov V.D., Nesterenko L.V., Sofronov I.D., Statsenko V.P. Chisl. Met. Mekh. Splosh. Sredy, Novosibirsk, v.5, No.1, 1974.
5. Numerical solution of the problem of channel shutting-off in a wall under action gas pressing it. Glagoleva Yu.P., Malshakov V.D., Rodigin V.N., Sofronov I.D., Shustova E.F. Chisl. Met. Mekh. Splosh. Sredy, Novosibirsk, v.6, No.4, 1976.

## METHOD FOR MATERIAL FAILURE AND FRAGMENTATION COMPUTATION IN EGAK PROGRAM SYSTEM

Gorodnichev A.V., Simonov G.P., Yanilkin Yu.V.

RFNC-VNIIEF, Sarov (Arzamas-16)

The presentation describes the Lagrangian-Eulerian technique implemented in the program system EGAK [1] and designed for simulation of 2D multi-component media flows whose characteristic feature is presence of severe deformation, taking into consideration elastic-plastic material properties [2]. The technique under discussion makes use of the elastic-plastic Wilkins model with the Mises yield criterion.

The method of concentrations is used to compute the interfaces. In one computational cell there can be several components characterized with internal energies, as well as volume and mass concentrations. The components can be both various materials with their equations of state and elastic-plastic constants and vacuum, as well as a perfectly rigid body.

The technique for the material failure computation uses both simplest models based on prompt failure at achievement of limiting tensile stresses and more complex models proposed and studied in [3-6]. The latter involve the evolutionary equations for the parameters characterizing the material porosity degree which allows to take into account the history of damage accumulation in the material to determine the time of its failure.

The material rigid component yield strength and pressure are assumed to be a function of the parameters characterizing the material porosity degree.

The proposed technique also implements the capability to take into consideration material fragmentation following material failure under the high-velocity deformation conditions. To do this, the concepts developed by Grady [7] and Ivanov *et al.* [8] were considered.

The purpose of using the dynamic fragmentation model is determination of the fragment sizes from the material failure. At a high-velocity collision the fragmentation occurs when the collision velocity is higher than some critical value. The fragmentation characteristics immediately depend on the failure type and material parameters at the failure time.

The presentation discusses computed data for several problems: steel ball piercing through a two-layer aluminum and textolit barrier; collision of two copper plates; steel ball piercing through a plastic barrier; etc. The latter problem was used to test the fragmentation computation methods.

The computed data is compared with the analytical solutions, with experimental data and results of computations with other techniques. In all the computation series conducted the agreement of the computed data with analytical solutions and experimental data was good. Note that the model of Kanel *et al.* [4] proved most efficient and currently this is the basic in the EGAK system. By way

of example consider the computed results for piercing through a two-layer aluminum and composite barrier by a steel ball flying at velocity 2.7 km/s. The initial computation geometry is presented in Fig.1a. One computation did not use the failure model, the other used Kanel's model. The equations of state were taken in the Mie-Grueneisen form. Fig.1b.c shows the piercing pattern for two times. In the experiment the composite and aluminum hole diameters are 60 mm and 70 mm, respectively, close values were found in the computation taking into account the failure.

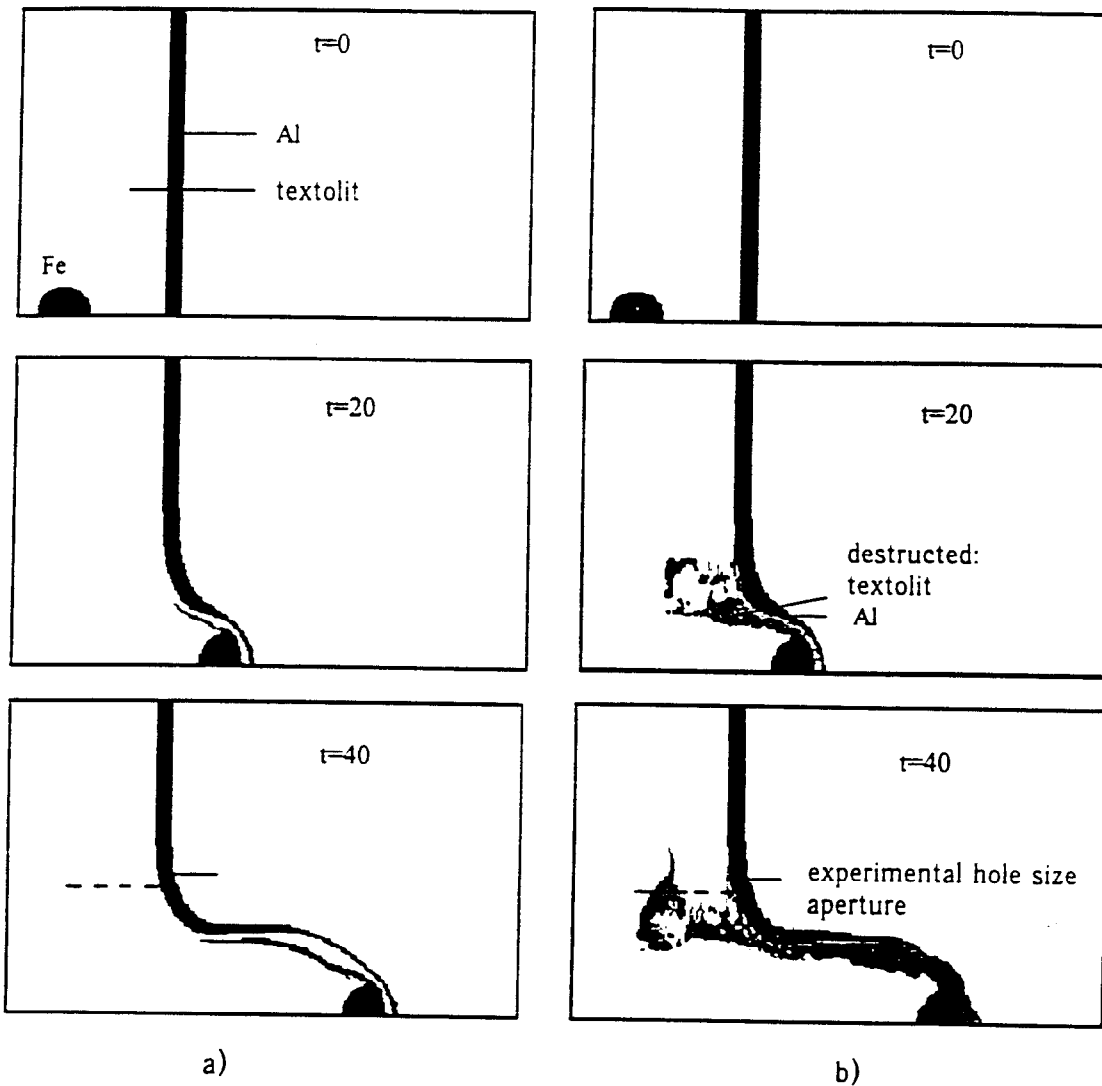


Fig.1. Raster pattern of two-layer barrier piercing:  
a) computation without account of failure, b) computation with  
account of failure (time in microseconds).

## REFERENCES

1. Yanilkin Yu.V., Shanin A.A., Kovalev N.P., Gavrilova E.S., Gubkov E.V., Darova N.S., Dibirov O.A., Znarova G.V., Kalmanovich A.I., Paviusna I.N., Samigulin M.S., Simonov G.P., Sin'kova O.G., Sotnikova M.G., Tarasov V.I., Toropova T.A. VANT. Ser.MMFP, No.4, 1993.
2. Toropova T.A., Yanilkin Yu.V. VANT. Ser. Mat. odelir. Fiz. Protsesov. 1994, No.4.
3. Glushak B.L., Novikov S.A., Ruzanov A.I., Sadyrin A.I. Failure of strained media at pulsed loads. Nizhi Novgorod State University Publishing House, Nizhi Novgorod, 1992.
4. Kanel G.I., Sugak S.G., Fortov V.E. Problemy Prochnosti. 1983, No.8, p.40-44.
5. Volkov I.A. Elasticity. Nizhi Novgorod, 1993, p.19-24.
6. Barbee T.W., Seaman L., Crewdsone R., Curran D. J. Materials, 1972, 7, N 3, p. 393-401.
7. Grady D.E. J. Appl.Phys., 1985, v.53. №1, P. 322-325.
8. Ivanov A.G., Rayevsky V.A., Vorontsova O.S. Fizika Goreniya i Vzryva, 1995, V.31, No.2.



# Molecular Dynamics Simulation of Permeation in Solids

Phillip I. Pohl, Grant S. Heffelfinger, Diana K. Fidler and David M. Ford  
Sandia National Laboratories, Albuquerque, NM 87185

## Abstract

In this work we simulate permeation of gases and cations in solid models using molecular mechanics and a dual control volume grand canonical molecular dynamics technique. The molecular sieving nature of microporous zeolites are discussed and compared with that for amorphous silica made by sol-gel methods. One mesoporous and one microporous membrane model are tested with Lennard-Jones gases corresponding to He, H<sub>2</sub>, Ar and CH<sub>4</sub>. The mesoporous membrane model clearly follows a Knudsen diffusion mechanism, while the microporous model having a hard-sphere cutoff pore diameter of ~3.4Å demonstrates molecular sieving of the methane (σ=3.8Å) but anomalous behavior for Ar (σ=3.4Å). Preliminary results of Ca<sup>+</sup> diffusion in calcite and He/H<sub>2</sub> diffusion in polyisobutylene are also presented.

## INTRODUCTION

The diffusion of gases in porous solids is governed by physical and chemical features of both the solid and the gas. The diffusion of a species, *i*, in a direction, *x*, is related to the gradient of concentration or density, *ρ*, by Fick's law:

$$J_i^x = -D_i^x \frac{d}{dx} \rho_i(x). \quad (1)$$

Permeability, *F*, a more appropriate parameter used in flow across membranes is found by modifying (1) slightly, i.e.,

$$J_i^x = \frac{F}{Ax} \Delta P_i. \quad (2)$$

Where  $\Delta P$  is the pressure drop across a membrane of thickness *x*, per cross sectional area *A*. If *x* is not known exactly, then it is absorbed into *F* and takes the name permeance.

Recently, Xiao and Wei gave a detailed analysis of the diffusion mechanisms of hydrocarbons in zeolites [1]. Their unified diffusion theory describing gaseous, liquid, Knudsen, solid and configurational (molecular sieving) diffusion, has a diffusivity expressed by

$$D = guLe^{-\frac{E}{RT}} \quad (3)$$

where  $g$  is a geometric term,  $u$  is a characteristic velocity,  $L$  the characteristic path length, and  $E$  the activation energy. The activation energy is only used for solid and configurational diffusion, and is cause for the sieving effect important in microporous membrane separations.

More recently, Shelekin et al., discussed the permeability of gases across disordered silica membranes. In these porous materials, Knudsen diffusion, surface diffusion and molecular sieving behavior dominate depending on the gas-surface interaction. For pores large relative to the molecular size of the permeating gases, Knudsen diffusion is the likely mechanism controlling the rate of transport. In this instance, the gases permeate proportionally to their molecular velocity, and hence, inversely proportional to the square root of their molecular weight. For similar membranes that strongly attract the permeating gases, surface diffusion will enhance the rate relative to Knudsen diffusion. In this study, Ar and CH<sub>4</sub> are much more strongly adsorbing than He and H<sub>2</sub>, so are possibly subject to this effect. When the pores of the membrane are roughly the same size as the gas molecule's diameter, then molecular sieving may take place. Like configurational diffusion described above, this mechanism is characterized by a strong temperature dependence and more importantly, sharp dropoffs in permeabilities for larger gas molecules.

Computer simulations of microporous solids have grown considerably in the past decade due to the advent of improved classical and quantum mechanical algorithms and the rapid growth of parallel computer hardware (Figure 1). These simulations can aid in understanding the structure-property relationships between the diffusing gases and the membrane.

To test the assumptions used in arriving at equation 3, we recently employed a number of simulation techniques [2] including molecular mechanics to predict  $E$ , grand canonical Monte Carlo (GCMC) to simulate the concentration in model pores and analysis of available pore space for different sized molecules to evaluate porosity/tortuosity effects. The focus of the present work has been an alternative to this three pronged approach. That is, simulate pressure driven gas transport in pores, which is more like the actual experiments carried out in testing zeolite [3] or silica [4] membranes. It is generally known that the chemical potential gradient is the true driving force for diffusion. Hence, simulation in the grand canonical ensemble (constant  $\mu VT$ ) is the most appropriate construct. To completely investigate pore diffusion, we have

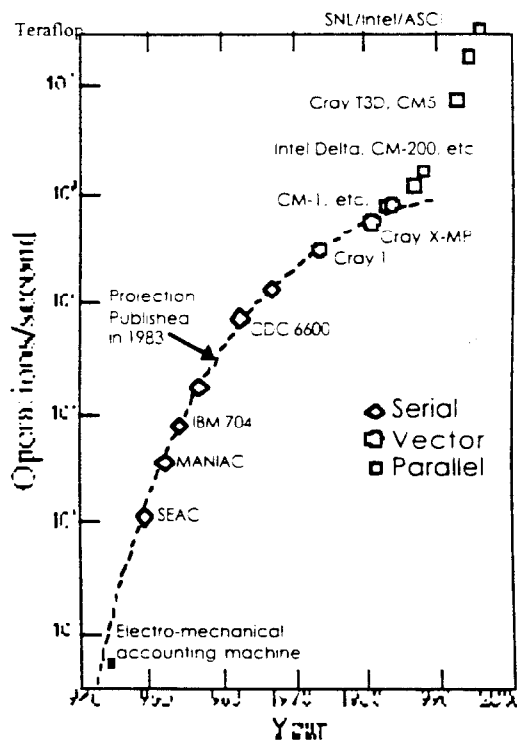


Figure 1 Growth of Computing Power

simulated gas movement driven by a chemical potential gradient in microporous silica using a newly developed dual control volume grand canonical molecular dynamics method [5].

### POROUS MODELS

The wall atoms, which did not move, were positioned according to the coordinates of a silica model made by expanding an amorphous glass model to a density of 1.5g/cc and then further to a density of 0.5 g/cc as in ref 6. The pore size of current generation sol-gel derived silica membranes consists of a distribution and all indications suggest that it may be similar to that of our model (Figure 2). That is, Brinker and Seghal [4] have been able to demonstrate molecular sieving by preparing membranes that exclude CH<sub>4</sub> at detectable levels, but allow He to permeate at a rate of  $2.25 \times 10^{-5}$  cm<sup>3</sup>/cm<sup>2</sup>-s-cmHg at 313K. In the present work, He, H<sub>2</sub>, Ar, and CH<sub>4</sub> (modeled as Lennard-Jones particles at 300K, 450K and 600K) permeability are determined for the silica models. The technique described below was applied recently to the simulation of He, H<sub>2</sub> and CH<sub>4</sub> permeation across silicalite membranes [7]. Results in that system showed considerably accuracy in comparison with experiments and suggested that the experimentally usable cross-sectional area in [3] was approximately 40 times less than ideal. Insights like this are indeed one benefit of molecular level computer simulations.

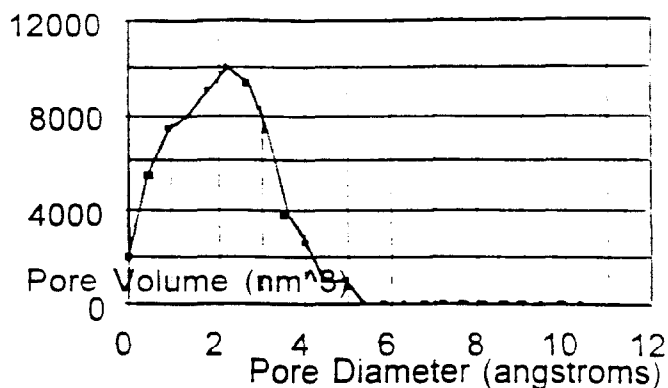


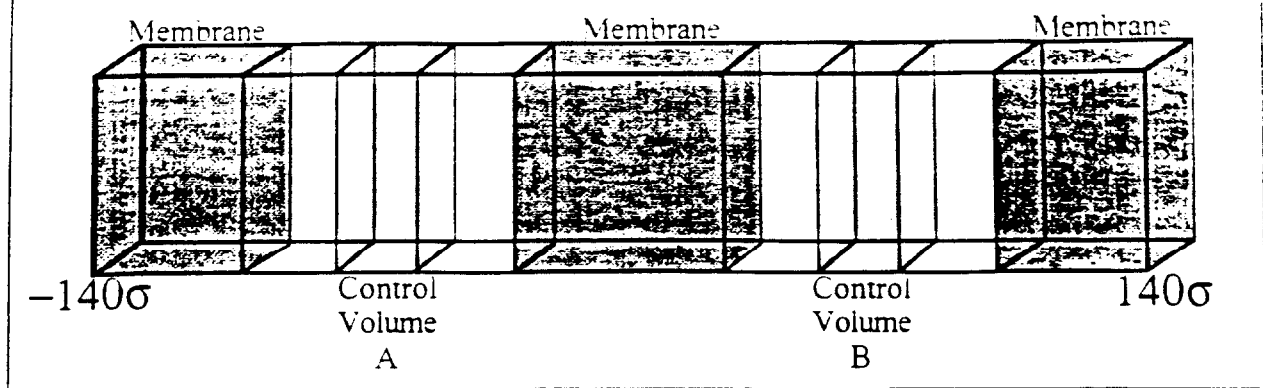
Figure 2 Silica Model Pore Size Distribution

### GCMD

The Dual Control Volume Grand Canonical Molecular Dynamics (DCV-GCMD) method has recently been adapted to investigate pressure-driven transport of a pure component fluid through a model zeolite [7]. While the DCV-GCMD method employs molecular dynamics (MD) moves throughout the system, each MD move is followed by a series of GCMC-like insertions and deletions of fluid molecules in each of two control volumes in order to maintain the chemical potential in the control volumes constant at a desired value. By measuring the flux and the gradient of the resulting steady-state density profile, the diffusivity of each fluid component, i. in the presence of a chemical potential or pressure gradient, transport parameter can be determined from equations 1 and 2. While DCV-GCMD has been demonstrated for binary color diffusion [5], in this work we have extended the method to model a fluid experiencing a pressure gradient while confined in a porous system [7] as well as running the code on a massively parallel computer. The pressure gradient is achieved for a pure component fluid simply by choosing chemical potentials in the two control volumes which produce two different fluid densities. Gradient driven gas diffusion simulations in pores is being tried by several others [8,9,10,11].

The fluid-fluid and fluid-wall interactions were modeled with the cut and shifted Lennard-Jones potential, the cut-off distance taken to be  $2.5\sigma$  for all interactions. The parameters were taken as those for silica hydroxyl oxygens [12] and He, H<sub>2</sub>, CH<sub>4</sub> and Ar [13] ( $\sigma_0=3.0$  Å).

Figure 3 Setup of Grand Canonical Molecular Dynamics computer simulation.



$\epsilon_{O/k}=230K$ ;  $\sigma_H=2.6 \text{ \AA}$ .  $\epsilon_H/k=10K$ ;  $\sigma_M=3.8 \text{ \AA}$ .  $\epsilon_M/k=148K$ ;  $\sigma_A=3.4 \text{ \AA}$ .  $\epsilon_A/k=130K$ ; ), and Lorentz-Bertholot combining rules used. The Si atoms in the silica model were neglected as they are effectively shielded by the Os making up the tetrahedral network. The densities in the system were initially set only to give ample flux for study but can be controlled to the desired bulk pressure. the temperature was 300K, 450K, and 600K, and the MD time step 2.9 fs.

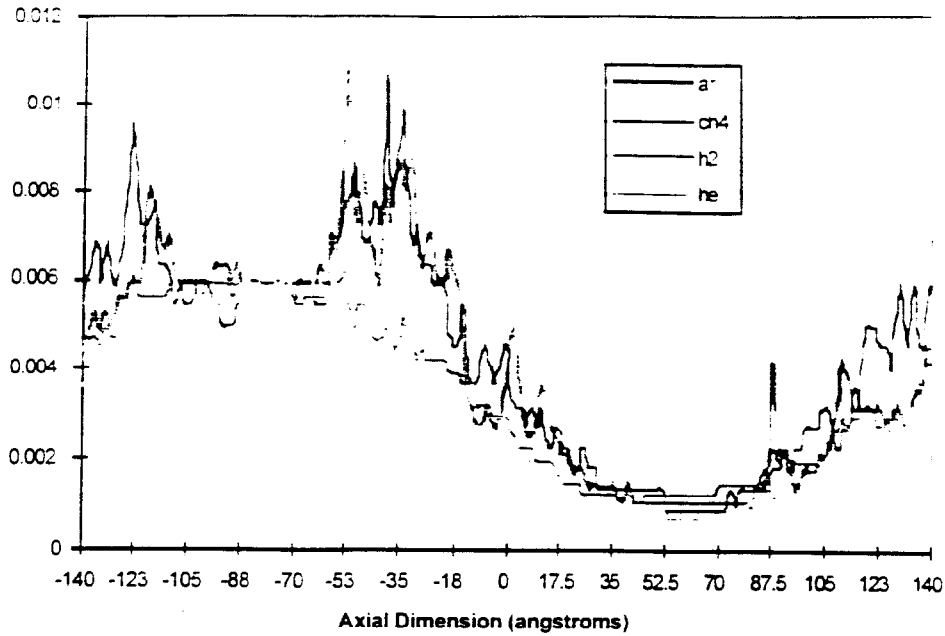
The silica system was  $139.0\sigma_H$  long consisting of  $8 \times 3 \times 3$  of the models described above, thus the x coordinate stretched from 0.0 to  $139.0\sigma_H$ . Periodic boundary conditions were employed along all planes and at  $x = 0.0$  and  $x = 139\sigma_H$ . Each control volume encompassed the entire pore cross section (Figure 3). While we have positioned the control volumes for both systems inside the pore, they could just as easily have been positioned outside the pore, enabling one to model entrance effects.

The simulation was equilibrated for 100,000 timesteps after which averages were accumulated for  $>100,000$  steps. The simulations were carried out only long enough to see a reliable and repeatable flux. At this point, the permeability can be computed based on the known pressure drop and membrane thickness. The algorithm employed in this work is a massively parallel version of the DCV-GCMD. Briefly, this parallel algorithm employs a superposition of two different parallel algorithms: spatial GCMC and spatial MD. With this parallel DCV-GCMD algorithm, simultaneous insertions/deletions can be attempted in each control volume thus for this work, 64 insertions and/or deletions were attempted in each control volume after each MD step. For this simulation, carried out on 250 processors of Sandia's Intel Paragon, each MD timestep and its associated 64 attempted insertions/deletions in each control volume took  $\sim 1$  cpu second depending on the number of gas particles.

## RESULTS

The axial density profile ( $\rho(x)$ ), determined by averaging the number of fluid molecules in  $1 \sigma_H$  wide bins is shown in Figure 4. From this figure, we can see that the density in control volumes A and B are  $\rho\sigma_H^3 = 0.030$  and  $0.0035$ , which correspond to bulk pressures of 20 and 2 atm, respectively. While these conditions are currently unattainable experimentally, the results should still be valid if the Gas-Gas interactions are much fewer than the Gas-Membrane interactions. Based on the low densities, we have assumed this is the case and a concentrations dependence is not expected. The axial density profile in Figure 4 shows approximate Fickian behavior, namely the dropping density from the high pressure to low pressure surfaces. We have

Figure 4 Axial density profiles in microporous silica membrane model (reduced units)



calculated the flux via two different methods [11], the flux plane method and the control volume flux method ( $\mathcal{J}$  and  $\xi$ , respectively):

$$\mathcal{J} = \frac{j^{LTP} - j^{RTL}}{\Delta t A_{yz} N_{planes}} \quad (4)$$

$$\xi^x = \frac{M(B) - M(A)}{4 \Delta t A_{yz} N_{steps}} \quad (5)$$

where  $j^{LTP}$  and  $j^{RTL}$  represent the net number of fluid molecules which move through each flux plane (two were used in this work, one at  $x = 70.0\sigma_H$  and another at the periodic boundary,  $x = 0$  and  $140.0\sigma_H$ ) and  $N_{planes}$  is the number of flux planes (2 for this work).  $M(B)$  and  $M(A)$  are the net number of insertions (accepted insertions - deletions) in control volumes A and B, respectively.  $\Delta t$  is the MD timestep.  $A_{yz}$  is the cross sectional area of the model, and  $N_{steps}$  is the number of MD timesteps. The fluxes, calculated via both methods (reduced by multiplying by  $\sigma_H^3(m_H/\epsilon_H)$ ), and the resulting permeabilities computed from equation 2 are shown in Table I.

From Table I we see that the fluxes calculated via the two methods agree quite well and yield a value for the permeabilities, for silica[1]. These values are considerably higher than the experimental values given above at 313K suggest that the density of this particular model is too low for comparison with the molecular sieving membranes of Brinker et al. [4]. The reason for this is that the relative elementary volume for the thin films is probably on the order of 100nm or essentially the thickness of the layer. Since our model is less than one tenth of that, the density of the real system overall can be greater than that of our model and still have the same permeability. Another view of the results through the mesoporous model can be seen in Figure 5, where the permeabilities are plotted as a function of the inverse square of the molecular weight.

Table I. Fluxes and permeabilities from DCV-GCMD simulations

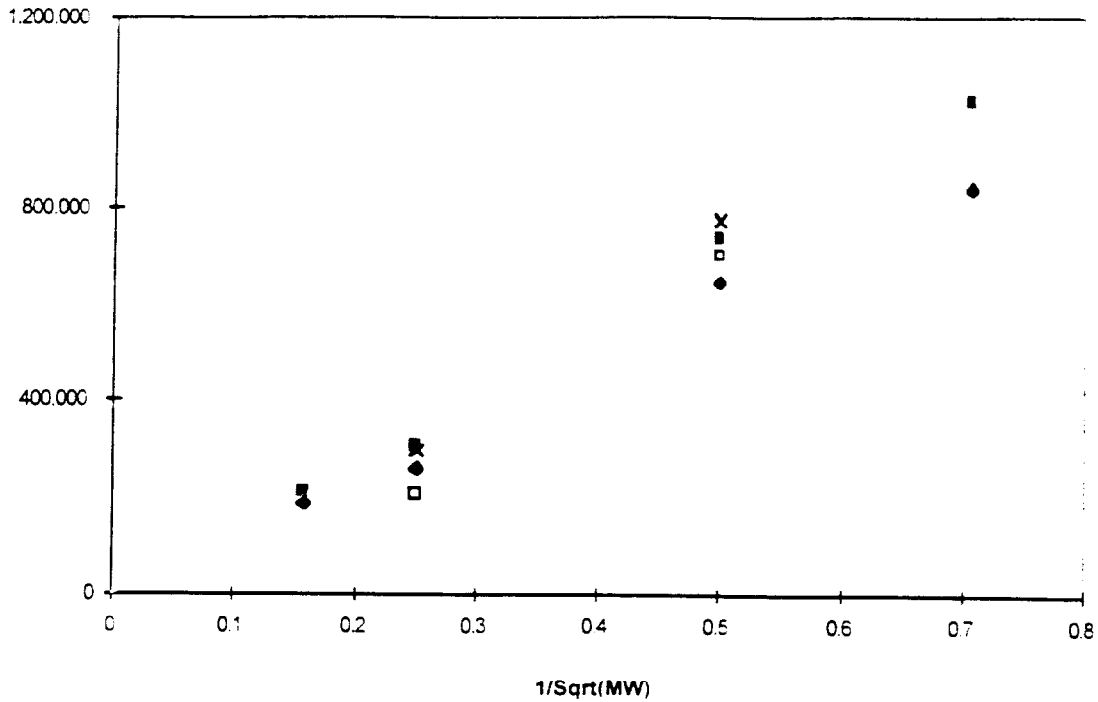
	$J \sigma^3 \sqrt{\frac{m}{\epsilon}}$	$\frac{J}{\sigma^3} \sqrt{\frac{m}{\epsilon}}$	permeability (Barrers*)
1.5 g/cc Silica Model			
He(450K)	3.6e-5	3.7e-5	3.300
He(300K)	3.5e-5	3.8e-5	3.500
H <sub>2</sub> (450K)	2.4e-5	1.9e-5	2.300
H <sub>2</sub> (300K)	3.3e-5	3.2e-5	3.000
Ar(600K)	4.7e-6	4.0e-6	180
Ar(450K)	2.3e-6	3.5e-6	205
Ar(300K)	3.2e-6	3.5e-6	190
CH <sub>4</sub> (600K)	3.1e-4	2.8e-4	300
CH <sub>4</sub> (450K)	8.0e-7	7.0e-7	80
CH <sub>4</sub> (300K)	1.1e-7	3.1e-7	<10
He (Mixed 300K)	1.4e-5	1.3e-5	2.700
CH <sub>4</sub> (Mixed 300K)	3.0e-5	3.0e-5	<10
0.5 g/cc Silica Model			
He(450K)	4.8e-4	4.7e-4	646.000
He(300K)	4.7e-4	4.8e-4	737.000
H <sub>2</sub> (450K)	5.7e-4	6.0e-4	841.000
H <sub>2</sub> (300K)	7.0e-4	7.1e-4	1.020.000
Ar(450K)	9.4e-5	9.1e-5	184.000
Ar(300K)	1.3e-4	1.3e-4	213.000
CH <sub>4</sub> (450K)	1.0e-4	1.0e-4	260.000
CH <sub>4</sub> (300K)	1.6e-4	1.5e-4	307.000
He (Mixed-450K)	1.4e-4	1.4e-4	700.000
CH <sub>4</sub> (Mixed-450K)	4.0e-5	4.0e-5	206.000
He (Mixed-300K)	2.3e-4	2.3e-4	776.000
CH <sub>4</sub> (Mixed-300K)	9.0e-5	8.0e-5	300.000

A straight line through the origin should reveal the knudsen permeation expected from mesoporous membranes where the molecular velocity dictates the fluid transport.

### DENSE SOLIDS

While the above discussion concerned the permeation of gases in meso- and microporous solids, the following examples describe the diffusion in denser solids. The applications are different, but the study techniques remain the same. That is, making proper assumptions about the interaction potentials and solid structure are paramount to obtaining useful information about

Figure 6 Permeability vs. Inverse molecular weight squared for mesoporous model (line drawn as guide for eye).



the transport properties of the diffusing body within a reasonable simulation time frame. Again, massively parallel supercomputing helps when applicable.

The first example concerns the diffusion of cations through calcite, and is part of a program funded by the National Aeronautic and Space Administration to assess the prospects of Figure 5 Experimental (below) and simulated diffusion of Ca<sup>2+</sup> in calcite.

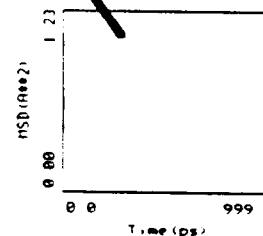
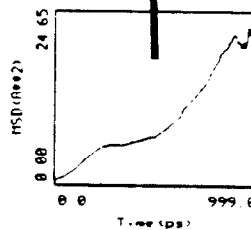
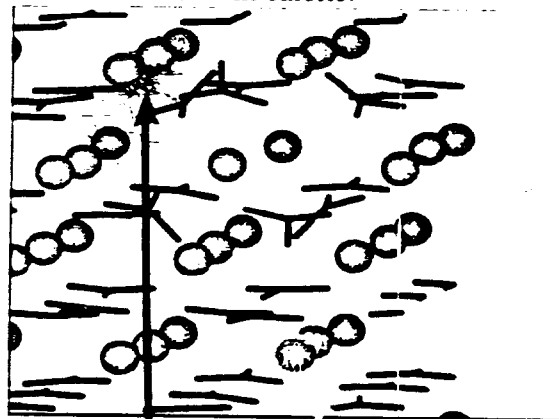
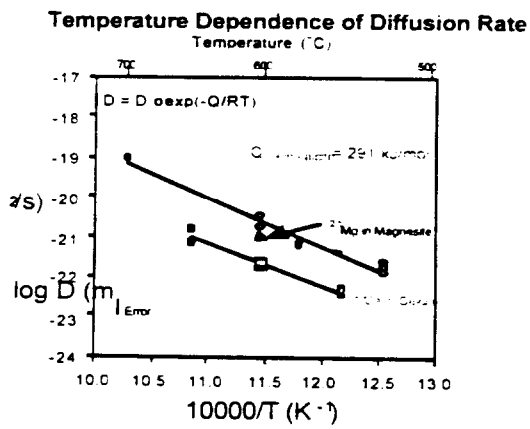
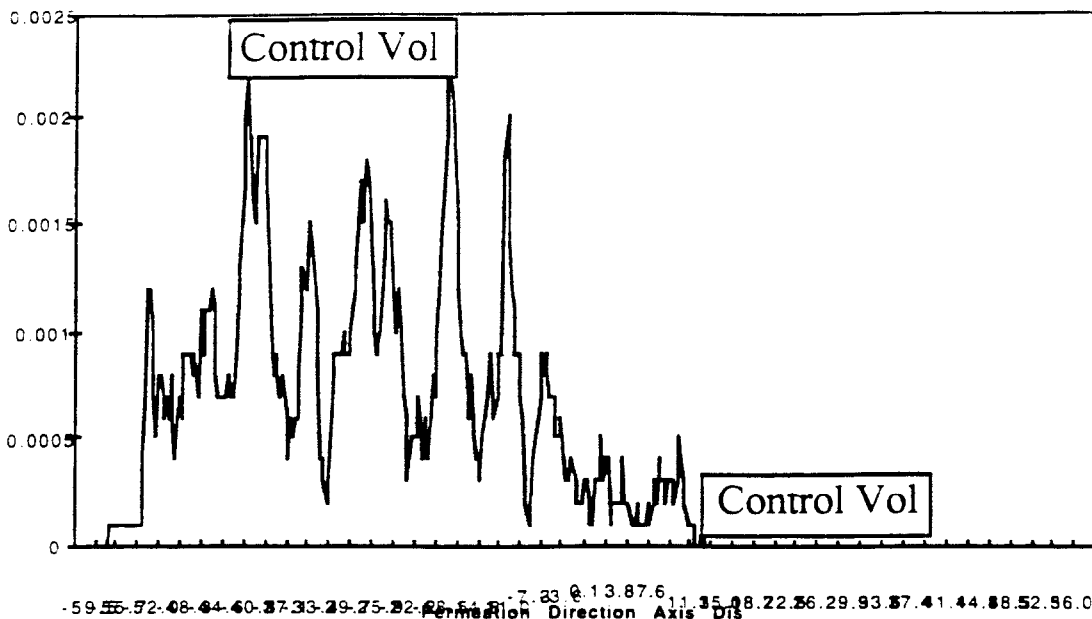


Figure 7 The density profile of He/H<sub>2</sub> in polyisobutylene



organic species on mars. Figure 6 shows the results of the experimental and simulated diffusion of Ca in calcite. The agreement is reasonable and suggests that the activation energy is approximately 300 kcal/mol [17]. The second example is of the permeation of He and H<sub>2</sub> down a concentrations gradient within a model of polyisobutylene. Figure 7 gives a plot of the gas density as a function of position within the polymer model [18]. Initial conclusions of this work suggest that the timesteps were so small, that a relatively long time was required to reach equilibrium.

## CONCLUSIONS

We have demonstrated the usefulness of DCV-GCMD for investigating the sieving nature of microporous materials by applying the method to a model silica system. Work is currently underway to apply DCV-GCMD to multicomponent fluids under different conditions in other silica and zeolite models. In this work we tried to exhibit the power and usefulness of massively parallel computer simulation in understanding gas flow in microporous solids. The theories in use for zeolites may work well for amorphous silica membranes if the pores are of molecular dimensions. DCV-GCMD simulation allows comparison with the most relevant experiments in membrane research, that is permeation of gases and gas mixtures.

## LITERATURE CITED

1. Xiao, J., and J. Wei. "Diffusion Mechanism of Hydrocarbons in Zeolites-I. Theory", Chem. Engr. Sci., 1992, 47(5), 1123.
2. Pohl P.I. and D.M. Smith. "Molecular Simulation of Porous Silicates", *Advances in Porous Materials*, MRS Vol 371, 27-33, 1995.

3. Yan, Y., M. E. Davis, and G.R. Gavalas. "Preparation of Zeolite ZSM-5 Membranes by In-Situ Crystallization on Porous  $\alpha$ -Al<sub>2</sub>O<sub>3</sub>". *Ind. Eng. Chem. Res.*, 34, 1652-1661, 1995.
4. Seghal, R., PhD Dissertation, University of New Mexico, 1995.
5. Heffelfinger, G. S., and F. van Swol. *J. Chem Phys.*, 1994, 100(10), 7548.
6. Pohl, P.I., J.L. Faulon, and D.M. Smith. "Molecular Dynamics Computer Simulation of Silica Aerogels". *J. Non-Cryst. Solids*, 186, 349-355, 1995.
7. Pohl, P.I., G.S. Heffelfinger, and D. M. Smith. "Molecular dynamics computer simulation of gas permeation in thin silicalite membranes". *Mol. Phys.*, 89(6), 347-354, 1996.
8. MacElroy, J.M.D., "Nonequilibrium Molecular Dynamics Simulation of Diffusion and Flow in Thin Microporous Membranes". *J. Chem. Phys.*, 101(6), 5274-5280, 1994.
9. Cracknell, R. F., D. Nicholson, and N. Quirke. "Direct Molecular Dynamics Simulation of Flow Down a Chemical Potential Gradient in a Slit-Shaped Micropore". *Phys. Rev. Lett.*, 74(13), 2463-2466, 1995.
10. Fritzsche, S., R. Haberlandt and J. Kärger. "An MD Study on the Correlation between Transport Diffusion and Self-Diffusion in Zeolites". *Z. Phys. Chem.(Munich)*, 189, 211-220, 1995.
11. Ford, D. M. and E. D. Glandt. "Molecular Simulation of the Surface Barrier Effect. Dilute Gas Limit". *J. Chem. Phys.*, 99, 11543-11549, 1995.
12. MacElroy, J.M.D., and K. Raghavan. "Adsorption and Diffusion of a Lennard-Jones Vapor in Microporous Silica". *J. Chem. Phys.*, 93(3), 2068-2079, 1992.
13. Hirshfelder, J. O., C. F. Curtiss, and R. B. Bird. *Molecular Theory of Gases and Liquids*. John Wiley & Sons, New York, 1954.
14. G. S. Heffelfinger. "Massively Parallel Dual Control Volume Grand Canonical Molecular Dynamics with LADERA". *in preparation*.
15. Fidler, D.K. and R.T. Cygan. "Diffusion of Isotopes of Magnesium and Calcium in Calcite". *submitted to American Mineralogist* (1997).
16. Ford, D.M. and G.S. Heffelfinger. "Modeling Gradient-Driven Diffusion of Small Molecules in Polymers with Dual-Control Volume Grand Canonical Molecular Dynamics". presented at the Winter Meeting of the American Institute of Chemical Engineers, Los Angeles, CA, Nov. 17, 1997.



## MONTE-CARLO SIMULATION OF BIOLOGICAL PROTECTION FOR REPETITIVE PULSE ELECTRON ACCELERATOR

Ya.Z. Kandiev, V.V. Plokhoi

**Russian Federal Nuclear Center - All-Russia Scientific-Technical Institute of Technical  
Physics (RFNC-VNIITF), Snezhinsk, Russia, 456770**

### Introduction

Currently there is a development effort underway at VNIITF focused on studying the kinetics of processes that decompose sulfur and nitrogen oxides in flue gases by repetitive pulse electron beam. In the framework of this effort there is ongoing development of the accelerator with parameters: beam current  $I=2$  kA, accelerated electrons energy up to 1 MeV, pulse duration  $\tau=50$  ns and pulse repetition frequency up to 500 Hz. Electron beam will exit through thin titanium foil of output window and will be slowed down in air layer  $\sim 1.5$  m thick, some beam energy will be transformed into Bremsstrahlung with ended energy 1 MeV.

In spite of the fact that the portion of beam energy converted into Bremsstrahlung in air per pulse is small, repetitive mode of operation with fairly high pulse repetition rate can lead to fairly big radiation exposure dose for personnel, if there is no biological shielding in place to surround the accelerator

To determine required thickness of biological shielding walls, in several federal points there has been performed computation of Bremsstrahlung dose resulting from interaction between 1 MeV electron beam from the repetitive-pulse accelerator and output window's foil, beam decelerating air layer, assuming various wall thickness.

It was demonstrated that high pulse repetition rate  $\sim 500$  Hz necessitates selection of concrete shielding walls  $\sim 100$  cm thick to protect personnel against radiation.

The computation was performed by PRIZMA code [Ref.1] which enables consideration of the problem in full formulation. The code incorporates versatile capabilities in describing geometry, sources, composition of materials, and computation results. It allows for computation of paths for different nature particles (neutrons, photons, electrons, positrons, and ions) accounting for their mutual transformations. For the purpose of solving the problems requiring computation of small probabilities-linked functionals (for instance, protection against radiation, detection problems, etc.) there has been developed cost function simulation method which permits to tune algorithm onto features of the specific problem. Development of this method relied on the assessment by "visits", i.e. required result is taken only in the case if a particle crosses integration region (detector)

If, in computations based on this method, one evaluates the number of particles which for the first time have visited integration region along with evaluation of required functionals, it becomes possible to get the assessment of benefit  $k_E$  obtained in comparison against analogue simulation method

$$k_E = \frac{t_1}{I_n \sigma_n t_n}$$

where  $t_1$  - time of computing one history by analogue method,

$I_n$ ,  $\sigma_n$ ,  $t_n$  - average number of particles - first time visitors of integration region, relative error of this result, and total time of computations, respectively, in non-analogue simulation method

To vindicate produced results, there has been done computation of the dose created by scattering on air of  $\gamma$ -radiation from  $^{60}\text{Co}$ -source at a big distance from the source, in the geometry described in [Ref.2]. The results of computation are compared against the results of "benchmark" experiment [Ref.2], thus serving as a test for the method developed to evaluate Bremsstrahlung dose beyond accelerator's biological protection.

For the same purpose there were performed tests of the method for computation of Bremsstrahlung production and energy-angle distribution of photons by comparison of measurement results presented in [Ref.3] against results under PRIZMA code.

The above-named problems, because of big optical thickness of barriers and relatively small sizes of detectors, are reduced to small values assessment problem. Thus, there is a need in use of non-analogue simulation apparatus incorporated in the software complex PRIZMA. Brief description of non-analogue simulation method as it is implemented in this software complex is given in [Ref.4].

### Computation of Bremsstrahlung Dose Behind Accelerator's Biological Protection - Formulation of the Problem

Computation of Bremsstrahlung radiation dose which is created in interaction of accelerator electron beam with output window foil, layer of air, and with concrete, was carried out for the points #1-7 shown on figure 1.

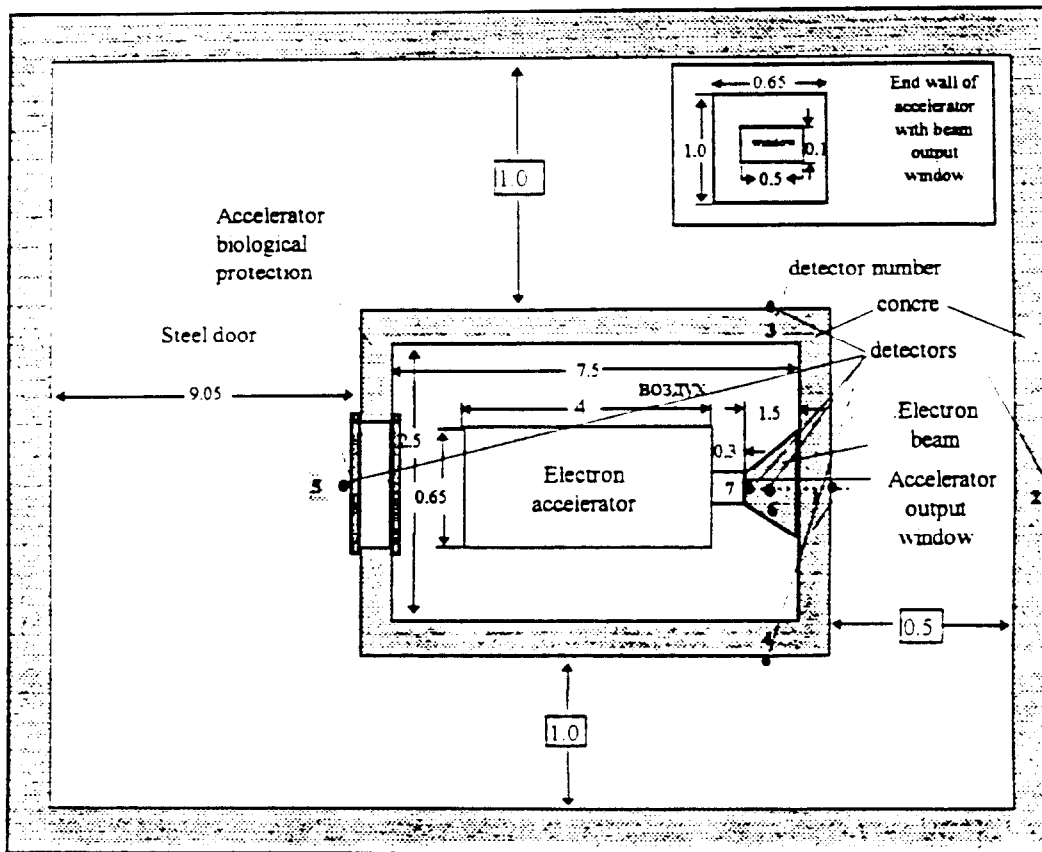


Figure 1. Relative position and sizes of the accelerator and test box (unequal scale, all sizes are in m)

Detector #6 is located above upper roofing of the test box, detectors #1-4 are located on horizontal plane which goes through beam axis, detector #5 is located on the level 2.125 m. Detector #7 is inside test box and is situated 15 cm above beam axis in vertical plane, and is shifted 1 cm

forward from output window surface. Internal height of the test box is 2.5 m. Accelerated electrons energy is 1 MeV. The electron source is specified as surface, monodirectional and monoenergetic on the internal surface of the foil in accelerator's output window and has an area  $0.5 \times 0.1 \text{ m}^2$ .

Electrons are normal incident onto window's foil internal surface, they are uniformly distributed through the surface

Walls of the accelerator box are made of steel, 0.8 cm thick. Concrete's formulation (weight): 0.0056 H, 0.4983 O, 0.0171 Na, 0.0024 Mg, 0.0456 Al, 0.3158 Si, 0.0012 S, 0.0192 K, 0.0826 Ca, 0.0122 Fe, density  $\rho = 2.3 \text{ g/cm}^3$ . Output window's foil is made of titanium  $2 \cdot 10^{-3} \text{ cm}$  thick. Weight composition of the air: 0.755 N, 0.232 O, 0.013 Ar ; density equals to normal value. Thickness of hall's brick walls is 0.4 m, hall's height - 9 m.

### Computation of the Dose from $^{60}\text{Co}$ -source Gamma-radiation Scattered on Air (test 1)

Correctness of photon transport in barriers with big optical thickness and complex geometry was performed through comparison of the dose from air-scattered gamma-radiation emitted by  $^{60}\text{Co}$  special configuration (see fig. 2) source, as it was computed by PRIZMA code, and measured in experiments in the vicinity to the ground surface.

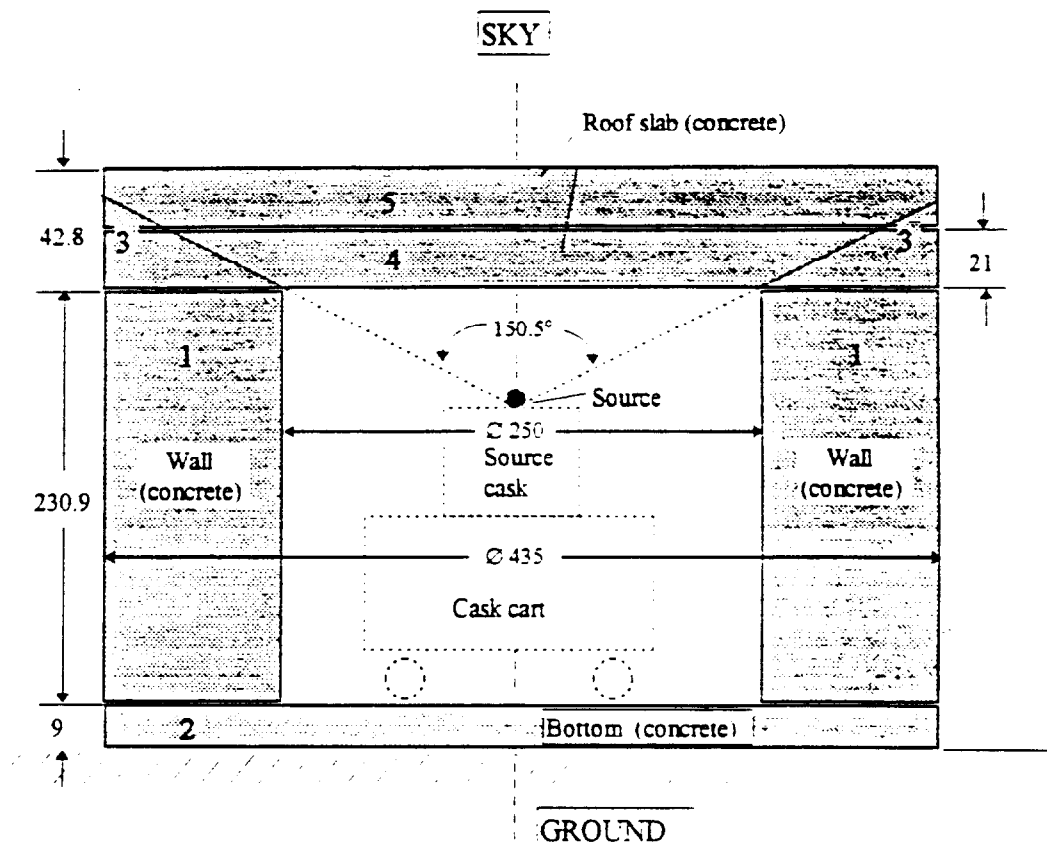


Figure 2. Vertical cross-section of protective box, with concrete roof slab 43 cm thick shown, which corresponds to the configuration of confined source in experiments on measurement of atmosphere-scattered radiation

Figure 2 shows the geometry of protective concrete box for  $^{60}\text{Co}$  isotope source used in computations, the geometry, with maximal approximation (we do not know the design of the cart and container for the source), describes geometry of the box used in experiments [Ref.2]

The computations used three source configurations

- open source with a beam, collimated in vertical cone with solid angle of  $150.5^\circ$ , in this case conic ring 3 was put on the edges of walls 1, beam is formed by the ring
- the source covered by concrete slab 21 cm thick.
- the source covered by concrete slab 42.8 cm thick

Radiation detectors used in computations are air-filled spheres 10 cm in diameter. Detectors were placed at various distances from the source in the range 50-700 m. Height of detectors relative to the earth surface is 1 m.

Analyzing the problem of computing exposure dose for an open source we decompose it on following elementary problems [4].

1. Radiation transport into detector located in emitting and scattering medium. System's geometry - spherical, 10 cm diameter detector is situated in the center of the system. Solution method - method of concentric detectors.
2. Radiation transport in optically thick air layers. System's geometry - spherical, in the center of the system is located 10 cm diameter detector. Solution method - exponential transformation.
3. Radiation transport in optically thick soil layers. System's geometry - planar, soil-air boundary serves as the detector. Solution method - exponential transformation.

When calculating exposure dose for confined source, one more problem is added to the three above-named elementary problems:

4. Radiation transport in optically thick layers of concrete. System's geometry is determined by the geometry of protective box, external surface of the protective box acts as detector. Solution method - exponential transformation.

Comparison of computation results versus experiment for the power of exposure dose at various distances from the source is given in tables 1-3.

Table 1

Measured and computed exposure dose ( $\mu\text{R}/\text{h}^{-1}\text{Ci}^{-1}$ ) for open source with the beam collimated in vertical cone of  $150.5^\circ$  solid angle

Distance, m	Experiment	PRIZMA		
	Exposure dose, $\mu\text{R}/\text{h}^{-1}\text{Ci}^{-1}$	Exposure dose, $\mu\text{R}/\text{h}^{-1}\text{Ci}^{-1}$	Number of photons incident on detector (per source photon)	Benefit $k_b$
50	$27.0 \pm 0.087$	$21.3 \pm 0.51$	$(2.20 \pm 0.048) 10^{-7}$	$1.2 10^4$
100	$10.5 \pm 0.087$	$8.39 \pm 0.2$	$(9.07 \pm 0.22) 10^{-8}$	$3.6 10^4$
200	$2.74 \pm 0.058$	$2.22 \pm 0.02$	$(2.44 \pm 0.024) 10^{-8}$	$1.7 10^5$
300	$0.86 \pm 0.038$	$0.811 \pm 0.013$	$(8.89 \pm 0.17) 10^{-9}$	$3.9 10^5$
400	$0.302 \pm 0.003$	$0.321 \pm 0.0077$	$(3.54 \pm 0.095) 10^{-9}$	$5.2 10^5$
500	$0.112 \pm 0.0022$	$0.128 \pm 0.0027$	$(1.41 \pm 0.037) 10^{-9}$	$1.4 10^6$
600	$0.0523 \pm 0.0026$	$0.0574 \pm 0.0013$	$(6.33 \pm 0.19) 10^{-10}$	$2.5 10^6$
700	$0.0267 \pm 0.00016$	$0.0246 \pm 0.00039$	$(2.62 \pm 0.057) 10^{-10}$	$5.4 10^6$

Table 2

Measured and computed exposure dose ( $\mu\text{R}/\text{h}^{-1}\text{Ci}^{-1}$ ) for the source covered by a layer of concrete 21 cm thick

Distance, m	Experiment	PRIZMA		
	Exposure dose, $\mu\text{R}/\text{h}^{-1}\text{Ci}^{-1}$	Exposure dose, $\mu\text{R}/\text{h}^{-1}\text{Ci}^{-1}$	Number of photons incident on detector (per source photon)	Benefit $k_e$
50	$2.53 \pm 0.039$	$2.28 \pm 0.064$	$(3.87 \pm 0.011) 10^{-6}$	$6.9 10^{-7}$
100	$0.802 \pm 0.0022$	$0.822 \pm 0.025$	$(1.38 \pm 0.044) 10^{-6}$	$2.4 10^{-7}$
200	$(1.64 \pm 0.022) 10^{-1}$	$(1.68 \pm 0.055) 10^{-1}$	$(2.79 \pm 0.10) 10^{-9}$	$1.3 10^{-9}$
300	$(4.43 \pm 0.013) 10^{-2}$	$(4.89 \pm 0.10) 10^{-2}$	$(8.29 \pm 0.21) 10^{-10}$	$4.3 10^{-9}$
400	$(1.59 \pm 0.011) 10^{-2}$	$(1.62 \pm 0.065) 10^{-2}$	$(2.71 \pm 0.14) 10^{-10}$	$7.1 10^{-9}$
500	$(4.99 \pm 0.11) 10^{-3}$	$(5.46 \pm 0.17) 10^{-3}$	$(8.69 \pm 0.35) 10^{-11}$	$2.7 10^{-9}$
600	$(1.78 \pm 0.11) 10^{-3}$	$(2.19 \pm 0.10) 10^{-3}$	$(3.60 \pm 0.23) 10^{-11}$	$3.6 10^{-9}$
700	$(6.63 \pm 1.3) 10^{-4}$	$(7.70 \pm 0.2) 10^{-4}$	$(1.14 \pm 0.039) 10^{-11}$	$1.4 10^{-9}$

Table 3

Measured and computed exposure dose ( $\mu\text{R}/\text{h}^{-1}\text{Ci}^{-1}$ ) for the source covered by a layer of concrete 42.8 cm thick

Distance, m	Experiment	PRIZMA		
	Exposure dose, $\mu\text{R}/\text{h}^{-1}\text{Ci}^{-1}$	Exposure dose, $\mu\text{R}/\text{h}^{-1}\text{Ci}^{-1}$	Number of photons incident on detector (per source photon)	Benefit $k_e$
50	$(2.22 \pm 0.022) 10^{-1}$	$(2.39 \pm 0.10) 10^{-1}$	$(3.99 \pm 0.13) 10^{-9}$	$5.2 10^{-7}$
100	$(6.49 \pm 0.18) 10^{-2}$	$(7.24 \pm 0.32) 10^{-2}$	$(1.25 \pm 0.047) 10^{-9}$	$1.9 10^{-9}$
200	$(1.31 \pm 0.013) 10^{-2}$	$(1.58 \pm 0.076) 10^{-2}$	$(2.71 \pm 0.11) 10^{-10}$	$1.1 10^{-9}$
300	$(3.16 \pm 0.11) 10^{-3}$	$(4.08 \pm 0.12) 10^{-3}$	$(7.31 \pm 0.22) 10^{-11}$	$3.4 10^{-9}$
400	$(1.01 \pm 0.13) 10^{-3}$	$(1.21 \pm 0.067) 10^{-3}$	$(2.10 \pm 0.14) 10^{-11}$	$5.8 10^{-9}$
500	--	$(4.28 \pm 0.23) 10^{-4}$	$(7.49 \pm 0.55) 10^{-12}$	$9.0 10^{-9}$
600	--	$(1.41 \pm 0.076) 10^{-4}$	$(2.33 \pm 0.15) 10^{-12}$	$5.3 10^{-9}$
700	--	$(5.45 \pm 0.20) 10^{-5}$	$(8.23 \pm 0.34) 10^{-13}$	$1.3 10^{-9}$

Apparent to the eye is satisfactory matching of computation and experimental results for confined source, and some discrepancy at small distances for the open source. The existing discrepancies, to our view, are explained by the absence of accurate information on concrete formulation and source cart (for more accurate accounting for scattered radiation inside concrete pit, for the case of open source)

### Computation of Bremsstrahlung Yield from Be, Al, and Fe Targets (Test 2)

Computation method which determines yield of Bremsstrahlung radiation generated from interaction between accelerated electrons and air, and elements of accelerator's structure was tested by comparing PRIZMA-computed and experimental values [Ref.3] of the total yield and angular distribution of Bremsstrahlung generated in Be, Al, and Fe targets irradiated by 1 MeV electron beam. Target thickness was chosen from the condition of complete electron stopping, experiment's schematics is shown on Figure 3.

In this case decomposition gave only one elementary problem.

1. Radiation transport into detector located in vacuum. Detectors with radius 0.1 cm are located on 1 m radius sphere in the points corresponding to various polar angles relative to the symmetry axis of the system. Solution method - method of probe particles.

Computed results of total Bremsstrahlung yield for various targets are compared versus experimentally measured in Table 4. Angle distribution computed results are compared against experiment on figure 4. Comparison of provided results gives grounds to speak of satisfactory accuracy in computation of Bremsstrahlung characteristics for the situation of Bremsstrahlung generation in interaction between the electron beam and air or accelerator's structure elements.

**Table 4**

Computed and measured total energy of Bremsstrahlung (MeV/electron) radiated from thick Be, Al, and Fe targets. Incident electrons energy is 1 MeV.

Target	Be	Al	Fe
PRIZMA	$(1.98 \pm 0.014) \cdot 10^{-3}$	$(6.11 \pm 0.037) \cdot 10^{-3}$	$(1.15 \pm 0.092) \cdot 10^{-3}$
Experiment	$(1.56 \pm 0.4) \cdot 10^{-3}$	$(5.12 \pm 0.8) \cdot 10^{-3}$	$(1.05 \pm 0.1) \cdot 10^{-3}$

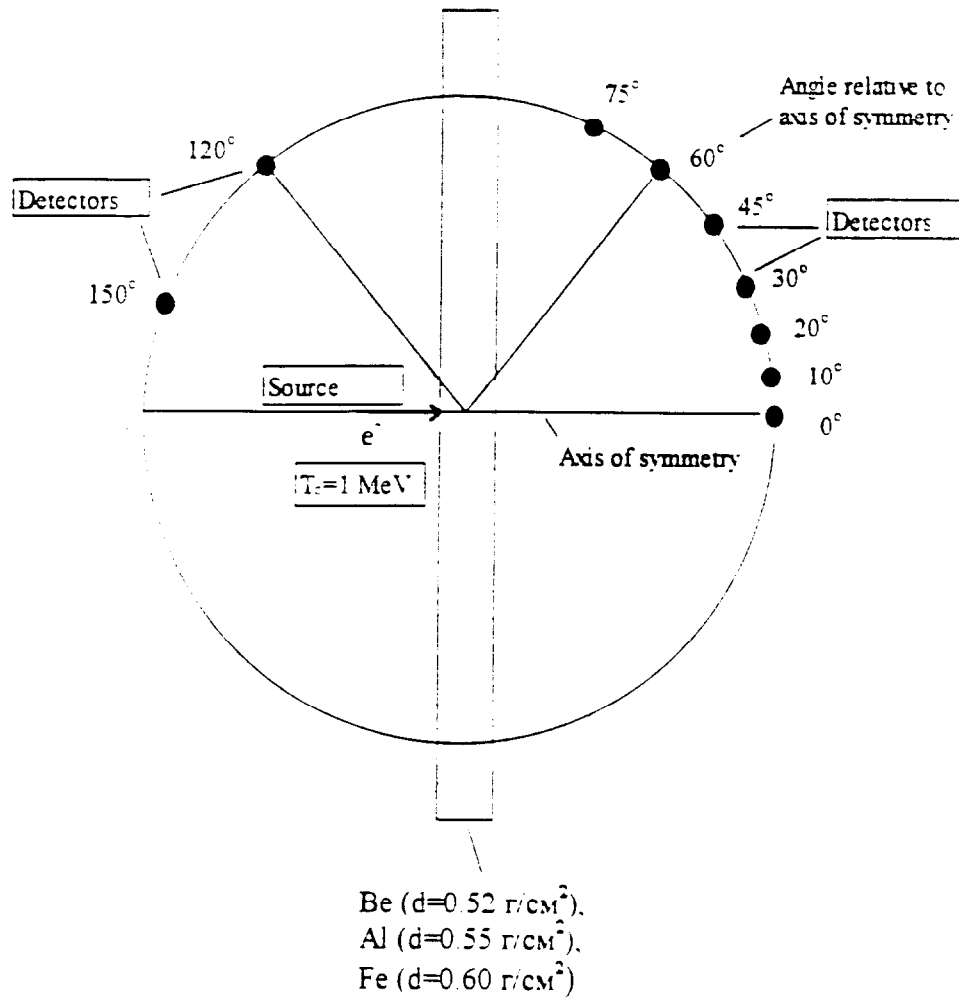


Figure3 Geometry of experiment on measuring characteristics of Bremsstrahlung radiated from the thick layer of Be, Al, and Fe. under irradiation by 1 MeV electrons

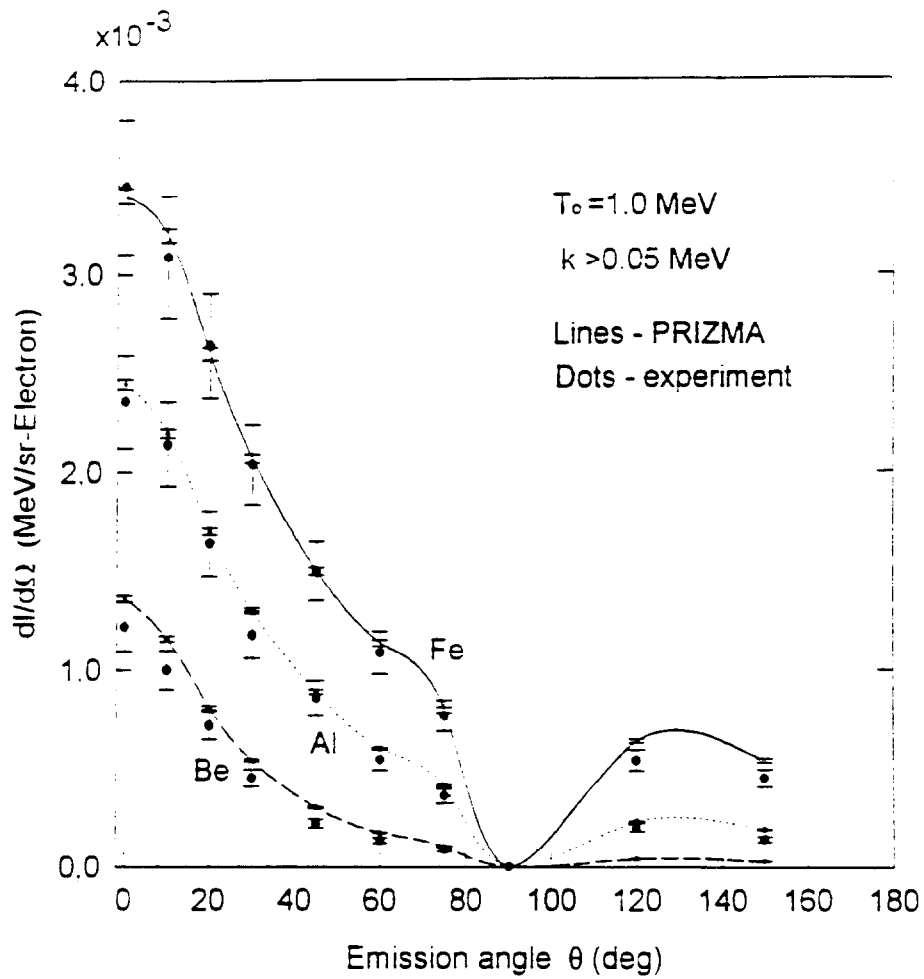


Figure 4. Angle distribution of Bremsstrahlung for photons with energy  $k > 0.05$  MeV for thick targets of Be, Al, and Fe. Incident electron energy is 1 MeV.

### Computation of Bremsstrahlung Dose Beyond Accelerator's Biological Protection

Analyzing the problem of computing the dose of Bremsstrahlung generated in interaction of accelerator's electron beam with output window foil, with layer of air and concrete, at the point right beyond accelerator's biological protection, we were able to outline two elementary problems

1. Radiation transport into detector located in emitting and scattering medium. System's geometry - spherical, detector 0.1 cm in radius is placed at the system's center. Solution method - method of concentric detectors
2. Radiation transport in optically thick medium. System's geometry is determined by the geometry of accelerator's protective box, external surface of the protective box acts as the detector. Solution method - exponential transformation.

By means of preliminary computations thickness of all walls in test box, except the front one, was chosen equal to 1.0 m, thickness of the front wall was taken equal to 1.2 m, thickness of steel doors - 2x9 cm.

After performing computations for the chosen sizes of protecting system, following values of absorbed dose D of Bremsstrahlung were obtained, the values are per one source (beam) electron for detector locations.

1. Detector #1 -  $D=1.28 \cdot 10^{-27}$  Gray/electron,  $\sigma=8.3 \%$
2. Detector #3,4,6 -  $D=0.98 \cdot 10^{-27}$  Gray/electron,  $\sigma=9.3 \%$
3. Detector #5 -  $D=1.82 \cdot 10^{-27}$  Gray/electron,  $\sigma=8.4 \%$

Benefits  $k_b$  for Detector #1-6 are shown in Table 5.

Table 5

Detector number	Number of photons incident on detector (per source electron)	Benefit $k_b$
Detector #1	$3.72 \cdot 10^{-17}$ , $\sigma=8.3 \%$	$2.9 \cdot 10^{14}$
Detector #3,4,6	$3.18 \cdot 10^{-17}$ , $\sigma=9.3 \%$	$2.6 \cdot 10^{15}$
Detector #5	$4.66 \cdot 10^{-17}$ , $\sigma=8.3 \%$	$5.2 \cdot 10^{15}$

The dose inside test box was estimated by means of detector #7 and through computation of dose in detector #1 for the case when front wall thickness is equal 0.2 cm (for electron capture), we assigned number #1a to this detector for further cases. The computation gives following values of absorbed dose for these detectors:

1. Detector #1a -  $D=2.27 \cdot 10^{-19}$  Gray/electron,  $\sigma=5.8 \%$
2. Detector #7 -  $D=0.73 \cdot 10^{-19}$  Gray/electron,  $\sigma=9 \%$

For the purpose of studying the feasibility of reducing thickness of the front wall, there were computations done for the case when front wall is 1 m thick. Following values of absorbed dose in detectors #1 (assigned number #1b to this detector) and 2 were obtained for this case

1. Detector #1b -  $D=3.73 \cdot 10^{-26}$  Gray/electron,  $\sigma=8.8 \%$
2. Detector #2 -  $D=1.64 \cdot 10^{-27}$  Gray/electron,  $\sigma=10.4 \%$

Recalculating obtained results into absorbed dose power P for the hardest (in the sense of requirements to biological protection) accelerator's operating mode with beam current  $I=2$  kA, pulse duration  $\tau=50$  ns, and pulse repetition frequency 500 Hz gives following results

1. Detector #1 -  $P=1.44 \cdot 10^{-6}$  Gray/hour,  $\sigma=8.3$  %
2. Detector #3,4,6 -  $P=1.10 \cdot 10^{-6}$  Gray/hour,  $\sigma=16$  %
3. Detector #5 -  $P=2.05 \cdot 10^{-6}$  Gray/hour,  $\sigma=8$  %

For the thickness of front wall of 1 m similar recalculation gives following values

1. Detector #1b -  $P=4.20 \cdot 10^{-5}$  Gray/hour,  $\sigma=8.8$  %
2. Detector #2 -  $P=1.85 \cdot 10^{-6}$  Gray/hour,  $\sigma=10.4$  %

For the power of absorbed dose inside test box we obtain:

1. Detector #1a -  $P=2.55 \cdot 10^{-2}$  Gray/hour,  $\sigma=5.8$  %
2. Detector #7 -  $P=0.82 \cdot 10^{-2}$  Gray/hour,  $\sigma=9$  %

The above given results attest to the fact that chosen parameters of the test box assure dose levels in possible personnel locations do not exceed allowed level of the Norms of Radiation Safety NRB-96 of  $10^{-5}$  Gray/hour.

Worth noting is that the above given values of the benefit are somewhat understated, since when estimating  $k_E$ , the number of first-time visits was substituted by the total number of visits.

## References

- [1] Ya. Z. Kandiev, E.S. Kuropatenko, I.V. Lifanova et al. // Collection of abstracts. 3<sup>rd</sup> All-Union Scientific Conference on Protection of Nuclear-Engineering Installations from Ionizing Radiation. Tbilisi, TGU, 1981. page 24
- [2] R.R.Nason, J.K.Shultis, R.E.Saw and C.E.Clifford, "A Benchmark  $\gamma$ -Ray SkyShine Experiment", Nucl. Sci. Eng., 79, 404-416, (1981).
- [3] D.H.Rester, W.E.Dance and J.H.Derrickson, "Thick Target Bremsstrahlung Produced by Electron Bombardment of Targets Be, Sn and Au in the Range 0.2-2.8 MeV", Journ. Appl. Phys., vol.41, No.6, 2682-2692, (1970).
- [4] M.A.Arnautova, Ya.Z.Kandiev, B.E.Lukhminsky, G.N.Malishkin, Nucl. Geophys. Vol.7.No.3, pp. 407-418,1993.

# MULTI-PARAMETER MODEL OF TURBULENT MIXING IN TWO-DIMENSIONAL FLOWS

V.V. Nikiforov, Yu.V. Yanilkin, G.V. Zharova, Yu.A. Yudin.  
RFNC-VNIIEF, 607190, Sarov (Arzamas-16), Russia

## ABSTRACT

The paper describes Nikiforov's multi-parameter model of turbulent mixing implemented in the EGAK program system [1]. The model uses 9 independent variables for which evolutionary equations are solved. For the variables all the Reynolds tensor components, turbulent energy dissipation rate, two components of mass turbulent flow velocity, squared density fluctuations and total turbulent energy are used. The model is a 2D analog of 1D VIKHR' technique model [2] and involves turbulence generation both due to gravitational and tangent instabilities.

### 1. EQUATIONS FOR AVERAGED QUANTITIES

$$\frac{\partial}{\partial t}(\rho \bar{u}) + \operatorname{div}(\rho \bar{u} \bar{u}) = -\nabla P - \operatorname{div} \sigma_T,$$

$$\frac{\partial}{\partial t}(\alpha_i \rho) + \operatorname{div}(\alpha_i \rho \bar{u}) = \operatorname{div}(\rho D \nabla \alpha_i),$$

$$\frac{\partial}{\partial t} \beta_i + \operatorname{div}(\beta_i \bar{u}) = \beta_i \operatorname{div} \bar{u}_i + \operatorname{DIF}(\beta_i),$$

$$\frac{\partial}{\partial t}(\alpha_i \rho \varepsilon_i) + \operatorname{div}(\alpha_i \rho \varepsilon_i \bar{u}) = \operatorname{div}(\rho D \nabla \alpha_i \varepsilon_i) - \beta_i P_i \operatorname{div}(\bar{u} - \bar{w}) + \alpha_i \rho \varepsilon \frac{\Phi}{e^T}.$$

Viscous stress tensor  $\sigma_T$  has four components in 2D case

$$\sigma_T = \begin{Bmatrix} \sigma_{11} & \sigma_{12} & 0 \\ \sigma_{21} & \sigma_{22} & 0 \\ 0 & 0 & \sigma_{33} \end{Bmatrix} \quad \begin{aligned} \sigma_{ik} &= 2\rho \sigma'_{ik}, \\ \sigma'_{ik} &= 2\rho \frac{e_{ik}^T}{e^T} \Phi. \end{aligned}$$

### 2. EQUATIONS FOR TURBULENT QUANTITIES

$$\begin{aligned} \frac{de_1^T}{dt} &= \Pi_{11} - e_1^T \operatorname{div} \bar{w} - 2e_1^T V_{11} - 2e_{12}^T V_{12} + \left(1 - \frac{2}{10} k\right) f_1 w_1 g_1 + \frac{1}{10} k f_1 w_2 g_2 - \\ &\quad - \gamma \omega \left( e_1^T - \frac{1}{3} e^T \right) - k_1 \omega e_1^T; \end{aligned}$$

$$\begin{aligned}
\frac{de_1^T}{dt} &= \Pi_{22} - e_2^T \operatorname{div} \bar{w} - 2e_2^T V_{22} - 2e_{12}^T V_{21} + \left(1 - \frac{2}{10}k\right) f_1 w_2 g_2 - \frac{1}{10} k f_1 w_1 g_1 - \\
&\quad - \gamma \omega \left( e_1^T - \frac{1}{3} e^T \right) - k_2 \omega e_2^T; \\
\frac{de_2^T}{dt} &= \Pi_{33} - e_3^T \operatorname{div} \bar{w} - 2e_3^T V_{33} + \frac{1}{10} k f_1 (w_1 g_1 + w_2 g_2) - \gamma \omega \left( e_3^T - \frac{1}{3} e^T \right) - k_3 \omega e_3^T; \\
\frac{de_{12}^T}{dt} &= \Pi_{12} - e_{12}^T \operatorname{div} \bar{w} - e_1^T V_{21} - e_2^T V_{12} - e_{12}^T (V_{11} + V_{22}) + \\
&\quad + \frac{1}{2} \left(1 - \frac{3}{20}k\right) (w_1 g_2 + w_2 g_1) f_1 - \gamma \omega e_{12}^T; \\
\frac{dw_1}{dt} &= \Pi_1^w - w_1 V_{11} - w_2 V_{12} + 2e_1^T A_1 + 2e_{12}^T A_2 + f_1 R g_1 - k_w \omega w_1; \\
\frac{dw_2}{dt} &= \Pi_2^w - w_2 V_{22} - w_1 V_{21} + 2e_2^T A_2 + 2e_{12}^T A_1 + f_1 R g_2 - k_w \omega w_2; \\
\frac{dR}{dt} &= \Pi^R + R \operatorname{div} \bar{w} + 2(w_1 A_1 + w_2 A_2) - k_R \omega R; \\
\frac{d\Phi}{dt} &= \Pi^\Phi - 2\sigma'_{ij} V_{ij} - \bar{w} \frac{d\bar{u}}{dt} - \omega \Phi; \\
\frac{d\varepsilon}{dt} &= \Pi^\varepsilon - \varepsilon \operatorname{div} \bar{w} - \frac{4}{3} \varepsilon \operatorname{div} (\bar{u} - \bar{w}) - 2 \frac{\varepsilon^2}{k e^T} - \\
&\quad - c_{\varepsilon 1} \gamma \frac{\varepsilon}{e^T} \left\{ \left( e_1^T - \frac{1}{3} e^T \right) V_{11} + \left( e_2^T - \frac{1}{3} e^T \right) V_{22} + \left( e_3^T - \frac{1}{3} e^T \right) V_{33} + e_{12}^T (V_{12} + V_{21}) \right\} + \\
&\quad + c_{\varepsilon 2} f_1 \frac{\varepsilon}{3 \bar{e}^T} (w_1 g_1 + w_2 g_2) + \\
&\quad + c_{\varepsilon 3} \varphi(R) \left\{ k f_1 \left( \frac{2}{10} w_1 g_1 - \frac{1}{10} w_2 g_2 \right) + \gamma \omega \left( e_1^T - \frac{1}{3} e^T \right) \right\} w_1 A_1 + \\
&\quad + c_{\varepsilon 3} \varphi(R) \left\{ k f_1 \left( \frac{2}{10} w_2 g_2 - \frac{1}{10} w_1 g_1 \right) + \gamma \omega \left( e_2^T - \frac{1}{3} e^T \right) \right\} w_2 A_2 + \\
&\quad + c_{\varepsilon 3} \varphi(R) \left\{ \frac{3}{20} k f_1 (w_1 - w_2) (g_2 - g_1) + \gamma \omega e_{12}^T \right\} (w_1 A_2 + w_2 A_1);
\end{aligned}$$

where  $\bar{u}(u_1, u_2)$  - velocity vector;  $\rho$  - average density of medium;  $\rho_i$  - density of the  $i$ -th component of medium;  $e_i$  - specific internal energy of the  $i$ -th component

of medium:  $P$  - average pressure of medium;  $P_i$  - pressure of the  $i$ -th component of medium;  $\beta_i$  - volume concentration of the  $i$ -th component ( $\beta_i = V_i/V$ );  $\alpha_i$  - mass concentration of the  $i$ -th component ( $\alpha_i = M_i/M$ );  $\varepsilon$  - viscous dissipation rate for turbulent energy;  $e_{ij}^T$  - components of velocity component fluctuation tensor;  $V_{ij}$  - components of deformation rate tensor;  $\bar{w}(w_1, w_2)$  - velocity vector for turbulent mass flow;  $R$  - relative mean square for density fluctuations;  $\bar{\varepsilon}$  - rate of viscous dissipation of turbulence energy,  $\omega = \varepsilon/e^T$ ;  $\Phi = \langle u'_j u'_j \rangle + \frac{1}{\rho} \langle \rho' u'_j u'_j \rangle$  - total turbulence energy.

$$e_{ii}^T \equiv e_i^T = \frac{1}{2} \langle u'_i u'_i \rangle, \quad i = 1, 2, 3; \quad e^T = \sum_i e_i^T; \quad e_{12}^T = \frac{1}{2} \langle u'_1 u'_2 \rangle;$$

$$w_i = \frac{1}{\rho} \langle \rho' u'_i \rangle, \quad i = 1, 2; \quad R = \frac{1}{\rho^2} \langle \rho'^2 \rangle; \quad \bar{\varepsilon} = \frac{1}{\rho} \nabla P;$$

$$\varphi(R) = \frac{1+R}{R}; \quad \omega = \frac{\varepsilon}{e^T}.$$

Superscripts 1, 2 denote longitudinal and radial components, respectively.

Transport terms  $\Pi$ , being divergences of third order tensors, have quite a bulky form. Therefore, in the original version of the numerical method we use a diffusion approximation for them in the following form:

$$\begin{aligned} \Pi_{ik} &= \text{div} \left( D_T^e \nabla e_{ik}^T - \bar{w} e_{ik}^T \right), & \Pi^\Phi &= \text{div} \left( D_T^\Phi \nabla \Phi - \bar{w} \Phi \right), \\ \Pi_1^w &= \frac{1}{\rho} \text{div} \rho \left( D_T^w \nabla w_1 - \bar{w} w_1 \right), & \Pi_2^w &= \frac{1}{\rho} \text{div} \rho \left( D_T^w \nabla w_2 - \bar{w} w_2 \right), \\ \Pi^R &= \frac{1}{\rho^2} \text{div} \rho^2 \left( D_T^R \nabla R - \bar{w} R \right), & \Pi^\varepsilon &= \text{div} \left( D_T^\varepsilon \nabla \varepsilon - \bar{w} \varepsilon \right). \end{aligned}$$

### 3. EXPRESSIONS FOR COEFFICIENTS

$$k_i = \frac{e^T}{3e_i^T}, \quad k_R = 1.5, \quad k = 3\sqrt{3} \frac{\sqrt{e_1^T e_2^T e_3^T}}{(e^T)^3},$$

$$k_w = \frac{e^T}{6\bar{\varepsilon}^T} + \frac{1}{10} c_{e^T} k f_1 \frac{\bar{w} \cdot \nabla P}{\bar{\varepsilon}^T} \frac{e^T}{\varepsilon} \frac{1}{\rho} \frac{\gamma}{2} + \frac{k_R}{2},$$

where  $|\bar{w}| = \sqrt{w_1^2 + w_2^2}$ ,

$$f_i = \frac{1}{1+R - \frac{D_T}{|\mathbf{w}} \frac{dR}{dl}}, \quad \frac{dR}{dl} = \frac{dR}{dx} \frac{w_1}{|\mathbf{w}} - \frac{dR}{dy} \frac{w_2}{|\mathbf{w}}$$

$$\tilde{\mathbf{e}}^T = e_1^T \cos^2 \varphi + 2e_{12}^T \cos \varphi \sin \varphi + e_2^T \sin^2 \varphi, \quad \cos \varphi = \frac{w_1}{|\mathbf{w}|}, \quad \sin \varphi = \frac{w_2}{|\mathbf{w}|}.$$

$\tilde{\mathbf{e}}^T$  is a component of the tensor  $e_{jk}$  in a local coordinate system where one of the axes coincides with the direction of the turbulent mass flow.

$$\gamma = 1 - \frac{\varphi_2}{2} - \frac{\varphi_3}{2} + \sqrt{\left(\frac{\gamma_1 - 1}{2}\right)^2 + \frac{\varphi_2^2}{4}} + \sqrt{\left(\frac{\gamma_1 - 1}{2}\right)^2 + \frac{\varphi_3^2}{4}},$$

$$\varphi_2 = \gamma_2 \frac{w_1 A_1 + w_2 A_2}{R \omega},$$

$$\varphi_3 = -\gamma_3 \frac{e_1^T V_{11} + e_2^T V_{22} + e_3^T V_{33} + e_{12}^T (V_{12} + V_{21})}{\varepsilon},$$

$$\bar{A} = \bar{A}_S + (\bar{A}_T - \bar{A}_S) [1 - y(\varphi)],$$

$$\bar{A}_S = \frac{1}{\rho} \frac{\partial \rho}{\partial P} \Big|_S \nabla P - \frac{\nabla \rho}{\rho}, \quad \bar{A}_T = \frac{1}{\rho} \frac{\partial \rho}{\partial P} \Big|_T \nabla P + \frac{1}{\rho} \frac{\partial \rho}{\partial T} \Big|_P \nabla T - \frac{\nabla \rho}{\rho},$$

where  $y(\varphi) = \frac{1}{\varphi} (1 - e^{-\varphi})$ ,  $\varphi = \frac{\chi}{\rho c_p l_t \sqrt{2e^T}}$ ,  $\chi$  - heat conductivity,

$l_t \approx \frac{\sqrt{2e^T}}{\omega}$  - scale of turbulence;

$$D_T^{(e_1^T)} = D_T^{(e_2^T)} = D_T^{(e_3^T)} = D_T^{(e_{12}^T)} = D_T^\Phi = 3D_T,$$

$$D_T^w = 2D_T, \quad D_T^R = D_T, \quad D_T^\varepsilon = \frac{5}{3}D_T,$$

$$D_T = 2c_{D_T} \frac{\tilde{\mathbf{e}}^T \mathbf{e}^T}{k_\gamma \varepsilon} \frac{1}{1+b},$$

$$b = \frac{1}{4} \frac{k_R}{k_\gamma} (\psi + |\psi|), \quad \psi = \frac{2(w_1 A_1 + w_2 A_2) e^T}{k_R \varepsilon R} - 1,$$

$$k_\gamma = \frac{3}{2} + \frac{e^T}{6e_1^T} + \frac{\gamma}{2}.$$

$V_{11}, V_{22}, V_{33}$  - components of deformation rate tensor,

$$V_{11} = \frac{\partial(u_1 - w_1)}{\partial x}, \quad V_{22} = \frac{\partial(u_2 - w_2)}{\partial r}, \quad V_{33} = \frac{(u_2 - w_2)}{r},$$

$$V_{12} = \frac{1}{2} \left( \frac{\partial(u_1 - w_1)}{\partial r} - \frac{\partial(u_2 - w_2)}{\partial x} \right)$$

Results of computations with the EGAK-B technique based on the above-discussed model are presented for known problems on studying turbulent mixing in 1D and 2D flows. The following problems are considered: turbulent mixing at gravitational and shear instabilities, Meshkov experiments in cylindrical geometry and shock tubes. The computed data is compared with experimental data and results of computations with other techniques. The agreement is good.

#### REFERENCES

1. Yanilkin Yu.V., Shanin A.A., Kovalev N.P. et al. VANT, Ser.MMFP, No.4, 1993.
2. Andronov V.A., Bakhrakh S.M., Meshkov E.E., Mokhov V.N., Nikiforov V.V., Pevnitsky A.V., Tolshmyakov A.I. ZhETF, v.71, No.2(8), p.806-811, 1976.



# " Numerical modeling of experiments with fuel pellets at pulse reactor "

Kandiev Ya. Z. Kozybayev R.M

Russian Federal Nuclear Center - All-Russia Scientific-Technical Institute of Technical Physics (RFNC-VNIITF), Snezhinsk, Russia, 456770

To solve the problems connected with numerical modeling of experiments, carried out at pulse reactors, the updating of the PRIZMA base code - the code PRIZMA-D has been developed at VNIITF.

Peculiarity of this code is the special source - fission points distributed by eigenfunction within reactor core.

To diminish restrictions on application of nonanalog modeling, the process of deriving a source and the process of modeling trajectories to obtain necessary results are separated

This organization of calculation cycle allows to increase efficiency of calculations essentially.

Besides, the special method of modeling particles trajectories which is realized in the PRIZMA complex allows to obtain correlated results of several versions of a problem in one calculation.

To illustrate the capabilities of the code, the problems of numerical modeling of experiments with fuel tablets at pulse reactor are considered.

## 1. Introduction

At present Monte-Carlo the calculations of linear problems of radiation transport in various compositions and units of facilities are carried out at VNIITF using PRIZMA code[1] Broad capabilities for describing geometry, sources, structure of materials, for ordering the results are incorporated in the code. The possibility is provided to carry out calculations of particles cascade transport including (neutrons, photons, electrons, positrons and ions) with allowance made for their transmutation. To solve the problems in which it is necessary to calculate functionals connected with small probabilities (e.g. problems of radiation shielding, problems of detection, etc.), importance biasing scheme has been developed which permits to adapt modeling algorithms to a specific problem while developing this method due account was given to the fact that in the code the evaluation "on visits" is applied, i.e. the required result is rerecorded only if particle intersects the area of integration detector.

If using this method in addition to required functionals one evaluates the number of particles visiting the area of integration for the first time it is possible to obtain an estimate of a prize  $k_p$  in comparison with the analog method of modeling

$$k_p = \frac{t_1}{I_n \sigma_n t_n}$$

where  $t_1$  - is such time of one history using analog method,

$I_n$ ,  $\sigma_n$ ,  $t_n$  - are average number of particles visiting the area of integration for the first time, relative error of this result and total run time, respectively, for nonanalog method of modeling

All this enables to model numerically experiment and ensures necessary accuracy of the results with much lower expenses than those spent on organization and conduct of experiment. Similar calculations allow to predict behaviour of radiation in an experiment, compare results of calculation and experiment, update parameters of the experiment.

At the same time there are classes of problems, in which either source, or results have such specific features, that they cannot be solved by the PRIZMA code. Therefore, there is a necessity of creating specialized codes with the same main capabilities as PRIZMA code. PRIZMA.D code is one of them. It is intended for solving problem connected with estimation of nuclear reactors and critical assemblies.

Experimental Physics Division of VNIITF calculated experiments on melting tablets of reactor fuel in a retort placed along the axis of channel of pulse reactor IGRUK [2].

The report describes briefing capabilities of PRIZMA.D code and calculations results obtained during planning these experiments.

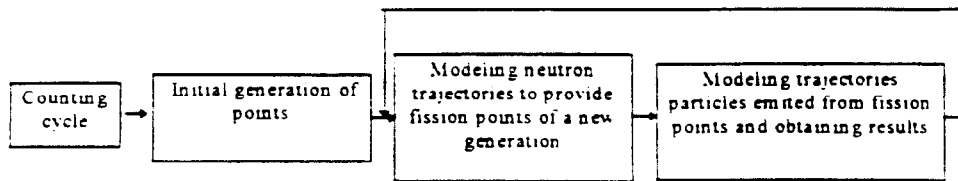
## 2. PRIZMA.D code.

Peculiarity of the code is in special source - fission points distributed by eigenfunction within reactor core. Depending on conditions of a problem, fission points can emit:

- a) neutrons and photons of fission spectrum
- b) only neutrons of fission spectrum.

To diminish restrictions on application of nonanalog modeling, the process of deriving a source and the process of modeling trajectories for obtaining required results are separated.

Calculation cycle is schematically as follows:



This organization of calculation cycle allows to apply nonanalog method of modeling in the second part of this cycle without restrictions.

In PRIZMA complex special method of modeling trajectories (based on marking of a particle) is implemented which permits to obtain correlated results of several versions of a problem differing a little in some local area of a system. There are three types of such problems.

1. Version with varying composition. Versions differ in composition of substance filling some volume  $V$ .
2. Versions with increasing volume  $V$ . Volume varies according to the rule  

$$V(1) = V_1, V(2) = V_1 - V_2, \dots, V(k) = V_1 + V_2 + \dots + V_k$$
3. Versions with moving volume. Versions differ in the fact that volumes  $V(i)$ ,  $i = 1, k$  are located in different places of a system.

The essence of the special method of modeling consists in the following: certain type of mark corresponds to each version of a problem (a source particle is marked by all types of marking), when particle enters perturbed volume, it splits into two particles, and one continues random walk in geometry corresponding to the version with perturbed volume with a mark corresponding to this version, another one does the same in geometry corresponding to the version with undisturbed volume with an appropriate mark. In one calculation the combination of various cases is allowed. Plots of particles trajectories prior to the entry into of perturbation area are the same for each case. Therefore, appropriate calculation results for the versions are correlated positively to some extent. Besides, total time of calculation for versions is saved.

Special method of modeling is used in PRIZMA.D code in assumption of small

perturbations. In this case, distribution of fission points of the source is the same for all versions of the problem and corresponds to distribution of the version without perturbed volume.

### 3. Problem description and results of calculations

The calculations were performed using PRIZMA.D code with BAS constants [3]. The results of calculations are normalized to one fission in the core of the reactor. In all the tables standard deviations are given in percentage.

Geometry of the experiment is shown in Fig. 1, 2. A fuel tablet of  $UO_2$  (diameter and length of the tablet are 0.58 and 1.5 cm, respectively, the density of uranium oxide is 10.5 g/cm<sup>3</sup>) is located in a protective retort, which is placed in a centerline of the reactor channel, centre of the retort having the coordinate  $z = 37.5$  cm (Fig. 1). To increase the fraction of thermal neutrons, the converter of polyethylene is used contiguous to the lateral surface of reactor working zone. Channel is closed by a carbon fuse from outside. It is required to calculate energy yield in the fuel tablet.

The following conditions of the problem were considered:

1. Determination of optimum thickness of the converter; five variants of converter thickness were considered: 2, 3, 4, 5 and 6 cm (case with increasing volume).
2. Evaluation of influence of protective retort material on energy in a fuel tablet, four variants (the case with moving volume) were considered:
  - a. fuel tablet without retort,
  - b. tablet with an iron retort ( $\rho = 7.8$  g/cm<sup>3</sup>),
  - c. tablet with a titanium retort ( $\rho = 4.5$  g/cm<sup>3</sup>),
  - d. tablet with a carbon retort ( $\rho = 1.7$  g/cm<sup>3</sup>).
3. Evaluation of influence of  $^{235}U$  concentration on radial distribution of energy release in a fuel tablet. Four variations (case with varying composition) were considered:

a.  $U_{0.05}^{235}U_{0.95}^{238}O_2$ ,

b.  $U_{0.1}^{235}U_{0.9}^{238}O_2$ ,

c.  $U_{0.36}^{235}U_{0.64}^{238}O_2$ ,

d.  $U_{0.95}^{235}U_{0.05}^{238}O_2$ .

Using special method of modeling allowed to obtain the results for 80 versions of the problem in one calculation.

Table 1 gives energy yield averaged over the mass of fuel tablet.

Fig. 4 shows the results for various thicknesses of the converter and for various materials of the protective retort.

In Table 2 and in Fig. 5 radial distributions of energy in fuel tablet for various  $^{235}U$  concentrations are given (tablet is without a protective retort, thickness of polyethylene is 5 cm).

To evaluate the efficiency of main calculation, comparative calculation was performed of a variant for converter with a moderator 4 cm thick, with an iron protective retort and with the structure of retort (3.b). The time spent to obtain energy release value of  $7.01e-3$  with  $\sigma = 4.3\%$  was one-third of the total run time spent on all 80 versions of the main problem. Relative efficiency was  $K_v = 17.3$ . The average number of neutrons hitting in the fuel tablet is  $6.54e-4$ . Inference is that run time of all 80 versions using the analog method with appropriate errors would be approximately 400-fold.

Here the fact is not taken into account that in one calculation positively correlated results of all versions of the problem were obtained.

To improve dependence of radial distribution, the calculation with six various (2.5 %, 5 %, 10 %, 15 %, 36 %, 90 %) concentrations of  $^{235}\text{U}$  was carried out. Results are given in Tab. 3 and in Fig. 5.

Analysis of the results obtained showed that radial distribution of energy in a tablet depends practically on concentration of  $^{235}\text{U}$  in it.

To evaluate gradient of density of neutron field along the axis of the reactor channel, calculation was carried out for six variants of fuel tablet location ( $z = 11.75, 15.75, 19.75, 23.75, 27.75, 31.75$  cm). This calculation corresponds to the case with moving volume. The results are given in Table 4 and in Fig. 6.

#### 4. References

1. M.A. Arnautova, Ya.Z. Kandiev, B.E. Lukhminsky and G.N. Malyshkin, " Monte Carlo Simulation In Nuclear Geophysics. Intercomparison of the PRIZMA Monte Carlo Code and Benchmark Experiments ", Nucl. Geophys. Vol.7., pp.407-418, 1993
2. A.P. Vasilyev, N.V. Gorin, R.M. Kozybayev et al., " Experimental capabilities of IGRUK reactor in research on safety of nuclear reactors ", International Topical Meeting, Obninsk, Russia, October 3-7, 1994 (in Russian).
3. A.P. Vasilyev, Ya.Z. Kandiev, V.I. Chitaikin. Neutron physics, V.2, pp. 119-123, M., 1984 (in Russian).

Table 1. Energy release in the fuel tablet (MeV/g)

Concentration of $^{235}\text{U}$	$\Delta\text{CH}_2$ (cm)	Tablet without shell	Shell from Fe	Shell from Ti	Shell from C
5%	2.0	5.95e-3 5.4%	5.24e-3 6.3%	5.21e-3 6.1%	4.54e-3 5.3%
	3.0	4.85e-3 5.2%	3.95e-3 5.9%	3.64e-3 5.0%	5.03e-3 5.0%
	4.0	5.72e-3 5.4%	4.65e-3 5.6%	5.92e-3 5.8	5.04e-3 5.2%
	5.0	5.08e-3 5.6%	4.29e-3 6.6%	4.01e-3 6.3%	5.05e-3 6.0
	6.0	4.65e-3 6.3%	3.21e-3 7.3%	3.37e-3 6.9%	4.81e-3 6.0%
	2.0	7.00e-3 4.0%	5.64e-3 4.4%	5.21e-3 4.6%	7.22e-3 4.1%
10%	3.0	8.23e-3 4.0%	6.40e-3 4.2%	6.30e-3 4.3%	8.18e-3 4.0%
	4.0	9.13e-3 4.2%	6.97e-3 4.6%	6.44e-3 4.4%	8.95e-3 4.2%
	5.0	9.01e-3 4.8%	6.90e-3 5.3%	6.51e-3 5.0%	8.95e-3 5.0%
	6.0	7.30e-3 5.1%	5.36e-3 5.8%	5.37e-3 5.0%	7.57e-3 5.2%
	2.0	1.28e-2 4.6%	1.01e-2 5.0%	9.72e-3 5.2%	1.34e-2 4.5%
	3.0	1.49e-2 4.5%	1.17e-2 4.8%	1.10e-2 4.7%	1.60e-2 4.2%
36%	4.0	1.69e-2 4.6%	1.33e-2 4.0%	1.21e-2 4.0%	1.69e-2 4.7%
	5.0	1.05e-2 5.0%	1.31e-2 5.8%	1.24e-2 5.6%	1.55e-2 4.7%
	6.0	1.45e-2 5.6%	9.81e-3 6.4%	1.02e-2 6.0%	1.44e-2 5.6%
	2.0	1.58e-2 4.3%	1.28e-2 4.6%	1.20e-2 4.8%	1.62e-2 4.2%
	3.0	1.80e-2 4.3%	1.41e-2 4.6%	1.41e-2 4.5%	1.85e-2 4.1%
	4.0	2.00e-2 4.5%	1.58e-2 4.7%	1.45e-2 4.8%	2.02e-2 4.5%
95%	5.0	1.94e-2 4.8%	1.55e-2 5.5%	1.48e-2 5.3%	1.84e-2 5.1%
	6.0	1.00e-2 5.4%	1.10e-2 6.2%	1.15e-2 5.8%	1.64e-2 5.4%

Table 2. Distribution of energy release (MeV/g) in the layers  $\Delta R$  of the fuel tablet (tablet without retort)

Concentration of $^{235}\text{U}$	$\Delta\text{CH}_2$ (cm)	$R_1\text{--}R_2$ (0.0--0.10cm)	$R_2\text{--}R_3$ (0.10--0.15cm)	$R_3\text{--}R_4$ (0.15--0.20cm)	$R_4\text{--}R_5$ (0.20--0.23cm)	$R_5\text{--}R_6$ (0.23--0.26cm)	$R_6\text{--}R_7$ (0.26--0.29cm)
5%	5.0	$5.02\text{e-}3$ 13%	$4.72\text{e-}3$ 11%	$4.59\text{e-}3$ 10%	$5.81\text{e-}3$ 9.6%	$4.98\text{e-}3$ 3.6%	$5.45\text{e-}3$ 7.8%
10%	5.0	$8.37\text{e-}3$ 7.3%	$8.14\text{e-}3$ 6.6%	$8.61\text{e-}3$ 6.1%	$9.03\text{e-}3$ 6.3%	$1.01\text{e-}2$ 6.1%	$9.53\text{e-}3$ 5.5%
36%	5.0	$1.16\text{e-}2$ 11%	$1.13\text{e-}2$ 9.4%	$1.25\text{e-}2$ 7.7%	$1.60\text{e-}2$ 7.5%	$2.01\text{e-}2$ 7.0%	$2.43\text{e-}2$ 6.5%
95%	5.0	$6.09\text{e-}3$ 14%	$8.07\text{e-}3$ 11%	$1.00\text{e-}2$ 8.8%	$1.58\text{e-}2$ 7.6%	$2.49\text{e-}2$ 6.7%	$4.41\text{e-}2$ 5.6%

Table 3. Distribution of energy release (MeV/g) in layers  $\Delta R$  of the fuel tablet (tablet without retort)  $\Delta\text{CH}_2=4.5\text{cm}$

Concentration of $^{235}\text{U}$	$\Delta\text{CH}_2$ (cm)	$R_1\text{--}R_2$ (0.0--0.10cm)	$R_2\text{--}R_3$ (0.10--0.15cm)	$R_3\text{--}R_4$ (0.15--0.20cm)	$R_4\text{--}R_5$ (0.20--0.23cm)	$R_5\text{--}R_6$ (0.23--0.26cm)	$R_6\text{--}R_7$ (0.26--0.29cm)
2.5%	4.5	$2.72\text{e-}3$ 4.3%	$2.81\text{e-}3$ 3.8%	$2.72\text{e-}3$ 3.3%	$2.93\text{e-}3$ 3.5%	$2.80\text{e-}3$ 3.2%	$2.93\text{e-}3$ 3.0%
5%	4.5	$4.58\text{e-}3$ 4.8%	$4.78\text{e-}3$ 4.3%	$4.82\text{e-}3$ 3.7%	$4.70\text{e-}3$ 3.9%	$5.42\text{e-}3$ 3.4%	$5.47\text{e-}3$ 3.2%
10%	4.5	$7.23\text{e-}3$ 4.5%	$7.40\text{e-}3$ 4.1%	$7.97\text{e-}3$ 3.5%	$8.59\text{e-}3$ 3.7%	$8.69\text{e-}3$ 3.5%	$9.49\text{e-}3$ 3.1%
15%	4.5	$9.09\text{e-}3$ 4.1%	$9.93\text{e-}3$ 3.7%	$9.64\text{e-}3$ 3.4%	$1.11\text{e-}2$ 3.6%	$1.17\text{e-}2$ 3.2%	$1.30\text{e-}2$ 3.0%
36%	4.5	$9.70\text{e-}3$ 4.2%	$1.08\text{e-}2$ 3.8%	$1.27\text{e-}2$ 3.2%	$1.60\text{e-}2$ 3.3%	$1.89\text{e-}2$ 3.0%	$2.39\text{e-}2$ 2.7%
90%	4.5	$5.13\text{e-}3$ 5.0%	$6.73\text{e-}3$ 4.3%	$9.89\text{e-}3$ 3.5%	$1.58\text{e-}2$ 3.2%	$2.36\text{e-}2$ 2.0%	$4.29\text{e-}2$ 2.4%

Table 4. The energy release (MeV/g) in the fuel tablet moving along of channel axis

Concentration of $^{235}\text{U}$	$\Delta\text{CH}_2$ (cm)	Center coordinate of the fuel tablet (cm)					
		11.75	15.75	19.75	23.75	27.75	31.75
10%	4.5	$6.50\text{e-}3$ 3.7%	$6.77\text{e-}3$ 3.3%	$7.28\text{e-}3$ 3.0%	$7.92\text{e-}3$ 2.0%	$8.34\text{e-}3$ 2.8%	$8.62\text{e-}3$ 2.9%

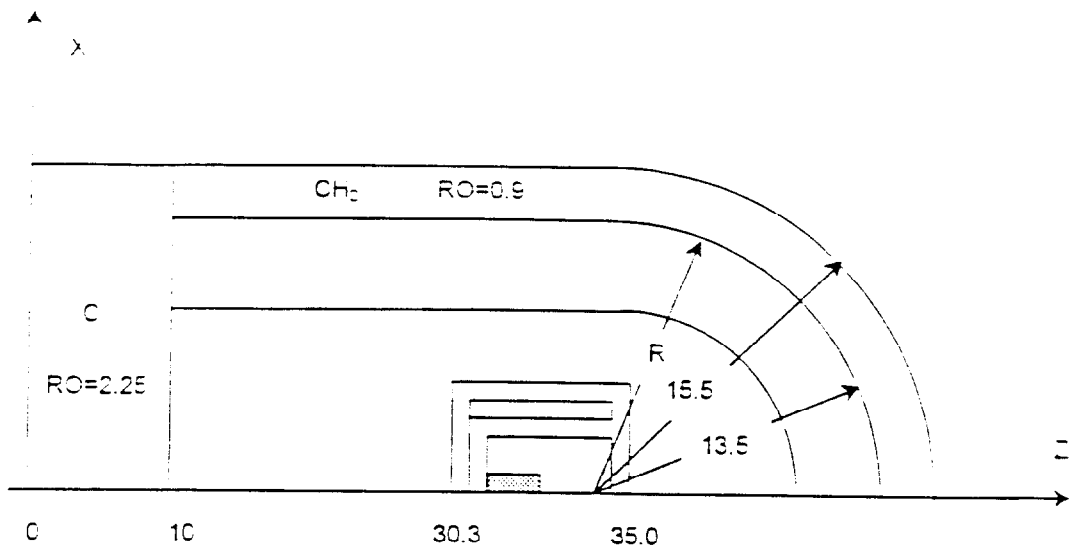


Fig. 1 Experimental setup.

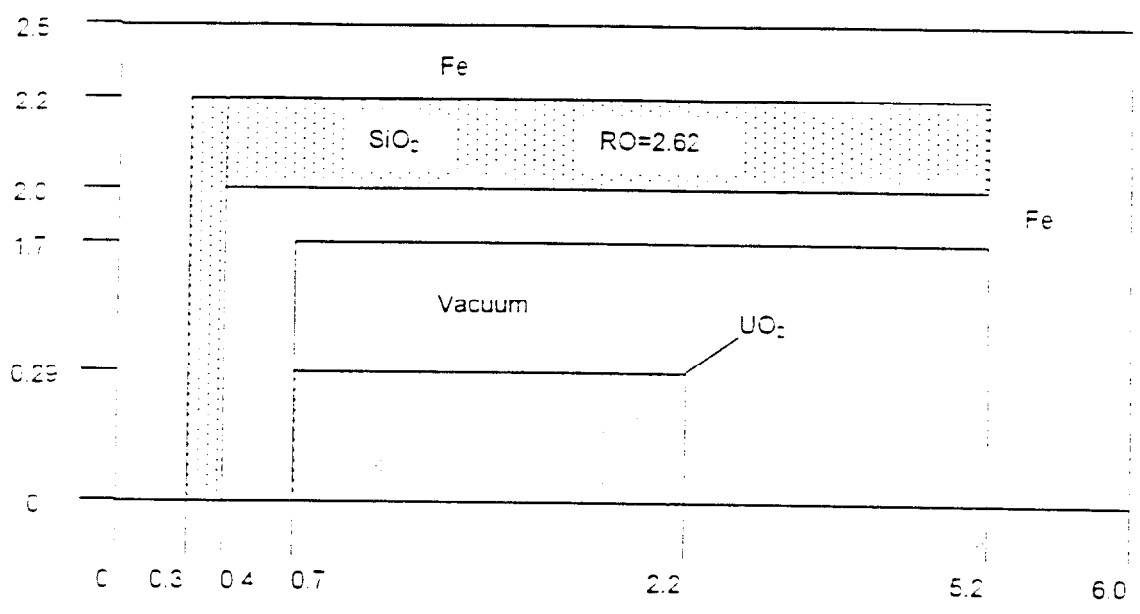


Fig. 2 Retort geometry

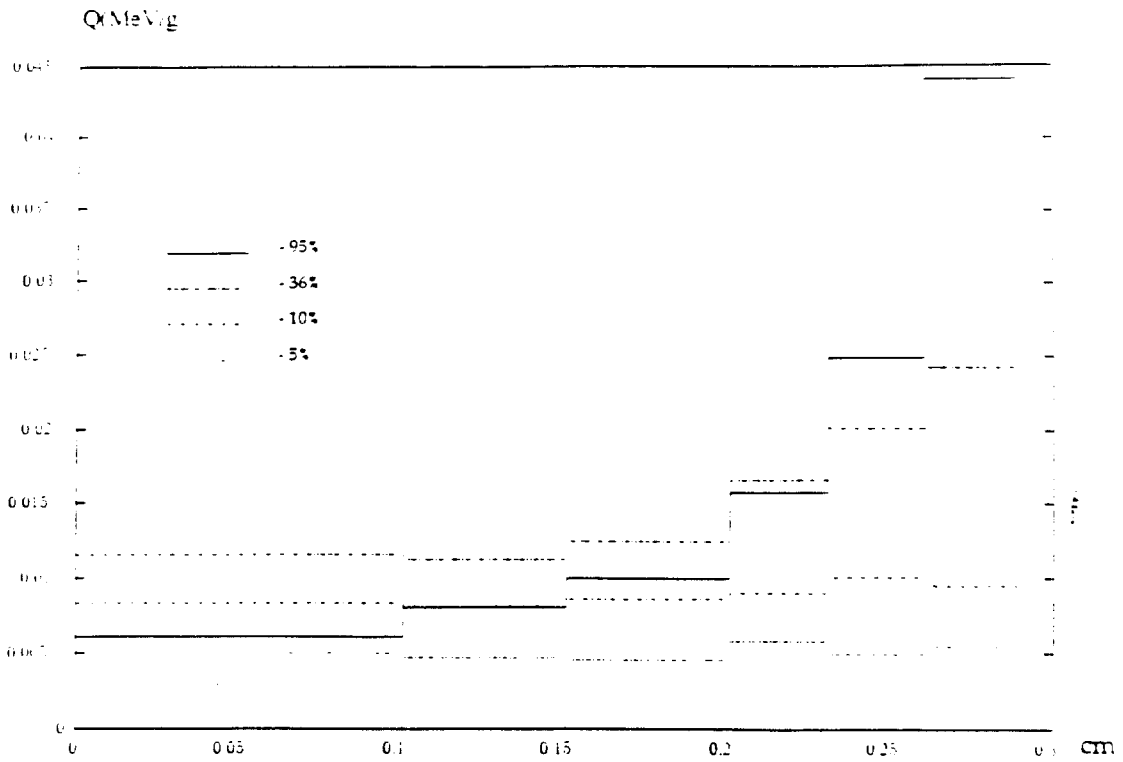


Fig 3. Distribution of energy release in the layers  $\Delta R$  of fuel tablet (tablet without retort)  $\Delta CH_2=5.0\text{cm}$

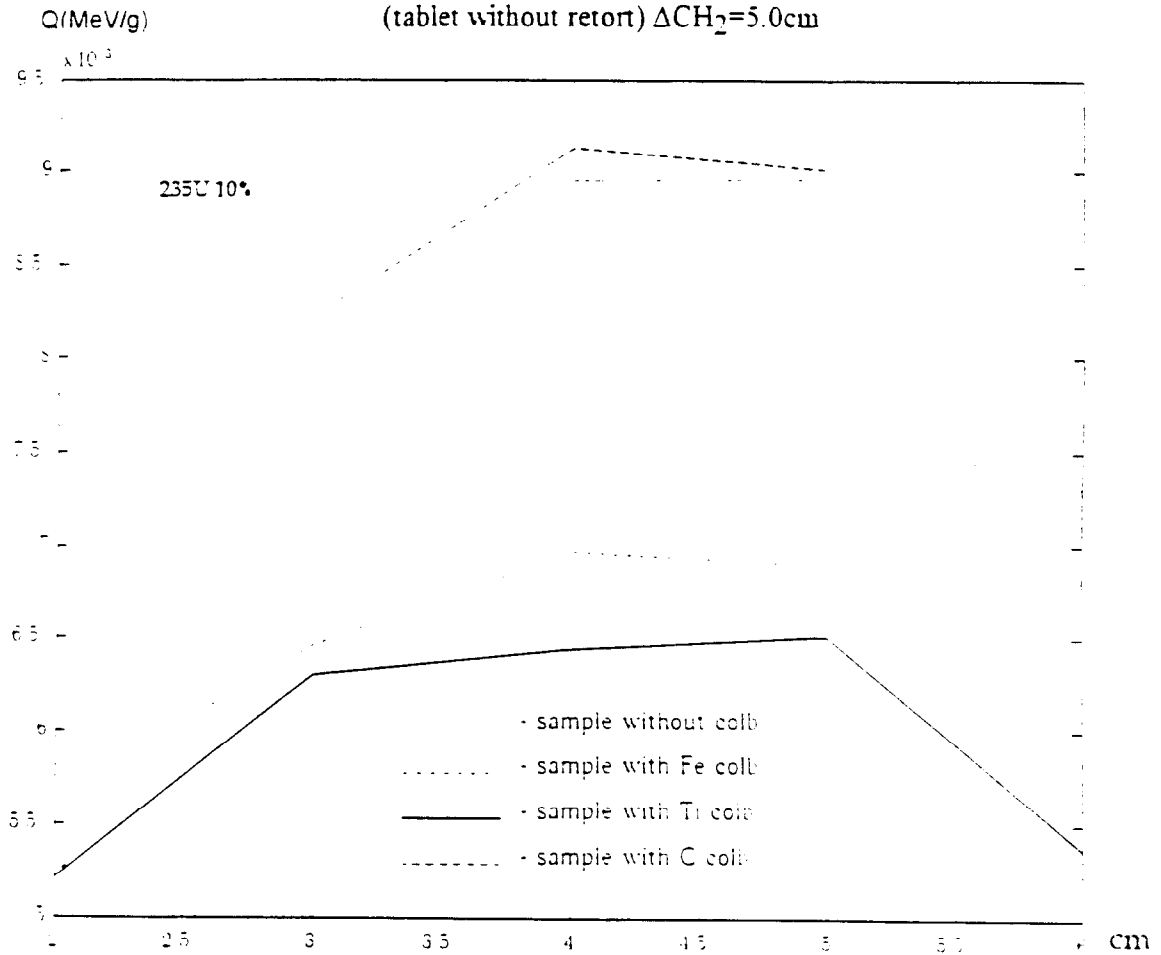


Fig 4. Distribution of energy release in the fuel tablet for various thickness of polyethylene

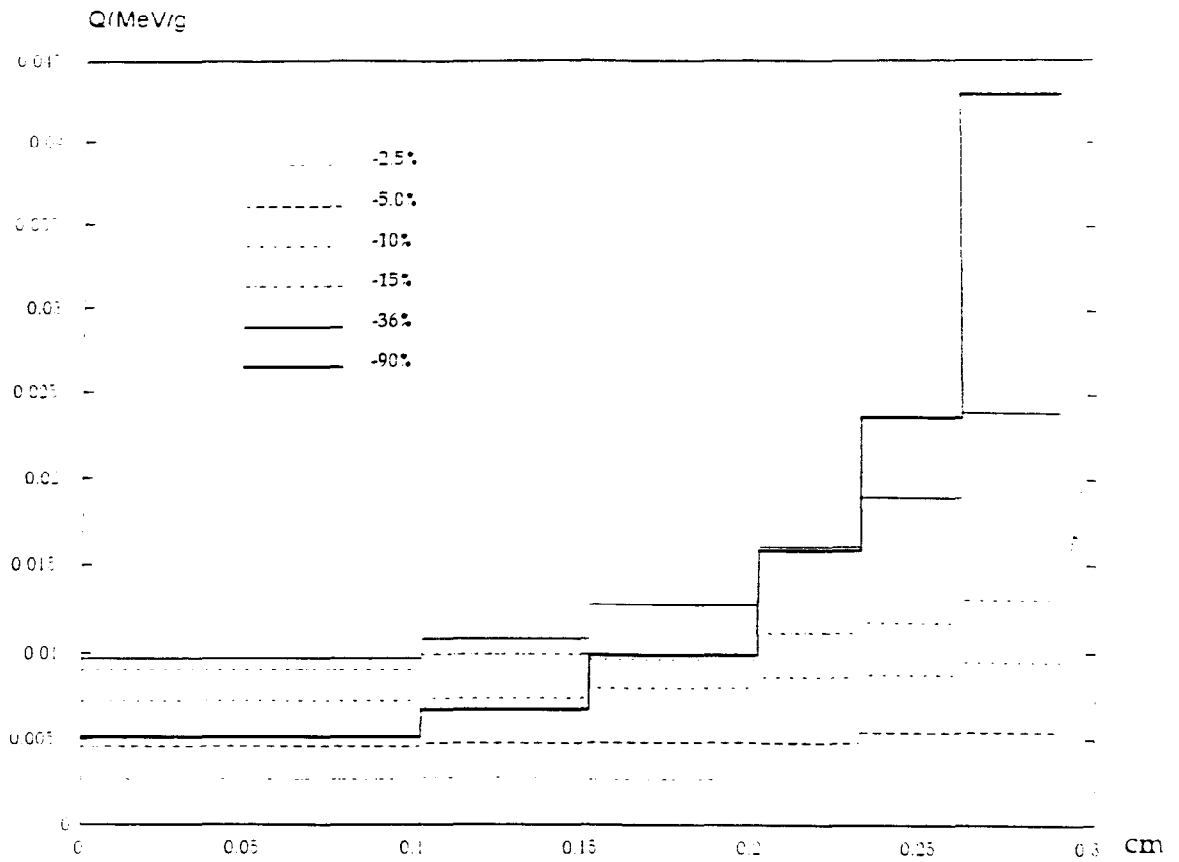


Fig 5. Distribution of energy release in layers  $\Delta R$  of fuel tablet (tablet without retort)  $\Delta CH_2 = 4.5$  cm

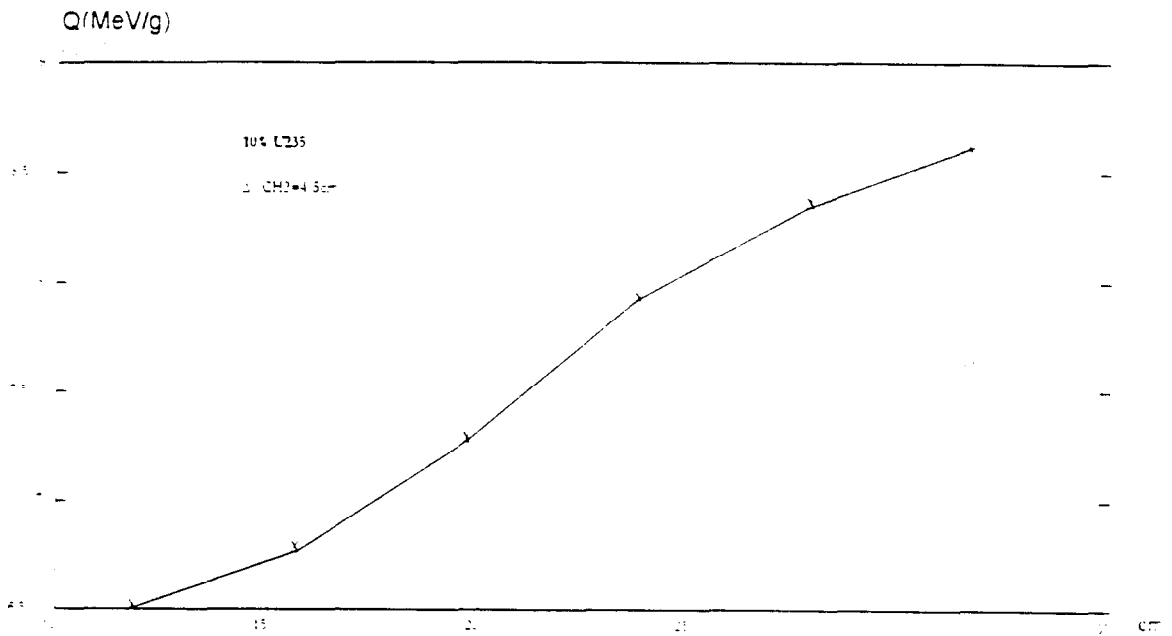


Fig 6. The energy release in the fuel tablet moving along of channel axis



# NUMERICAL SIMULATION OF NEAR AND FAR AREAS OF ACCIDENTAL RELEASES AND EXPLOSIONS

Yanilkin Yu.V., Sofronov V.N., Tarasov V.I., Statsenko V.P.,  
Piskunov V.N., Kovalev N.P., Dibirov O.A., Stadnik A.L., Toropova T.A.,  
Ivanova G.G., Shanin A.A.  
RFNC-VNIIEF, 607190, Sarov (Arzamas-16), Russia

## ABSTRACT

The presentation describes the 3D program package designed for numerical simulation of dynamics of accidental explosions and releases and their consequences in the global scale. The package is implemented within the program system TREK [1].

## INTRODUCTION

Simulation of a full-scale problem relating to accidental releases is a complex problem due to both a large number of physical processes to be taken into account and different scales of flows at various process phases. The package includes two phases of the process under consideration: explosion cloud rising up to the stabilization height and aerosol transport in the atmosphere over the orphographically and thermally inhomogeneous underlying surface.

The simulation is based on simultaneous solution of the following physical processes:

### **at the first stage:**

- gas-dynamical flow of polydisperse medium;
- turbulent mixing;
- change in aerosol particle disperse composition due to coagulation;

### **at the second stage:**

- atmosphere hydrothermodynamics;
- particle transport and turbulent diffusion.

Quite a great number of methods have been recently developed for simulation of the polydisperse media flows under discussion. However, irrespective of the plenty of various methods, in the literature there is practically no papers discussing methods suitable for simulation of full-scale problems, that is the accidental release dynamics from the process beginning to the end.

Within the system TREK an attempt was made to integrate the programs designed for numerical simulation of the flows discussed in full measure, that is for simulation of the accidental release dynamics from the process beginning to deposition onto the ground surface.

The package does not allow to simulate flows from the problem beginning to the end without computation interruption. Each process stage is also computed separately, however, using the programs within a single system considerably facilitates the transfer of the computed data for one stage for simulation of the second. This procedure can be automated in many respects. The principal service and computation package modules have been recently developed which allows to use the package for simulation of principal physical processes occurring at accidental releases and explosions.

Note that for the near area many problems are 2D in their formulation, and the authors earlier developed 2D programs within the EGAK program system [2.3] for simulation of such flows.

## 1. FIRST STAGE FLOW MODEL

The following basic assumptions are used for description of the polydisperse medium flows:

- the carrying phase is a gas-vapor mixture composed of several components with their equations of state;
- each carrying phase component is described completely with specific energy and volume concentrations;
- the medium molecular viscosity is taken into consideration only in the interphase exchange processes;
- the disperse phase is a polydisperse impurity composed of several coagulating components of the active fraction and several components of the composite fraction;
- the collisions of disperse phase particles with one another are not taken into account both for each separate fraction and for particles from different fractions;
- separate disperse phase fractions can exchange mass between themselves and carrying phase due to the processes of coagulation, condensation, fragmentation and aerodynamical entrainment;
- the disperse phase material is incompressible;
- the heat exchange between the carrying phase and particles is not taken into account;
- the turbulence is simulated within the  $k-\epsilon$  model.

## 2. SECOND STAGE FLOW MODEL

- The processes are studied in which the horizontal sizes are considerably larger than the vertical ( $X \sim Y \gg Z$ ). In this case the statics equation is used instead of the equation of motion for the vertical velocity component. If the condition ( $X \sim Y \gg Z$ ) is not met, the equations for three velocity vector components are solved;
- Meteorological fields will be set as sums of given background large-scale components and their deviations which are small. This allows to linearize the initial equations through rejection of small values;

- The atmosphere is formally segregated into two layers: near-ground and boundary layer located above the near-ground. The near-ground layer is taken into consideration parametrically, that is by setting effective boundary conditions on the upper near-ground layer boundary basing on known phenomenological relations;
- The space and time variations in density are assumed small, therefore the incompressibility condition is used;
- The turbulence is simulated both within the k- $\epsilon$  model and algebraic model of Reynolds stresses.

### 3. NUMERICAL RESULTS

Numerical solutions for a number of test problems are exemplified:

- Gaussian profile transport;
- Aerosol transport taking into account the turbulent diffusion;
- Aerosol transport taking into account the turbulent diffusion and sedimentation;
- Aerosol transport by height-variable wind;
- Ekman problem;
- Prandtl problem of slope wind.

The above examples demonstrate a sufficient efficiency and accuracy of the programs integrated in the package.

### REFERENCES

1. Gavrilova E.S., Dibirov O.A., Stadnik A.A., Tarasov V.I., Toropova T.A., Shanin A.A., Yanilkin Yu.V. Abstract of presentation for the 11-th All-Russian Conference "Theoretic fundamentals and construction of numerical algorithms for solving computational physics problems", Pushchino, October 5-9, 1996. 24, 1996.
2. Yanilkin Yu.V., Shanin A.A., Kovalev N.P., Gavrilova E.S., Gubkov E.V., Darova N.S., Dibirov O.A., Zharova G.V., Kalmanovich A.I., Pavlusha I.N., Samigulin M.S., Simonov G.P., Sin'kova O.G., Sotnikova M.G., Tarasov V.I., Toropova T.A. VANT. Ser.MMFP, No.4, 1993.
3. Yanilkin Yu.V., Dibirov O.A., Golubev A.I., Ismailova N.A., Piskunov V.N., Gavrilova E.S., Gubkov E.V., Darova N.S., Zharova G.V., Tarasov V.I., Shanin A.A. Abstract of presentation for the 11-th All-Russian Conference "Theoretic fundamentals and construction of numerical algorithms for solving computational physics problems", Pushchino, October 5-9, 1996.



Mention the principal features of taking into account some of the above processes in the program package /1/.

The X radiation transport and radiation-material interaction process is computed in the multi-group kinetic or multi-group diffusion approximation depending on the class of problems being solved.

For the 2D multi-group kinetic approximation the following system is solved

$$\frac{1}{c} \frac{\partial \varepsilon}{\partial t} + L\varepsilon_i + \chi_{\cdot i} \varepsilon_i = \frac{\chi_{\alpha}}{2\pi} \varepsilon_{ip} + \sum_{j=1}^{i-1} a_{ij} \chi_{\eta} \varepsilon_j^{(0)} + Q_i, \quad i = \overline{1, i_1} \quad (1)$$

$$L\varepsilon_i = \mu \frac{\partial \varepsilon}{\partial z} - \frac{1}{r} \frac{\partial}{\partial \alpha} \left( r \sqrt{1-\mu^2} \cos \varphi \varepsilon_i \right) - \frac{1}{r} \frac{\partial}{\partial \varphi} \left( \sqrt{1-\mu^2} \sin \varphi \varepsilon_i \right) \quad (2)$$

$$\frac{1}{\rho} \frac{\partial \mathcal{E}_i}{\partial \alpha} = \sum_{i=1}^{i_1} \chi_{\alpha} \varepsilon_i^{(0)} \Delta \omega_i - \sum_{i=1}^{i_1} \chi_{\alpha} \varepsilon_{ip} \Delta \omega_i - \sum_{i=1}^{i_1} \sum_{j=1}^{i_1} a_{ij} \chi_{\eta} \varepsilon_j^{(0)} \Delta \omega_i \quad (3)$$

$$\varepsilon_i = \varepsilon_i(r, z, \mu, \varphi, \omega_i, t),$$

$$E_i = E_i(\rho, T_e),$$

$$\chi_{\alpha} = \chi_{\alpha}(\rho, T_e, \omega_i),$$

$$\chi_{\eta} = \chi_{\eta}(\rho, T_e, \omega_i),$$

$$\chi_{\cdot i} = \chi_{\alpha i} + \chi_{\eta i},$$

$$\varepsilon_{ip} = \varepsilon_{ip}(T_e, \omega_i).$$

$$Q_i = Q_i(r, z, p, \mu, \varphi, t) - \text{an independent source.}$$

Computations of many thermonuclear fusion problems are known to require a very accurate account of X radiation transport processes using the kinetic approximation, and, on the other hand, computer simulation of X radiation transport processes in the multi-group kinetic approximation involves fairly high computer costs. Taking into account the above circumstances, at development of the package /1/ a particular attention was attached to designing effective numerical methods and algorithms for solving the multi-group kinetic equation.

Mention some features of the methods implemented here. The 2D transport equation is approximated on quadrangular spatial grids by a difference scheme with an extended template /3/. To solve the obtained essentially non-linear equation system, the KM-method of iteration convergence acceleration /4/ is used

As it is known, many of the computed thermonuclear fusion systems are characterized with a fairly small optical thickness which imposes especially high requirements for accuracy of the kinetic equation approximation by angular

**NUMERICAL SIMULATION OF THERMONUCLEAR FUSION  
NON-EQUILIBRIUM  
PROCESSES USING 2D SOFTWARE PACKAGES**

RFNC-VNIIEF  
607190, Nizhni Novgorod region, Sarov

Belyakov I.M., Belkov S.A., Vatulin V.V., Vakhlamova L.L.,  
Vinokurov O.A., Garanin S.G., Yermolovich V.F., Pleteneva N.P.,  
Remizov G.N., Rezhnikov V.Yu., Ryabikina N.A., Sofronov I.D.,  
Fedotova L.P., Shagaliev R.M.

In works on studying and solving thermonuclear fusion problems an important role is played by computer simulation of running processes. The computer simulation methods allow not only to study one or another physical scheme and approach to solving the problem, but also promote reduction in a large number of expensive experiments and, eventually, determination of promising lines for solution of the posed problem.

This presentation is devoted to discussion of principal capabilities for numerical simulation of material radiation and energy transfer processes in 2D thermonuclear fusion problems implemented in the framework of connection of two VNIIEF program packages, i.e. the multi-dimensional program package for computing particle transport processes taking into account particle-medium interaction /1/ and multi-dimensional program package for computing gas-dynamical processes /2/. The following is taken into account within the program package for computing particle transport processes:

1. Spectral X radiation transport and radiation-medium interaction
2. Energy transfer by electrons and ions taking into account medium non-equilibrium.
3. Energy transfer by heavy ions and absorption of this energy by medium in heavy-ion fusion problems.
4. Laser radiation energy transfer and absorption.
5. Ionization kinetics in the mean ion approximation.

variables. To secure such an accuracy, the following two approaches are used in the package /1/.

1. The numerical solution of the kinetic equation in optically transparent regions is implemented in two stages with separation of "primary" and "secondary" photons, where the primary photons are photons which have got into the system from volume and surface sources, respectively; accordingly, the secondary photons are photons generated in the system from radiation-medium interaction (scattering, absorption). In other words, solution of the original problem is represented as a combination of solutions of two individual problems set up for the primary photons and secondary photons, respectively.

Note that in the package /1/ the numerical solution of the equations corresponding to the primary and secondary photons uses essentially different angular grids differing both in selection of the quadrature formulas and in the number of the photon flight directions used. As the computation experience shows, such an approach secures the possibility to conduct detailed computations with simultaneous considerable increase in the computation accuracy.

The presentation provides a more detailed discussion of this approach. Examples of numerical computations are given.

2. The weight factors in the additional relations used at the difference approximation of the equations of transport by angular variables are selected taking into consideration the curvilinear geometry.

Two methods are therewith implemented in the program, one of which is based on the known paper by Reed W.H. and Lathrop K.D. /5/. As the presentation demonstrates, using such methods also considerably increases accuracy of the numerical solution obtained.

For the 2D multi-group diffusion approximation the following equation system is solved:

$$\frac{1}{c} \frac{\partial u_i}{\partial t} - \text{div} D_i \text{grad} u_i + \chi_i u_i = \chi_i u_{i,p} - \sum_{j=i}^i a_{ij} \chi_j u_j, \quad i = \overline{1, I}$$

$$\rho \frac{\partial E}{\partial t} = \sum_{i=1}^n \chi_i u_i \Delta \omega_i - \sum_{i=1}^n \chi_{a,i} u_{i,p} \Delta \omega_i - \sum_{i=1}^n \sum_{j=1}^n a_{ij} \chi_j u_j \Delta \omega_i$$

$$\begin{aligned}
u_i &= u_i(r, z, \omega, t), \\
E_e &= E_e(\rho, T_e), \\
u_{ip} &= u_{ip}(T_e, \omega_i), \\
D_i &= D_i(\rho, T_e, \omega_i), \\
\chi_\alpha &= \chi_\alpha(\rho, T_e, \omega_i), \\
\chi_n &= \chi_n(\rho, T_e, \omega_i), \\
\chi_i &= \chi_\alpha + \chi_n,
\end{aligned}$$

### Energy transfer by electrons and ions

$$\rho \frac{\partial E_e}{\partial t} = \text{div} D_e \text{grad} T_e + \theta_e (T_e - T_i)$$

$$E_e = E_e(\rho, T_e),$$

$$D_e = D_e(\rho, T_e),$$

$$T_e = T_e(r, z, t).$$

$$\rho \frac{\partial E_i}{\partial t} = \text{div} D_i \text{grad} T_i + \theta_i (T_i - T_e)$$

$$E_i = E_i(\rho, T_i),$$

$$D_i = D_i(\rho, T_i),$$

$$T_i = T_i(r, z, t).$$

The spatial and time approximation of the diffusion type equations is constructed on the regular difference grid composed of arbitrary quadrangles. The possibility of using both direct methods and iterative methods of incomplete Cholesky decomposition type is provided for solving the obtained algebraic equation system. To achieve an economical computation, special acceleration methods are used.

Energy transfer by heavy ions is computed in the one-particle approximation taking into account the Coulomb deceleration on free and bound medium electrons and ions.

The model for accounting laser radiation absorption is implemented in the geometric optics approximation.

To compute spectral optical properties of non-equilibrium, non-stationary, multi-component, multi-charge plasma, the ionization kinetics in the mean ion approximation was used.

The gas-dynamical motion of multi-component non-equilibrium medium, as it was already mentioned, is computed with the program /2/ using the Lagrangian-Eulerian method.

The program package under discussion uses non-orthogonal spatial grids which enables to take into account features of geometries computed within a required degree of detail.

The method of computing over subregions (computational domains) is therewith used. The domain inter-influence is taken into account through communication of internal boundary conditions. In so doing the possibility to simulate most complex processes in various approximations is implemented. For example, the spectral radiation transport processes can be computed in some regions in the multi-group kinetic approximation, in other regions in the multi-group diffusion approximation.

This capability is based on the conservative combined scheme of computation using special internal boundary conditions.

The above program package finds a wide application in studies of various thermonuclear fusion structures.

The presentation exemplifies some of such computations.

## REFERENCES

1. Belyakov I.M., Butneva O.V., Bukharova V.Ya. et al. SATURN system arrangement. VANT. Ser. Mat. Modelir. Fiz. Protsessov. 3,1992, p.49-51
2. Sofronov I.D., Afanasyeva E.A., Vinokurov O.A. et al. MIMOZA program system for solving multi-dimensional continuum mechanics problems on ELBRUS computer. VANT. Ser. Mat. Modelir. Fiz. Protsessov. 2,1990, p.3-9.
3. Pleteneva N.P., Shagaliev R.M. 2D transport equation approximation on quadrangular and polygonal spatial grids by the difference scheme with an extended template. VANT. Ser. Mat. Modelir. Fiz. Protsessov. 3,1989.
4. L.P.Fedotova, R.M.Shagaliev.  
The finite-difference KM method for computer simulation of 2-D nonstationary transport in multigroup kinetic approximation. //Mathematical approximation, 1991, v.3, №6, p.29-42.

5. Reed W.H., Lathrop K.D.

Truncation Error Analysis of Finite Difference Approximations to the Transport Equation. Nucl. Sci. Eng., 1970, 41, №2.

**PARALLELIZATION METHODS FOR NUMERICAL  
SOLUTION OF 3D GROUP  
NON-STATIONARY EQUATION OF NEUTRON DIFFUSION  
FOR NUCLEAR POWER PLANT SAFETY CALCULATIONS**

Alekseyev A.V., Zvenigorodskaya O.A., Shagaliev R.M.

Russian Federal Nuclear Center- VNIIEF,  
37 Mir ave., Sarov, Nizhni Novgorod region, 607190

Presently numerical simulation is one of the principal methods allowing to predict behavior of nuclear power plants (NPP) at various (design and accidental) modes of operation. This method capabilities have always been and seemingly will be limited with computer powers. The advent of massively parallel computers has created new capabilities for development of software tools (ST) for NPP simulation.

As was already reported at the previous fourth Mathematical Conference, VNIIEF has developed the 3D program package TENAR designed for numerical simulation of NPP behavior at various modes of operation, beginning with design and ending with serious accidents (but where the NPP equipment structure is preserved).

The package includes programs allowing to take into account the following processes: neutron transport and interaction with medium, delayed neutron and isotope burnup kinetics, coolant flow in the circulation circuit and NPP vessel, heat transfer in solid elements, fuel element thermomechanics. The package can be augmented with new components allowing to take into account needed processes

For numerical solution of 3D stationary and non-stationary problems of neutron transport in the group diffusion approximation this package uses the program KORAT 3D [1]. As the numerical solution of the neutron diffusion problem in the reactor computations is characterized with considerable amounts of computer operations, of particular urgency is parallelizing this problem on multi-processor computers, primarily, on high-performance distributed-memory systems.

It should be noted that the issues of development of effective diffusion problem parallelization methods are currently attached quite a significant attention to. Several approaches are therewith used. One of most common is that based on the geometry decomposition principle on which we will dwell in more detail somewhat further. The idea of some 3D diffusion equation parallelization techniques (see, e.g., /2-4/) is that on multi-processor computers the conventional method for numerical solution of mesh diffusion equations is used entirely in the whole domain of solution. In so doing special parallelizable algorithms for solution of mesh diffusion equation systems on multi-processor computers are used. Thus, for example, while on one-processor computer the known iterative method of conjugate gradients with incomplete Cholesky type expansion was used for numerical solution of grid diffusion equations, such an approach employs the parallelized version of the method of conjugate gradients /2/.

Mention one more approach frequently used on a computer with a small number of processors: this is the method of parallelization by energy groups.

This presentation discusses the iterative method of 3D diffusion problem parallelization based in the program KORAT 3D. It is based of the geometry decomposition principle.

As it is known, the geometry decomposition method idea is that the domain of solution of the original problem is split into a number of subdomains (hereinafter we will refer to them as computational domains) and the diffusion equation is solved separately by the computational domains. This permits splitting both into geometrically non-intersecting and geometrically intersecting sets of the computational domains. Then the inter-influence of the solutions found in different computational domains is taken into account through internal boundary conditions which are communicated at special iterations. We will call these iterations as iterations by internal boundary conditions.

A number of implementation versions of the geometry decomposition method have been recently considered for numerical solution of the multi-dimensional diffusion equation. They differ both in the technique of splitting into the computational domains and the technique of setting the internal boundary conditions. As our experience and analytical estimations of the geometry

decomposition method efficiency show, in the general case both these factors have quite a considerable bearing on efficiency of numerical solution with this method

Various approaches are currently used to set the internal boundary conditions. For example, the well-known RM (Response Matrix) method for parallel machines /5,6/ is based on transfer of one-side flows to neighboring computational domains. Some other papers /7/ use Dirichlet-Dirichlet or Dirichlet-Neumann type conditions for the boundary conditions.

An important feature of the parallelization method implemented in the program KORAT 3D is using a special type of internal boundary conditions /8/. These internal boundary conditions are a combination of the complete flow function and desired function, with the coefficient in this combination being computed basing on a multi-dimensional analog of the limiting sweep factor /9/. This setting of internal boundary conditions is aimed at a higher efficiency of the method iterative in the internal boundary conditions.

The presentation provides a more detailed discussion of the iterative parallelization algorithm /10/ implemented in the program KORAT 3D. A simplest 1D problem is used as an example to make a comparative analytical estimation of the convergence rate of the iterative method implemented in the program KORAT 3D and some other iterative methods in internal boundary conditions. The proposed parallelization algorithm is numerically studied using an essentially 3D non-stationary two-group problem for the RBMK type reactor facility.

## REFERENCES

1. Fedotova L.P., Shagaliev R.M.  
Computational technique KORAT 3D for numerical solution of 3D group neutron diffusion problems on regular and irregular spatial meshes. VANT.Ser. Met i Progr. Chisl. Resh. Zad. Mat. Fiziki. No.4, 1994. P.3-10.
2. Scott Hutchinson, Edward Hensel, Steven Castilio, Kim Dalton  
"The Finite Element Solution of Elliptical Systems on a Data Parallel Comp

uter. "International Journal for Numerical Methods in Engineering, Vol. 22, 347-362 (1991).

3. S. Rajagopalan, A. Jentra, M. D. Ghodgaonkar, S. V. G. Menon  
"Parallel Iterative Algorithms for Solving Fundamental Mode  
Neutron Flux Distribution," Ann.  
nucl. Energy, Vol. 18, No.2, pp. 81-86, 1991

4. Butnev O.I., Bykov A.N., Voronin B.L., Skrypnik S.I., Sofronov I.D.  
Parallel algorithms for solution of 3D heat conduction equations and results of  
demonstration problem computations on eight-processor distributed-memory computer  
system MP-3. VANT. Ser. Mat. Modelir. Fiz. Protsessov. No.3, 1996. P.77-84.

5. U. R. Hanebutte, E. E. Lewis  
"A Discrete Ordinate Response Matrix Method for Massively Parallel Computers,"  
Proc. Int. Topl. Mtg. Advances in Mathematics, Computers and Reactor Physics,  
Pittsburg, Pennsylvania, April 28 - May 2, 1991

6. U. R. Hanebutte, C. B. Carrico, E. E. Lewis  
"Comparison of  $S_n$  and  $P_n$  Response Matrix Methods for Massively Parallel Com-  
puters," Trans. Am. Nucl. Soc., 63, 180 (1991).

7. Yong Hee Kim, Nam Zin Cho  
"Domain Decomposition Parallel Solution of the Neutron Diffusion Equation  
on a Transputer Network," Trans. Am. Nucl. Soc., 64, 311 (1991)

8. Shagaliev R.M. On an unconditionally robust algorithm for separate  
computation by domains of 2D heat conduction equation by a node difference  
scheme. VANT. Ser. Met. i Progr. Chisl. Resh. Zad. Mat. Fiziki. No.3(17), 1984.

9. Sofronov I.D. On sweep factors. VANT. Ser. Met. i Progr. Chisl. Resh. Zad.  
Mat. Fiziki. No.2, 1982. P.3-13.

10. Alekseyev A.V., Sofronov I.D., Fedotova L.P., Shagaliev R.M. Numerical  
studies of algorithms for paralleling 3D diffusion and neutron transport problems  
in SATURN system on multi-processor computers. VANT. Ser. Met. i Progr.  
Chisl. Resh. Zad. Mat. Fiziki. No.4/1, 1996. P.16-23.

Propagation of an ultrashort, intense laser pulse in a  
relativistic plasma

Burke Ritchie and Christopher D. Decker

University of California  
Lawrence Livermore National Laboratory  
Livermore, California 94550

A Maxwell-relativistic fluid model is developed for the propagation of an ultrashort, intense laser pulse through an underdense plasma. The separability of plasma and optical frequencies ( $\omega_p$  and  $\omega$  respectively) for small  $\omega_p/\omega$  is not assumed; thus the validity of multiple-scales theory (MST) can be tested. The theory is valid when  $\omega_p/\omega$  is of order unity or for cases in which  $\omega_p/\omega \ll 1$  but strongly relativistic motion causes higher-order plasma harmonics to be generated which overlap the region of the first-order laser harmonic, such that MST would not be expected to be valid although its principal validity criterion  $\omega_p/\omega \ll 1$  holds.

It is the purpose of this paper to present a relativistic fluid model in which the approximate separation of optical and plasma frequencies is not made. The fluid model results are then benchmarked against PIC results as a test of our numerical methods.

The equations of the model are Maxwell's equations for the vector and scalar potentials in the Lorentz gauge, the continuity equation, and the fluid momentum equations,

$$\left(\nabla^2 - \frac{1}{c^2} \frac{\partial^2}{\partial t^2}\right) \vec{A} = - \frac{\omega_p^2 n \vec{p}}{e \gamma c} \quad (1a)$$

$$\left(\nabla^2 - \frac{1}{c^2} \frac{\partial^2}{\partial t^2}\right) \Phi = - \frac{m \omega_p^2 (n - n_i)}{e} \quad (1b)$$

$$\frac{\partial n}{\partial t} = - \vec{\nabla} \cdot \left( \frac{\vec{p} n}{m \gamma} \right) \quad (1c)$$

$$\left( \frac{\partial}{\partial t} + \frac{\vec{p} \cdot \vec{\nabla}}{m \gamma} \right) \vec{p} = - \frac{e}{c} \frac{\partial \vec{A}}{\partial t} - \vec{\nabla} e \Phi + \frac{e}{m c \gamma} (\vec{p} \times \vec{\nabla} \times \vec{A}) \quad (1d)$$

In Eqs. (1)  $n$  is the dimensionless normalized electron density and  $n_i$  the dimensionless normalized ion density, which is taken to be constant during the passage of a laser with a pulse length in the femto-second regime.

We difference Eqs. (1a) and (1b) in time but not in space, where the spatial problem is defined as a 2D slab with propagation along  $z$ . The use of Fast-Fourier Transform (FFT) methods to treat spatial derivatives has been described previously [1]; here we merely outline the techniques used for the equations of the Maxwell-fluid model. All terms containing differential operators are moved to the right side, which is assumed known from the previous time step. Then we Fourier transform the equations in space and advance the resulting algebraic equations one time step using the three-point central-difference algorithm for the second-order time derivative. Then we find the inverse Fourier transform. This constitutes one cycle in the temporal advance. We treat Eq. (1d) similarly, a procedure which has already been implemented by others [2] for the fluid momentum.

In this way spatial differencing is entirely avoided. This

procedure has the effect that spatial derivatives, which in real-space, finite-difference methods are distributed locally over a selected number of grid zones and can be the source of numerical instabilities, are smoothed globally over all space, thereby leading to robustly stable results. We use the standard FFT routine of Cooley and Tukey [3], which is a very fast algorithm on a vector machine. This procedure, as applied to Maxwell's equations, has been thoroughly benchmarked in other applications [1].

A similar procedure applied to Eq. (1c), however, does not yield numerically stable results. The following procedures, however, do yield numerically stable results. Our algorithm to advance the normalized electron density over an interval  $dt$  is,

$$n_a = e^{-\frac{dt}{2m\gamma} \vec{p} \cdot \vec{\nabla}} e^{-dt \vec{\nabla} \cdot \vec{p}/m\gamma} e^{-\frac{dt}{2m\gamma} \vec{p} \cdot \vec{\nabla}} n_r, \quad (2)$$

where the subscripts a, r designate the advanced, retarded function with respect to the interval  $dt$ . This algorithm is a form of the well-known split-operator FFT method [4], in which noncommuting exponential factors of the propagator are arranged over a single three-step interval as shown in Eq. (2). The outside factors, which contain differential operators, are evaluated in transform space and the middle factor is evaluated in real space. This procedure is obviously limited to first-order accuracy in  $dt$  because (in contrast to the conventional split-operator method of [4])  $\vec{p}/\gamma$  depends on space and thus higher-order terms in the expansion of the exponential are dropped as truncation errors. However this procedure is observed to be conditionally numerically stable.

The laser wavelength is  $1 \mu\text{m}$ . The plasma density is  $10^{20} \text{ cm}^{-3}$  such that the ratio of the plasma to optical frequency,  $\omega_p/\omega$ , is 0.296. In the calculations we use the scaled variables: time in units of  $\omega^{-1}$ , space in units of  $k^{-1}$ , fields in units of  $mc^2/e$ , and momentum in units of  $mc$ . The longitudinal and transverse widths of the Gaussian pulse are  $10 k^{-1}$  and  $17.67 k^{-1}$  respectively, where the FWHM is  $2\delta\sqrt{\ln 2}$  for a Gaussian width  $\delta$ . This corresponds to a pulse length of about 8.75 fs and a pulse width of about  $4.64 \mu\text{m}$ . For

maximum time of  $220 \omega^{-1}$ , transverse length of  $125 k^{-1}$ , and longitudinal length of  $500 k^{-1}$  we used 8001, 256, and 1024 mesh points respectively.

The PIC calculations were performed using the code WAVE [5], which has been thoroughly benchmarked over the last two decades [6]. We used  $10^6$  particles (sufficient to resolve the fifth-order laser harmonic) and 512, 256 mesh points for longitudinal, transverse lengths respectively equal to  $204.8 k^{-1}$ . The temporal interval is  $0.2 \omega^{-1}$ .

We present results for a laser pulse with a peak intensity of  $1.12 \times 10^{18} \text{ W cm}^{-2}$  (Fig. 1) incident on a cold plasma whose boundaries are sharply defined at  $-100 k^{-1}$  and  $100 k^{-1}$  longitudinally and at the grid boundaries transversely. The laser is polarized in the transverse direction and causes the transverse component of the fluid momentum to quiver as shown in Fig. 2. The EM fields are calculated from the potentials [Eqs. 1a-1b] from the relation,

$$\vec{E} = -\frac{1}{c} \frac{\partial \vec{A}}{\partial t} - \vec{\nabla} \Phi \quad (3)$$

In the wake of the laser a longitudinal EM field is generated (Figs. 3-4) which extends for many plasma wavelengths - a plasma wavelength is  $2\pi \omega/\omega_p$  in our scaled variables. The fluid and PIC models in Figs. 3 and 4 respectively show reasonable mutual agreement considering their theoretical differences. The poorest agreement is observed near the laser pulse and at the left-hand boundary of the plasma. This may reflect the use of damping terms in the fluid momentum equations to suppress motion outside of the plasma boundaries.

**Acknowledgements.** This work was performed under the auspices of the U. S. Department of Energy by Lawrence Livermore National Laboratory under Contract No. W-7405-ENG-48.

## References

1. B. Ritchie and M. E. Riley, Sandia Report Sand97-1205. UC-401 (1997); B. Ritchie, P. Dykema, and D. Braddy, Phys. Rev. E **57**, 2217 (1997).
2. Vadim Borue and Steven A. Orszag, Phys. Rev. E **51**, R856 (1995).
3. J. W. Cooley and J. W. Tukey, Math. Compt. **19**, 297 (1965).
4. J. A. Fleck, Jr., J. R. Morris, and M. D. Feit, Appl. Phys. **10**, 129 (1976) and M. D. Feit and J. A. Fleck, Jr., Appl. Opt. **17**, 3990 (1978).
5. R. L. Morse and C. W. Nielson, Phys. Fluids **14**, 830 (1971).
6. D. W. Forslund, J. M. Kindel, and E. Lindman, Phys. Fluids **8**, 1017 (1975); D. W. Forslund, J. M. Kindel, W. Mori, C. Joshi, and J. M. Dawson, Phys. Rev. Lett. **54**, 558 (1985); C. W. Decker, W. B. Mori, K. - C. Tzeng, and T. Katsouleas, Phys. of Plasmas **3**, 2047 (1996).

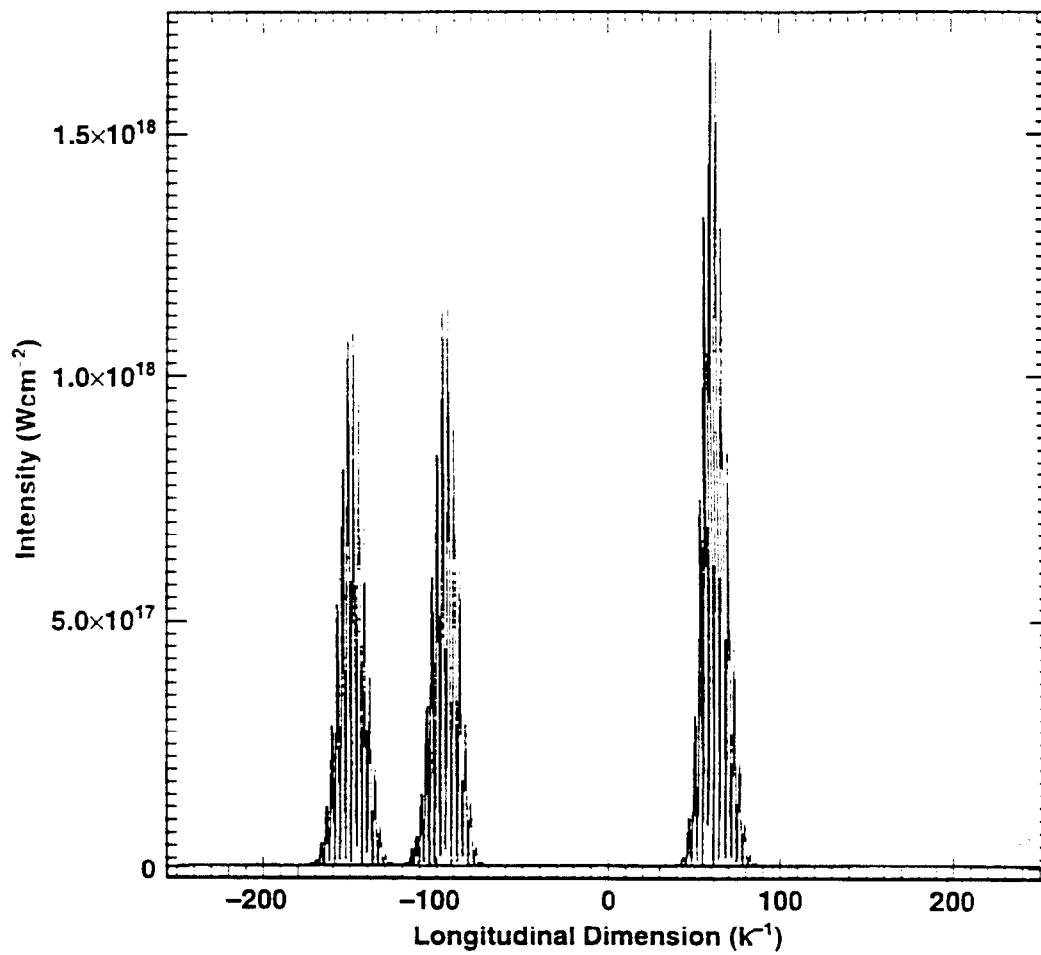
## Figure Captions

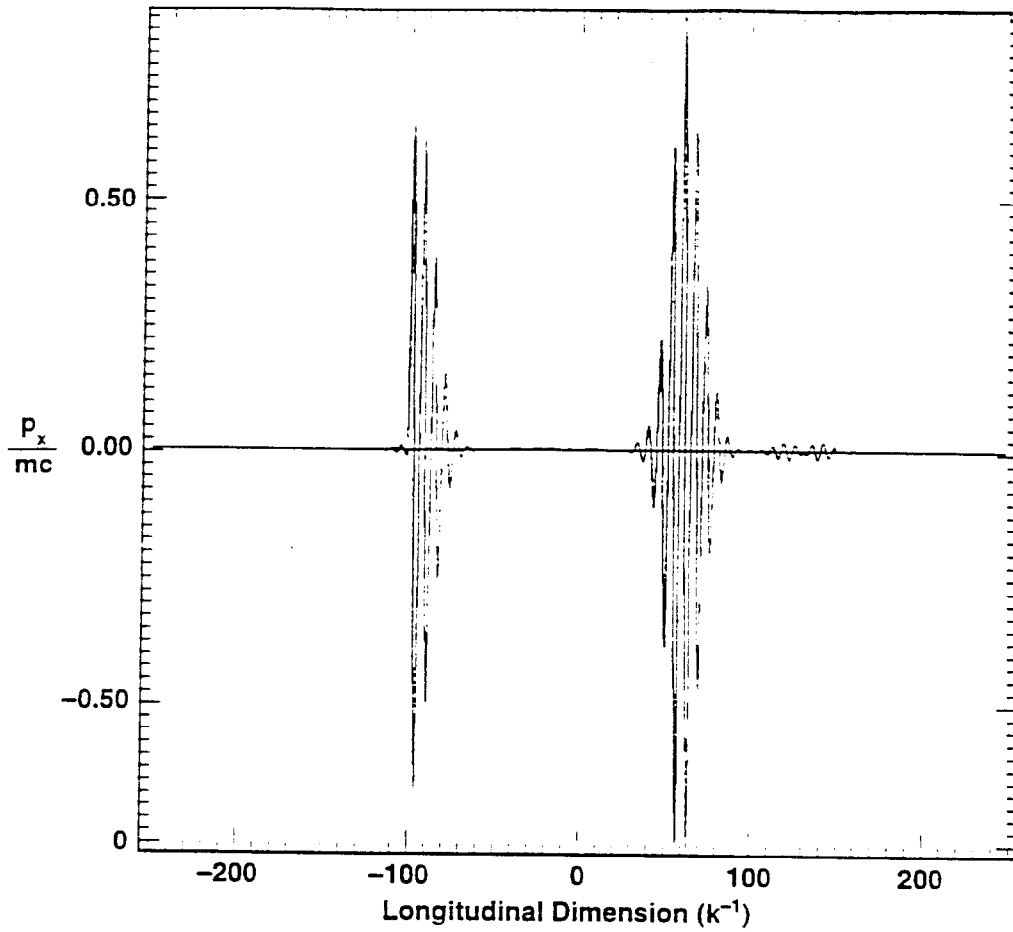
Figure 1. Three snapshots of laser intensity versus longitudinal distance. The laser enters the region of the plasma at  $-100 \text{ k}^{-1}$  and is self-focused as it passes through the region.

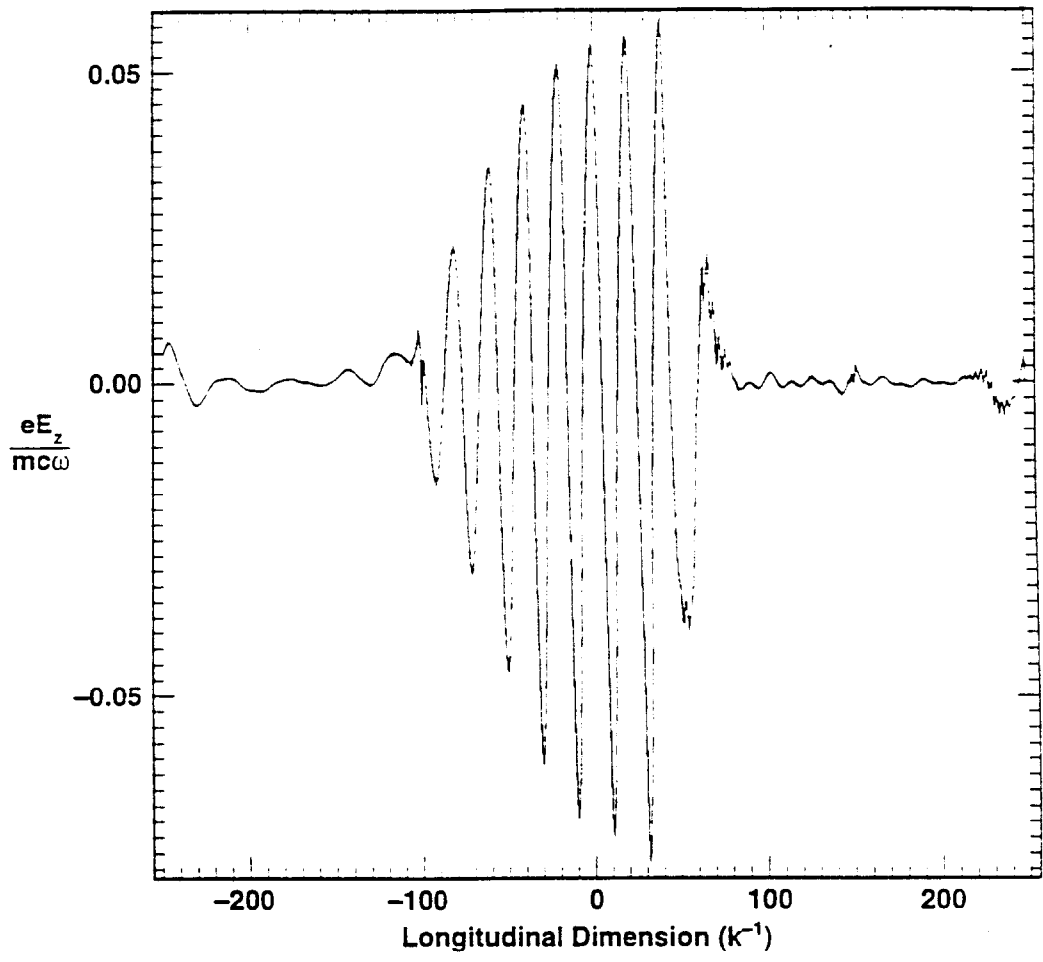
Figure 2. Snapshots of fluid quiver momentum versus longitudinal distance corresponding to the second and third snapshots from the left of Figure 1. The periodicity is on the optical frequency scale.

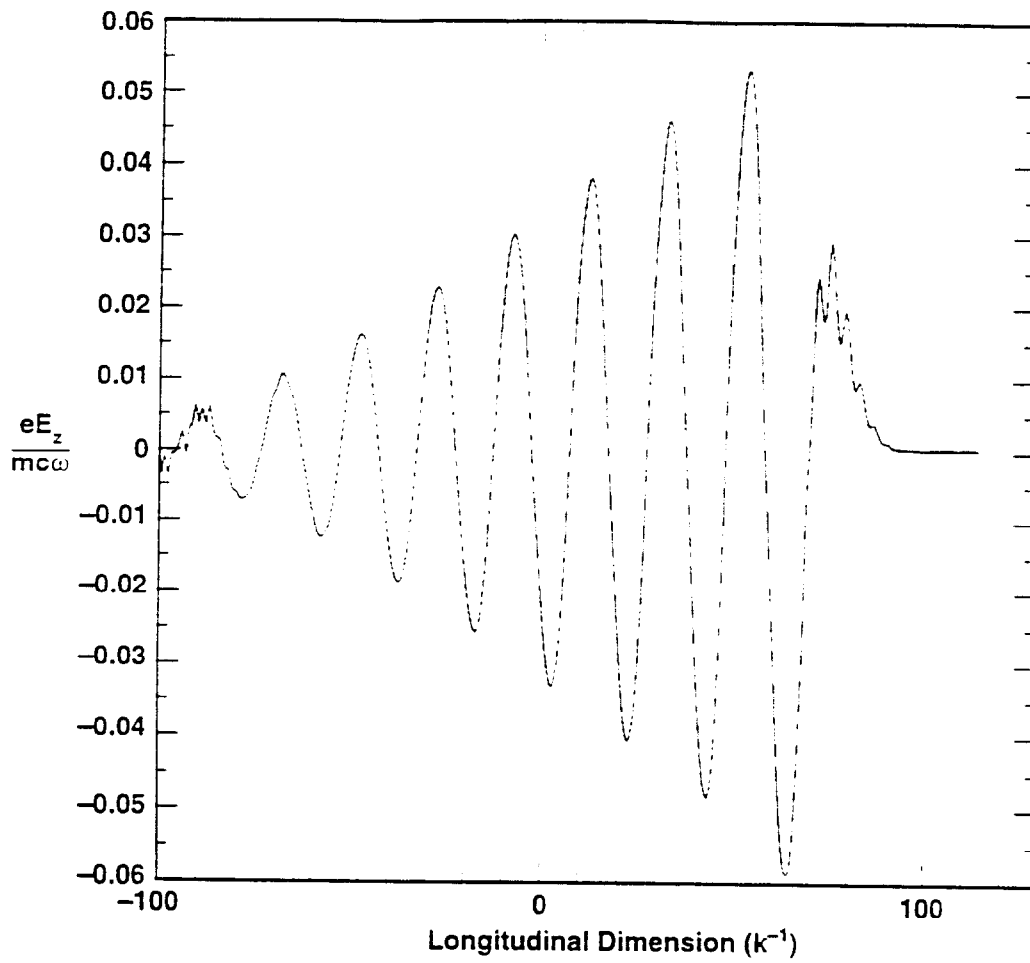
Figure 3. Wake EM field versus longitudinal distance for the right-hand pulse of Figure 1. The periodicity is on the plasma frequency scale, with optical-scale modulation clearly visible near the front of the pulse.

Figure 4. Wake EM field as given by the PIC model versus longitudinal distance as a comparison with the fluid-model wake field given in Figure 3.











# Source Description and Sampling Techniques in PEREGRINE Monte Carlo Calculations of Dose Distributions for Radiation Oncology

A. E. Schach von Wittenau, L. J. Cox, P. M. Bergstrom Jr., W.P. Chandler, C.L. Hartmann-Siantar, and S. M. Hornstein

Lawrence Livermore National Laboratory, Livermore, CA 94550

## Abstract

We outline the techniques used within PEREGRINE, a 3D Monte Carlo code calculation system, to model the photon output from medical accelerators. We discuss the methods used to reduce the phase-space data to a form that is accurately and efficiently sampled.

## Introduction

PEREGRINE is a 3D Monte Carlo code calculation system designed specifically for radiation therapy planning. Unlike current dose calculation methods, which approximate dose distributions in the patient based on water phantom measurements, PEREGRINE determines the dose in the patient by simulating the actual treatment, particle interaction by particle interaction.

Accurate Monte Carlo dose calculations rely on a detailed understanding of the radiation source. One of the operational requirements for Monte Carlo treatment planning is that this detailed understanding be expressed as a set of distributions which may be rapidly and efficiently sampled, but which still accurately represent the underlying phase-space used to derive those distributions.

The nature of the problem is perhaps best understood in the context of Figure 1. A monoenergetic beam of electrons (~2 mm diameter) strikes a thin (~1 mm) target made of a high-Z material such as tungsten. The resulting bremsstrahlung photons are collimated by conical collimator (typically tungsten).

The photon beam passes through a beam flattener (also known as a flattening filter), which is usually made of Cu, Pb, or steel. The beam flattener, being thicker in the center, attenuates the central portion of the bremsstrahlung photon distribution. This results in a flat energy fluence distribution at the patient plane. Although the energy fluence distribution is uniform, the energy distribution itself is not uniform, since the photons landing at different points on the patient plane will have gone through differing thicknesses of the beam flattener. In addition, non-negligible amounts of radiation will scatter from the collimator and the beam flattener and arrive at the patient plane. This radiation field needs to be characterized by several distributions of bremsstrahlung and scattered photons

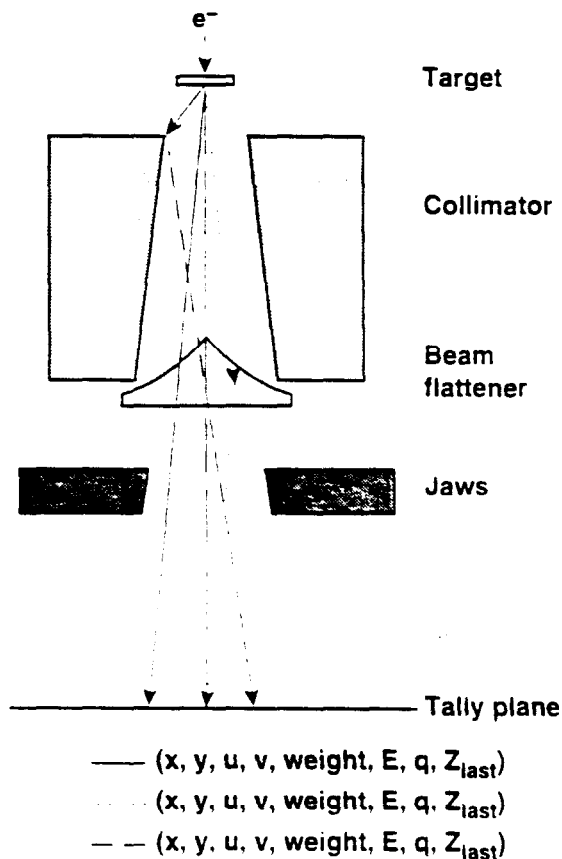


Figure 1. A stylized picture of the head portion of a medical accelerator. Monoenergetic electrons with energies of 4, 6, 8, 10, 15, or 18 MeV are incident on a thin (~1 mm), high-Z target such as tungsten. The bremsstrahlung radiation so produced is collimated by a primary collimator, also typically made from tungsten. The forward-peaked bremsstrahlung fluence distribution is 'flattened' by a conical piece of metal, typically made from copper. This filter, being thicker in the center, attenuates the center portion of the beam, primarily by attenuating the low energy portion of the photon distribution. Photons escaping the bottom of the accelerator head are tallied for later analysis.

This work was performed under the auspices of the U.S. Department of Energy by the Lawrence Livermore National Laboratory under contract number W-7405-ENG-48.

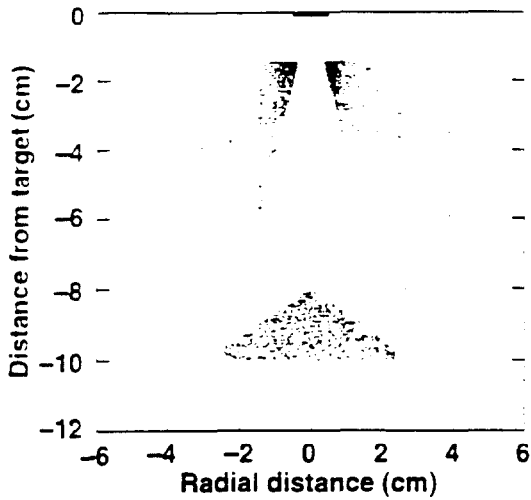


Figure 2. Backtracking the photons to their point of origin shows which portions of the accelerator head contribute to the output fluence

and may be further shaped by beam shaping hardware such as movable jaws and other devices. All of these distributions must be understood in order to develop a useful source model for input into PEREGRINE. In addition, the source model derived from this understanding must satisfy the operational needs of being easily and efficiently sampled within the overall problem.

In this paper we present methods currently used within PEREGRINE to satisfy these requirements.

### Methods and Materials

The simulations were performed using the Monte Carlo codes BEAM96 [1] and MCNP4B [2]. Machine drawings and materials data for the medical accelerators discussed in this paper were supplied by Varian, Inc [3]. Both BEAM and

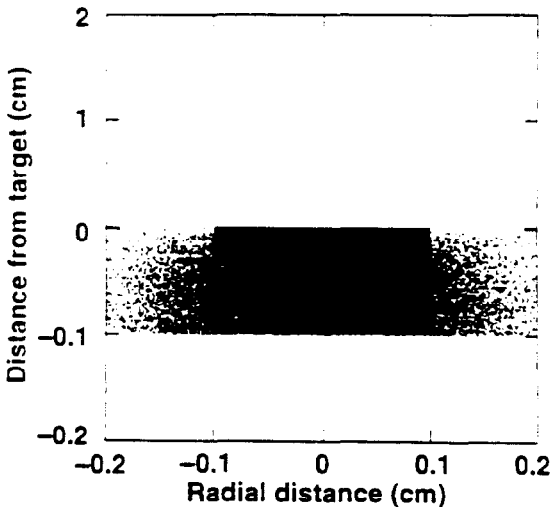


Figure 3. An expanded view of the region around the bremsstrahlung target of the stylized accelerator head shown in Figure 2. The sharp edges of the incident electron distribution are clearly visible, as is the broader, less intense distribution of photons that scatter within the target

MCNP have physics 'switches' which allow the biasing of the various physical processes that occur within the accelerator head. In addition, the BEAM code comes with the capability to record the 'position of last interaction' of a particle, as well as the number of the cell in which a given particle was created. Only those portions of the treatment head lying above the jaws were simulated, since this portion of the accelerator does not vary between treatments. Modeling of the movable jaws and patient-specific portions of the accelerator will be discussed elsewhere. A schematic of the modeling process is shown in Figure 1. The bremsstrahlung photons are tracked through the accelerator head. Photons arriving at the bottom of the head are tallied. Their position ( $x, y$ ), their direction cosines ( $u, v$ ), as well as their particle type, energy, weight (to account for the various physics-biasing schemes used), and position of last interaction  $z_{last}$  are written to the phase-space file. The  $z$  coordinate for each particle, being merely the tally-plane position, and the direction cosine  $w$ , known from

$$w = \sqrt{1 - u^2 - v^2}$$

do not need to be written to the file. Approximately  $5 \times 10^6$  incident electrons are used in the simulations. Given the variance reduction schemes used (e.g., forced collisions, particle splitting), the resulting phase-space files contain information for several tens of millions of photons (of varying weights) and occupy ~1 GB of disk space each. To date we have simulated eight accelerators made by Varian, Inc. Work has started on accelerators made by Siemens, Inc.

### Analysis of Phase Space Files

The first step in the analysis is to 'backtrack' the photons to their place of creation. This is done using the equations:

$$x_s = x + (z_{last} - z_{tally}) \times u / w$$

$$y_s = y + (z_{last} - z_{tally}) \times v / w$$

A scatter plot of  $x_s$  vs.  $z_{last}$  for a stylized accelerator head is shown in Figure 2. This step in the phase-space analy-

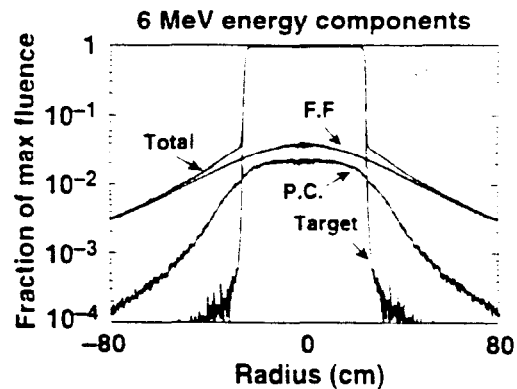


Figure 4. The fluence at the patient plane comprises contributions from the target, the primary collimator, and the flattening filter. The target is the major source of the energy reaching the patient

1. We have since added this capability to MCNP, along with a number of other diagnostics which are not covered here

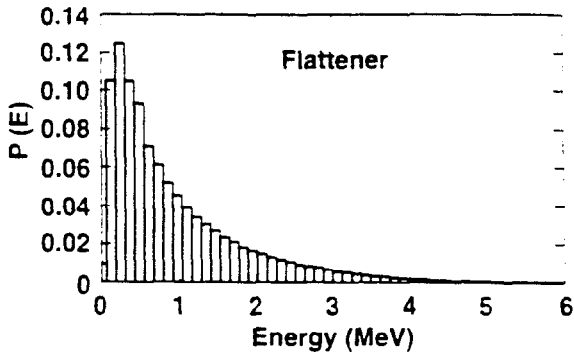
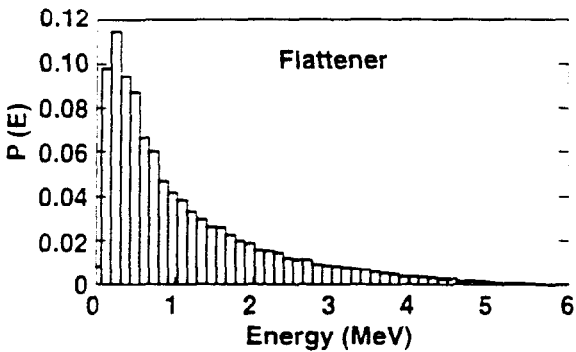
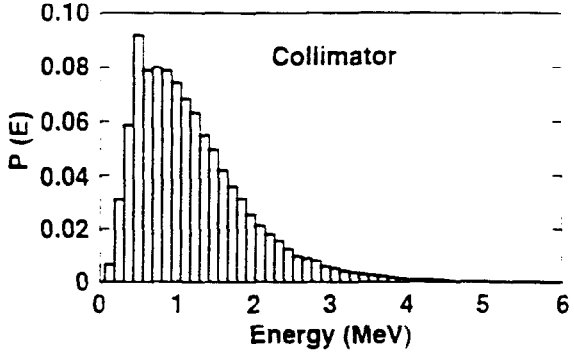
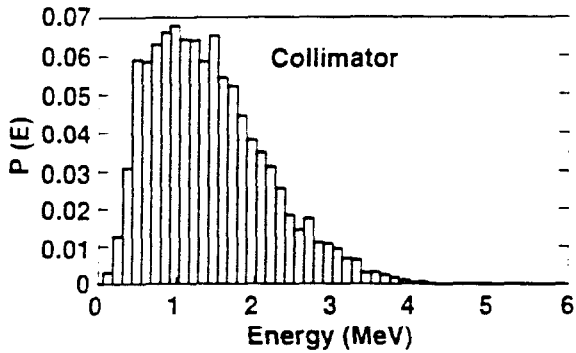
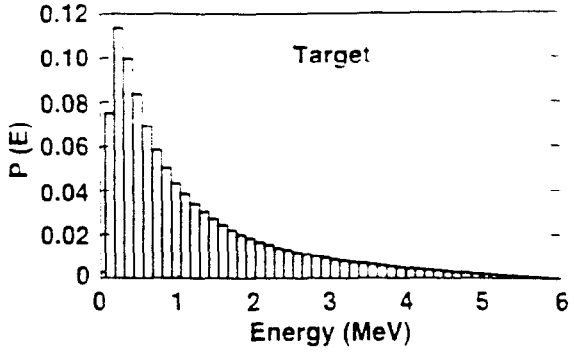
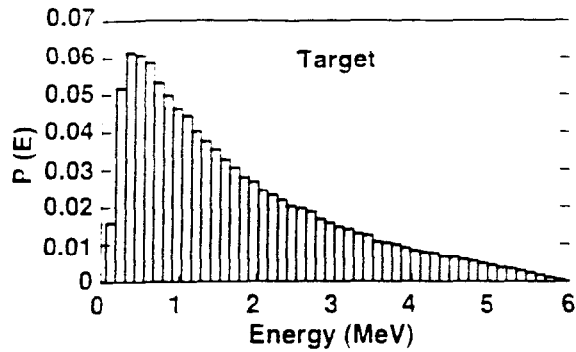


Figure 5. The photon energy distributions vary strongly with the piece of hardware in which they are created. Photons from the target have energies ranging from the energy of the initial electrons down to low, but not quite zero, energy. This is consistent with the flattening filter's removal of the lower energy photons. The energy distribution from the primary collimator reflects both this filtering process (on the low energy side) and the fact that the photons are Compton scattered through a non-negligible angle (thus affecting the high energy side). The photon distribution from the flattening filter reflects both the lack of low-energy filtering as well as the possibility for small angle scattering (and consequently little energy loss).

sis serves two purposes — the first being practical, the second being conceptual. First, it is a useful check on the input deck, since the locations of the photon creations should correlate with the physical structure of the accelerator head. Second, it gives us a feel for how each portion of the hardware contributes to the output of the machine. For the example shown in Figures 2 and 3, we see that photons originating from the target come from a well defined spot. Photons coming from the primary collimator are fewer in number, and they tend to come from the upper edge of the collimator. Thus, the inner surface of the primary collimator is not a uniform source of

Figure 6. The photon energy distributions shown in Figure 5 change with increasing distance from the central axis of the accelerator. The energy distributions at a radius of 20 cm are shown.

photons. Rather, the primary collimator appears to be more of a 'ring' source. The flattening filter is also a source of photons. Unlike the primary collimator, however, the flattening filter is much more uniformly 'filled'.

We next analyze the fluence distributions at the patient plane. This is shown in Figure 4 for an accelerator operating at 6 MeV. We see that most of the energy comes directly from the target, with contributions at the several percent level from the flattening filter and the primary collimator.

### Energy Distribution

We show in Figure 5 the photon energy distributions from the various components at the center of the patient plane. The photon energy distributions vary strongly with the piece of hardware in which they are created. Photons from the target have energies ranging from the energy of the initial incident

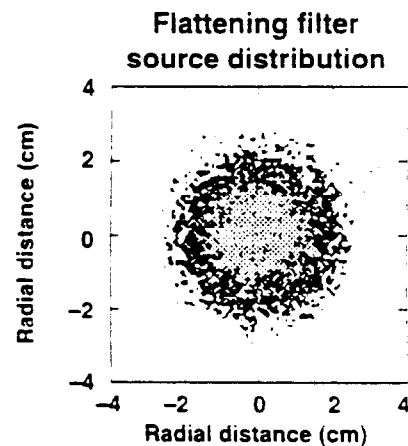
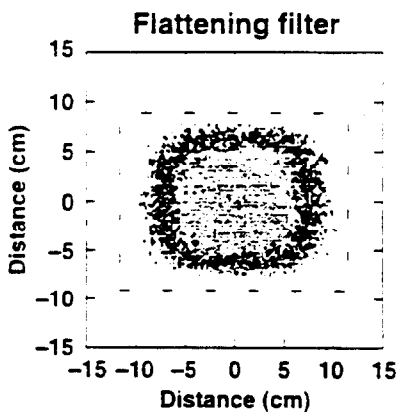
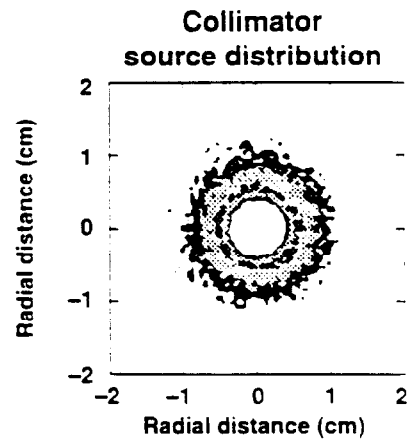
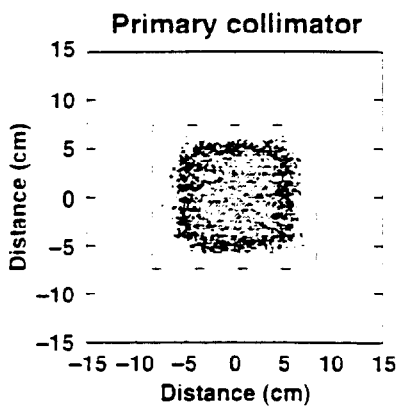
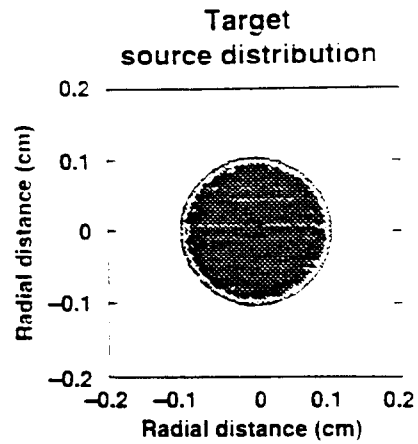
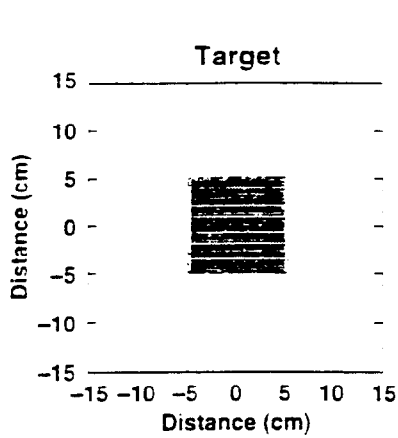


Figure 7. Each subsource illuminates a different amount of the patient surface. This area is a function both of the source 'size' as well as its distance to the jaws. The 'target' source is most sharply defined. The other sources illuminate larger areas of the patient. The dashed lines in the lower two panels denote a suitable area for Monte Carlo sampling.

Figure 8. The effective source distributions, looking upwards from the patient plane towards the bremsstrahlung target. The photons coming from the target appear to come from a 2 mm diameter disk, those photons coming from the primary collimator appear to come from a ring-like source (compare with Figure 2), and those photons coming from the flattening filter appear to come from a broad, almost Gaussian-like source. Note the different diameters of the various sources.

electrons down to low, but not quite zero, energy. This is consistent with the flattening filter's removal of the lower energy photons. The energy distribution from the primary collimator reflects both this filtering process (on the low energy side) and the fact that the photons are Compton scattered through a non-negligible angle (thus setting an upper bound on the high energy side). The photon distribution from the flattening filter reflects both the lack of low-energy filtering (since this is the last piece of hardware transited by the photons) as well as the possibility for small-angle scattering (and consequently little energy loss) of the high energy photons coming from the target.

The energy distributions shown in Figure 5 change as we move to larger distances from the central axis of the beam. This is shown in Figure 6. We find that the distributions show an increase in the proportion of low energy (here,  $\sim 1$  MeV) photons with increasing distance from the central axis, which correlates with the decrease in the thickness of the flattening filter traversed by these photons.

### Energy Fluence at Patient

The fluence patterns at the patient from each of the sub-sources for a  $10\text{ cm} \times 10\text{ cm}$  field (that is, where the jaws in Figure 1 have been moved so that the photons from the target illuminate a  $10\text{ cm} \times 10\text{ cm}$  square) are shown in Figure 7. We see that, as expected, the target photons illuminate the desired area. Photons from the primary collimator illuminate a larger area of the patient. This is expected, since the 'source' of these particular photons is both closer to the jaws and larger (Figure 2). This trend becomes even more pronounced for the photons from the flattening filter. Indeed, these photons illuminate a slightly rectangular area, a result of the different aspect ratio of the x- and y-jaw pairs. Analysis indicates that, at this field size, 93% of the photon energy reaching the patient comes from the target, 2% from the primary collimator, and 5% from the flattening filter.

While the area of illumination at a given field size is different for each subsource, it is true, on the other hand, that each subsource will illuminate a specific area of the patient for a specific jaw setting. The areas of illumination shown in Figure 7 can be studied for other jaw settings and the results tabulated for later use.

### Photon Origin Distribution

The subsources, in addition to illuminating different size areas of the patient, also have markedly different source distributions. Figure 8 shows the radial distribution of the photon energy for each subsource when the photons are backtracked to planes at positions corresponding to the locations shown in Figure 2. The 'target' photons source is a flat disk, the 'primary collimator' photons come from a ring-like source, and the 'flattening filter' photons come from a broad, almost Gaussian source. While these distributions are quite different, each is well described by a radial distribution and an angular distribution.

## Source Algorithm

We now have enough information to develop a source algorithm for use in PEREGRINE. The 'source problem', as described in the Introduction, was to be able to generate photons in a manner that was both accurate and efficient. Let us consider the problem for a treatment consisting of one field size for one machine; the generalization to multiple field sizes is straightforward.

For a given field size, we know what proportion of the energy reaching the patient comes from each subsource (Figures 4 and 7).

- Step 1: Decide which subsource will be sampled.
- Step 2: For this subsource and field size, determine the x and y limits of illumination (Figure 7). Generate a random, uniformly distributed  $(x,y)$  coordinate within this area.
- Step 3: Given this  $(x,y)$  pair, calculate  $r$ . Adjust the weight of the particle to account for the slowly-varying fluence (Figure 4) of this subsource. Sample the particle's energy from the energy distribution for this subsource, at this  $r$  (Figures 5 and 6).
- Step 4: Given the subsource being sampled, sample an initial position for the photon by choosing a starting radius and angle from the appropriate distribution (Figure 8).

At this point, we have the particle's energy and weight (Steps 2 and 3), as well as two points defining its trajectory (Steps 3 and 4). The trajectory-defining points define the particle's direction cosines, and we have all the required phase-space information needed to start tracking this particle in the patient. Sampling from the various distributions is performed using the alias sampling method [4]. 'Step 2' above keeps the efficiency of the overall algorithm high, since we tend to pick only those photons that will hit the patient.

## Conclusion

We have given an overview of the approaches used within the PEREGRINE project to model medical accelerators. We have described the variations in the energy and angular distributions of the radiation produced in or scattered by various portions of the accelerator. We have outlined our procedures for sampling these distributions to yield an algorithm that is both efficient and rapid.

## References

1. D.W.O. Rogers, B.A. Faddegon, G.X. Ding, C.-M. Ma, J. We, T.R. Mackie, *Med. Phys.*, 22, 503 (1995).
2. J.F. Briesmeister, MCNP - A General Monte Carlo N-Particle Transport Code, LA-12625-M, Los Alamos National Laboratory (1997).
3. Varian Oncology Systems.
4. A.J. Walker, *ACM Trans. Math. Software*, 3, 253, (1977).



## The technique for solving 3D hydrodynamics problems on irregular Lagrangian grids

V.N.Motlokhov, V.V.Rasskazova, P.A.Rasskazov, A.N.Shaporenko  
Russian Federal Nuclear Center- All-Russian Scientific Research Center  
of Experimental Physics (VNIEF), Sarov

### Introduction

The necessity in a mathematical technique development allowing to compute a material motion in 3D space is related to the fact that in the majority of practically significant situations the phenomena geometry is three-dimensional.

In practice, there are a great number of problems when domains of solutions originally have a complex structure and it is very difficult to construct a regular grid. And construction of a regular grid with a preset property even within domains of simple structure may be practically impossible. The use of an irregular grid will allow to avoid these difficulties.

In problems with strong deformations closely located gas particles have a trend to become widely separated from each other. In these cases flow simulation on regular Lagrangian grids appears to be impossible. In mathematical models operating in Eulerian coordinates which do not use metric closeness the determination of various material boundaries is a quite difficult task though in many cases it becomes significant.

The proposed technique uses Lagrangian representation of gas dynamics equations and the difference computational grid connected to a material and moving along with it.

The space filling up by figures as computational grid cells without folds and gaps is performed in irregular way with the use of Dirichlet-Voronoy convex polyhedrons at the initial time of integration.

The Lagrangian technique is an extremely powerful technique for solving hydrodynamics problems. But its disadvantage is that grid distortion takes place during the process of computation of flows with strong material deformations and this, in its turn, leads to a time step value decrease and in some cases to the impossibility of further computations.

To eliminate the Lagrangian grid computational distortions during the numerical experiment, the ways of preserving three-edged angles to be convex and local grid reconstruction by cutting some cells or pasting together two neighboring cells are used.

The interest in unstructured and irregular grids may be also explained by the fact that they may be much easier reconstructed in different ways and, additionally, allow to localize grid areas which are to be reconstructed more simply.

Under local reconstruction all integral characteristics of the problem remain and this fact positively affects the computation accuracy.

Topological grid structure is determined by connections of its nodes. Each node of a triangular grid has strictly four neighbors. This grid feature is the most important for the development of the local grid reconstruction technique.

Assume that the volume of cells surrounding cells being reconstructed is not changed during operations of cell cutting and pasting together. This condition is useful both for recomputation of hydrodynamic grid values and satisfaction of the requirement of convexity of all cells after the grid reconstruction completion.

### Cells cutting and pasting together

While cutting a cell  $J$ , a plane which cuts a cell in two new ones shall be specified. After points of this plane intersection with a cell edges have been found and new connections between cells and nodes have been determined, we obtain two new cells  $J_1$  and  $J_2$  (see Fig.1).

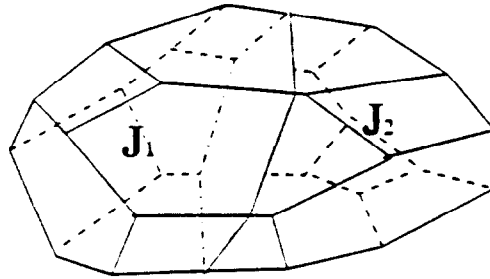


Fig.1. Example of cutting a polyhedral cell by a plane.

Following the idea of preservation of cell volumes while executing operations of the local grid reconstruction we need to relocate cell's nodes being connected to nodes of an edge occurring as a result of cell cutting, so that we could restore cell volumes.

The following dimensionless values are selected to estimate the grid status:

$R_1$  is a ratio between a typical cell size and a length of its maximal diagonal:

$R_2$  is a ratio between a typical cell size and an average value of this parameter over the whole domain:

$R_3$  is a ratio between a cell volume and an average volume value of cells surrounding it.;

$R_4$  is a number of this cell edges.

A typical cell size may be determined by the formula:

$D = \sqrt{\frac{V}{d_m}}$ , where  $V$  is a cell volume,  $d_m$  is a maximal diagonal length. As experience

showed, such approach to a typical cell size computation reflects in the best way specific features of polyhedral cells.

A certain cell cutting is performed depending on values of estimated  $R_i$  join parameters.

Each cell cutting is performed completely by the plane normal to linear section which connects centers of maximally distant from each other edges and dividing this section in two.

The correct choice of a neighbor is a significant enough factor for combining a cell with one of its neighbors. The choice of a neighbor was performed according to the following criteria:

- a cell volume should be minimal;
- surface area of an edge separating cells being pasted should be maximal;
- maximal diagonal of a cell obtained as a result of pasting should be minimal.

Be sure to remove cells being tetrahedrons.

### Grid correction using elastic impact.

At the initial time of integration a grid consists of convex polyhedrons only. This requirement may be easily implemented and is strictly performed in grid structure at the initial time. Each time we obtain a new set of polyhedron's vertices, verification of the requirement that a value of any three-edged angle is less than  $2\pi$  is performed. This means that volume of the pyramid in which vertex the three-edged angle under consideration is situated and the base of which is a plane passing through nodes surrounding this angle and being nearest neighboring nodes over edges is a positive value.

As a result of motion of all polyhedron's vertices at the next  $(n+1)$  time step of integration the volume value may change its sign. This means that there is a time point  $t^*$ , when this volume value equals zero.  $V(t^*) = 0$ . This is possible, when four grid nodes belonging to one three-edged angle lie in the same plane.

To determine this time point, write the expression of a triangular pyramid volume in the form of cubic polynomial by introducing an integration time continuity parameter. Cubic equation within the integration time range has an odd number of roots: either one or three and only one positive.

To preserve a three-edged angle convexity, introduce an elastic impact on a weightless rotating plane.

Impact is a phenomenon of finite change of solid velocities within a very short time range. Therewith, if impulsive forces are potential, then this impact is called quite elastic one. The set of masses grouped in grid nodes we consider solids of finite mass.

Use conservation laws for a closed system of points:

- momentum conservation law;
- kinetic energy conservation law;
- rotational moment conservation law.

Note that a closed system is a system of bodies when no one of them is affected by external forces.

The given system of equations includes seven equations with twelve unknowns. For unique determination of new velocity values subordinate to these conservation laws, add the condition of elastic impact on a rigid weightless wall. In this case conservation of velocity tangent components on this wall is performed and modification of only normal components of velocities in relation to this wall is considered.

Using some not difficult transformations we obtain this system solution.

From the analysis of formulas describing the system solution one may see that the use of elastic impact resulted in the fact that a volume value of a three-edged prism has changed its sign for an opposite after the impact of all its vertices on the plane where they were located at this moment. I.e. in this case the corresponding three-edged angle will be convex.

Using the procedure (similar to the procedure for 2D case) of sequential look through all vertices of all polyhedrons and composing a list of numbers of those three-edged angles which are to be corrected sequentially using elastic impact, we'll obtain a set of convex polyhedrons by the end of one time step integration.

In the next task the material motion was computed using 3D Lagrangian hydrodynamics program. Cubic region was filled up by the ideal gas and restricted by rigid walls. A conical subregion was selected inside this region with the cone axis being parallel to Oz axis, of opening angle equal to  $\pi/12$  and with a vertex in the cube side laying in Oxy plane. In the conical subregion filled up with the same gas the rotational flow was given at the initial time being defined by velocities in every point according to the following formulas:

$$U_x = y - y_k,$$

$$U_y = x_k - x,$$

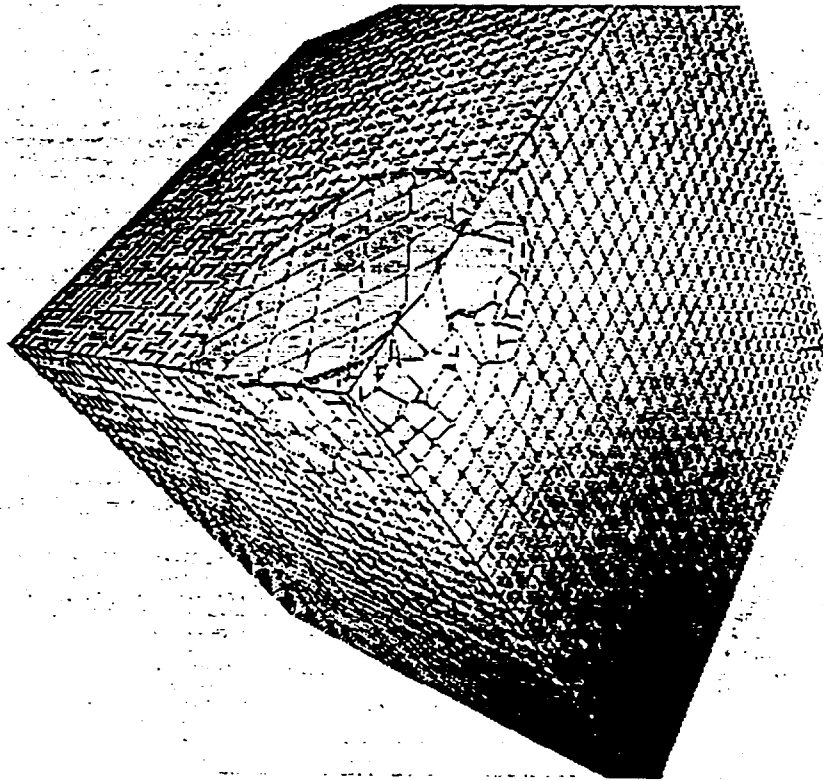
$$U_z = 0$$

where  $(x_k, y_k, 0)$  are coordinates of the cone vertex.

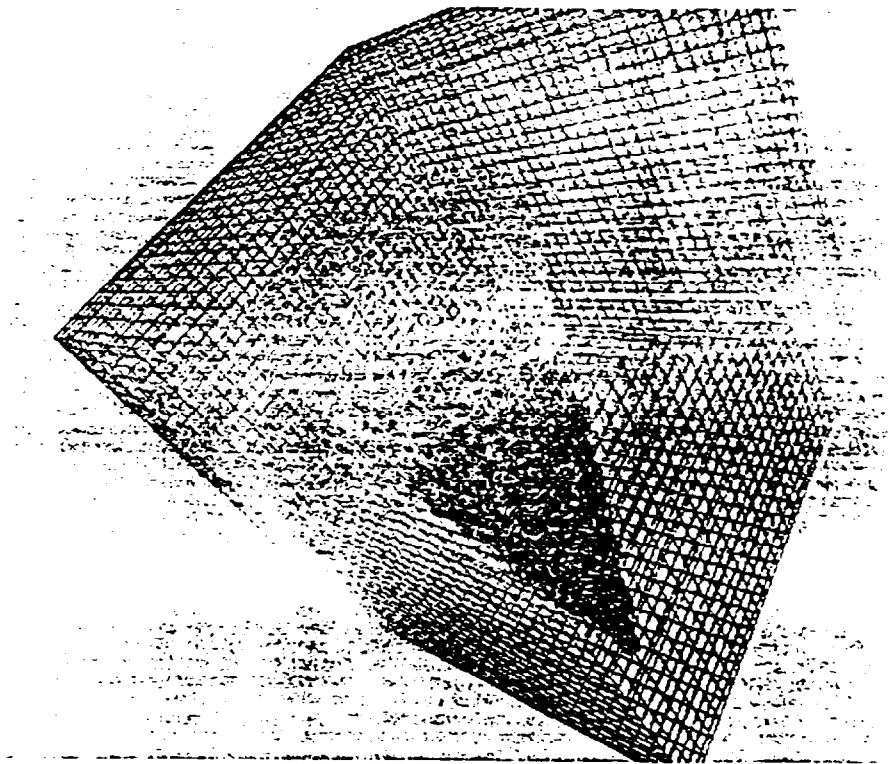
During the process of involving a unperturbed part of the region in this motion strong material deformation arose near the conical surface that caused the computational grid distortion.

The computation of the given task was performed with local grid reconstructions.

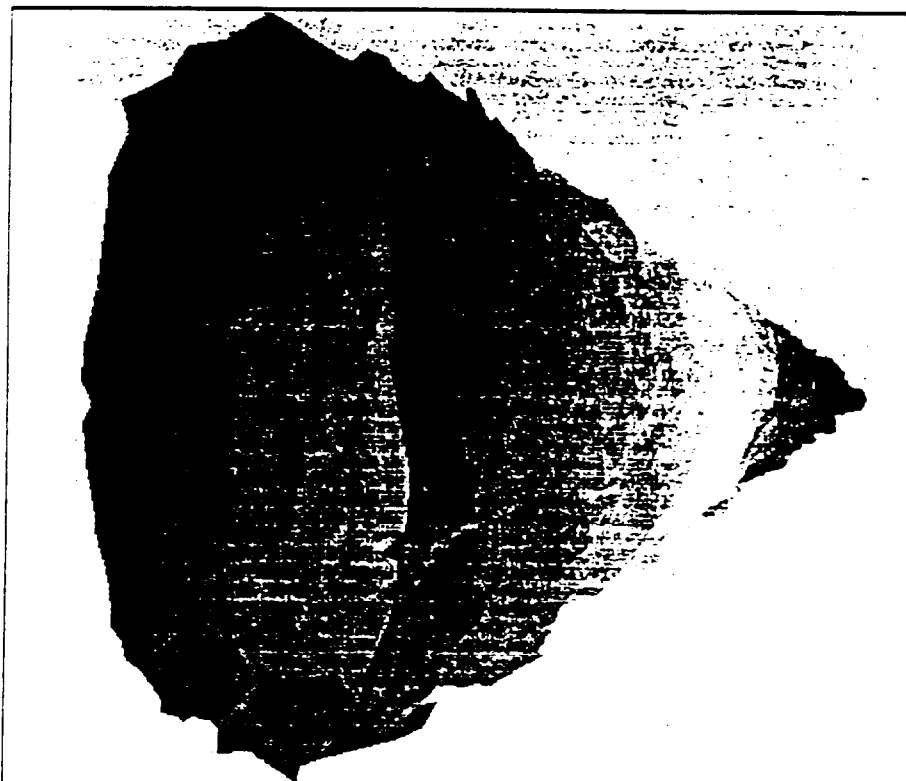
Projections of the task deformed region are given below.



Projection of the task deformed region.



Vortex conical flow field inside the cube.



Conical surface.



# A THREE DIMENSIONAL FINITE ELEMENT FORMULATION FOR THERMOVISCOELASTIC ORTHOTROPIC MEDIA

Marvin A. Zocher

Los Alamos National Laboratory  
XXH, MS-F664  
Los Alamos, NM 87545

## ABSTRACT

A numerical algorithm for the efficient solution of the uncoupled quasistatic initial/boundary value problem involving orthotropic linear viscoelastic media undergoing thermal and/or mechanical deformation is briefly outlined.

**Introduction:** This discussion is concerned with the development of a numerical algorithm for the solution of the uncoupled quasistatic initial/boundary value problem involving orthotropic linear viscoelastic media undergoing thermal and/or mechanical deformation. The algorithm has been incorporated into a three dimensional FE program written by the author. This code is a general purpose tool capable of predicting the response of a mathematical domain to complex loading/thermal histories. Phenomena such as creep, relaxation, and creep-and-recovery can all be predicted using this program. This discussion is based in large part on the work previously presented in Zocher, Groves, and Allen.<sup>1</sup> Related work may be found in Lin and Hwang,<sup>2,3</sup> Lin and Yi,<sup>4</sup> Hilton and Yi,<sup>5</sup> Yi,<sup>6</sup> and Kennedy and Wang.<sup>7</sup>

In the following, a brief statement of the problem of interest is provided. This is followed by a discussion of the conversion through incrementalization of the thermoviscoelastic constitutive equations into a form suitable for implementation in a finite element formulation. Next the finite element formulation which is based on these incrementalized constitutive equations is presented.

**Problem statement:** The problem to be solved, or more precisely, the class of problems for which a method of solution is presented, may be referred to as the linear three-dimensional quasistatic orthotropic uncoupled thermoviscoelastic initial/boundary value problem. The governing field equations are equilibrium.

$$\sigma_{ji,j} + \rho f_i = 0 \quad (1)$$

strain-displacement.

$$\epsilon_{ij} = \frac{1}{2} (u_{i,j} + u_{j,i}) \quad (2)$$

and constitution.

$$\sigma_{ij}(x_k, \xi) = \int_0^\xi C_{ijkl}(x_k, \xi - \xi') \frac{\partial \epsilon_{kl}(x_k, \xi')}{\partial \xi'} d\xi' - \int_0^\xi \beta_{ij}(x_k, \xi - \xi') \frac{\partial \theta(x_k, \xi')}{\partial \xi'} d\xi' \quad (3)$$

with constraints imposed on the solution by the following boundary and initial conditions:

$$\begin{aligned} u_i &= \bar{u}_i & \text{on} & \partial\Omega_1 \\ T_i &= \sigma_{ji}n_j = \bar{T}_i & \text{on} & \partial\Omega_2 \end{aligned} \quad (4)$$

$$\begin{aligned}
\Theta(\mathbf{x}_k, t) &= 0 \\
u_i(\mathbf{x}_k, t) &= 0 \quad \text{for } t < 0 \\
\sigma_{ij}(\mathbf{x}_k, t) &= 0
\end{aligned} \tag{5}$$

In the above,  $f_i$  is the body force,  $T_i$  is the surface traction,  $n_j$  is the unit outer normal on  $\partial\Omega$  (the boundary of the domain  $\Omega$ ), and  $\rho$  is the mass density. The terms  $C_{ijkl}$  and  $\beta_{ij}$  represent the fourth order tensor of orthotropic relaxation moduli relating stress to mechanical strain, and the second order tensor of relaxation moduli relating stress to thermal strain, respectively. The symbol  $\Theta$  is used to represent the difference between the current temperature and a stress-free reference temperature. The reader will recognize from the form of the constitutive relationship that we have assumed the material to be possibly nonhomogeneous, nonaging, orthotropic, and thermorheologically simple. The symbol  $\xi$  in (3) is the reduced time of the time-temperature superposition principle.

**Incrementalization of the Constitutive Equations:** To accomplish the aforementioned incrementalization, we begin by subdividing the time line (reduced time) into discrete intervals and assume that the state of stress is known at the beginning of a time step. We then seek the state of stress at the end of a time step, or equivalently  $\Delta\sigma_{ij}$ . In accomplishing the incrementalization, four approximations and one assumption are made. The nature each of the approximations is the same, that the variation in a given quantity (such as strain or temperature) across a time step is linear. The assumption is that the relaxation moduli can be represented in the form of Wiechert thermomechanical analogs (Dirichlet-Prony series).

The result is that the constitutive equation, given in (3), is converted into an incremental form given by

$$\Delta\sigma_{ij} = C_{ijkl}' \Delta\epsilon_{kl} - \beta_{ij}' \Delta\Theta + \Delta\sigma_{ij}^R \tag{6}$$

where  $C_{ijkl}'$ ,  $\beta_{ij}'$ ,  $\Delta\epsilon_{kl}$ , and  $\Delta\Theta$  are given by:

$$C_{ijkl}' \equiv C_{ijkl\infty} + \frac{1}{\Delta\xi} \sum_{m=1}^{M_{ijkl}} \eta_{ijklm} \left( 1 - e^{-\frac{\Delta\xi}{\tau_{ijklm}}} \right) \quad (\text{no sum on } i, j, k, l)$$

$$\beta_{ij}' \equiv \beta_{ij\infty} + \frac{1}{\Delta\xi} \sum_{p=1}^{P_{ij}} \eta_{ijp} \left( 1 - e^{-\frac{\Delta\xi}{\tau_{ijp}}} \right) \quad (\text{no sum on } i, j)$$

$$\Delta\epsilon_{kl} \equiv R_\epsilon \Delta\xi \quad \Delta\Theta \equiv R_\Theta \Delta\xi$$

and  $\Delta\sigma_{ij}^R$  is given by:

$$\Delta\sigma_{ij}^R = - \sum_{k=1}^3 \sum_{l=1}^3 A_{ijkl} + \sum_{p=1}^{P_{ij}} \left( 1 - e^{-\frac{\Delta\xi}{\tau_{ijp}}} \right) B_{ijp}(\xi_n) \quad (\text{no sum on } i, j)$$

where

$$A_{ijkl} = \sum_{m=1}^{M_{ijkl}} \left( 1 - e^{-\frac{\Delta\xi}{\tau_{ijklm}}} \right) S_{ijklm}(\xi_n) \quad (\text{no sum on } i, j, k, l)$$

$$S_{ijklm}(\mathbf{x}_k, \xi_n) = e^{-\frac{\Delta\xi}{\tau_{ijklm}}} S_{ijklm}(\mathbf{x}_k, \xi_n - \Delta\xi) + \eta_{ijklm} R_\epsilon \left( 1 - e^{-\frac{\Delta\xi}{\tau_{ijklm}}} \right) \quad (\text{no sum on } i, j, k, l)$$

$$B_{1j_r}(x_k, \xi_n) = \epsilon^{-\frac{\Delta t}{t_{j_r}}} B_{1j_r}(x_k, \xi_n - \Delta t) - \gamma_{1j_r} R_{\Theta} \left( 1 - \epsilon^{-\frac{\Delta t}{t_{j_r}}} \right) \quad (\text{no sum on } j_r)$$

This incremental form of the constitutive equations is well suited to implementation in a finite element program.

**Finite Element Formulation:** Using the incrementalization given in (6) in the method of weighted residuals, one arrives in a straightforward manner to a system of algebraic equations of the form:

$$[k^\epsilon][\Delta u^\epsilon] = [f_1^\epsilon] - [f_2^\epsilon] - [f_3^\epsilon] + [f_4^\epsilon] + [f_5^\epsilon] \quad (7)$$

where

$$\begin{aligned} [k^\epsilon] &= \int_{\Omega_\epsilon} [B^\epsilon]^T [C'^\epsilon] [B^\epsilon] dV \\ [f_1^\epsilon] &= \int_{\Omega_\epsilon} [z^{n+1}]^T \rho [f^{n+1}] dV \\ [f_2^\epsilon] &= \int_{\partial\Omega_{2h}^\epsilon} [z^{n+1}]^T [T^{n+1}] dS \\ [f_3^\epsilon] &= \int_{\Omega_\epsilon} [B^\epsilon]^T [\sigma^n] dV \\ [f_4^\epsilon] &= \int_{\Omega_\epsilon} [B^\epsilon]^T [\Delta\sigma^R] dV \\ [f_5^\epsilon] &= \int_{\Omega_\epsilon} [B^\epsilon]^T [\beta'^\epsilon] dV \end{aligned} \quad (8)$$

$[k^\epsilon]$  is referred to as the element stiffness matrix,  $[f_1^\epsilon]$ ,  $[f_2^\epsilon]$ ,  $[f_3^\epsilon]$ ,  $[f_4^\epsilon]$ , and  $[f_5^\epsilon]$ , are contributions to the element load vector due to body forces, surface tractions, stresses at the start of the time step, change of stresses during the time step, and thermal effects, respectively. Summation of the contributions from all elements results in a simple set of algebraic equations of the form:

$$[K] \{\Delta u\} = \{F\} \quad (9)$$

**Conclusions** A three-dimensional finite element formulation has been developed and incorporated into a three-dimensional finite element code. This development provides the analyst with a versatile tool with which he can easily predict the response of an orthotropic body (isotropic and transversely-isotropic bodies are considered subsets) to a wide range of loading/temperature histories. Demonstrative example problem solutions can be found in reference 1.

#### References:

1. Zocher, M.A., S.E. Groves and D.H. Allen, 'A Three-Dimensional Finite Element Formulation for Thermo-viscoelastic Orthotropic Media,' *International Journal for Numerical Methods in Engineering*, Vol. 40, No. 12, 1997, pp. 2267-2288.
2. Lin, K.Y. and I.H. Hwang, 'Thermo-viscoelastic analysis of composite materials,' *Journal of Composite Materials*, Vol. 23, 1989, pp. 554-569.
3. Lin, K.Y. and I.H. Hwang, 'Thermo-viscoelastic response of graphite/epoxy composites,' *Journal of Engineering Materials and Technology*, Vol. 110, 1988, pp. 113-116.
4. Lin, K.Y. and S. Yi, 'Analysis of interlaminar stresses in viscoelastic composites,' *International Journal of Solids and Structures*, Vol. 27, 1991, pp. 929-945.

5. Hilton, H.H. and S. Yi. 'Anisotropic viscoelastic finite element analysis of mechanically and hygrothermally loaded composites.' *Composites Engineering*, Vol. 3, 1993, pp. 123-135.
6. Yi, S.. 'Thermoviscoelastic analysis of delamination onset and free edge response in laminated composites.' *AIAA Journal*, Vol. 31, 1993, pp. 2320-2328.
7. Kennedy, T.C. and M. Wang. 'Three-dimensional, nonlinear viscoelastic analysis of laminated composites.' *Journal of Composite Materials*, Vol. 28, 1994, pp. 902-925.

**3D PARALLEL PROGRAM FOR NUMERICAL SOLUTION  
OF GAS DYNAMICS PROBLEMS WITH HEAT CONDUCTION  
ON DISTRIBUTED-MEMORY COMPUTERS.  
RESULTS OF COMPUTATIONS ON MP-3, MEIKO CS-2  
AND SP2 COMPUTERS.**

Sofronov I.D., Voronin B.L., Burnev O.I., Bykov A.N.,

Yerofeev A.M., Skrypnik S.I.

(VNIEF)

D.Nielsen, Jr., M.Uyemura, R.Evans, S.Brandon,

M.Nemanic, C.Okuda

(LLNL)

The goal of this effort is development of a 3D parallel program for numerical solution of gas dynamics problems with heat conduction on distributed-memory computer systems satisfying the condition of the numerical result independency on the number of processors involved. The program was developed on the eight-processor computer system MP-3 developed by VNIEF and was adapted by joint efforts of VNIEF and Lawrence Livermore National Laboratory (LLNL) employees to the massively parallel computer Meiko CS-2 located in LLNL. A large series of numerical experiments was conducted on the Meiko CS-2 computer with a various number of processors, up to 256, and parallelization efficiency estimations depending on the number of the processors and other parameters were made.

### INTRODUCTION

VNIEF Mathematical Division has gained wide experience of parallel computations. Parallel computations of 2D problems were conducted on multiple computer complexes BESM-4, BESM-6 and Elbrus-1 [1,2]. Later on parallel application programs were developed on the multiprocessor computer Elbrus-2, i.e. shared main memory computer [7]. Recently, with the advent of the eight-processor distributed-memory computer MP-3 [8] the problem of parallel program development for such computers has become urgent.

The problem of program development for massively parallel distributed-memory computers requires development of efficient parallelization algorithms and methods taking

into consideration the specificity of these computers. Some of the numerical schemes which have showed themselves to advantage appear to be well parallelizable, others contain a non-parallelizable part.

So in some cases achievement of a high parallelization performance is possible only when the numerical methods used for the problem solution have been considerably developed.

## 2. SOLUTION METHOD

Recently we have pursued the development of the parallel program based on the Eulerian-Lagrangian technique for numerical solution of 3D non-stationary gas dynamics problems taking into account heat conduction /3,4/.

The heat conducting medium motion is described with the differential equation system of gas dynamics taking into account heat conduction either in the single- or multi-component formulation.

Implicit approximations combined with the direction-splitting method /5/ lead both in the case of the heat conduction equation and in the case of gas dynamics equations to the set of finite-difference equations of the form:

$$A \cdot \bar{u}^{n+1} = B \cdot \bar{u}^n,$$

$\bar{u}$  — desired grid function,  $A$  — three-diagonal matrix.

The three-diagonal matrix equation system is solved with the sweep method /6/.

## 3. PARALLELIZATION METHODS

The development of techniques and programs for computing complex 2D and then 3D problems on available integrated computers has been always paid much attention to at VNIIEF Mathematical Division.

At each of these computer development phases the question of adequate problem representation in a form accessible for parallel processing was solved in its own way.

The inter-machine computer systems were used for large-block parallelization through problem geometry segmentation into fragments each of which was computed in the parallel mode on its own computer, while the fragment interaction was through the boundary condition communication between computers involved in the computer system.

On the multiple computer complex Elbrus-2 the parallelization algorithms both with static and dynamic balancing of processor load were implemented. In both the cases the timestep computation scheme was a sequential computation of all the three spatial directions. The computation of each spatial direction was a set of "one-dimensional" problems. At the static balancing the set of the "one-dimensional" problems was split over processors (the problem decomposition by parallelepipeds) and each computer computed a fixed set of computational grid columns.

At the dynamic balancing each processor computed a "free" uncomputed column at a given time.

We use the problem geometry decomposition to arrange the massively parallel computations on distributed-memory computer systems.

We have developed two basically different approaches to the massively parallel computation arrangement. The first approach uses the timestep reconstructable decomposition of the 3D data matrix and is an extension of the parallelization algorithms for multi-processor shared main memory computer systems. The decomposition change consists in double or triple transposition of the 3D data matrix distributed over multi-processor computer nodes. The second approach is based on using the 3D data matrix non-reconstructable within the timestep.

At the first approach the commutation system load per one processor increases with the increasing number of processors, at the second this load is invariable, but the initial computational algorithms contain a non-parallelizable part. Achievement of a high parallelization efficiency (close to 100% up to 100 processors) required combination of the computation (arithmetic operation) with communications (communication operation) at the first arrangement approach and a considerable sweep algorithm modification at the second.

The sweep formulas are recurrent, i.e. are functions of running computation in the forward and backward directions.

We considered three methods of sweep parallelization.

The first method is using the "counter-sweep" formulas.

Implementation of this method provides a speedup of 2 at the sweep formula computation which means complete parallelization at the number of processors in the "line"

equal to 2: when the processors in the "line" number more than 2, we will have losses in the parallelization efficiency as earlier.

The second method is the sweep pipelining.

Taking into account that the computation of each spatial direction should implement the sweep formulas on a line set, one can begin the forward run on the following lines when waiting for the backward sweep run for a given line. Implementation of this method brought out a high parallelization efficiency at the number of processors in the "line" on the order of several hundreds.

The third method is the sweep parallelization proposed in the paper by Yanenko et al. 10.

This method implementation also showed a high parallelization efficiency.

The developed algorithms were used to make a parallel program for numerical solution of 3D gas dynamics problems with heat conduction for massively parallel computers. The program was developed on the eight-processor computer system MP-3 using the MPI Standard for the interprocessor communication arrangement.

The block-matrix type computational grids can be employed to solve problems with using the large-block parallelization algorithms between blocks and each block being distributed over processors using one of three decomposition types: lines, columns, cubes.

The first decomposition type corresponds to splitting the problem geometry by one spatial direction, the second to that by two and the third to that by three spatial directions.

The program is arranged so, that each problem can be computed on an arbitrary number of computer system processors. The computed data is independent on the number of the processors involved in the problem solution.

#### **4. SETTING UP TEST PROBLEM COMPUTATIONS AND THEIR RESULTS**

The test demonstration problems of three-axes gas ellipsoid expansion into vacuum and problem of heated homogeneous cube cooling /3,4/ were taken for numerical experiments.

In all the computations the numerical result error was no more than  $1-3\%$  relative to the exact values.

A computation series was conducted for numerical study of the parallelization efficiency for various problem geometry decomposition methods, for two modes of processor loading and depending on the ratio of the arithmetic and communication operations.

Some results demonstrating the parallelization efficiency are presented in the figures. (See. Application).

## 5. CONCLUSIONS

Analyzing the results obtained, we can infer that we managed to develop efficient parallelization methods and 3D parallel program allowing to bring out a very high scalability (close to the theoretic) on massively parallel distributed memory computer systems involving ~100-300 processors.

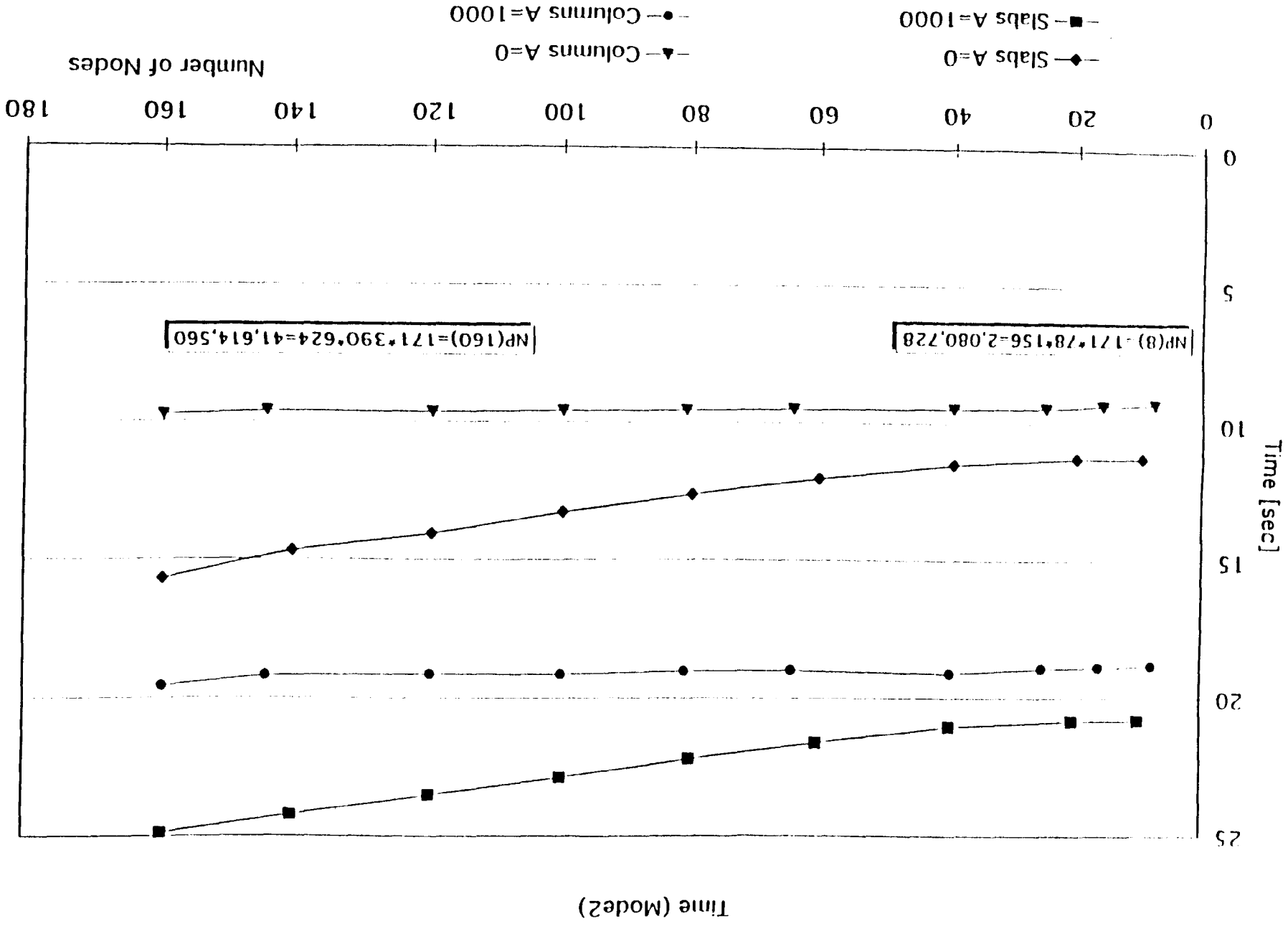
Apparently, further work is needed on development both of parallelization methods and of the parallel program itself in order to retain this scalability level on computer systems involving thousands of processors.

To conclude with, two important circumstances should be mentioned relating to development of programs for massively parallel computers. The first is the data input output problems. We took and implemented the principle of distributed formation of the initial data and output data files of a problem. This allowed to avoid bottlenecks relating to input output, especially at the parallel program debugging and testing phase where it is necessary to make a great number of relatively short computer runs. The second is that parallel program debugging and quality study requires special toolkit: parallel program debuggers and profilers.

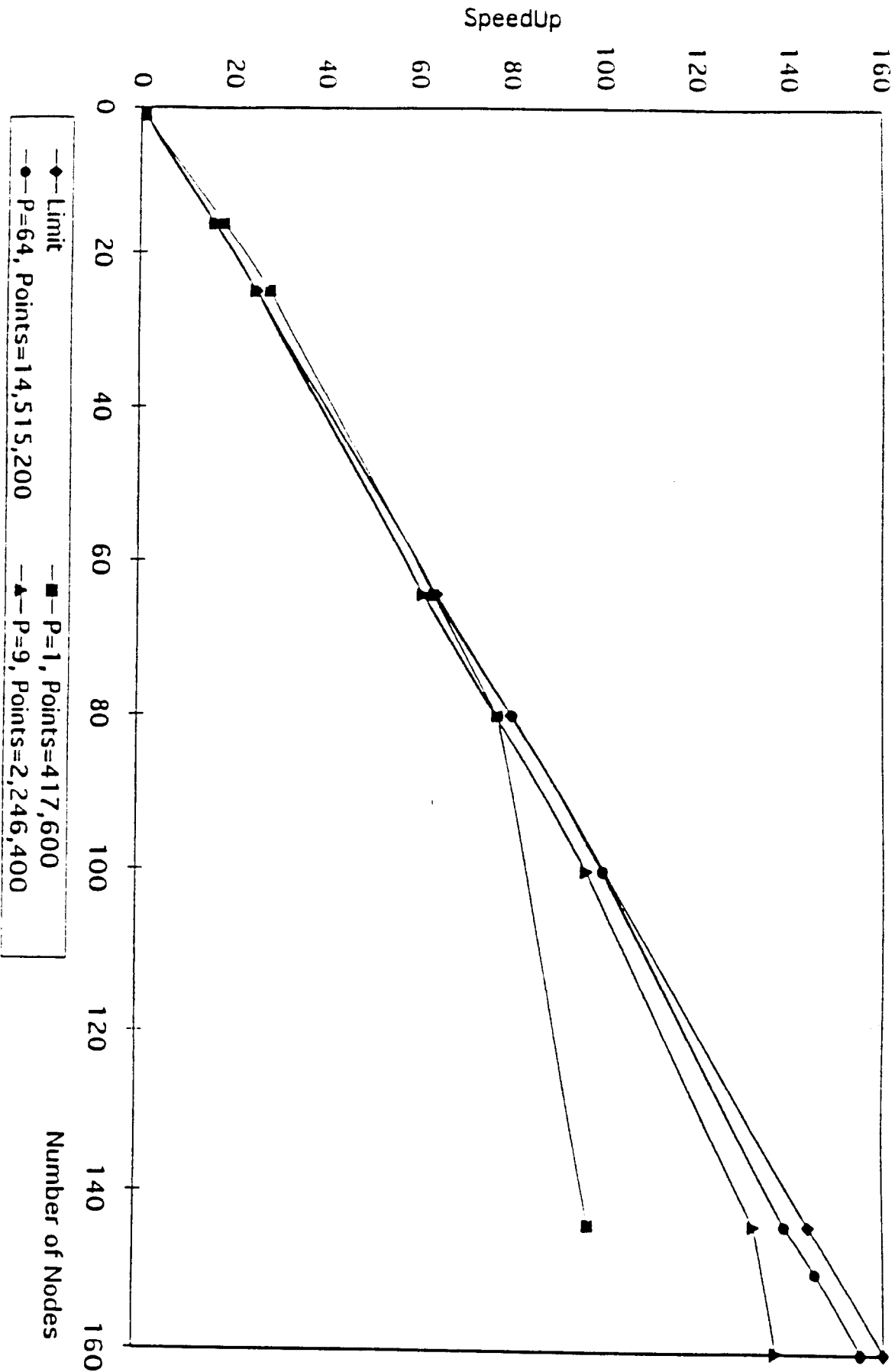
## REFERENCES

1. Bartenev Yu.G., Gorbunov V.N., Yeliseyev G.M. et al. Arrangement of parallel computations on multi-machine system BESM-6. Proc.6th Conference on BESM-6 computer. Tbilisi, USSR Academy of Sciences Computer Center.

2. Bartenev Yu.G., Demin I.V., Lukin A.I., Sarayev V.A., Sofronov I.D. 2D non-stationary continuum mechanics problem computation distribution on special processors Elbrus-1 in SIGMA system. VANT. Ser. Met. i Progr. Chisl. Resh. Zad. Mat. Fiziki. 1988. No.1, p.70-74.
3. Voronin B.L., Skrypnik S.I., Sofronov I.D. Eulerian-Lagrangian technique for numerical solution of 3D time-dependent problems of gas dynamics with account of heat conduction. VANT. Ser. Met. i Progr. Chisl. Resh. Zad. Mat. Fiziki. 1988. No.3, p.3-8.
4. A.N.Bykov, B.L.Voronin, A.G.Kozub, S.I.Skrypnik, I.D.Sofronov, A.V.Urm. Numerical Simulation of Heat Conductive Medium Spatial Shock - Wave Movements in Eulerian - Lagrangian Coordinates. //Russian/U.S. Weapons Laboratories Introductory Technical Exchange in Computational and Computer Science.
5. Yanenko N.N. The fractional step method for solving multi-dimensional computational physics problems. Novosibirsk, Nauka Publishers, 1967.
6. Lokutsievsky O.V. Numerical methods for solving partial differential equations/ Uspekhi Matematicheskikh Nauk, 1956, v.XI, No.3.
7. Abramov N.N., Kukhtin V.M., Lukin A.I. et al. Multi-user network. Computational simulation technology. Collected scientific works. Ed.by V.P.Ilyin. Novosibirsk, 1990, p.12-19.
8. Stepanenko S.A., Gusev V.A., Lyakishev A.M. et al. Multi-processor computer systems MP-X-Y. In: Issues of mathematical simulation, computational mathematics and information science. Moscow- Arzamas-16, 1994, p.101-103.
9. Voronin B.L., Kazarin A.A., Skrypnik S.I. Parallel algorithms for numerical solution of gas dynamics problems with heat conduction with the method of splitting by directions on shared-memory computer systems. VANT, No.3, 1997, p.1-6.
10. Yanenko N.N., Kovalev A.N., Bugrov A.N., Shustov G.V. On parallel computation arrangement and sweep "parallelization"// In: "Numerical Methods of Continuum Mechanics". Novosibirsk, 1978, v.9, No.7, p.139-146.



# SpeedUp (Mode 1)



Comparing of MP3 with Meiko



## Comparison of Meiko with SP-2

Meiko		SP-2				
Eff [%]	Sp	Time	Nodes	Time	Sp	Eff [%]
100	1	632	1	496	1	100
114.3	11	55.3	10	52.4	9.45	94.5
108.3	22	29.5	20	26.7	18.5	92.7
104.5	31	20.2	30	18.2	27.2	90.8

# Time Dependent View Factor Methods

Ronald C. Kirkpatrick

Los Alamos National Laboratory

**Abstract :** View factors have been used for treating radiation transport between opaque surfaces bounding a transparent medium for several decades. However, in recent years they have been applied to problems involving intense bursts of radiation in enclosed volumes such as in the laser fusion hohlraums. In these problems, several aspects require treatment of time dependence.

## View Factors

View factors are commonly used to compute the transport of radiation through a vacuum between sets of opaque surfaces. A view factor is simply a coupling coefficient that gives the fraction of radiation emitted from one surface that is intercepted by another, assuming that the emission is isotropic [1]:

$$C_{12} = \iint d_{12}^{-2} \cos \alpha_1 \cos \alpha_2 dA_1 dA_2 ,$$

$$VF_{12} = C_{12} / A_1 ,$$

where  $d_{12}$  is the distance between the surfaces,  $\alpha$  is the angle of incidence measured from the normal to the surface, and  $A$  is the surface area. For simple problems, conservation can be insured down to round-off accuracy, but the accuracy of the view factors depends on the method used for computing them, some of which are restrictive. Here we are concerned not with the methods for computation of the view factors, but with methods for treating time dependence in view factor codes.

In the simplest view factor codes the geometry is fixed, specified albedos (the fraction of incident radiation that is diffusely reflected or emitted) are used to describe the surface properties, and the times of flight between the surfaces are ignored. However, for many physical problems these simplifications are unsatisfactory. First, the surfaces may have anisotropic properties. Second, the surface properties may be time dependent or depend on the condition of the surface, which may change with time. For some problems (e.g., some radiation symmetry studies) it may not be necessary to treat the time dependence of the surface properties, but in most cases changing surface properties are very important. Third, the geometry can change significantly when the surfaces move (e.g., in response to rapid heating), and fourth, for some problems (e.g., illumination of an interstellar cloud by a supernova) the radiation may be rapidly varying on a time scale shorter than the time of flight between surfaces. Finally, many problems involve a tenuous medium between the surfaces [2].

For the case of anisotropic surfaces properties it is possible to use angular bins, but it is often more convenient to use angular moments of view factors:

$$C_{12}^n = \iint d_{12}^{-2} \cos^{n+1} \alpha_1 \cos \alpha_2 dA_1 dA_2 .$$

For other problems, more detailed treatment of time changing properties of the surfaces must be considered. For example an opaque surface may absorb and re-emit radiation. If

that surface is optically thick and has uniform temperature the radiation will be Planckian. but this is seldom the case for a dynamic problem. It can be shown that for planar geometry, the first angular moment ( $n=1$ ) of the view factor is sufficient to treat the anisotropy due to a simple gradient in the source function:

$$\mu dI/d\tau = -I + S$$

where  $\mu = \cos \alpha$ ,  $I$  is the radiation intensity,  $\tau$  is the optical depth, and  $S$  is the source function. This has the formal solution:

$$I = - \int_{\tau} S e^{(\tau-\tau_0)/\mu} d\tau/\mu,$$

So that if  $S = S_0 + S'\tau$ , then

$$I_{out} = - \int_{\tau} (S_0 + S'\tau) e^{-\tau/\mu} d\tau/\mu \quad (\mu < 0),$$

which leads to

$$I_{out} = S_0 + S' \cos \alpha.$$

Thus, the first moment of the view factor is sufficient for treating a constant gradient of the source function in an opaque surface. Absorbing surfaces exhibit limb brightening, which is analogous to limb darkening seen for emitting surfaces such as the sun. This can lead to radiation energy flowing in the direction opposite that which would be dictated by energy density gradients computed in a diffusion code, which emphasizes the need for matching the computational technique to the physical problem.

There are some cases in which the time of flight becomes important, and also some work has been done on including the effect of a (more or less complex) medium between the surfaces [2]. Henceforth, we confine our discussion to time dependent surface properties and handling the effects of time of flight. We will discuss some specific models, but there are many special applications of view factor codes that require other approaches. We only suggest ways to handle changing geometry, since we have never implemented this capability.

### Models for Absorbing/Re-emitting Surfaces

While there are many ways to model changing surface properties, one of practical interest for inertial confinement fusion (ICF) is the use of non-linear heat diffusion [3]. In ICF hohlraum problems [4], soft X-ray radiation is absorbed by the surface which (as it heats up) emits soft X-ray radiation with a different spectrum, until it comes into equilibrium with the other surfaces that couple with it. Once equilibrium is obtained (if ever), the emission comes into balance with the incident radiation, so the effective albedo is unity. Otherwise, it differs from unity in a complex way that depends on both the amount and rate of the incident radiation.

There are several options for modeling these types of surfaces. One that has received only a little attention is the uniform flux approximation [5]. It is based on the observation that in the similarity solution for the non-linear heat diffusion equation with a power law opacity,

treated. Thus effects such as limb darkening (as is the case for the sun) and limb brightening can be included.

### **Time of Flight**

Only a little work has been done on including the time of flight effects in view factor codes. This is because for most practical problems it is not important. However, for the case of sudden illumination of an interstellar cloud by a supernova, or some similar physical problem, the distant observer sees the cloud first illuminated and then the light scattered from the cloud reaching the distributed parts of the cloud. Analytic solutions for the case of a spherical shell surrounding a central pulsed source have been obtained [7,8]. If the scattering has a high effective albedo, then multiple brightenings may occur. Similar behavior can occur in fast diagnostics for ICF, etc..

One successful method for treating time of flight uses temporal bins associated with the destination surface. Here, the energy emitted by each surface during a time step is apportioned to the proper destination surface in accord with the view factor for each pair, and then the portion is divided between two temporal bins for the destination surface based on the centroid time of flight of flight between the pair. Between each time step, the energies in all the bins are shifted, so that after several (constant) time steps the energy emitted earlier arrives at the destination surface. Numerical results compare favorably with the analytic results of Hoffman [7] and Zahrt [8]. An attempt to improve on this approach by using a time of flight weighted by the contribution to the view factor gave nonsensical results. For the case of a cylindrical pipe the radiation using the weighted times of flight can travel at super-luminal speeds to the other end. Only in the case of very few surfaces does the use of weighted times of flight seem to improve the relevant conservation property: the sum of the products of the distances between surface pairs and the view factors should be  $4\pi$  times the volume.

The above method is restrictive, requiring a constant time step. In addition, no distinction is made between the various source surfaces, so information on the angle of incidence for the radiation arriving at the destination surface is lost. Retention of this information would require a set of temporal bins for each pair of surfaces. Memory requirements would then limit the total number of surfaces that could be used in the problem, but the faithfulness to the physics would be greatly improved. However, another way to retain the angular information with less expense for memory is to use angular moments of view factors, using a destination based set of temporal bins for each moment included. To my knowledge, this has not been done.

### **Changing Geometries**

For most problems that view factor methods have traditionally been applied to, the geometry is fixed. This means that the view factors can be computed once and used over and over again to solve the problem. However, there are some problems that are most efficiently handled by view factor methods which do have changing geometries during the course of the solution. One crude approach would be to simply recompute the view factors at intervals, but since the expense for computing the view factors for  $N$  surfaces goes as  $N^2$  at best, and as  $N^3$  for cases with a great deal of partial blockage (i.e., shadowing), this could be very expensive for complex problems requiring a large number of surfaces.

However, there is some hope for handling problems involving changing geometries. First, it should be noted that for surfaces with no blockage the straight-forward double areal integral for computing view factors can be transformed into a double line integral [9]. This

the flux deep into the surface is nearly uniform up to the head of the diffusion front, where it diminishes rapidly to zero. If one neglects the radiation energy density ( $aT^4$ ) relative to internal energy of the material, an integral relation connects the flux history with the depth of penetration for a power law opacity dependence on temperature ( $\kappa = \kappa_1 \theta_1^n / \theta^n$ ) can be found:

$$E(t) = \int c_v T(x,t) dx = (n+4) c_v x_0(t) T_0(t) / (n+5),$$

$$x_0(t) T_0(t) = \sqrt{2K} \int T_0^{n+5} dt ,$$

where  $x$  is the depth (in gm/cm<sup>2</sup>),  $K = 4ac(n+5) / (n+4)^2 c_v \kappa_1 \theta_1^n$ ,  $T_0(t)$  is the boundary temperature, and  $x_0(t)$  is the penetration depth. This leads to

$$f(t) = K T_0^{n+5} / \sqrt{\int T_0^{n+5} dt} ,$$

but since  $f(t) = F(t) - \sigma T_0^4(t) ,$

$$F(t) = \sigma T_0^4 + K T_0^{n+5} / \sqrt{\int T_0^{n+5} dt} .$$

Inversion of the results from the last equation provides  $T_0(F(t), t)$ . Use of the uniform flux approximation is restricted to a constant or continually increasing temperature at the surface, which this is typically the case for ICF, because it fails badly when the boundary temperature starts to decrease. It is also possible to get a solution for the case of an arbitrary dependence of opacity on temperature.

Another option is to do a radiation hydrodynamics calculation for each surface and couple them to each other through the view factors. However, a simplistic implementation of this approach may compromise some important physics. Some years ago a modified radiation diffusion treatment was developed to allow the in-depth absorption of radiation from a hot source, yet utilize efficient radiation diffusion in the deeper zones in a 1-D problem [6]. Starting with the formal solution

$$I(\tau_0, \mu) = - \int_{\tau} S(\tau) e^{-(\tau-\tau_0)/\mu} d\tau/\mu ,$$

The intensity is split into direct and diffusion parts:  $I = I_{dir} + I_{diff}$ , where  $I_{dir} = I_{inc} e^{-\tau/\mu}$ .  $I_{inc}$  is the intensity of the radiation incident on the surface, and  $I_{diff}$  is the contribution to the intensity of the radiation that due to the source function inside the opaque surface. Integration over angle to get the flux results in:  $F = F_{dir} + F_{diff}$ , where

$$F_{dir} = \int_{\mu} I_{inc}(\mu) e^{-\tau/\mu} d\mu$$

and  $F_{diff} = 4\pi S'(\tau) \{ 1 - (1 + \tau/4) e^{-\tau} + \tau^2 E_2(\tau)/4 \} / 3 .$

Rather than use a flux or temperature boundary condition as is often done for diffusion problems, the exponentially attenuated radiation that should be absorbed by each zone was calculated and used as a source of heating. Properly applied, this allows the effect of both hot Planckian sources and non-Planckian sources, as well as an anisotropic distribution of sources to be treated. An additional modification allows the anisotropic re-radiation to be

means that if a surface changes shape (e.g., is warped) but does not change its boundary as seen from the other surface of the pair, then the view factor doesn't change. Second, view factors scale. If two surfaces are moved apart and expanded to keep the angular outline the same, then their view factors are unchanged. Therefore, for a geometry that changes due to a uniform expansion (or contraction) of the whole problem, all the view factors remain the same. If a surface is uniformly tilted, then to first order the change in the view factor is proportional to the change in the cosine of the angle between the normal of the tilted surface and the line between them. Finally, the viewfactor for a surface that is so warped as to slope across its apparent original boundary changes only in proportion to that part which slopes across the original boundary. This means that small changes in geometry can be handled by simply scaling the view factors appropriately. One can periodically recalculate the view factors to track the accuracy as scaling effects accumulate over many time steps.

## References

- [1] C.O. Mackey, L.T. Wright, Jr., R.E. Clark, and N.R. Gray, "Radiant Heating and Cooling. Part I, Angle Factors for Calculations on Radiant Heating and Cooling", Cornell U. Engr. Expt. Station, Bull. 34 (1943); R. Siegel and J.R. Howell, "Thermal Radiation Heat Transfer", McGraw Hill, New York (1960).
- [2] D. J. Drake, "A View Factor Method for Solving Time-dependent Radiation Transport Problems Involving Fixed Surfaces with Intervening, Participating Media", J. Computational Physics 87 (1990) 73.
- [3] R.E. Marshak, Los Alamos Scientific Laboratory Report LA-230 (1945); also, "Effect of Radiation on Shock Wave Behavior", Physics of Fluids 1 (1958) 24.
- [4] A. Caruso, "High Gain Radiation-Driven Targets", Inertial Confinement Fusion Course and Workshop (Varenna, Italy, 1988. A. Caruso and E. Sindoni, ed.)
- [5] A.G. Petschek, R.E. Williamson, and J.K. Wooten, "The Penetration of Radiation with Constant Driving Temperature", University of California Los Alamos National Laboratory Report LAMS-2421 (1960); R. Pollock, "Radiation Penetration under Monotone Increasing Boundary Temperature", Los Alamos internal memo (1971).
- [6] A.J. Cooper, "Combining Radiative Transfer and Diffusion", University of California Los Alamos National Laboratory Report LA-UR-82-573 (1982).
- [7] N. Hoffman, "Exact Solutions to a Time-Dependent Vacuum Transport Problem", J. Quantitative Spectroscopy and Radiation Transfer 34 (1985) 435.
- [8] V. Faber, and J.D. Zahrt, Transport Theory and Statistical Physics 21 (1992) 151.
- [9] A.B. Shapiro, "FACET, A Radiation View Factor Computer Code for Axisymmetric 2-D and 3-D Geometries with Shadowing", University of California Lawrence Livermore National Laboratory Report UCID-19887 (1983).



VARIATIONAL-DIFFERENCE FLOW-TYPE SCHEME  
FOR 3D DIFFUSION EQUATION ON GRIDS  
OF ARBITRARY HEXAHEDRONS.

Bazhenov S.V., Belayaev S.P., Bondarenko Yu.A., Gorev V.V., Korolkova T.V., Pevnaya P.I.

The paper addresses the construction and numerical study of difference scheme for 3D equation of non-stationary linear isotropic and anisotropic diffusion by variational method using the diffusion equation of flow type ( A.P.Favorsky method generalized for a 3D anisotropic case [1]).

A linear 3D diffusion equation is under consideration:

$$Q \cdot \frac{\partial U}{\partial t} = -\text{div } \bar{W}, \quad x \in \Omega, \quad (1)$$

where  $\bar{W} = (W_1, W_2, W_3)$  is the heat flow vector whose components are equal to

$$W_i(t,x) = - \sum_j D_{ij}(t,x) \cdot \frac{\partial U}{\partial x_j}, \quad i=1,2,3. \quad (2)$$

Here  $U$  is temperature,  $Q$  is volume heat capacity,  $D_{ij}$  is a symmetrical positively defined matrix of diffusion coefficients, in anisotropic case  $D_{ij} = D \cdot \delta_{ij}$ . The boundary is specified by a flow and/or flow-temperature combination ( including only temperature)

$$\langle \bar{W}(t,x) \cdot \bar{n}(x) \rangle = v(t,x), \quad x \in \Gamma_2 = \partial\Omega; \quad (3)$$

$$\gamma(t,x) \cdot \langle \bar{W}(t,x) \cdot \bar{n}(x) \rangle + \beta(t,x) \cdot U(t,x) = f(t,x), \quad x \in \Gamma_1 = \partial\Omega \setminus \Gamma_2. \quad (4)$$

Here  $\bar{n}(x)$  is the external normal,  $\langle \bar{a} \cdot \bar{b} \rangle$  is a scalar product. (4) assumes that  $\beta \neq 0, \gamma \cdot \beta \leq 0, \forall x \in \Gamma_1$ .

Similarly to [1], both the flow definition (2) and boundary condition (4) result simultaneously from minimality condition for convex functional

$$\Phi(\bar{W}) = \int_{\Omega} \left( \sum_{i,j} L_{ij} \cdot W_i \cdot W_j - 2U \cdot \text{div } \bar{W} \right) d\Omega - \int_{\Gamma} \frac{\gamma \cdot \langle \bar{W} \cdot \bar{n} \rangle^2 - 2f \langle \bar{W} \cdot \bar{n} \rangle}{\beta} d\Gamma. \quad (5)$$

where  $L = \{L_{ij}\}$  matrix is reverse to  $D = \{D_{ij}\}$  matrix. In the case, when computing the minimality condition for functional (5) it is only the  $\bar{W}$  flow that is varied, while the boundary condition (3) is accounted as an additional restriction, i.e. normal flow variations are assumed to be equal to zero on the boundary section  $\Gamma_2$ .

To solve the problems (1)-(4) numerically we use the grid composed of arbitrary hexahedral cells whose faces might be represented by linear surfaces stretched over the straight edges of hexahedron. The  $U_{i,j,k}$  temperature, specified in cell centers, is an average volume temperature in cells. The volume of hexahedral  $V_{i,j,k}$  cell is found by familiar formulas, for example, [2]. Normal components  $W_{\xi_{i,j,k}}, W_{\zeta_{i,j,k}}$  and  $W_{\eta_{i,j,k}}$  for the  $\bar{W}$  heat flows, averaged over the surfaces of corresponding faces, are specified on hexahedron faces having  $S_{\xi_{i,j,k}}, S_{\zeta_{i,j,k}}$  и  $S_{\eta_{i,j,k}}$  areas. The law of conservation (1) is approximated in each cell in the regular way (see Fig.1)

$$Q_{i,j,k} \frac{U_{i,j,k}^{n-1} - U_{i,j,k}^n}{\Delta t} = -\text{DIV}_{i,j,k} \bar{W}^{n-1} \quad (6)$$

$$\text{DIV}_{i,j,k} \bar{W}^{n-1} = \frac{1}{V_{i,j,k}} (S_{\xi 2} \cdot W_{\xi 2} - S_{\xi 1} \cdot W_{\xi 1} + S_{\eta 2} \cdot W_{\eta 2} - S_{\eta 1} \cdot W_{\eta 1} + S_{\zeta 2} \cdot W_{\zeta 2} - S_{\zeta 1} \cdot W_{\zeta 1}) \quad (7)$$

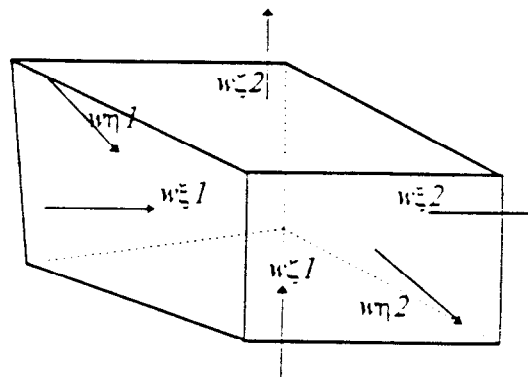


Fig. 1

To approximate the ratios (2) and boundary conditions (4) it is necessary to approximate functional (5) on the grid and to compute its minimality condition. The surface integral in (5) is substituted by an evident sum of  $\Phi_{\text{ond}}$  over the boundary edges of quadratic expressions from normal flow components. Volume integral (5) over the volume of one hexahedral cell is substituted by the expression

$$\Phi_{i,j,k} = V_{i,j,k} \left( \frac{1}{8} \sum_{m=1}^8 \left\langle \bar{W}_m \cdot \bar{L}_{i,j,k} \bar{W}_m \right\rangle - 2 \cdot U_{i,j,k}^{n-1} \cdot \text{DIV}_{i,j,k} \bar{W}^{n-1} \right) \quad (8)$$

where  $m$  is the number of hexahedral cell vertex, while the difference flow divergence is specified by formula (7). Vector flow  $\bar{W}_m$  in (8) at each vertex is computed independently by solving the system of equations

$$W_{\xi} = (\bar{W} \cdot \bar{e}_{\xi}) \quad , \quad W_{\zeta} = (\bar{W} \cdot \bar{e}_{\zeta}) \quad , \quad W_{\eta} = (\bar{W} \cdot \bar{e}_{\eta}) \quad ,$$

where  $\bar{e}_{\xi}$ ,  $\bar{e}_{\zeta}$  and  $\bar{e}_{\eta}$  are identity normals to hexahedron faces meeting in one given common vertex.

Difference equations result from differentiating the functional over the flows and making the derivatives equal to zero

$$\frac{\partial \left( \sum_{i,j,k} \Phi_{i,j,k} + \Phi_{\text{bnd}} \right)}{\partial W_{\xi_{i,j,k}}} = 0 \quad , \quad \frac{\partial \left( \sum_{i,j,k} \Phi_{i,j,k} + \Phi_{\text{bnd}} \right)}{\partial W_{\zeta_{i,j,k}}} = 0 \quad , \quad \frac{\partial \left( \sum_{i,j,k} \Phi_{i,j,k} + \Phi_{\text{bnd}} \right)}{\partial W_{\eta_{i,j,k}}} = 0 \quad .$$

Then  $U^{m-1}$  temperatures are excluded in the equations obtained by the equation of balance (6) and that leads to equations for normal flow components

$$A_{\xi_{i,j,k}} \cdot W_{\xi_{i-1,j,k}} - B_{\xi_{i,j,k}} \cdot W_{\xi_{i,j,k}} + C_{\xi_{i,j,k}} \cdot W_{\xi_{i+1,j,k}} = F_{\xi_{i,j,k}} (W_{\zeta}, W_{\eta}, U^n) \quad ;$$

$$A_{\zeta_{i,j,k}} \cdot W_{\zeta_{i,j,k-1}} + B_{\zeta_{i,j,k}} \cdot W_{\zeta_{i,j,k}} + C_{\zeta_{i,j,k}} \cdot W_{\zeta_{i,j,k+1}} = F_{\zeta_{i,j,k}} (W_{\eta}, W_{\xi}, U^n) \quad ;$$

$$A_{\eta_{i,j,k}} \cdot W_{\eta_{i,j,k-1}} + B_{\eta_{i,j,k}} \cdot W_{\eta_{i,j,k}} + C_{\eta_{i,j,k}} \cdot W_{\eta_{i,j,k+1}} = F_{\eta_{i,j,k}} (W_{\xi}, W_{\zeta}, U^n) \quad .$$

This system of equations is computed by block iterations according to Seidel, each iteration uses the runs along the corresponding grid line, the right parts are computed each time with the values known. When iterations are completed and flows are defined, new temperatures are computed from the equations of balance (6), (7). Since the functional being minimized is strictly convex, the iteration process of the kind is sure to always converge. The test problems computed on orthogonal and rather oblique grids testify to the number of such iterations to be approximately proportional to the square root of Courant number. In isotropic case with a grid composed of rectangular parallelepiped, the constructed difference scheme allows to exclude the flows completely and to obtain an ordinary seven-point implicit scheme.

To exemplify the accuracy of the constructed difference scheme we would refer to computation results of a problem on cube cooling, both isotropic [3] and anisotropic. At the initial moment  $t=0$  inside the cube we have  $\Omega = \{0 < x < L, 0 < y < L, 0 < z < L\}$ ,  $L = 1$ , the temperature is constant  $U(x,y,z,0) = 1$ ,  $(x, y, z) \in \Omega$ , the boundary is specified by the temperature  $U(x, y, z, t) = 0$ ,  $(x, y, z) \in \partial\Omega$ ,  $t > 0$ . Heat capacity  $Q=1$ , matrix of diffusivity factors is diagonal  $D_{ij} = D_i \cdot \delta_{ij}$ , with  $D_1 = D_2 = D_3 = 1$  for isotropic case and  $D_1 = 3$ ,  $D_2 = D_3 = 1$  for anisotropic case. A accurate solution of the problem looks like follows:

$$U^a(x,y,z,t) = \psi(x, L, D_1, t) \cdot \psi(y, L, D_2, t) \cdot \psi(z, L, D_3, t) \quad ;$$

$$\psi(x, L, D, t) = 4 \cdot \sum_{m=1}^{\infty} \frac{L}{\pi \cdot (2m-1)} \cdot \exp \left[ -t \cdot \left( \frac{\pi \cdot (2m-1)}{L} \cdot D \right)^2 \right] \cdot \sin \left( \frac{\pi \cdot (2m-1)}{L} \cdot x \right) \quad .$$

All computations used a time step  $\Delta t=0.0005$  on the grid  $N \times N \times N$  with  $N=20$  and  $N=40$ , each time on a uniform orthogonal grid and on an oblique one from Fig.2

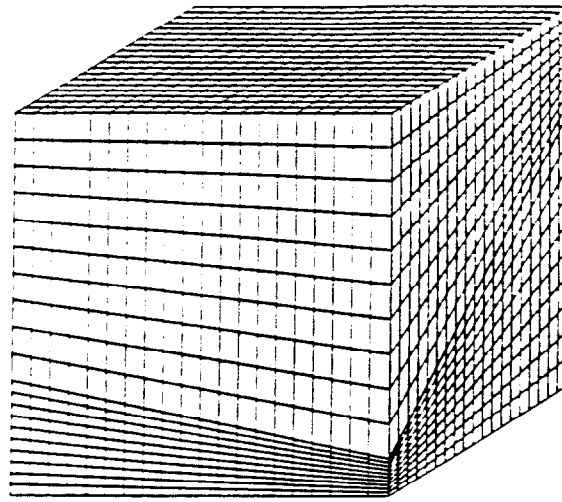


Fig. 2

Errors  $\varepsilon_N = \max_{i,j,k} |U_{i,j,k} - U^a(x_{i,j,k}, y_{i,j,k}, z_{i,j,k}, t)|$  at time  $t=0.08$  are given in the Table

problem	grid	$\varepsilon_{20}$	$\varepsilon_{40}$	$R_1$	$R_2$
isotropic	orthogonal	$4.745 \cdot 10^{-3}$	$3.659 \cdot 10^{-3}$	6.60	0.579
isotropic	oblique	$5.000 \cdot 10^{-3}$	$3.735 \cdot 10^{-3}$	6.63	0.675

$R_1$  and  $R_2$  values, given in the Table, result from the error  $\varepsilon_N$  decomposed in terms of formula  $\varepsilon_N = R_1 \cdot \Delta t + R_2 \cdot \left(\frac{L}{N}\right)^2 = O(\Delta t + \Delta x^2)$ . These values be close in both cases for orthogonal and oblique grids, the formula proves to be correct for the error and inaccuracy on oblique grid proves to be insignificant.

The program of numerical solution for 3D diffusion equations based on the difference scheme described, both for isotropic and anisotropic cases, is used presently to simulate turbulent diffusion when problems on aerosol and other atmospheric pollutant transfer are computed in frames of TREK code [4].

## REFERENCES

1. V.F.Tishkin, A.P.Favorsky, M.Yu. Shashkov. Variational-difference schemes for heat conduction equation on irregular grids. Papers of the USSR Academy of Sciences. - 1979. - Volume 246. #6. p.1342-1346.
2. A.S.Shvedov. Equations for cell volumes. // mathematical notes. - 1986. - Volume 39. #4. - p.597-605.
3. O.I.Butnev, A.N.Bykov, B.L.Voronin, S.I.Skripnik, I.D.Sofronov. Parallel algorithms for 3D heat conduction equation solution and computational results of a demonstration problem on a distributed-memory 8-processor computational system MP-3. // VANT. Computational simulation of physical processes. - 1996. - #3. - p.77-84.
4. A.L.Stadnik, A.A.Shanin and Yu.A.Yanilkin. Eulerian technique TREK for computing 3D gas-dynamical multi-component medium flows. // VANT. Ser. Mat. Modelir. Fiz. Protssesov. - 1994. - #4. - p.71-78.

## Index of Authors & Co-Authors

Adamkevich, G. A. ....	3	Glosli, J. ....	13
Aleoshin, V. V. ....	37, 135	Gorev, V. V. ....	8, 291
Alexeyev, A. V. ....	4, 245	Gorodnichev, A. V. ....	26, 195
Andreyev, E. S. ....	5	Greenberg, D. ....	27
Atkins, J. ....	28	Gusev, V. Yu. ....	5
Baidin, G. V. ....	3	Gustavsen, R. L. ....	57
Bakhrakh, S. M. ....	6, 69	Hart, W. ....	28
Bazhenov, S. V. ....	7, 8, 83, 291	Hartmann-Sinatar, C. L. ....	19, 259
Bazin, A. A. ....	9, 79	Heffelfinger, G. S. ....	45, 199
Beklov, S. A. ....	11, 239	Heinstein, M. W. ....	34
Belak, J. F. ....	10, 13	Hendrickson, C. ....	16
Belyakov, I. M. ....	11, 239	Hixson, R. ....	57
Belyayev, S. P. ....	8, 291	Holm, E. A. ....	23
Bergstrom, Jr., P. M. ....	19, 259	Hornstein, S. M. ....	19, 259
Blanford, M. ....	12	Istrail, S. ....	28
Boercker, D. B. ....	13	Ivanova, G. G. ....	63, 235
Bondarenko, Yu. A. ....	8, 291	Kandiev, Ia. Z. ....	30, 32, 33, 149, 209, 225
Brandon, S. ....	53, 275	Kelly, A. ....	57
Bucheron, E. A. ....	54	Key, S. W. ....	34
Butnev, O. I. ....	53, 275	Kirkpatrick, R. C. ....	35, 36, 50, 97, 285
Bykov, A. N. ....	53, 275	Klishin, G. S. ....	37, 135
Caramana, E. J. ....	14, 15	Korolkova, T. V. ....	8, 291
Chandler, W. P. ....	19, 259	Kovalyov, N. P. ....	63, 235
Clouse, C. ....	16	Kozmanov, M. Yu. ....	5
Clover, M. R. ....	17	Kozybayev, R. M. ....	33, 225
Collins, L. ....	18	Kress, J. ....	18
Cox, L. ....	19, 259	Kwon, I. ....	18
Cranfill, C. W. ....	17	Lenosky, T. ....	18
Decker, C. D. ....	49, 249	Lindemuth, I. R. ....	50
Delov, V. I. ....	60, 87	Linn, R. ....	38
Dementyev, Yu. A. ....	9, 79	Litvinenko, I. A. ....	3
Dibirov, O. A. ....	63, 235	Malshakov, V. D. ....	62, 159, 165
Diegert, C. ....	20	Malyshkin, G. N. ....	30, 149
Dilts, G. ....	21	Margolin, L. G. ....	39, 51
Elsukov, V. P. ....	22, 105, 123	Medsen, N. ....	53
Evans, R. ....	53, 275	Mironova, V. F. ....	9, 79
Faehl, R. J. ....	50	Mitchell, S. A. ....	40
Fang, H. E. ....	23	Morel, J. ....	41
Fedotova, L. P. ....	11, 239	Mosso, S. J. ....	42
Ferguson, J. ....	16	Motlokhov, V. N. ....	265
Ferguson, J. M. ....	25	Nielsen, Jr., D. ....	53, 275
Fisler, D. K. ....	45, 199	Nemanic, M. ....	275
Ford, D. M. ....	45, 199	Nikiforov, V. V. ....	43, 219
Fye, R. M. ....	23	O'Rourke, P. J. ....	58
Garanin, S. G. ....	11, 239	Ober, C. C. ....	44

## Index of Authors & Co-Authors

Okuda, C. ....	275	Tarasov, V. I. ....	63, 235
Petrov, D. V. ....	22, 105, 123	Tautges, T. J. ....	40
Pevnaya, P. I. ....	7, 8, 83, 291	Taylor, P. A. ....	56
Piskunov, V. N. ....	63, 235	Thissell, W. R. ....	57
Pleteneva, N. P. ....	11, 239	Tikhomirov, B. P. ....	9, 79
Plokhoy, V. V. ....	32, 209	Tikhomirova, E. N. ....	9, 79
Pohl, P. I. ....	45, 199	Tonks, D. L. ....	57
Porter, V. L. ....	23	Toropova, T. A. ....	63, 235
Procassini, R. J. ....	46	Trease, H. E. ....	58
Rasskazov, P. A. ....	265	Troullier, N. ....	18
Rasskazova, V. V. ....	47, 265	Trucano, T. ....	59
Rathkopf, J. ....	55, 91	Uyemura, M. ....	275
Remizov, G. N. ....	11, 239	Vakhlamova, L. L. ....	11, 239
Rezchikov, V. Yu. ....	11, 239	Vatulin, V. V. ....	9, 11, 79, 239
Riley, M. E. ....	48, 143	Vershinin, V. B. ....	60
Ritchie, A. B. ....	48, 49, 143, 249	Vinokurov, O. A. ....	11, 239
Rotko, V. A. ....	3	Volkov, S. G. ....	62, 159, 165
Ryabikina, N. A. ....	11, 239	Voronin, B. L. ....	53, 275
Sahota, M. S. ....	58	Vorthman, J. E. ....	57
Schach von Wittenau, A. E. ....	19, 259	Weatherby, J. R. ....	54
Seleznev, V. E. ....	37, 135	Whalen, P. ....	15
Senilova, O. V. ....	60, 87	Wong, M. K. ....	54
Shagaliyev, R. M. ....	4, 11, 239, 245	Yanilkin, Yu V. ....	26, 43, 63, 195, 219, 235
Shanin, A. A. ....	63, 235	Yermolovich, V. F. ....	11, 239
Shaporenko, A. N. ....	265	Yerofeyev, A. M. ....	53, 275
Shashkov, M. J. ....	14	Yudin, Yu A. ....	43, 219
Sheehy, P. T. ....	50	Zharova, G. V. ....	43, 219
Shubin, O. N. ....	22, 105, 123	Zhogov, B. M. ....	62, 159, 165
Simonenko, V. A. ....	22, 105, 123	Zocher, M. A. ....	65, 271
Simonov, G. P. ....	6, 26, 69, 195	Zurek, A. K. ....	57
Skidan, G. I. ....	9, 79	Zvenigorodskaya, O. A. ....	4, 245
Skripnik, A. I. ....	53, 275		
Smolarkiewiez, P. K. ....	51		
Sofronov, I. D. ....	11		
	52, 53, 60, 62, 75, 87, 159, 165, 239, 275		
Sofronov, V. N. ....	63, 235		
Stadnik, A. L. ....	63, 235		
Statsenko, V. P. ....	63, 235		
Stone, C. M. ....	34		
Summers, R. M. ....	54		
Svatos, M. ....	55, 91		
Swartz, B. K. ....	42		

DISTRIBUTION:

- 1 MS-9018 Central Technical Files. 8940-2
  - 2 MS-0899 Technical Library. 4916
  - 2 MS-0619 Review & Approval Desk. 12690  
For DOE/OSTI
- 
- 67 MS-0441 9225  
To be distributed to conference attendees